



Université de Bourgogne–Franche Comté
Laboratoire Interdisciplinaire Carnot de Bourgogne
Ecole doctorale n°553
école doctorale Carnot-Pasteur

THÈSE

pour obtenir le grade de docteur en physique

présentée par

Vardan Martikyan

**Optimal Control and Shortcuts to Adiabaticity
Techniques in Linear and Non-Linear Systems:
from Ion Cyclotron Resonance to Nuclear Magnetic Resonance**

soutenue à Dijon, le 15 Décembre 2021 devant le jury composée de:

Claude Leroy	Professeur	Président & Examineur
Xi Chen	Professeur	Rapporteur
Dionisis Stefanatos	Professeur	Rapporteur
Eric Van Reeth	Maître de Conférence	Examineur
Francesca Chittaro	Maître de Conférence	Examineur
Dominique Sugny	Professeur	Directeur de Thèse

Par la Sagesse, la
Connaissance et la Science,
l'univers a été établi.

— Livre des Proverbes

La lutte elle-même vers les
sommets suffit à remplir un
cœur d'homme. Il faut
imaginer Sisyphe heureux.

— Albert Camus, Le Mythe de
Sisyphe

Abstract

The goal of our research is to develop efficient and robust control protocols for classical and quantum systems. To this end, we have applied Optimal Control Theory (OCT) and Shortcuts to Adiabaticity (STA) with inverse engineering and motion planning approaches in three different examples, which are Resistor Capacitor (RC) circuits, Fourier Transform-Ion Cyclotron Resonance (FT-ICR), and Nuclear Magnetic Resonance (NMR). Some of our results are not limited to these systems but are rather general. We apply OCT and STA with inverse engineering approach to control the time-evolution of the charge on a capacitor. We show that OCT solution is a member of the family of STA solutions. In order to control an ensemble of spins and apply it in NMR, we harness the method of mapping spins to springs. We give a more illustrative explanation of this method, hence it becomes clear why this works both under OCT and STA control pulses. The mutual advantages and drawbacks of OCT and STA are discussed. By using the Rotating Wave Approximation (RWA), we show that the control pulses developed for an ensemble of springs are applicable in FT-ICR. In a first step, we have designed robust pulses without any constraint on the amplitude of the pulse following the framework of OCT. Moreover, in a second step, adapting the Gradient Ascent Pulse Engineering (GRAPE) algorithm we have taken into account an important experimental limitation, which is the constraint on the amplitude of the pulse. The OCT and STA control pulses have been compared with standard adiabatic and Stored Waveform Inverse Fourier Transform (SWIFT) pulses. This is the first time that OCT is applied in FT-ICR.

*

Le but de ce travail de recherche est de développer des protocoles de contrôle efficaces et robustes pour les systèmes classiques et quantiques. À cette fin, nous avons appliqué les approches de théorie du contrôle optimal et de "Shortcuts to Adiabaticity" (STA) basé pour cette dernière sur des méthodes inverses dans trois exemples distincts : la charge d'une capacité dans un circuit électrique RC, la résonance cyclotron d'ion par transformée de Fourier (FT-ICR) et la Résonance Magnétique Nucléaire (NMR). Certains de ces résultats ne sont pas limités à ces systèmes mais sont plus généraux. Nous avons utilisé OCT et STA pour contrôler l'évolution temporelle de la charge d'une capacité. Nous montrons que OCT peut être vu comme un membre de la famille des solutions STA. Dans le but de contrôler un ensemble de spins pour des applications en NMR, nous exploitons la connexion entre les spins et les ressorts. Nous donnons une description qualitative de cette approche, ce qui nous permet d'expliquer pourquoi celle-ci fonctionne à la fois avec des impulsions OCT et STA. Les avantages et les inconvénients de OCT et STA sont discutés. En utilisant l'approximation des ondes tournantes, nous montrons que les pulses de contrôle développés pour un ensemble de ressorts sont applicables en FT-ICR. Dans une première étape, nous avons mis en forme des impulsions robustes sans contrainte sur son amplitude à partir des méthodes du contrôle optimal. De plus, dans une seconde étape, nous avons pris en compte les limitations expérimentales sur les limites

de l'intensité de l'impulsion. Les impulsions OCT et STA ont été comparées avec les solutions standards adiabatiques et SWIFT (Stored Waveform Inverse Fourier Transform). Il s'agit de la première fois que le contrôle optimal est appliqué en FT-ICR.

Dedication and Acknowledgments

Acknowledgments

All acknowledgments that have to be strictly respected are given in the preface. Here I want to freely express myself without thinking about numbers and obligations.

I want to thank my supervisor Prof. Dr. Domimique Sugny for his patience and willingness to help me over the years of my Ph. D. studies. It was truly an honor and pleasure to work with him and learn from him.

Special thanks go to the author of this article [1]. I hope that my thesis mostly violates the tips given there.

I have to mention the important role of the QuSCo (Quantum Enhanced Sensing via Quantum Control) project. My scientific journey of the last three years would not have been possible if I had not been involved in QuSCo as an early stage researcher. I especially thank Mattia Giardini (project manager), Prof. Dr. Christiane Koch (project coordinator) and Athina Zampara (project adviser) for the great job they have done over the last years.

I am very thankful to my friends and all the early stage researchers of QuSCo for their precious friendship and partnership.

My abiding love and gratitude to my teachers for sharing their universal wisdom and experience with me during all those long years of studies.

And last, but always first, I am so grateful to God for he has blessed me with so many wonderful people and has helped me face the shipwreck predicament courageously. Thanks to God's guidance, I have met the true heroes of my life and have become a part of a new crew, a part of a brotherhood. The battle will be won at all costs for there is no freedom without victory. Who knows will see.

Dedication

To my big family

God has also blessed me with a great family who I am enormously thankful to. My father, mother, big mother, godfather and brothers nourished me with their love, faith and knowledge and have always been there for me during good and bad times despite the distance of thousands of miles. They are my angels and watchful guardians whose caring and everlasting love will stay in my heart for eternity.

Love you all.

Vardan Martikyan
University of Burgundy, Department of Physics
October 2021

Table of Contents

	Page
List of Figures	xi
List of Tables	xiii
List of Abbreviations	xvi
List of Symbols	xvii
Preface	1
Introduction	5
1 Applications of STA and OCT Techniques to a Simple Model	7
1.1 RC Circuits	8
1.2 Simplified Problem	9
1.3 General Problem	10
1.3.1 Singular Case	11
1.3.2 Regular Case	13
1.3.3 Analytic Solution in the Regular Case	15
1.3.4 True Hamiltonian and Regularized Cost Functional	19
1.4 Shortcuts to Adiabaticity	22
1.4.1 Polynomial Family of STA Solutions	22
1.4.2 Trigonometric Family of STA Solutions	25
1.4.3 Exponential Family of STA Solutions	27
1.4.4 Exponential Solution vs Regular Solution	29
1.5 Limits	32
1.5.1 Exponential Solution vs Singular Solution	32
1.5.2 Regularized Cost vs Singular Cost	34
1.5.3 Limit of the Derivative of Regularized Cost	37
1.6 Generalization to Higher Orders	38
1.6.1 Generalized Problem	38

TABLE OF CONTENTS

1.6.2	Regular Control	40
1.6.3	Linear Quadratic Optimal Control Theory	42
1.7	Conclusions	45
2	Ensemble Control of Springs and Spins	47
2.1	Optimal Control of a Single Spring	48
2.2	Ensemble Controllability	52
2.2.1	Control of an Ensemble of Springs	55
2.3	Fidelity Plots	60
2.3.1	Fidelity of the Control Process	60
2.4	Mapping Spins to Springs	62
2.4.1	Spin Systems vs Nonlinear Oscillators	65
2.4.2	Simulations for One Control Case	68
2.5	STA Solutions	70
2.5.1	One Control Input: Springs	71
2.5.2	One Control Input: Spins	74
2.5.3	Two Control Inputs: Springs	75
2.5.4	Two Control Inputs: Spins	78
2.5.5	Continuous Case	79
2.6	Pulses	82
2.6.1	Excitation Pulse	82
2.6.2	Concatenated Pulse	85
2.6.3	Selective Control Pulses	87
2.6.4	Adiabatic Control	89
2.6.5	Optimal Control	91
2.7	Conclusions	92
3	Ion Cyclotron Resonance Mass Spectrometry	95
3.1	Experimental Setup	95
3.1.1	Model Dynamics	97
3.1.2	Rotating Wave Approximation	99
3.2	Pulses	101
3.2.1	Adiabatic Excitation	101
3.2.2	Optimal Pulse with RWA	103
3.2.3	SWIFT Pulse	105
3.2.4	Optimal Gradient-Based Algorithm	108
3.2.5	Application of LQOCT to ICR	109
3.2.6	Numerical Computations	111
3.3	Detection Process	113

3.3.1	Green's Reciprocity Principle	113
3.3.2	Parallel-Plate Capacitor	114
3.3.3	Charge Induction in the System of Parallel Plates	114
3.3.4	Signal Processing	115
3.3.5	Analyzing the Signals	117
3.3.6	Detection of Ions by Means of the Adiabatic Pulse	118
3.4	Conclusions	119
A	Basics of Optimal Control Theory	121
A.1	Optimal Control Theory: PMP	121
A.2	Gradient Based Algorithm	123
A.3	Application of the Gradient Based Algorithm	124
B	Ensemble of Springs	127
B.1	Inversion of a Matrix Using its Eigenvalues	127
B.2	Reversing the Direction of Steering	128
B.3	Different Ways of Solving the Main Dynamical Equation	129
C	Special Integrals and Approximations	135
C.1	Fresnel and Imaginary Error Functions	135
C.2	Special Integrals	137
C.3	Stationary Phase Approximation	138
C.4	Rotating Wave Approximation	139
	Conclusions	142
	Bibliography	143

List of Figures

Figure	Page
1.1 Scheme of a Simple RC Circuit	8
1.2 Evolution of RC Circuit in New Variables	20
1.3 Regularized Cost Functional	21
1.4 STA Solutions: Polynomial Family	24
1.5 STA Solutions: Trigonometric Family	27
1.6 STA Solutions: Exponential Family	28
1.7 STA Solutions: Exponential Family in the Limit	31
1.8 Limit of the Regularized Cost	37
1.9 Generalized Case	42
2.1 Control of a Single Spring	51
2.2 Illustration of a Controllability Theorem	55
2.3 Control of an Ensemble of Springs	58
2.4 An Example of a Control Problem	61
2.5 Contour Plot of the Fidelity	62
2.6 Dependence of the Average Fidelity on a Pair of Offsets	63
2.7 Comparison between Minimum-Energy and Quadratic Control	65
2.8 Optimal Control to Apply in a Spin System	68
2.9 Spring and Spin Trajectories	69
2.10 Comparison of Spring and Spin Trajectories	69
2.11 Spin Trajectories on a Bloch Sphere	70
2.12 Springs: OCT and STA Control Pulses in the Case of One Control	73
2.13 Springs: OCT and STA Trajectories in the Case of One Control	74
2.14 Spins: OCT and STA Control Pulses in the Case of One Control	75
2.15 Spins: OCT and STA Trajectories in the Case of One Control	76
2.16 Comparison of OCT and STA Fidelities: without Additional Constraints	77
2.17 Comparison of OCT and STA Fidelities: with Additional Constraints	78
2.18 Springs: Comparison of OCT and STA Control Pulses in the Case of Two Controls: with Additional Constraints	79

2.19 Spins: Comparison of OCT and STA Control Pulses in the Case of Two Controls: with Additional Constraints	80
2.20 Spins: Comparison of OCT and STA Trajectories in the Case of Two Controls: with Additional Constraints	81
2.21 $\pi/2$ Excitation Pulse	83
2.22 Inversed $\pi/2$ Excitation Pulse	84
2.23 Excitation of Spins	84
2.24 Concatenated Pulses	86
2.25 Selective Control Pulse: Two Control Inputs	87
2.26 Selective Control Pulse: One Control Input	88
2.27 Stationary Phase Approximation	90
3.1 Experimental Cell of FT-ICR MS	96
3.2 Adiabatic Excitation of Ions	102
3.3 Comparison of Adiabatic and OCT Excitation Pulses	104
3.4 Comparison of OCT and SWIFT Excitation Pulses	107
3.5 Gradient Based Computations	112
3.6 Detection of Ions by Adiabatic Excitation	118
3.7 Detection Signal Obtained by Adiabatic Excitation	119

List of Tables

Table	Page
1.1 Numerical Values of Different Parameters and Costs of STA and OCT Solutions .	31
3.1 Experimental Values of 2D FT-ICR MS	96

List of Abbreviations

STA Shortcuts to Adiabaticity	4
OCT Optimal Control Theory	4
RC Resistor Capacitor	5
PMP Pontryagin's Maximum Principle	7
LQOCT Linear Quadratic Optimal Control Theory	38
2D Two Dimensional	95
FT-ICR Fourier Transform-Ion Cyclotron Resonance	5
MS Mass Spectrometry	5
SWIFT Stored Waveform Inverse Fourier Transform	5
RWA Rotating Wave Approximation	5
NMR Nuclear Magnetic Resonance	4
MRI Magnetic Resonance Imaging	4

LIST OF TABLES

RF Radio Frequency	4
GRAPE Gradient Ascent Pulse Engineering	108

List of Notations

\bar{A}	Complex conjugate of A
A^*	A Corresponding to the optimal solution
\mathcal{C}	Cost functional
\mathcal{C}_R	Regularized cost functional
\mathcal{F}	Fidelity
H_p	Pontryagin Hamiltonian
$\Re(z)$	Real part of a complex number z
$\Im(z)$	Imaginary part of a complex number z
T, t_f	Control duration
\mathbf{I}_n	n th order identity matrix
x_n^P	Polynomial solution of the order n
x_n^{Tg}	Trigonometric solution consisting of n sine functions
x^{Ex}	Exponential solution

Preface

This research has been carried out at the University of Burgundy, department of quantum interactions and control. I have been working on this project since 2018 as a Ph. D. student at the laboratory ICB with the supervision of Prof. Dr. D. Sugny. The research project has received funding from the European Union's Horizon 2020 research and innovation program under the Marie Skłodowska-Curie grant agreement No. 765267 (QuSCo). I am one of the 15 early stage researchers in QuSCo (Quantum Enhanced Sensing via Quantum Control). The results of this manuscript are a product of valuable collaborations with the group of Prof. Dr. S. J. Glaser (Technical University of Munich) and his Ph. D. student A. Devra who is also an early stage researcher in QuSCo, Prof. Dr. D. Guéry-Odelin (University of Toulouse) and the group of Prof. Dr. M-A. Delsuc (University of Strasbourg). I acknowledge the contribution of Lilit Avagyan in the design of ICR's figure. I am thankful to Xavier Laforgue for helpful discussions about LaTeX and technical support.

Introduction

Scientific problems are conventionally divided into direct and inverse problems. A direct problem is about predicting the set of observations from a set of causal factors that produce them. A good classical example is the Newton's direct problem: the force field at a given time, the mass of a solid object of interest and the initial state (position, orientation and velocity) are known, and the goal is to predict the state at a given time in the future or the final state. This is the direct problem and the way most of us were introduced to classical mechanics at school. There are also good examples in the theory of electricity and gravity: the charge distribution and currents or mass distribution are given and the goal is to predict the characteristics of electromagnetic or gravitational fields that an experimenter will observe. Opposed to direct or forward problem, the inverse or backward problem starts with the effects (e.g. a set of observations) to calculate the causes. Little does general public know that inverse problems are more interesting and practical. For instance, the counterpart inverse problem of Newton could be formulated in this way: the mass of a solid object of interest, the initial and the final states are known, and the goal is to calculate the force field that drove the object from its initial state into the final state. Similarly, a counterpart example of inverse problems in the theory of electricity and gravity could be given in the following way: an experimenter measures the electromagnetic or gravitational fields and the goal is to calculate the charge distribution and currents or mass distribution. The last example indicates the greater utility of inverse problems in real life applications. Indeed, we first observe the gravitational field of Earth and then put forward the inverse problem of finding the mass distribution and structure of Earth. A historical astronomical example of a solved inverse problem is the theoretical prediction of existence of the 8th solar planet later called Neptune from the perturbed trajectory of Uranus by John Couch Adams [2] and Urbain Jean Joseph Le Verrier [3]. Another historical example is Weyl's conjecture about the relation between the eigenfrequencies and shape (area, perimeter) of a drum. In some sense, this indicates the possibility of hearing the shape of a drum [4]. The field of inverse problems was later scratched by Soviet-Armenian astronomer Viktor Ambartsumian. Essentially, he examined the inverse Sturm-Liouville problem or if we put it in another way, he examined the possibility of finding the form of equations given a family of eigenvalues. Ambartsumian's studies in this direction were published and remained in obscurity and oblivion for a long time until Swedish mathematicians would develop his ideas after the Second World War [5].

*

Along with the development of inverse problems, a new direction that we call Optimal Control Theory (**OCT**) started to emerge as an extension of the calculus of variations which is applied to solve inverse problems [6]. **OCT** problems can also be viewed as a combination of direct and inverse problems. As a brief historical overview, it is worth to recall two of the earliest problems posed by Galileo Galilei in 1638 that were later solved by the calculus of variations [7–9] and established the beginning of the control theory. The first is the brachistochrone problem [8] of shaping a wire such that a frictionless bead sliding along it traverses the distance between two end points in minimum time. The second is the heavy chain problem of finding the shape assumed by a heavy chain hanging between two points [10]. Later, **OCT** started to enter into the area of technological sciences. For instance, one of aircraft applications of **OCT** was the calculation of the minimum time-to-climb (time-optimal solution [11–14]) path to an altitude of $20km$ using aerodynamic data from McDonnell and thrust data from General Electric. This path was tested in January of 1962 and provided substantially shorter time than had been achieved by cut-and-try [10]. The fuel-optimal solution is thoroughly discussed in [15, 16]. There is a very nice example of applying **OCT** in a simple mechanical system [17]. For another example of a simple mechanical system where **OCT** is compared with Shortcuts to Adiabaticity (**STA**) see the reference [18]. **OCT** has also been applied to quantum systems first in the context of physical chemistry to steer chemical reactions or control specific degrees of freedom [19, 20], followed by control of spin dynamics [21, 22] for applications in Nuclear Magnetic Resonance (**NMR**) [11, 23–30], Magnetic Resonance Imaging (**MRI**) [31–34] and quantum systems in general [35–37]. Quantum optimal control approaches as well as the state of the art are described in details [38]. The link between quantum speed limit and the energetic cost expenditure has been described [39].

**

Many approaches and methodologies in control theory apart from **OCT** are applied including but not limited to adiabatic control and **STA**. Adiabatic methods [40–43] aim to achieve excitation insensitive to spatial inhomogeneities of the Radio Frequency (**RF**) magnetic field or off-resonances in the sample and are widely used thanks to their simplicity and intuitive scheme but require a long control duration, which could be undesirable. As an alternative to that, **STA** protocols [44–53] constitute driving schemes to control classical and quantum systems without the need of slow driving [47, 50, 54]. **STA** protocol has a myriad of applications in different disciplines including quantum thermodynamics, superconducting qubits, nitrogen-vacancy centers and ultracold gases [55], just to name a few [54]. Furthermore, engineered swift equilibration protocol that shortcuts time-consuming relaxations of a Brownian particle trapped in an optical potential could also be referred to **STA** technique [56]. Different approaches are known in **STA** such as fast-forward approach [57], enhanced **STA** approach [58], counterdiabatic approach [59, 60]. A new method of driving an ultracold gas in potential box with **STA** was proposed [61]. State of the art of **STA** is thoroughly discussed [47, 50].

This thesis is devoted to the in-depth exploration of **STA** and **OCT** techniques for linear and non-linear dynamical systems. In the first chapter, **OCT** and **STA** techniques are applied in a linear system of a Resistor Capacitor (**RC**) circuit. We compare the mutual advantages and drawbacks of **STA** and **OCT** control pulses. We show that **OCT** is included in the family of **STA** solutions in this example. In the second chapter, we focus on a quite challenging problem of ensemble control. This chapter mainly focuses on the application of **OCT** and **STA** in an ensemble of springs and spins. We give an original explanation of an established connection between those two ensemble control problems [62]. We tackle the problem of finding a robust control pulse for this physical system. We design new analytic pulses for the robust or selective control of two-level quantum systems, which could be useful in **NMR**, **MRI** or quantum computing applications. In the third chapter, we apply **OCT** and **STA** in Fourier Transform-Ion Cyclotron Resonance (**FT-ICR**) Mass Spectrometry (**MS**), which is an experimental technique designed for measuring the masses of ions e.g. in unknown natural extracts. We introduce the Rotating Wave Approximation (**RWA**) thereby indicating on the applicability of the control pulses developed for an ensemble of springs in **FT-ICR**. Then, we compare the newly designed **OCT** pulses with standard adiabatic and Stored Waveform Inverse Fourier Transform (**SWIFT**) pulses. All the necessary mathematical tools are presented in the Appendices. The gradient based algorithm is described in Subsecs. 3.2.4, A.2. Some useful tips for inverting a matrix and reversing the direction of steering of an ensemble of springs are given in Appendix B. Fresnel integral, imaginary error function, some important integrals and stationary phase approximation are introduced in Appendix C.

All chapters are based on original scientific publications that are mentioned below.

Chapter 1

- V. Martikyan, D. Guéry-Odelin, and D. Sugny, Comparison between optimal control and shortcut to adiabaticity protocols in a linear control system, Phys. Rev. A 101, 013423 Published 15 January 2020

Chapter 2

- V. Martikyan, A. Devra, D. Guéry-Odelin, S. J. Glaser, and D. Sugny, Robust control of an ensemble of springs: Application to ion cyclotron resonance and two-level quantum systems, Phys. Rev. A 102, 053104 Published 4 November 2020

Chapter 3

- V. Martikyan, C. Beluffi, S. J. Glaser, M-A Delsuc, and D. Sugny, Application of Optimal Control Theory to Fourier Transform Ion Cyclotron Resonance, Molecules 2021, 26(10), 2860

Applications of STA and OCT Techniques to a Simple Model

In this chapter we deal with simple RC series circuit subjected to a driving voltage source. The objective is to reach the stationary regime corresponding to sinusoidal driving in a time much shorter than the characteristic time of the circuit [63]. This approach can also be harnessed to reach fast discharge of a capacitor or sudden change of the driving frequency [63]. The same mathematical framework can be applied to control the motion of a charged particle in a medium by an external electric field [64]. This differential system has the very interesting property of being linear which considerably simplifies its study. We apply the general STA and OCT methods to this simple model and we derive the analytic STA and OCT solutions. Boundary conditions are also taken into account at the initial and final times. The STA trajectory is derived with reverse engineering approach, which consists in imposing the desired evolution of the dynamics and inferring from it the required control pulse [65, 66]. The STA pulse can be expanded over several function bases [64]. The optimal control problem is defined through a cost functional, which allows smooth evolution of the system. The optimal trajectory is achieved from Pontryagin's Maximum Principle (PMP) both in the singular and regular cases. Different works have compared STA and OCT in a nonlinear setting [36, 37, 67]. Here, we revisit this comparison for a linear system. We discuss the advantages and drawbacks of STA and OCT protocols and the way they can mutually benefit from each other. In Sec. 1.1 we describe the physical model, and we formulate the main objectives of the control problem. In Sec. 1.2 we solve the optimal control problem with the only boundary conditions on the charge at initial and final times. In Sec. 1.3 we tackle the general problem with additional boundary conditions on the current and we provide an analytic solution. We also discuss the behavior of the regularized cost functional near the origin. In Sec. 1.4 we derive the STA solutions. We prove that exponential STA and regular optimal solutions are equivalent. In Sec. 1.5 we show that the limit of the regular optimal solution as $\lambda \rightarrow 0$ coincides with the singular optimal protocol.

Note that λ is a small parameter allowing to regularize the singular solution. Details will be given below. Furthermore, the regular cost converges to the singular cost as $\lambda \rightarrow 0$. In Sec. 1.6 we generalize this approach to additional boundary conditions on higher order derivatives of the charge. Imposing such conditions, one ensures smooth behavior at initial and final times for the time evolution of the system while securing the robustness of the control pulse with respect to control time. Such conditions are typical for STA but not for OCT.

1.1 RC Circuits

We consider a simple electric circuit made of a resistor placed in series with a capacitor driven by a time dependent voltage source (see Fig. 1.1). Charge on the capacitor obeys a first order

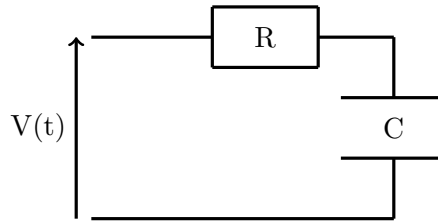


Figure 1.1: Scheme of a simple RC circuit

differential equation [63]:

$$(1.1) \quad \dot{q}(t) + \frac{q(t)}{\tau} = \frac{V(t)}{R},$$

with $\tau = RC$, which comes from Kirchhoff's voltage law:

$$\sum_{i=1}^k V_k = 0.$$

The Kirchhoff's second fundamental law states that the algebraic sum of all the voltages around any closed loop in a circuit is equal to zero.

Let us discuss a particular case of Eq. (1.1) with $\tau = 1\text{s}$, that is the dynamical system:

$$(1.2) \quad \dot{x}(t) + x(t) = u(t),$$

where $V(t)/R = u(t)$ is the control function with a dimension of current, and $x(t) \equiv q(t)$. The goal of the control is to drive the system from the state $x(0) = 0$ to $x(T) = 1$ ($x(t) \in \mathbb{R}$) in a fixed time T with additional constraints $\dot{x}(0) = 0$, $\dot{x}(T) = 0$ while minimizing the running cost $\mathcal{E} = \int_0^T [x^2(t) + \dot{x}^2(t)] dt$.

Summary

- The physical model we consider in this chapter is depicted in Fig. 1.1.
- In physical terms, the goal of the control is to charge an initially uncharged capacitor of a RC circuit in a fixed control time while holding the current equal to zero at the initial and final times and minimizing the dissipated energy and the average energy of the capacitor.
- As a first step towards a final solution, we first consider in Sec. 1.2 a simplified problem without any boundary constraints on the current.

1.2 Simplified Problem

Here, our goal is to drive the state of the system $x(t)$ governed by the dynamics given in Eq. (1.2) from $x(0) = 0$ to $x(T) = 1$ in a fixed time T without any constraint on the derivative of the state. Our analysis is based on the mathematical theory of optimal processes (a brief overview is given in Appendix A). We first construct Pontryagin's Hamiltonian of the system under study [68]:

$$H_p = p(u - x) - \frac{1}{2}(x^2 + (u - x)^2),$$

which corresponds to the linear dynamics given in Eq. (1.2) and where p is the adjoint state. The cost functional physically represents the dissipated energy and the average energy of capacitor:

$$(1.3) \quad \mathcal{E} = \int_0^T [x(t)^2 + \dot{x}(t)^2] dt.$$

Hamilton's equations are:

$$\begin{cases} \dot{x} = u - x \\ \dot{p} = p + 2x - u \end{cases}$$

Since there is no constraint on u , the optimal control satisfies the maximization condition of PMP [68–70] $\frac{\partial H_p}{\partial u} = 0$, which leads to $u^* = x + p$. The optimal trajectories can be expressed as:

$$\begin{cases} \dot{x} = p \\ \dot{p} = x \end{cases}$$

The general solution is:

$$x(t) = c_1 e^t + c_2 e^{-t},$$

where the constants c_1 and c_2 can be found from the boundary conditions $x(0) = 0$ and $x(T) = 1$:

$$c_1 = -c_2 = c, \quad c = \frac{1}{e^T - e^{-T}},$$

This gives:

$$(1.4) \quad x(t) = \frac{\sinh(t)}{\sinh(T)}.$$

Using the hyperbolic trigonometric identities:

$$\begin{aligned} \cosh(2t) &= \sinh^2(t) + \cosh^2(t) \\ \sinh(2t) &= 2\sinh(t)\cosh(t) \end{aligned}$$

and substituting the dynamics given in Eq. (1.4) into Eq. (1.3) one can obtain the minimum cost, which is expressed by a cotangent hyperbolic function:

$$(1.5) \quad \mathcal{C}^* = \coth(T).$$

Summary

- Here, we have discussed the simple case with no boundary constraint on the current.
- We have obtained the corresponding dynamics and the running cost which are given by Eqs. (1.4), (1.5).
- The value of the cost functional when $T = 1$ is $\mathcal{C}^*(T = 1) = \coth 1 \approx 1.3130$.
- In Sec. 1.3 we will discuss the general case with boundary constraints on the current.

1.3

General Problem

We introduce the notations $y := \dot{x}$ and $z := u$ in order to tackle the problem with additional constraints $\dot{x}(0) = \dot{x}(T) = 0$. The idea is to transform the problem with boundary conditions that is difficult to deal with in optimal control into an extended control problem without any constraint on derivatives. The price to pay is the increase of the size of the system under study i.e. its dimension. The modified dynamics in new variables is obtained by taking a first order derivative from both sides of Eq. (1.2):

$$\ddot{x} + \dot{x} = \dot{u} = v,$$

where $v := \dot{u}$ is a new control. The dynamical system is now defined in \mathbb{R}^2 :

$$(1.6) \quad \begin{cases} \dot{y} = v - y \\ \dot{z} = v \end{cases}$$

with boundary conditions $y(0) = y(T) = 0$ and $z(0) = 0, z(T) = 1$. The original variables can be retrieved simply going back to the relations $x = z - y$ and $u = z$. The cost functional \mathcal{C} to minimize is given by:

$$(1.7) \quad \mathcal{C} = \int_0^T [(z - y)^2 + y^2] dt.$$

The control field v does not explicitly appear in the integrand of the cost functional. There are two approaches of finding a solution to this singular problem. Both approaches are discussed later on. Corresponding singular and regular solutions have been compared by numerical simulations.

1.3.1

Singular Case

We solve this problem in this subsection in a very general setting without any constraint on the control. In this case, we show that singular solutions with unbounded fields minimize the cost functional. Singular control fields have been exhibited in quantum physics in different examples [11, 71–73]. Another work where singular control is used for a problem from quantum optics is [74]. In the singular case, the goal is to directly derive the optimal solution. Pontryagin's Hamiltonian can be expressed as:

$$H_p = p_y(v - y) + p_z v - \frac{1}{2} [(z - y)^2 + y^2]$$

Hamilton's equations are:

$$(1.8) \quad \begin{cases} \dot{p}_y = p_y + 2y - z \\ \dot{p}_z = z - y. \end{cases}$$

The singular control v^* is a solution of PMP:

$$\frac{\partial H_p}{\partial v} = 0,$$

which leads to a singular set: $p_y + p_z = 0$. Note that this condition does not allow to explicitly obtain the control. A few manipulations have to be made to find the optimal solution. Since the relation $p_y + p_z = 0$ is valid on a time interval, we may take a first order derivative of both sides of this equation:

$$\dot{p}_y + \dot{p}_z = 0 \Rightarrow p_y = -y \Rightarrow \dot{p}_y + \dot{y} = 0 \Rightarrow v^* = z$$

The initial differential system (1.6), taking into account that $v^* = z$, can be expressed as:

$$\begin{cases} \dot{y} = z - y \\ \dot{z} = z \end{cases}$$

This leads to a singular trajectory:

$$(1.9) \quad \begin{cases} y_s = y_0 e^{-t} + z_0 \sinh(t) \\ z_s = z_0 e^t, \end{cases}$$

which does not satisfy the boundary conditions. In order to sew this solution to the boundary values we assume that the optimal solution has a structure B-S-B (this structure is the general solution of PMP) where **B** is a bang pulse, and **S** is a singular one. Since there is no constraint on the control field, the bang control is a Dirac pulse of amplitude v_τ and of duration τ such that $v_\tau \tau = \mathcal{A}$ with \mathcal{A} being the area of the pulse. The time τ can be chosen as small as needed. We denote by \mathcal{A}_1 and \mathcal{A}_2 the areas of the first and second bangs respectively. During the bang pulse of very large amplitude, the dynamical system is governed by the following system (we can neglect y with respect to v):

$$\begin{cases} \dot{y} = v \\ \dot{z} = v \end{cases}$$

Note that $y(t)$, $z(t)$ satisfy the same differential equation. We have:

$$\lim_{\tau \rightarrow 0} v\tau = \mathcal{A}_1 \quad \text{and} \quad \lim_{\tau \rightarrow T} v(T-\tau) = \mathcal{A}_2$$

At time $t = 0$:

$$\begin{aligned} \dot{y}(0) = v(0) &\Rightarrow \lim_{\tau \rightarrow 0} \frac{y(\tau) - y(0)}{\tau} = v(0) \Rightarrow y(\tau) = y(0) + v(\tau)\tau + o(\tau) \\ \tau \rightarrow 0 &\Rightarrow y(0^+) = y(0) + \mathcal{A}_1 \end{aligned}$$

At time $t = T$:

$$\begin{aligned} \dot{y}(T) = v(T) &\Rightarrow \lim_{\tau \rightarrow T} \frac{y(\tau) - y(T)}{\tau - T} = v(T) \Rightarrow y(\tau) = y(T) - v(\tau)(T - \tau) - o(T - \tau) \\ \tau \rightarrow T &\Rightarrow y(T^-) = y(T) - \mathcal{A}_2 \end{aligned}$$

Here $y(0^+)$ is the right limit of $y(\tau)$ as τ approaches 0 from the right side. Similarly, $y(T^-)$ is the left limit of $y(\tau)$ as τ approaches T from the left side. $o(\tau)$ is an infinitely small term of higher order than τ itself as $\tau \rightarrow 0$ such that the ratio $o(\tau)/\tau$ is still infinitely small as τ approaches 0. We have:

$$\begin{cases} y(0^+) = y(0) + \mathcal{A}_1 \\ z(0^+) = z(0) + \mathcal{A}_1 \\ y(T^-) = y(T) - \mathcal{A}_2 \\ z(T^-) = z(T) - \mathcal{A}_2, \end{cases}$$

which can be simplified by taking into account the boundary conditions $y(0) = y(T) = 0$ and $z(0) = 0, z(T) = 1$:

$$(1.10) \quad \begin{cases} y(0^+) = \mathcal{A}_1 \\ z(0^+) = \mathcal{A}_1 \\ y(T^-) = -\mathcal{A}_2 \\ z(T^-) = 1 - \mathcal{A}_2 \end{cases}$$

Substituting these relations back into Eq. (1.9) at time $t = T$ we obtain:

$$\begin{cases} \mathcal{A}_1(e^{-T} + \sinh(T)) + \mathcal{A}_2 = 0 \\ \mathcal{A}_1 e^T + \mathcal{A}_2 = 1 \end{cases}$$

which has a solution:

$$\mathcal{A}_1 = \frac{1}{\sinh(T)}, \quad \mathcal{A}_2 = -\coth(T)$$

According to Eqs. (1.10), the constants $y_0 = y(0^+)$, $z_0 = z(0^+)$ are equal $y_0 = z_0 = \mathcal{A}_1$. Thus the singular solution (see Eqs. (1.9)) reads:

$$(1.11) \quad y_s = \frac{\cosh(t)}{\sinh(T)}; \quad z_s = \frac{e^t}{\sinh(T)}; \quad x_s = z_s - y_s = \frac{\sinh(t)}{\sinh(T)}$$

The bang pulses bring and remove the system instantaneously from the trajectory of the unconstrained problem such that the boundary conditions are eventually satisfied. As it follows from Eq. (1.7), the minimum cost functional \mathcal{C}^* is equal to the one of the simplified problem: $\mathcal{C}^* = \coth(T)$. For $T = 1$, we have: $\mathcal{C}^* \approx 1.3130$. Here, we assume that the bang pulses have no contribution to the cost.

1.3.2 Regular Case

Regular approach of solving the general problem consists in artificially introducing the control field v into the integrand of the cost functional (see Eq. (1.7)):

$$(1.12) \quad \mathcal{C}_R = \int_0^T [(z - y)^2 + y^2 + \lambda v^2] dt,$$

where \mathcal{C}_R is the so called regularized cost functional, and λ is the positive parameter that is mentioned in the introduction of this chapter. The singular case is obtained in the limit $\lambda \rightarrow 0$. We will verify that this limit is well defined. The way to solve the regular problem is the same. We first construct Pontryagin's Hamiltonian:

$$(1.13) \quad H_p = p_y(v - y) + p_z v - \frac{1}{2} [(z - y)^2 + y^2 + \lambda v^2].$$

Then we write down the dynamics of the adjoint state from Hamilton's equations:

$$\begin{cases} \dot{p}_y = -\frac{\partial H_p}{\partial y} = p_y - z + 2y \\ \dot{p}_z = -\frac{\partial H_p}{\partial z} = z - y. \end{cases}$$

According to [PMP](#), the optimal field v^* must satisfy the following equation:

$$\left. \frac{\partial H_p}{\partial v} \right|^* = 0,$$

therefore

$$(1.14) \quad v_R^* = \frac{p_y + p_z}{\lambda}.$$

Substituting v_R^* into the dynamics of the system (see Eq. (1.6)) we arrive at:

$$\begin{cases} \dot{y} = -y + \frac{1}{\lambda}(p_y + p_z) \\ \dot{z} = \frac{1}{\lambda}(p_y + p_z). \end{cases}$$

The final system of differential equations of the optimal state (y, z, p_y, p_z) is:

$$(1.15) \quad \begin{cases} \dot{y} = -y + \frac{1}{\lambda}(p_y + p_z) \\ \dot{z} = \frac{1}{\lambda}(p_y + p_z) \\ \dot{p}_y = 2y - z + p_y \\ \dot{p}_z = -y + z. \end{cases}$$

Let $\vec{X} := (y, z, p_y, p_z)^\top$ be the state of the physical system where \top stands for transpose. With this new notation, Eq. (1.15) can be rewritten in a matrix form:

$$(1.16) \quad \dot{\vec{X}} = M_\lambda \vec{X},$$

where M_λ is a matrix:

$$(1.17) \quad M_\lambda = \begin{pmatrix} -1 & 0 & 1/\lambda & 1/\lambda \\ 0 & 0 & 1/\lambda & 1/\lambda \\ 2 & -1 & 1 & 0 \\ -1 & 1 & 0 & 0 \end{pmatrix}.$$

In the following, an analytic solution is given to Eq. (1.16).

1.3.3

Analytic Solution in the Regular Case

The formal analytic solution of Eq. (1.16):

$$(1.18) \quad \vec{X} = e^{M_\lambda t} \vec{X}(0),$$

where $\vec{X}(0)$ is the initial state of the system, contains a matrix exponential $e^{M_\lambda t}$. The two unknowns keeping us away from an explicit solution are the matrix exponential $e^{M_\lambda t}$ and the initial state $\vec{X}(0)$. In the following, we derive the explicit form of the matrix exponential by solving the eigenvalue and eigenvector problem of the matrix M_λ :

$$M_\lambda \vec{X} = \mu \vec{X}.$$

Finding eigenvalues $\mu_1, \mu_2, \mu_3, \mu_4$, and eigenvectors $\vec{X}_1, \vec{X}_2, \vec{X}_3, \vec{X}_4$ is a standard procedure:

$$\mu_1 = -1, \quad \mu_2 = 1, \quad \mu_3 = -\frac{1}{\sqrt{\lambda}}, \quad \mu_4 = \frac{1}{\sqrt{\lambda}}$$

$$X_1 = c_1 \begin{pmatrix} 1 \\ 0 \\ -1 \\ 1 \end{pmatrix}, \quad X_2 = c_2 \begin{pmatrix} 1 \\ 2 \\ 2\lambda - 1 \\ 1 \end{pmatrix}$$

$$X_3 = c_3 \begin{pmatrix} 1 \\ 1 - \sqrt{\lambda} \\ -\sqrt{\lambda} \\ \lambda \end{pmatrix}, \quad X_4 = c_4 \begin{pmatrix} 1 \\ 1 + \sqrt{\lambda} \\ \sqrt{\lambda} \\ \lambda \end{pmatrix}$$

Normalization constants c_1, c_2, c_3, c_4 of eigenvectors do not play any role in the eigendecomposition of M_λ , therefore we can choose $c_1 = c_2 = c_3 = c_4 = 1$. Block matrix P with its i th column equal to the right eigenvector \vec{X}_i of M_λ :

$$(1.19) \quad P = \begin{pmatrix} 1 & 1 & 1 & 1 \\ 0 & 2 & 1 - \sqrt{\lambda} & 1 + \sqrt{\lambda} \\ -1 & 2\lambda - 1 & -\sqrt{\lambda} & \sqrt{\lambda} \\ 1 & 1 & \lambda & \lambda \end{pmatrix}$$

is invertible if $\lambda \neq 1$, and $\det(P) = 4\lambda^{1/2}(1 - \lambda)^2$. This is not an obstacle since we are interested in values of λ relatively close to 0. Long calculations of the inverse of the matrix P using cofactors

are omitted:

$$(1.20) \quad P^{-1} = \begin{pmatrix} \frac{1-2\lambda}{2(1-\lambda)} & -\frac{1}{2(1-\lambda)} & \frac{1}{2(1-\lambda)} & \frac{1}{1-\lambda} \\ \frac{1}{2(1-\lambda)} & \frac{1}{\sqrt{\lambda}} & -\frac{1}{2(1-\lambda)} & 0 \\ \frac{1}{2(1-\lambda)} & \frac{1}{\sqrt{\lambda}} & \frac{1}{2\sqrt{\lambda}(1-\lambda)} & \frac{1}{2(\lambda-\sqrt{\lambda})} \\ \frac{1}{2(1-\lambda)} & -\frac{1}{2(1-\lambda)} & \frac{1}{2\sqrt{\lambda}(1-\lambda)} & \frac{1}{2(\lambda+\sqrt{\lambda})} \end{pmatrix}$$

The fundamental property of eigenvectors entails $M_\lambda P = PD$ or $M_\lambda = PDP^{-1}$ where D is the diagonalized form of P with its diagonal elements equal to the eigenvalues of M_λ :

$$D = \begin{pmatrix} -1 & 0 & 0 & 0 \\ 0 & 1 & 0 & 0 \\ 0 & 0 & -\frac{1}{\sqrt{\lambda}} & 0 \\ 0 & 0 & 0 & \frac{1}{\sqrt{\lambda}} \end{pmatrix},$$

Expansion of $e^{M_\lambda t}$ into Taylor series results in a compact expression:

$$(1.21) \quad e^{M_\lambda t} = P e^{Dt} P^{-1},$$

where e^{Dt} is a diagonal matrix:

$$(1.22) \quad e^{Dt} = \begin{pmatrix} e^{-t} & 0 & 0 & 0 \\ 0 & e^t & 0 & 0 \\ 0 & 0 & e^{-\frac{t}{\sqrt{\lambda}}} & 0 \\ 0 & 0 & 0 & e^{\frac{t}{\sqrt{\lambda}}} \end{pmatrix}.$$

We denote by $N_1(t)$, $N_2(t)$, $N_3(t)$, $N_4(t)$ the column vectors of the block matrix $N(t) = e^{M_\lambda t}$:

$$(1.23) \quad N(t) = e^{M_\lambda t} = \begin{pmatrix} N_1(t) & N_2(t) & N_3(t) & N_4(t) \end{pmatrix}$$

$$N_1(t) = \frac{1}{2(1-\lambda)} \begin{pmatrix} (1-2\lambda)e^{-t} - e^t + e^{-\frac{t}{\sqrt{\lambda}}} + e^{\frac{t}{\sqrt{\lambda}}} \\ -e^{-t} + e^t + \sqrt{\lambda} e^{-\frac{t}{\sqrt{\lambda}}} - \sqrt{\lambda} e^{\frac{t}{\sqrt{\lambda}}} \\ e^{-t} - e^t - \frac{1}{\sqrt{\lambda}} e^{-\frac{t}{\sqrt{\lambda}}} + \frac{1}{\sqrt{\lambda}} e^{\frac{t}{\sqrt{\lambda}}} \\ 2e^{-t} - \left(1 + \frac{1}{\sqrt{\lambda}}\right) e^{-\frac{t}{\sqrt{\lambda}}} - \left(1 - \frac{1}{\sqrt{\lambda}}\right) e^{\frac{t}{\sqrt{\lambda}}} \end{pmatrix}$$

$$(1.24) \quad N_2(t) = \frac{1}{2(1-\lambda)} \begin{pmatrix} -2e^t + (1-\sqrt{\lambda})e^{-\frac{t}{\sqrt{\lambda}}} + (1+\sqrt{\lambda})e^{\frac{t}{\sqrt{\lambda}}} \\ 2e^t + (\sqrt{\lambda}-\lambda)e^{-\frac{t}{\sqrt{\lambda}}} - (\sqrt{\lambda}+\lambda)e^{\frac{t}{\sqrt{\lambda}}} \\ -2e^t + \left(1 - \frac{1}{\sqrt{\lambda}}\right)e^{-\frac{t}{\sqrt{\lambda}}} + \left(1 + \frac{1}{\sqrt{\lambda}}\right)e^{\frac{t}{\sqrt{\lambda}}} \\ \left(\frac{1}{\sqrt{\lambda}} - \sqrt{\lambda}\right)\left(-e^{-\frac{t}{\sqrt{\lambda}}} + e^{\frac{t}{\sqrt{\lambda}}}\right) \end{pmatrix}$$

$$N_3(t) = \frac{1}{2(1-\lambda)} \begin{pmatrix} -(1-2\lambda)e^{-t} + (1-2\lambda)e^t - \sqrt{\lambda}e^{-\frac{t}{\sqrt{\lambda}}} + \sqrt{\lambda}e^{\frac{t}{\sqrt{\lambda}}} \\ e^{-t} - (1-2\lambda)e^t - \lambda e^{-\frac{t}{\sqrt{\lambda}}} - \lambda e^{\frac{t}{\sqrt{\lambda}}} \\ -e^{-t} + (1-2\lambda)e^t + e^{-\frac{t}{\sqrt{\lambda}}} + e^{\frac{t}{\sqrt{\lambda}}} \\ -2e^{-t} + (1+\sqrt{\lambda})e^{-\frac{t}{\sqrt{\lambda}}} + (1-\sqrt{\lambda})e^{\frac{t}{\sqrt{\lambda}}} \end{pmatrix}$$

$$N_4(t) = \frac{1}{2(1-\lambda)} \begin{pmatrix} (1-2\lambda)e^{-t} - e^t + \lambda e^{-\frac{t}{\sqrt{\lambda}}} + \lambda e^{\frac{t}{\sqrt{\lambda}}} \\ -e^{-t} + e^t + \lambda\sqrt{\lambda}e^{-\frac{t}{\sqrt{\lambda}}} - \lambda\sqrt{\lambda}e^{\frac{t}{\sqrt{\lambda}}} \\ e^{-t} - e^t - \sqrt{\lambda}e^{-\frac{t}{\sqrt{\lambda}}} + \sqrt{\lambda}e^{\frac{t}{\sqrt{\lambda}}} \\ 2e^{-t} - (\sqrt{\lambda}+\lambda)e^{-\frac{t}{\sqrt{\lambda}}} + (\sqrt{\lambda}-\lambda)e^{\frac{t}{\sqrt{\lambda}}} \end{pmatrix}$$

N_{1i}, N_{2i}, N_{3i} and N_{4i} are the components of the blocks. Our next objective is to find the initial state $\vec{X}(0)$ and thereby the initial adjoint state of the system. This aim is reached by considering a partial explicit form of Eq. (1.18):

$$\begin{pmatrix} N_{13}(t) & N_{14}(t) \\ N_{23}(t) & N_{24}(t) \end{pmatrix} \begin{pmatrix} p_y(0) \\ p_z(0) \end{pmatrix} = \begin{pmatrix} y(t) - N_{11}(t)y(0) - N_{12}(t)z(0) \\ z(t) - N_{21}(t)y(0) - N_{22}(t)z(0) \end{pmatrix}$$

Taking into account the boundary conditions $y(0) = z(0) = 0$ we arrive at:

$$(1.25) \quad \begin{pmatrix} y(t) \\ z(t) \end{pmatrix} = \begin{pmatrix} N_{13}(t) & N_{14}(t) \\ N_{23}(t) & N_{24}(t) \end{pmatrix} \begin{pmatrix} p_y(0) \\ p_z(0) \end{pmatrix}.$$

In a similar way, from Eq. (1.18) and the boundary conditions $y(0) = z(0) = 0$, we deduce:

$$(1.26) \quad \begin{pmatrix} p_y(t) \\ p_z(t) \end{pmatrix} = \begin{pmatrix} N_{33}(t) & N_{34}(t) \\ N_{43}(t) & N_{44}(t) \end{pmatrix} \begin{pmatrix} p_y(0) \\ p_z(0) \end{pmatrix}.$$

We recall that $y(T) = 0$, and $z(T) = 1$, thus Eq. (1.25) implies:

$$\begin{pmatrix} p_y(0) \\ p_z(0) \end{pmatrix} = A^{-1} \begin{pmatrix} 0 \\ 1 \end{pmatrix},$$

where

$$A = \begin{pmatrix} N_{13}(T) & N_{14}(T) \\ N_{23}(T) & N_{24}(T) \end{pmatrix},$$

$$A^{-1} = \begin{pmatrix} N_{13}(T) & N_{14}(T) \\ N_{23}(T) & N_{24}(T) \end{pmatrix}^{-1} = \frac{1}{2(1-\lambda)\det(A)} \times \begin{pmatrix} \left(\frac{1}{\sqrt{\lambda}} - \sqrt{\lambda}\right) \left(-e^{-\frac{T}{\sqrt{\lambda}}} + e^{\frac{T}{\sqrt{\lambda}}}\right) & -2e^{-T} + \left(1 + \frac{1}{\sqrt{\lambda}}\right) e^{-\frac{T}{\sqrt{\lambda}}} + \left(1 - \frac{1}{\sqrt{\lambda}}\right) e^{\frac{T}{\sqrt{\lambda}}} \\ 2e^T - \left(1 - \frac{1}{\sqrt{\lambda}}\right) e^{-\frac{T}{\sqrt{\lambda}}} - \left(1 + \frac{1}{\sqrt{\lambda}}\right) e^{\frac{T}{\sqrt{\lambda}}} & e^{-T} - e^T - \frac{1}{\sqrt{\lambda}} e^{-\frac{T}{\sqrt{\lambda}}} + \frac{1}{\sqrt{\lambda}} e^{\frac{T}{\sqrt{\lambda}}} \end{pmatrix},$$

and

$$(1.27) \quad \det(A) = \frac{1}{4(1-\lambda)^2\sqrt{\lambda}} \left[\left(1 - \sqrt{\lambda}\right)^2 e^{-(1+\frac{1}{\sqrt{\lambda}})T} - \left(1 + \sqrt{\lambda}\right)^2 e^{-(1-\frac{1}{\sqrt{\lambda}})T} - \left(1 + \sqrt{\lambda}\right)^2 e^{(1-\frac{1}{\sqrt{\lambda}})T} + \left(1 - \sqrt{\lambda}\right)^2 e^{(1+\frac{1}{\sqrt{\lambda}})T} + 8\sqrt{\lambda} \right].$$

We finally obtain the initial adjoint state:

$$(1.28) \quad \begin{pmatrix} p_y(0) \\ p_z(0) \end{pmatrix} = \frac{1}{2(1-\lambda)\det(A)} \begin{pmatrix} -2e^{-T} + \left(1 + \frac{1}{\sqrt{\lambda}}\right) e^{-\frac{T}{\sqrt{\lambda}}} + \left(1 - \frac{1}{\sqrt{\lambda}}\right) e^{\frac{T}{\sqrt{\lambda}}} \\ e^{-T} - e^T - \frac{1}{\sqrt{\lambda}} e^{-\frac{T}{\sqrt{\lambda}}} + \frac{1}{\sqrt{\lambda}} e^{\frac{T}{\sqrt{\lambda}}} \end{pmatrix}.$$

Knowledge of the initial state enables us to extract the dynamics of the system from Eq. (1.25) and Eq. (1.26):

$$(1.29) \quad \begin{bmatrix} y \\ z \\ x \\ p_y \\ p_z \\ v_R \end{bmatrix} = \mathbf{a} \begin{bmatrix} y_1 & y_2 & y_3 & y_4 \\ z_1 & z_2 & z_3 & z_4 \\ x_1 & x_2 & x_3 & x_4 \\ p_{y1} & p_{y2} & p_{y3} & p_{y4} \\ p_{z1} & p_{z2} & p_{z3} & p_{z4} \\ v_1 & v_2 & v_3 & v_4 \end{bmatrix} \begin{bmatrix} e^{-t} \\ e^t \\ e^{-\frac{t}{\sqrt{\lambda}}} \\ e^{\frac{t}{\sqrt{\lambda}}} \end{bmatrix}$$

$$x = z - y, \quad v_R = \frac{p_y + p_z}{\lambda}$$

where

(1.30)

$$\begin{aligned} \mathbf{a} &= \frac{1}{4(1-\lambda)^2 \det(A)} = \\ &= \frac{1}{\sqrt{\lambda} \left[(1-\sqrt{\lambda})^2 e^{-(1+\frac{1}{\sqrt{\lambda}})T} - (1+\sqrt{\lambda})^2 e^{-(1-\frac{1}{\sqrt{\lambda}})T} - (1+\sqrt{\lambda})^2 e^{(1-\frac{1}{\sqrt{\lambda}})T} + (1-\sqrt{\lambda})^2 e^{(1+\frac{1}{\sqrt{\lambda}})T} + 8\sqrt{\lambda} \right]} \end{aligned}$$

$$\begin{aligned} (1.31) \quad y_1 &= -2e^T + \left(1 - \frac{1}{\sqrt{\lambda}}\right) e^{-\frac{T}{\sqrt{\lambda}}} + \left(1 + \frac{1}{\sqrt{\lambda}}\right) e^{\frac{T}{\sqrt{\lambda}}} \\ y_2 &= 2e^{-T} - \left(1 + \frac{1}{\sqrt{\lambda}}\right) e^{-\frac{T}{\sqrt{\lambda}}} - \left(1 - \frac{1}{\sqrt{\lambda}}\right) e^{\frac{T}{\sqrt{\lambda}}} \\ y_3 &= -\left(1 - \frac{1}{\sqrt{\lambda}}\right) e^{-T} + \left(1 + \frac{1}{\sqrt{\lambda}}\right) e^T - \frac{2}{\sqrt{\lambda}} e^{\frac{T}{\sqrt{\lambda}}} \\ y_4 &= -\left(1 + \frac{1}{\sqrt{\lambda}}\right) e^{-T} + \left(1 - \frac{1}{\sqrt{\lambda}}\right) e^T + \frac{2}{\sqrt{\lambda}} e^{-\frac{T}{\sqrt{\lambda}}} \end{aligned}$$

The rest of the multipliers z_1, z_2, \dots, v_4 can be expressed in terms of y_1, y_2, y_3, y_4 :

$$(1.32) \quad \begin{bmatrix} z_1 & z_2 & z_3 & z_4 \\ x_1 & x_2 & x_3 & x_4 \\ p_{y1} & p_{y2} & p_{y3} & p_{y4} \\ p_{z1} & p_{z2} & p_{z3} & p_{z4} \\ v_1 & v_2 & v_3 & v_4 \end{bmatrix} = \begin{bmatrix} 0 & 2y_2 & (1-\sqrt{\lambda})y_3 & (1+\sqrt{\lambda})y_4 \\ -y_1 & y_2 & -\sqrt{\lambda}y_3 & \sqrt{\lambda}y_4 \\ -y_1 & -(1-2\lambda)y_2 & -\sqrt{\lambda}y_3 & \sqrt{\lambda}y_4 \\ y_1 & y_2 & \lambda y_3 & \lambda y_4 \\ 0 & 2y_2 & \left(1 - \frac{1}{\sqrt{\lambda}}\right)y_3 & \left(1 + \frac{1}{\sqrt{\lambda}}\right)y_4 \end{bmatrix}$$

Some of the results achieved in the present section are represented in Fig. 1.2.

1.3.4

True Hamiltonian and Regularized Cost Functional

We have previously examined the evolution of the state of the system $\vec{X}(t) = (y, z, p_y, p_z)$. Time evolutions of the true Hamiltonian and regularized cost functional are also interesting aspects to explore. Substituting Eq. (1.14) into Eq. (1.13) we obtain the true Hamiltonian of the system:

$$(1.33) \quad \mathcal{H}^{true} = -p_y y - \frac{1}{2} \left[(z-y)^2 + y^2 \right] + \frac{(p_y + p_z)^2}{2\lambda},$$

which is a constant of motion. Our next goal is to plot the dependence of the cost functional on the regularization parameter λ . This computation allows us to explore the link between regular and singular trajectories. We recall the final formula of the regularized cost functional:

$$\mathcal{C}_R = \int_0^T G dt = \int_0^T \left[(z-y)^2 + y^2 + \lambda v_R^2 \right] dt$$

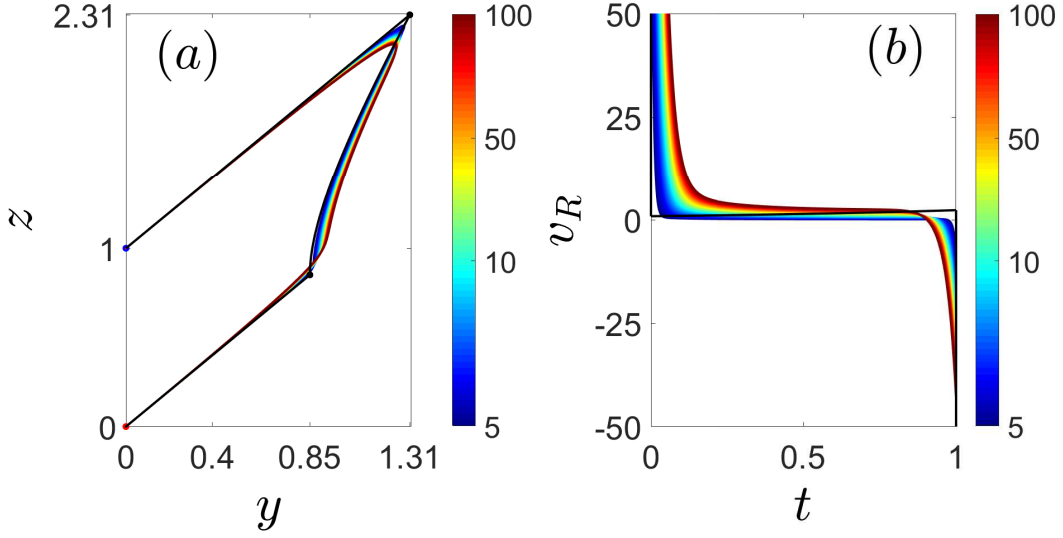


Figure 1.2: (a) Plot of the optimal regular and singular trajectories in the (y, z) plane. The red and blue dots indicate respectively the initial state and the target state. The black dots correspond to the end points of the trajectories associated with the bang pulses. (b) Plot of the time evolution of the regular control field v_R . The singular control field is derived from v_R in the limit $\lambda \rightarrow 0$. The black solid line corresponds to the singular solution, while the regular solutions are displayed in color. The color bar indicates the value of $\lambda \times 10^5$ for each regular process. Dimensionless units are used.

In order to plot this additional dependence we must calculate the terms λv_R^2 , y^2 , $(z - y)^2$:

$$\lambda v_R^2 = \alpha^2 \left(w_2^2 e^{2t} + w_3^2 e^{-\frac{2t}{\sqrt{\lambda}}} + w_4^2 e^{\frac{2t}{\sqrt{\lambda}}} + 2 \left[w_2 w_3 e^{\left(1 - \frac{1}{\sqrt{\lambda}}\right)t} + w_2 w_4 e^{\left(1 + \frac{1}{\sqrt{\lambda}}\right)t} + w_3 w_4 \right] \right)$$

$$w_2 = 2\sqrt{\lambda} y_2, \quad w_3 = -(1 - \sqrt{\lambda}) y_3, \quad w_4 = (1 + \sqrt{\lambda}) y_4$$

$$y^2 = \alpha^2 \left(y_1^2 e^{-2t} + y_2^2 e^{2t} + y_3^2 e^{-\frac{2t}{\sqrt{\lambda}}} + y_4^2 e^{\frac{2t}{\sqrt{\lambda}}} + 2 \left[y_1 y_2 + y_1 y_3 e^{-\left(1 + \frac{1}{\sqrt{\lambda}}\right)t} + y_1 y_4 e^{-\left(1 - \frac{1}{\sqrt{\lambda}}\right)t} + y_2 y_3 e^{\left(1 - \frac{1}{\sqrt{\lambda}}\right)t} + y_2 y_4 e^{\left(1 + \frac{1}{\sqrt{\lambda}}\right)t} + y_3 y_4 \right] \right)$$

$$(z - y)^2 = \alpha^2 \left(x_1^2 e^{-2t} + x_2^2 e^{2t} + x_3^2 e^{-\frac{2t}{\sqrt{\lambda}}} + x_4^2 e^{\frac{2t}{\sqrt{\lambda}}} + 2 \left[x_1 x_2 + x_1 x_3 e^{-\left(1 + \frac{1}{\sqrt{\lambda}}\right)t} + x_1 x_4 e^{-\left(1 - \frac{1}{\sqrt{\lambda}}\right)t} + x_2 x_3 e^{\left(1 - \frac{1}{\sqrt{\lambda}}\right)t} + x_2 x_4 e^{\left(1 + \frac{1}{\sqrt{\lambda}}\right)t} + x_3 x_4 \right] \right)$$

Integrand G can now be written in a compact form:

$$(1.34) \quad G = \alpha^2 \left\{ G_1 e^{-2t} + G_2 e^{2t} + G_3 e^{-\frac{2t}{\sqrt{\lambda}}} + G_4 e^{\frac{2t}{\sqrt{\lambda}}} + 2 \left[G_{13} e^{-(1+\frac{1}{\sqrt{\lambda}})t} + G_{14} e^{-(1-\frac{1}{\sqrt{\lambda}})t} + G_{23} e^{(1-\frac{1}{\sqrt{\lambda}})t} + G_{24} e^{(1+\frac{1}{\sqrt{\lambda}})t} \right] \right\},$$

where

$$\begin{aligned} G_1 &= 2y_1^2, & G_2 &= 2(1+2\lambda)y_2^2, & G_3 &= 2(1-\sqrt{\lambda}+\lambda)y_3^2, & G_4 &= 2(1+\sqrt{\lambda}+\lambda)y_4^2 \\ G_{13} &= (1+\sqrt{\lambda})y_1y_3, & G_{14} &= (1-\sqrt{\lambda})y_1y_4 \\ G_{23} &= (1-\sqrt{\lambda})(1-2\sqrt{\lambda})y_2y_3, & G_{24} &= (1+\sqrt{\lambda})(1+2\sqrt{\lambda})y_2y_4, \end{aligned}$$

The regularized cost functional \mathcal{C}_R is obtained by integrating G :

$$(1.35) \quad \begin{aligned} \mathcal{C}_R &= \alpha^2 \left\{ \frac{1}{2} \left[-\left(e^{-2T}-1\right)G_1 + \left(e^{2T}-1\right)G_2 \right] - \frac{\sqrt{\lambda}}{2} \left[\left(e^{-\frac{2T}{\sqrt{\lambda}}}-1\right)G_3 - \left(e^{\frac{2T}{\sqrt{\lambda}}}-1\right)G_4 \right] - \right. \\ &- 2 \frac{\sqrt{\lambda}}{1+\sqrt{\lambda}} \left[\left(e^{-(1+\frac{1}{\sqrt{\lambda}})T}-1\right)G_{13} - \left(e^{(1+\frac{1}{\sqrt{\lambda}})T}-1\right)G_{24} \right] + \\ &\left. + 2 \frac{\sqrt{\lambda}}{1-\sqrt{\lambda}} \left[\left(e^{-(1-\frac{1}{\sqrt{\lambda}})T}-1\right)G_{14} - \left(e^{(1-\frac{1}{\sqrt{\lambda}})T}-1\right)G_{23} \right] \right\} \end{aligned}$$

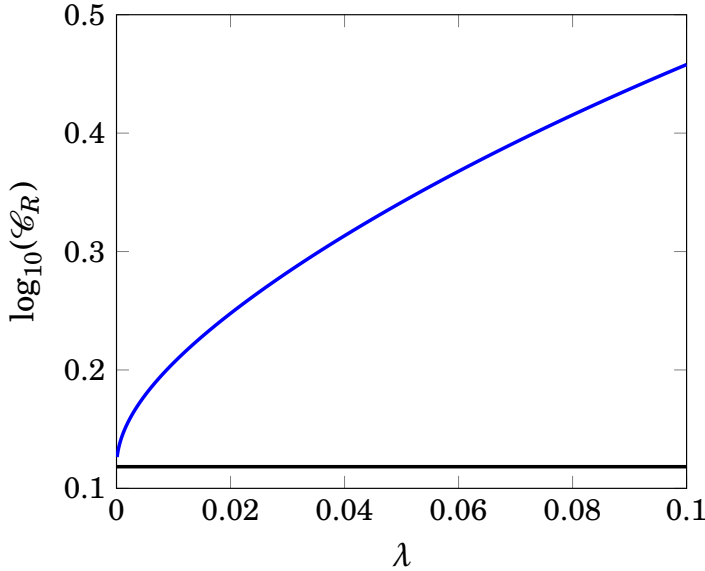


Figure 1.3: Plot of the regularized cost functional $\log_{10}(\mathcal{C}_R)$ as a function of the parameter λ (solid blue line). The solid horizontal black line indicates the value of the minimum cost functional $\log_{10}[\coth(1)]$ for the singular solution. In the limit when $\lambda \rightarrow 0$, the singular and regularized costs coincide $\log_{10}(\mathcal{C}_R) \rightarrow \log_{10}[\coth(1)]$.

Results concerning the behavior of the regularized cost functional for the values of λ close to 0 [64] is represented in Fig. 1.3. Analytically, it can be shown that the curves of the regularized and singular costs converge for the values $\lambda \ll 1$ (see Subsec. 1.5.2), however, we encounter some numerical problems because of exponential terms in Eq. (1.35), and therefore the regular solution is not depicted for the values $\lambda < 8.2 \times 10^{-6}$ in Fig. 1.8.

Summary

- The singular and regular solutions are obtained. We have shown that the singular solution coincides with that of the simplified problem.
- The regular solution, which has been analytically obtained, is anticipated to coincide with the singular solution when $\lambda \rightarrow 0$. This is rigorously discussed in Sec. 1.5.
- In Sec. 1.4 the reversely engineered STA solutions are derived and compared with the optimal solution.

1.4

Shortcuts to Adiabaticity

In the previous sections, we found the optimal solution of the control problem Eq. (1.2) with and without additional boundary conditions on the derivatives. The optimal solution is unique and corresponds to the energy minimum, therefore we will call it the global optimal solution. In this section, our aim is to solve the general control problem by using STA protocols with reverse engineering approach. We obtain polynomial, trigonometric, exponential families of STA solutions of different orders. Within each family and each order of STA solutions we find the one corresponding to the energy minimum by minimizing the cost functional with respect to the free parameters (the number of free parameters depends on the order of the expansion). These minima, that we call local optima, have been compared with the global optimum. Their advantages and drawbacks have been discussed.

1.4.1

Polynomial Family of STA Solutions

In OCT we first find the control field, and then we are able to extract the optimal trajectories. Here, we do the opposite. Trajectories are found first by narrowing our search within a family of functions, and then the control field is extracted from the dynamics. Since polynomial functions are the simple ones, let us start from them by assuming that $\mathbf{x}(t)$ is a polynomial function of the order n :

$$\mathbf{x}(t) = \sum_{k=0}^n \mathbf{a}_k t^k$$

From now on we assume that $T = 1$. The initial conditions $x(0) = \dot{x}(0) = 0$ impose $a_0 = a_1 = 0$, and therefore:

$$(1.36) \quad x(t) = \sum_{k=2}^n a_k t^k$$

From the final conditions $x(T = 1) = 1$, $\dot{x}(T = 1) = 0$, it follows:

$$(1.37) \quad \begin{cases} \sum_{k=2}^n a_k = 1 \\ \sum_{k=2}^n k a_k = 0 \end{cases}$$

There are 2 equations and $n - 1$ unknowns, thus there are $n - 3$ free parameters. Let us denote the solutions corresponding to polynomial, trigonometric and exponential functions respectively by x_n^P , x_n^{Tg} , x^{Ex} , where index n is the order of the family. The controls and cost functionals are denoted in the same way. The orders $n = 3, 4, 5, 6$ are considered one by one.

- If $n = 3$, there is no free parameter:

$$\begin{aligned} x_3^P(t) &= 3t^2 - 2t^3 \\ u_3^P(t) &= 6t - 3t^2 - 2t^3 \end{aligned}$$

The cost functional has been numerically evaluated: $\mathcal{C}_3^P \approx 1.57143$.

- If $n = 4$, there is one free parameter a :

$$\begin{aligned} x_4^P(t) &= (3 + a)t^2 - 2(1 + a)t^3 + at^4 \\ u_4^P(t) &= 2(3 + a)t - (3 + 5a)t^2 - 2(1 - a)t^3 + at^4 \end{aligned}$$

The minimization in this simple case can be done analytically. Just recall the expression for the cost functional:

$$\mathcal{C} = \int_0^1 [x^2(t) + \dot{x}^2(t)] dt$$

Substitution of the 4th order solution into the last expression yields:

$$\mathcal{C}_4^P = 2 \left[\left(\frac{1}{1260} + \frac{1}{105} \right) a^2 + \frac{1}{60} a + \frac{11}{14} \right],$$

and hence

$$\begin{aligned} a_{min} &= -\frac{1/60}{2(1/1260 + 1/105)} = -\frac{21}{26} \approx -0.8076923 \\ \mathcal{C}_4^P &= 2 \left[\left(\frac{1}{1260} + \frac{1}{105} \right) \left(\frac{21}{26} \right)^2 - \frac{1}{60} \left(\frac{21}{26} \right) + \frac{11}{14} \right], \end{aligned}$$

or $\mathcal{C}_4^P \approx 2(0.006730769 - 0.013461538 + 0.785714286) \approx 1.55797$

- If $n = 5$, there are two free parameters a and b :

$$x_5^{\text{P}}(t) = (3 + a + 2b)t^2 - (2 + 2a + 3b)t^3 + at^4 + bt^5$$

$$u_5^{\text{P}}(t) = 2(3 + a + 2b)t - (3 + 5a + 7b)t^2 + (-2 + 2a - 3b)t^3 + (a + 5b)t^4 + bt^5$$

Hereafter, the minimization is done numerically in the environment of "Mathematica" by the help of the functions "NMinimize" and "NIntegrate". The corresponding values for the free parameters and the cost functional are:

$$a \approx 23.636752, \quad b \approx -9.(7), \quad \mathcal{C}_5^{\text{P}} \approx 1.40276$$

- If $n = 6$, there are three free parameters a , b , and c :

$$x_6^{\text{P}}(t) = (3 + a + 2b + 3c)t^2 - (2 + 2a + 3b + 4c)t^3 + at^4 + bt^5 + ct^6$$

$$u_6^{\text{P}}(t) = 2(3 + a + 2b + 3c)t - (3 + 5a + 7b + 9c)t^2 + (-2 + 2a - 3b - 4c)t^3 + (a + 5b)t^4 + (b + 6c)t^5 + ct^6$$

The corresponding values for the free parameters and the cost functional are:

$$a \approx 6.956942, \quad b \approx 5.627256, \quad c \approx -5.135011, \quad \mathcal{C}_6^{\text{P}} \approx 1.39986$$

The polynomial solutions in comparison with singular and regular ones are depicted in Fig. 1.4.

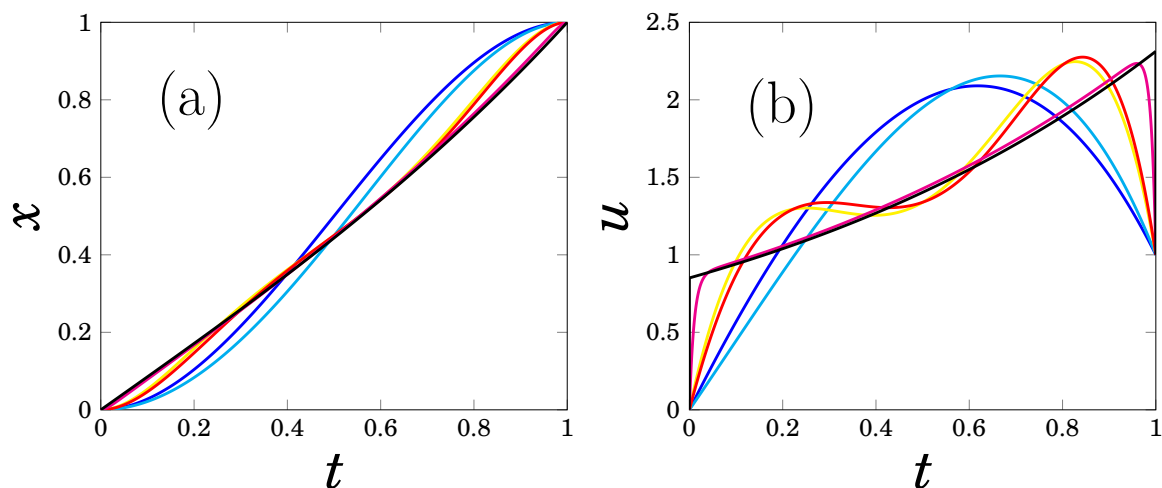


Figure 1.4: Comparison between the polynomial STA and OCT solutions. Panels (a) and (b) represent respectively the time evolution of the trajectory x and of the control field u . The black and magenta lines correspond respectively to the singular and regular solutions. The parameter λ is set to 10^{-4} . The polynomial STA solutions are plotted in blue, aqua, yellow and red for the respective orders $n = 3, 4, 5, 6$. Dimensionless units are used.

The value of λ is taken sufficiently small to illustrate the behavior of the regular solution when λ approaches 0. In the limit $\lambda \rightarrow 0$, the regular optimal solution coincides with the singular one.

1.4.2

Trigonometric Family of STA Solutions

Next we consider the family of trigonometric functions. Let $x(t)$ be a sum of sine functions:

$$(1.38) \quad x(t) = \sum_{k=1}^n a_k \sin\left(\frac{k\pi}{2}t\right)$$

The condition $x(0) = 0$ is automatically satisfied. The second condition $\dot{x}(0) = 0$ imposes:

$$(1.39) \quad \sum_{k=1}^n k a_k = 0$$

From $x(1) = 1$, $\dot{x}(1) = 0$, it follows:

$$(1.40) \quad \begin{cases} \sum_{k=1}^n a_k \sin\left(\frac{k\pi}{2}\right) = 1 \\ \sum_{k=1}^n k a_k \cos\left(\frac{k\pi}{2}\right) = 0 \end{cases}$$

There are 3 equations and n unknowns, hence there are again $n - 3$ free parameters. The cases $n = 3, 4, 5, 6$ are considered one by one.

- If $n = 3$, there is no free parameter.

$$\begin{aligned} x_3^{\text{Tg}}(t) &= \frac{3}{4} \sin\left(\frac{\pi}{2}t\right) - \frac{1}{4} \sin\left(\frac{3\pi}{2}t\right) \\ u_3^{\text{Tg}}(t) &= \frac{3}{4} \left(\frac{\pi}{2} \cos\left(\frac{\pi}{2}t\right) + \sin\left(\frac{\pi}{2}t\right) \right) - \frac{1}{4} \left(\frac{3\pi}{2} \cos\left(\frac{3\pi}{2}t\right) + \sin\left(\frac{3\pi}{2}t\right) \right) \end{aligned}$$

The corresponding value for the cost functional is:

$$\mathcal{C}_3^{\text{Tg}} \approx 1.70041$$

- If $n = 4$, there is one free parameter a .

$$\begin{aligned} x_4^{\text{Tg}}(t) &= \left(\frac{3}{4} - 2a\right) \sin\left(\frac{\pi}{2}t\right) + 2a \sin(\pi t) - \left(\frac{1}{4} + 2a\right) \sin\left(\frac{3\pi}{2}t\right) + a \sin(2\pi t) \\ u_4^{\text{Tg}}(t) &= \left(\frac{3}{4} - 2a\right) \left(\frac{\pi}{2} \cos\left(\frac{\pi}{2}t\right) + \sin\left(\frac{\pi}{2}t\right) \right) + 2a (\pi \cos(\pi t) + \sin(\pi t)) - \\ &\quad - \left(\frac{1}{4} + 2a\right) \left(\frac{3\pi}{2} \cos\left(\frac{3\pi}{2}t\right) + \sin\left(\frac{3\pi}{2}t\right) \right) + a (2\pi \cos(2\pi t) + \sin(2\pi t)) \end{aligned}$$

The corresponding values for the free parameter and the cost functional are:

$$a \approx 0.0202, \quad \mathcal{C}_4^{\text{Tg}} \approx 1.69843$$

- If $n = 5$, there are two free parameters a and b .

$$x_5^{\text{Tg}}(t) = \left(\frac{3}{4} - 2a\right) \sin\left(\frac{\pi}{2}t\right) + 2(a-b) \sin(\pi t) - \\ - \left(\frac{1}{4} + 2a - b\right) \sin\left(\frac{3\pi}{2}t\right) + (a-b) \sin(2\pi t) + b \sin\left(\frac{5\pi}{2}t\right)$$

$$u_5^{\text{Tg}}(t) = \left(\frac{3}{4} - 2a\right) \left(\frac{\pi}{2} \cos\left(\frac{\pi}{2}t\right) + \sin\left(\frac{\pi}{2}t\right)\right) + 2(a-b) (\pi \cos(\pi t) + \sin(\pi t)) - \\ - \left(\frac{1}{4} + 2a - b\right) \left(\frac{3\pi}{2} \cos\left(\frac{3\pi}{2}t\right) + \sin\left(\frac{3\pi}{2}t\right)\right) + (a-b) (2\pi \cos(2\pi t) + \sin(2\pi t)) + \\ + b \left(\frac{5\pi}{2} \cos\left(\frac{5\pi}{2}t\right) + \sin\left(\frac{5\pi}{2}t\right)\right)$$

The corresponding values for the free parameters and the cost functional are:

$$a \approx 0.785988, \quad b \approx -0.356639, \quad \mathcal{C}_5^{\text{Tg}} \approx 1.48104$$

- If $n = 6$, there are three free parameters a , b , and c .

$$x_6^{\text{Tg}}(t) = \left(\frac{3}{4} - 2a - 2b\right) \sin\left(\frac{\pi}{2}t\right) + (2a - 3c) \sin(\pi t) - \\ - \left(\frac{1}{4} + 2a + b\right) \sin\left(\frac{3\pi}{2}t\right) + a \sin(2\pi t) + b \sin\left(\frac{5\pi}{2}t\right) + c \sin(3\pi t)$$

$$u_6^{\text{Tg}}(t) = \left(\frac{3}{4} - 2a - 2b\right) \left(\frac{\pi}{2} \cos\left(\frac{\pi}{2}t\right) + \sin\left(\frac{\pi}{2}t\right)\right) + (2a - 3c) (\pi \cos(\pi t) + \sin(\pi t)) - \\ - \left(\frac{1}{4} + 2a + b\right) \left(\frac{3\pi}{2} \cos\left(\frac{3\pi}{2}t\right) + \sin\left(\frac{3\pi}{2}t\right)\right) + \\ + a (2\pi \cos(2\pi t) + \sin(2\pi t)) + b \left(\frac{5\pi}{2} \cos\left(\frac{5\pi}{2}t\right) + \sin\left(\frac{5\pi}{2}t\right)\right) + c (3\pi \cos(3\pi t) + \sin(3\pi t))$$

The corresponding values for the free parameters and the cost functional are:

$$a \approx 1.0407, \quad b \approx -0.312242, \quad c \approx -0.0105136, \quad \mathcal{C}_6^{\text{Tg}} \approx 1.48099$$

The trigonometric solutions in comparison with the singular and regular ones are depicted in Fig. 1.5. This family of functions has been considered in hope to reach a closer path in comparison with the regular and singular optimal solutions. Contrary to our expectations, the difference between STA and OCT paths is of the same order of magnitude for the polynomial (see Fig. 1.4) and trigonometric functions (see Fig. 1.5) but the polynomial appears to give better results.

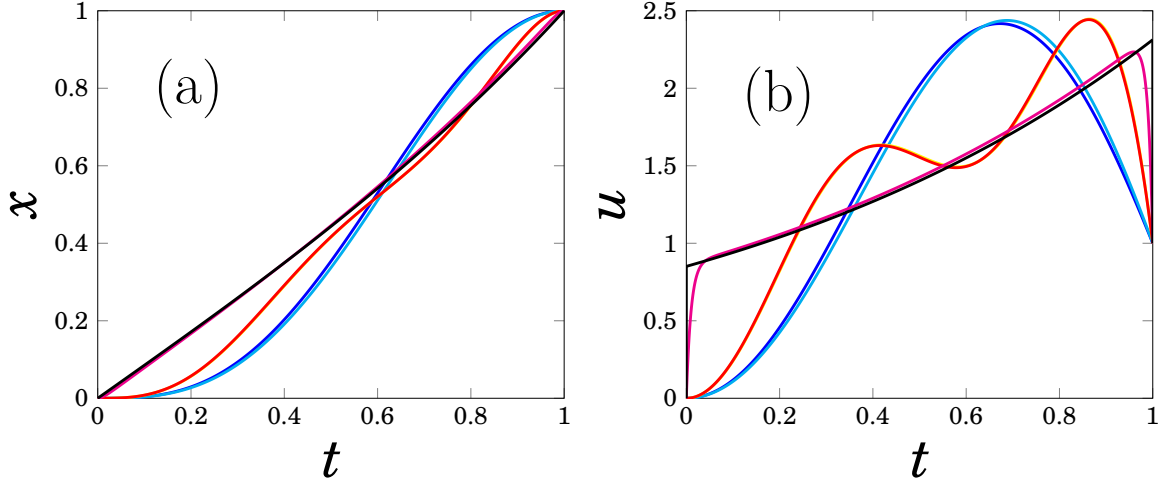


Figure 1.5: Same as Fig. 1.4 but for the trigonometric STA solutions. Dimensionless units are used.

1.4.3

Exponential Family of STA Solutions

In essence, the regular optimal solution given in Eq. (1.29) is a sum of real exponential functions. Inspired by this fact, we propose to consider the family of exponential functions:

$$(1.41) \quad x(t) = a e^t + b e^{-t} + c e^{kt} + d e^{-kt}$$

Here, the parameter k can be chosen according to the minimum energy requirement. We choose the coefficients a, b, c, d , complying with the boundary conditions $x(0) = 0, x(1) = 1, \dot{x}(0) = \dot{x}(1) = 0$. The following matrix equation then must be fulfilled:

$$B \vec{h} = \vec{s},$$

$$B = \begin{pmatrix} 1 & 1 & 1 & 1 \\ e & e^{-1} & e^k & e^{-k} \\ 1 & -1 & k & -k \\ e & -e^{-1} & k e^k & -k e^{-k} \end{pmatrix}, \quad \vec{h} = \begin{pmatrix} a \\ b \\ c \\ d \end{pmatrix}, \quad \vec{s} = \begin{pmatrix} 0 \\ 1 \\ 0 \\ 0 \end{pmatrix}$$

The coefficient vector \vec{h} can be expressed as:

$$(1.42) \quad \vec{h} = B^{-1} \vec{s},$$

$$(1.43) \quad B^{-1} = \frac{1}{\det B} \begin{pmatrix} |B|_{11} & |B|_{21} & |B|_{31} & |B|_{41} \\ |B|_{12} & |B|_{22} & |B|_{32} & |B|_{42} \\ |B|_{13} & |B|_{23} & |B|_{33} & |B|_{43} \\ |B|_{14} & |B|_{24} & |B|_{34} & |B|_{44} \end{pmatrix}.$$

$|B|_{11}, |B|_{12}, \dots$ are the cofactors of the B matrix, and $\det B$ is the determinant. \vec{h} can be rewritten in a simpler form:

$$\vec{h} = \frac{1}{\det B} \begin{pmatrix} |B|_{21} \\ |B|_{22} \\ |B|_{23} \\ |B|_{24} \end{pmatrix}.$$

The determinant and the cofactors are given in the following way:

$$(1.44) \quad \begin{aligned} \det B &= -(1-k)^2 e^{-(1+k)} - (1-k)^2 e^{1+k} + (1+k)^2 e^{-(1-k)} + (1+k)^2 e^{1-k} - 8k \\ |B|_{21} &= k \left(-2e^{-1} + (1+k)e^{-k} + (1-k)e^k \right) \\ |B|_{22} &= k \left(-2e + (1-k)e^{-k} + (1+k)e^k \right) \\ |B|_{23} &= k \left(\left(1 + \frac{1}{k}\right)e^{-1} + \left(1 - \frac{1}{k}\right)e - 2e^{-k} \right) \\ |B|_{24} &= k \left(\left(1 - \frac{1}{k}\right)e^{-1} + \left(1 + \frac{1}{k}\right)e - 2e^k \right), \end{aligned}$$

hence we derive the coefficients a, b, c, d :

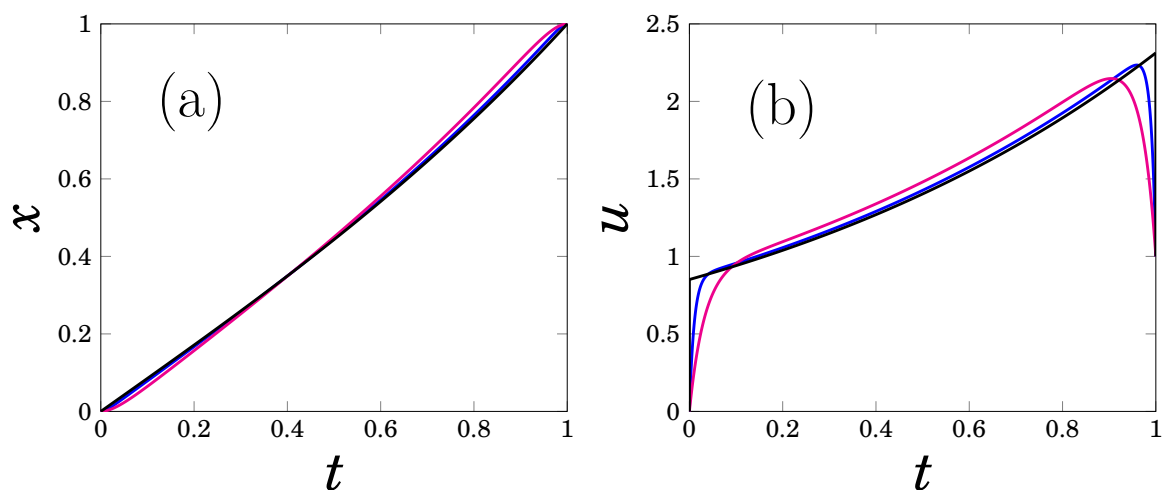


Figure 1.6: Comparison between the exponential STA and OCT solutions. Panels (a) and (b) represent respectively the time evolution of the trajectory x and of the control field u . The black and magenta lines correspond respectively to the singular and regular solutions. The parameters k and λ are set respectively to 100 and 10^{-3} . The exponential STA solution is plotted in blue. Dimensionless units are used.

$$\begin{aligned}
 a &= \frac{k \left(-2e^{-1} + (1+k)e^{-k} + (1-k)e^k \right)}{-(1-k)^2 e^{-(1+k)} - (1-k)^2 e^{1+k} + (1+k)^2 e^{-(1-k)} + (1+k)^2 e^{1-k} - 8k} \\
 b &= \frac{k \left(-2e + (1-k)e^{-k} + (1+k)e^k \right)}{-(1-k)^2 e^{-(1+k)} - (1-k)^2 e^{1+k} + (1+k)^2 e^{-(1-k)} + (1+k)^2 e^{1-k} - 8k} \\
 c &= \frac{k \left(\left(1 + \frac{1}{k}\right) e^{-1} + \left(1 - \frac{1}{k}\right) e - 2e^{-k} \right)}{-(1-k)^2 e^{-(1+k)} - (1-k)^2 e^{1+k} + (1+k)^2 e^{-(1-k)} + (1+k)^2 e^{1-k} - 8k} \\
 d &= \frac{k \left(\left(1 - \frac{1}{k}\right) e^{-1} + \left(1 + \frac{1}{k}\right) e - 2e^k \right)}{-(1-k)^2 e^{-(1+k)} - (1-k)^2 e^{1+k} + (1+k)^2 e^{-(1-k)} + (1+k)^2 e^{1-k} - 8k}
 \end{aligned}
 \tag{1.45}$$

In Fig. 1.6 the comparison of regular, singular and exponential solutions is illustrated. Later on, we will see that these solutions converge to each other as k goes to ∞ and λ approaches 0. The cost functional is computed numerically $\mathcal{C}^{Ex} \approx 1.325271$.

1.4.4

Exponential Solution vs Regular Solution

Here we are interested in comparing the exponential and regular solutions. Notice that Eqs. (1.29), (1.30) and (1.32), when $T = 1$, read:

$$x_R(t) = \mathbf{a} \left(x_1 e^{-t} + x_2 e^t + x_3 e^{-\frac{t}{\sqrt{\lambda}}} + x_4 e^{\frac{t}{\sqrt{\lambda}}} \right)
 \tag{1.46}$$

$$\mathbf{a} = \frac{\sqrt{\lambda}}{\left(1 - \sqrt{\lambda}\right)^2 e^{-\left(1 + \frac{1}{\sqrt{\lambda}}\right)} - \left(1 + \sqrt{\lambda}\right)^2 e^{-\left(1 - \frac{1}{\sqrt{\lambda}}\right)} - \left(1 + \sqrt{\lambda}\right)^2 e^{1 - \frac{1}{\sqrt{\lambda}}} + \left(1 - \sqrt{\lambda}\right)^2 e^{1 + \frac{1}{\sqrt{\lambda}}} + 8\sqrt{\lambda}}
 \tag{1.47}$$

$$x_1 = -y_1 = 2e - \left(1 - \frac{1}{\sqrt{\lambda}}\right) e^{-\frac{1}{\sqrt{\lambda}}} - \left(1 + \frac{1}{\sqrt{\lambda}}\right) e^{\frac{1}{\sqrt{\lambda}}}
 \tag{1.48}$$

$$x_2 = y_2 = 2e^{-1} - \left(1 + \frac{1}{\sqrt{\lambda}}\right) e^{-\frac{1}{\sqrt{\lambda}}} - \left(1 - \frac{1}{\sqrt{\lambda}}\right) e^{\frac{1}{\sqrt{\lambda}}}
 \tag{1.49}$$

$$x_3 = -\sqrt{\lambda} y_3 = -\left(1 - \sqrt{\lambda}\right) e^{-1} - \left(1 + \sqrt{\lambda}\right) e + 2e^{\frac{1}{\sqrt{\lambda}}}
 \tag{1.50}$$

$$x_4 = \sqrt{\lambda} y_4 = -\left(1 + \sqrt{\lambda}\right) e^{-1} - \left(1 - \sqrt{\lambda}\right) e + 2e^{-\frac{1}{\sqrt{\lambda}}},
 \tag{1.51}$$

where $x_R(t)$ is the regular solution. If $k \equiv \frac{1}{\sqrt{\lambda}}$, a connection between $\det \mathbf{B}$ and \mathbf{a} follows from Eqs. (1.44).

$$\det \mathbf{B} = -\frac{1}{\lambda} \left[\left(1 - \sqrt{\lambda}\right)^2 e^{-\left(1 + \frac{1}{\sqrt{\lambda}}\right)} - \left(1 + \sqrt{\lambda}\right)^2 e^{-\left(1 - \frac{1}{\sqrt{\lambda}}\right)} - \right.
 \tag{1.52}$$

$$\left. - \left(1 + \sqrt{\lambda}\right)^2 e^{\left(1 - \frac{1}{\sqrt{\lambda}}\right)} + \left(1 - \sqrt{\lambda}\right)^2 e^{\left(1 + \frac{1}{\sqrt{\lambda}}\right)} + 8\sqrt{\lambda} \right],$$

$$(1.53) \quad \frac{1}{\det B} = -\sqrt{\lambda} \mathbf{a}.$$

The coefficients a, b, c, d (see Eq. (1.45)) can be expressed by means of \mathbf{a} and the multipliers x_1, x_2, x_3, x_4 :

$$\begin{aligned} b &= -\frac{1}{\det B} \frac{1}{\sqrt{\lambda}} x_1 = \mathbf{a} x_1 \\ a &= -\frac{1}{\det B} \frac{1}{\sqrt{\lambda}} x_2 = \mathbf{a} x_2 \\ d &= -\frac{1}{\det B} \frac{1}{\sqrt{\lambda}} x_3 = \mathbf{a} x_3 \\ c &= -\frac{1}{\det B} \frac{1}{\sqrt{\lambda}} x_4 = \mathbf{a} x_4. \end{aligned}$$

With these new relations, the exponential solution (see Eq. (1.41)) can be rewritten in a new form:

$$(1.54) \quad \mathbf{x}^{\text{Ex}}(t) = \mathbf{a} \left(x_1 e^{-t} + x_2 e^t + x_3 e^{-\frac{t}{\sqrt{\lambda}}} + x_4 e^{\frac{t}{\sqrt{\lambda}}} \right).$$

From Eq. (1.46) and Eq. (1.54) we deduce that the regular and exponential solutions coincide:

$$(1.55) \quad \mathbf{x}^{\text{Ex}}(t) \equiv \mathbf{x}_R(t).$$

This statement is also visible numerically in Fig. 1.6, where $k = 100$ and $\lambda = 0.001$. In Fig. 1.7 the parameter k is increased and the parameter λ is decreased for a better illustration of the convergence of singular, regular and exponential solutions. Numerically, the maximum difference of exponential and regular solutions over time is almost zero for the values of k and λ respectively set to 100 and 10^{-4} .

$$\max \left| x_R(t) - x^{\text{Ex}}(t) \right| \approx 2 \times \text{eps},$$

where eps is the distance from 1.0 to the next larger double-precision number, and $\text{eps} \approx 2.2204 \times 10^{-16}$. In Table 1.1 all the numerical values for polynomial, trigonometric and exponential function families are summarized. Table 1.1 also gives the cost \mathcal{C} for different STA protocols and for the global optimal solution. As could be expected for polynomial and trigonometric expansions, the higher the order n is, the smaller \mathcal{C} is. We observe nevertheless that these solutions remain quite far from the global optimal solution, 6% and 12%, respectively, for the polynomial and trigonometric solutions at the order 6. The basis of real exponential functions seems to be more suited to the control problem since a small cost (1% larger than the optimal one) is achieved with the simple expansion proposed in Eq. (1.41).

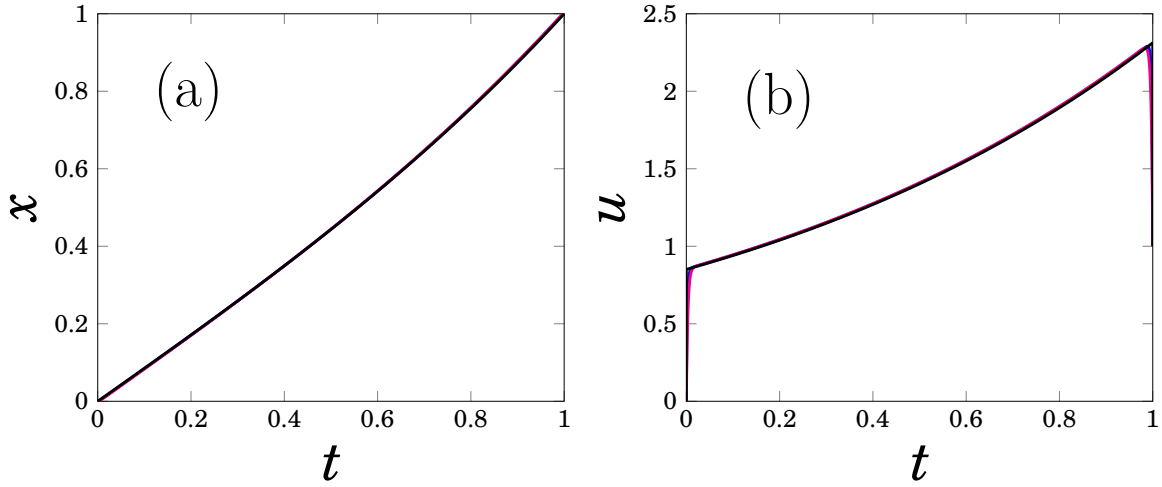


Figure 1.7: Same as Fig. 1.6. The parameters k and λ are set respectively to 500 and 10^{-5} . Dimensionless units are used.

	order	cost functional				
	n	\mathcal{C}	a	b	c	k
optimal solution	–	1.3130	–	–	–	–
polynomial	3	1.57143	–	–	–	–
	4	1.55797	–0.8076923	–	–	–
	5	1.40276	23.636752	–9.(7)	–	–
	6	1.39986	6.956942	5.627256	–5.135011	–
trigonometric	3	1.70041	–	–	–	–
	4	1.69843	0.0202	–	–	–
	5	1.48104	0.785988	–0.356639	–	–
	6	1.48099	1.0407	–0.312242	–0.0105136	–
exponential	–	1.325271	–	–	–	100

Table 1.1: Values of the coefficients a , b , and c for the polynomial and trigonometric expansions of the STA solution, value of the parameter k for the exponential STA solution and values of the costs \mathcal{C} for STA and singular OCT solutions.

Summary

- Reversely engineered polynomial, trigonometric and exponential STA solutions are obtained.
- The different STA solutions and the regular and singular solutions have been compared.
- We have shown that the exponential and regular solutions coincide.
- In Sec. 1.5, we explore the behavior of the regular solution and regularized cost in the limit when $\lambda \rightarrow 0$ with λ being the regularization parameter.

1.5 Limits

The aim of this section is to describe the behavior of the exponential or regular solution and regular cost for the values of the parameter λ in a neighborhood of 0. If everything has been done correctly, then the limit of the regular optimal solution and regular cost when λ approaches 0 must converge to the singular optimal solution and singular cost. Although, terms like $e^{\frac{T}{\sqrt{\lambda}} \sqrt{\lambda}}$, which diverge when the parameter λ is near 0, persist in the final physical results, we expect the sum of this kind of terms and thus the physical quantities to be convergent.

1.5.1 Exponential Solution vs Singular Solution

The physical insights, we have, lead us to the hypothesis that the limit of the exponential and regular solution, when $\lambda \rightarrow 0$, converges to the singular solution. Let us rigorously prove this statement. We recall:

$$\frac{1}{\alpha} = \sqrt{\lambda} \left[\left(1 - \frac{1}{\sqrt{\lambda}}\right)^2 e^{-(1+\frac{1}{\sqrt{\lambda}})T} - \left(1 + \frac{1}{\sqrt{\lambda}}\right)^2 e^{-(1-\frac{1}{\sqrt{\lambda}})T} - \left(1 + \frac{1}{\sqrt{\lambda}}\right)^2 e^{(1-\frac{1}{\sqrt{\lambda}})T} + \left(1 - \frac{1}{\sqrt{\lambda}}\right)^2 e^{(1+\frac{1}{\sqrt{\lambda}})T} \right] + 8.$$

The first and the third terms converge to zero, when $\lambda \rightarrow 0$:

$$\begin{aligned} \lim_{\lambda \rightarrow 0} \left[\sqrt{\lambda} \left(1 - \frac{1}{\sqrt{\lambda}}\right)^2 e^{-(1+\frac{1}{\sqrt{\lambda}})T} \right] &= \lim_{\lambda \rightarrow 0} \frac{\left(1 - \frac{1}{\sqrt{\lambda}}\right)^2}{\frac{1}{\sqrt{\lambda}} e^{(1+\frac{1}{\sqrt{\lambda}})T}} = 0 \\ \lim_{\lambda \rightarrow 0} \left[\sqrt{\lambda} \left(1 + \frac{1}{\sqrt{\lambda}}\right)^2 e^{(1-\frac{1}{\sqrt{\lambda}})T} \right] &= \lim_{\lambda \rightarrow 0} \frac{\left(1 + \frac{1}{\sqrt{\lambda}}\right)^2}{\frac{1}{\sqrt{\lambda}} e^{-(1-\frac{1}{\sqrt{\lambda}})T}} = 0. \end{aligned}$$

The second and the fourth terms diverge when $\lambda \rightarrow 0$:

$$\begin{aligned} \lim_{\lambda \rightarrow 0} \left[-\sqrt{\lambda} \left(1 + \frac{1}{\sqrt{\lambda}}\right)^2 e^{-(1-\frac{1}{\sqrt{\lambda}})T} \right] &= -\lim_{\lambda \rightarrow 0} \frac{\left(1 + \frac{1}{\sqrt{\lambda}}\right)^2 e^{-(1-\frac{1}{\sqrt{\lambda}})T}}{\frac{1}{\sqrt{\lambda}}} = -\infty. \\ \lim_{\lambda \rightarrow 0} \left[\sqrt{\lambda} \left(1 - \frac{1}{\sqrt{\lambda}}\right)^2 e^{(1+\frac{1}{\sqrt{\lambda}})T} \right] &= \lim_{\lambda \rightarrow 0} \frac{\left(1 - \frac{1}{\sqrt{\lambda}}\right)^2 e^{(1+\frac{1}{\sqrt{\lambda}})T}}{\frac{1}{\sqrt{\lambda}}} = +\infty \end{aligned} \tag{1.56}$$

In the end, we obtain an uncertainty:

$$\lim_{\lambda \rightarrow 0} \frac{1}{\alpha} = \infty - \infty.$$

In order to resolve this uncertainty, we have to combine the second and the fourth terms:

$$\begin{aligned} & \lim_{\lambda \rightarrow 0} \left\{ \sqrt{\lambda} \left(e^{\frac{T}{\sqrt{\lambda}}} \left[\left(1 - \frac{1}{\sqrt{\lambda}} \right)^2 e^T - \left(1 + \frac{1}{\sqrt{\lambda}} \right)^2 e^{-T} \right] \right) \right\} = \\ & = \lim_{\lambda \rightarrow 0} \left\{ \left(e^T - e^{-T} \right) \frac{e^{\frac{T}{\sqrt{\lambda}}}}{\frac{1}{\sqrt{\lambda}}} + \left[\frac{1}{\sqrt{\lambda}} \left(e^T - e^{-T} \right) - 2 \left(e^T + e^{-T} \right) \right] e^{\frac{T}{\sqrt{\lambda}}} \right\} = \\ & = +\infty + \infty = +\infty, \end{aligned}$$

hence it follows that:

$$\lim_{\lambda \rightarrow 0} \frac{1}{\mathbf{a}} = +\infty \Rightarrow \lim_{\lambda \rightarrow 0} \mathbf{a} = 0.$$

From Eqs. (1.47), (1.48), (1.49), (1.50) and (1.51), we obtain:

$$\begin{aligned} \lim_{\lambda \rightarrow 0} (\mathbf{a}x_i) &= 0 \times \infty; \quad i = 1 \dots 3 \\ \lim_{\lambda \rightarrow 0} (\mathbf{a}x_4) &= 0 \times \left(-e^{-T} - e^T \right) = 0. \end{aligned}$$

As one can deduce from Eq. (1.54), in order to calculate the limit of the exponential solution, when $\lambda \rightarrow 0$, we first have to resolve the following uncertainties:

$$\begin{cases} \lim_{\lambda \rightarrow 0} (\mathbf{a}x_1 e^{-t}) = 0 \times \infty \\ \lim_{\lambda \rightarrow 0} (\mathbf{a}x_2 e^t) = 0 \times \infty \\ \lim_{\lambda \rightarrow 0} (\mathbf{a}x_3 e^{-\frac{t}{\sqrt{\lambda}}}) = 0 \times \infty \\ \lim_{\lambda \rightarrow 0} (\mathbf{a}x_4 e^{\frac{t}{\sqrt{\lambda}}}) = 0 \times \infty. \end{cases}$$

Let us do that step by step. Using Eqs. (1.47), (1.48), (1.49), (1.50) and (1.51) we arrive at:

$$\begin{aligned} & \lim_{\lambda \rightarrow 0} [\mathbf{a}x_1] = \\ & = \lim_{\lambda \rightarrow 0} \left[\frac{2e^T \sqrt{\lambda} e^{-\frac{T}{\sqrt{\lambda}}} + (1 - \sqrt{\lambda}) e^{-\frac{2T}{\sqrt{\lambda}}} - (1 + \sqrt{\lambda})}{(1 - \sqrt{\lambda})^2 e^{-T} e^{-\frac{2T}{\sqrt{\lambda}}} - (1 + \sqrt{\lambda})^2 e^T e^{-\frac{2T}{\sqrt{\lambda}}} + 8\sqrt{\lambda} e^{-\frac{T}{\sqrt{\lambda}}} - (1 + \sqrt{\lambda})^2 e^{-T} + (1 - \sqrt{\lambda})^2 e^T} \right] = \\ & = -\frac{1}{e^T - e^{-T}} = -\frac{1}{2 \sinh T} \end{aligned}$$

$$\begin{aligned} & \lim_{\lambda \rightarrow 0} [\mathbf{a}x_2] = \\ & = \lim_{\lambda \rightarrow 0} \left[\frac{2e^{-T} \sqrt{\lambda} e^{-\frac{T}{\sqrt{\lambda}}} + (1 + \sqrt{\lambda}) e^{-\frac{2T}{\sqrt{\lambda}}} + (1 - \sqrt{\lambda})}{(1 - \sqrt{\lambda})^2 e^{-T} e^{-\frac{2T}{\sqrt{\lambda}}} - (1 + \sqrt{\lambda})^2 e^T e^{-\frac{2T}{\sqrt{\lambda}}} + 8\sqrt{\lambda} e^{-\frac{T}{\sqrt{\lambda}}} - (1 + \sqrt{\lambda})^2 e^{-T} + (1 - \sqrt{\lambda})^2 e^T} \right] = \\ & = \frac{1}{e^T - e^{-T}} = \frac{1}{2 \sinh T} \end{aligned}$$

$$\begin{aligned}
 & \lim_{\lambda \rightarrow 0} \left[\alpha x_3 e^{-\frac{t}{\sqrt{\lambda}}} \right] = \\
 & = \lim_{\lambda \rightarrow 0} \left[\frac{-\sqrt{\lambda} \left((1 - \sqrt{\lambda}) e^{-T} e^{-\frac{T}{\sqrt{\lambda}}} + (1 + \sqrt{\lambda}) e^T e^{-\frac{T}{\sqrt{\lambda}}} - 2 \right) e^{-\frac{t}{\sqrt{\lambda}}}}{\left((1 - \sqrt{\lambda})^2 e^{-T} e^{-\frac{2T}{\sqrt{\lambda}}} - (1 + \sqrt{\lambda})^2 e^T e^{-\frac{2T}{\sqrt{\lambda}}} + 8\sqrt{\lambda} e^{-\frac{T}{\sqrt{\lambda}}} - (1 + \sqrt{\lambda})^2 e^{-T} + (1 - \sqrt{\lambda})^2 e^T \right)} \right] = \\
 & = \frac{0}{e^T - e^{-T}} = 0
 \end{aligned}$$

$$\begin{aligned}
 & \lim_{\lambda \rightarrow 0} \left[\alpha x_4 e^{\frac{t}{\sqrt{\lambda}}} \right] = \\
 & = \lim_{\lambda \rightarrow 0} \left[\frac{-\sqrt{\lambda} e^{-\frac{(T-t)}{\sqrt{\lambda}}} \left((1 + \sqrt{\lambda}) e^{-T} + (1 - \sqrt{\lambda}) e^T - 2 e^{-\frac{T}{\sqrt{\lambda}}} \right)}{\left((1 - \sqrt{\lambda})^2 e^{-T} e^{-\frac{2T}{\sqrt{\lambda}}} - (1 + \sqrt{\lambda})^2 e^T e^{-\frac{2T}{\sqrt{\lambda}}} + 8\sqrt{\lambda} e^{-\frac{T}{\sqrt{\lambda}}} - (1 + \sqrt{\lambda})^2 e^{-T} + (1 - \sqrt{\lambda})^2 e^T \right)} \right] = \\
 & = \frac{0}{e^T - e^{-T}} = 0,
 \end{aligned}$$

where $0 \leq t \leq T$. These relations with Eq. (1.54) finally yield:

$$\lim_{\lambda \rightarrow 0} x^{\text{Ex}}(t) = \frac{1}{2 \sinh T} (e^t - e^{-t}) = \frac{\sinh t}{\sinh T} = x_s(t),$$

where $x_s(t)$ is the singular solution. The regular and exponential solutions coincide, thus:

$$(1.57) \quad \lim_{\lambda \rightarrow 0} x^{\text{Ex}}(t) = \lim_{\lambda \rightarrow 0} x_R(t) = x_s(t),$$

just as we guessed from our physical insights.

1.5.2 Regularized Cost vs Singular Cost

From the physical insights, we could guess that the regularized cost converges to the singular cost when $\lambda \rightarrow 0$. Let us rigorously prove this statement. Limits of all terms on the right side of Eq. (1.35), when λ approaches 0, are calculated one by one:

$$\begin{aligned}
 & \lim_{\lambda \rightarrow 0} \left[\alpha^2 G_1 \right] = \\
 & = \lim_{\lambda \rightarrow 0} \left[\frac{2 \left(-2e^T \sqrt{\lambda} e^{-\frac{T}{\sqrt{\lambda}}} - (1 - \sqrt{\lambda}) e^{-\frac{2T}{\sqrt{\lambda}}} + (1 + \sqrt{\lambda}) \right)^2}{\left[\left((1 - \sqrt{\lambda})^2 e^{-T} e^{-\frac{2T}{\sqrt{\lambda}}} - (1 + \sqrt{\lambda})^2 e^{-T} - (1 + \sqrt{\lambda})^2 e^T e^{-\frac{2T}{\sqrt{\lambda}}} + (1 - \sqrt{\lambda})^2 e^T + 8\sqrt{\lambda} e^{-\frac{T}{\sqrt{\lambda}}} \right)^2 \right]} \right] = \\
 & = \frac{2}{(e^T - e^{-T})^2} = \frac{1}{2 \sinh^2 T}
 \end{aligned}$$

$$\begin{aligned}
& \lim_{\lambda \rightarrow 0} \left[\alpha^2 G_2 \right] = \\
& = \lim_{\lambda \rightarrow 0} \left[\frac{2(1+2\lambda) \left(2e^{-T} \sqrt{\lambda} e^{-\frac{T}{\sqrt{\lambda}}} - (1+\sqrt{\lambda}) e^{-\frac{2T}{\sqrt{\lambda}}} + (1-\sqrt{\lambda}) \right)^2}{\left[(1-\sqrt{\lambda})^2 e^{-T} e^{-\frac{2T}{\sqrt{\lambda}}} - (1+\sqrt{\lambda})^2 e^{-T} - (1+\sqrt{\lambda})^2 e^T e^{-\frac{2T}{\sqrt{\lambda}}} + (1-\sqrt{\lambda})^2 e^T + 8\sqrt{\lambda} e^{-\frac{T}{\sqrt{\lambda}}} \right]^2} \right] = \\
& = \frac{2}{(e^T - e^{-T})^2} = \frac{1}{2 \sinh^2 T}
\end{aligned}$$

$$\begin{aligned}
& \lim_{\lambda \rightarrow 0} \left[\alpha^2 \sqrt{\lambda} \left(e^{-\frac{2T}{\sqrt{\lambda}}} - 1 \right) G_3 \right] = \\
& = \lim_{\lambda \rightarrow 0} \left[\frac{2\sqrt{\lambda} (1-\sqrt{\lambda} + \lambda) \left(e^{-\frac{2T}{\sqrt{\lambda}}} - 1 \right) \left((1-\sqrt{\lambda}) e^{-T} e^{-\frac{T}{\sqrt{\lambda}}} + (1+\sqrt{\lambda}) e^T e^{-\frac{T}{\sqrt{\lambda}}} - 2 \right)^2}{\left[(1-\sqrt{\lambda})^2 e^{-T} e^{-\frac{2T}{\sqrt{\lambda}}} - (1+\sqrt{\lambda})^2 e^{-T} - (1+\sqrt{\lambda})^2 e^T e^{-\frac{2T}{\sqrt{\lambda}}} + (1-\sqrt{\lambda})^2 e^T + 8\sqrt{\lambda} e^{-\frac{T}{\sqrt{\lambda}}} \right]^2} \right] = \\
& = \frac{0}{(e^T - e^{-T})^2} = 0
\end{aligned}$$

$$\begin{aligned}
& \lim_{\lambda \rightarrow 0} \left[\alpha^2 \sqrt{\lambda} \left(e^{\frac{2T}{\sqrt{\lambda}}} - 1 \right) G_4 \right] = \\
& = \lim_{\lambda \rightarrow 0} \left[\frac{-2\sqrt{\lambda} (1+\sqrt{\lambda} + \lambda) \left(e^{\frac{2T}{\sqrt{\lambda}}} - 1 \right) \left(-(1+\sqrt{\lambda}) e^{-T} - (1-\sqrt{\lambda}) e^T + 2e^{-\frac{T}{\sqrt{\lambda}}} \right)^2}{\left[(1-\sqrt{\lambda})^2 e^{-T} e^{-\frac{2T}{\sqrt{\lambda}}} - (1+\sqrt{\lambda})^2 e^{-T} - (1+\sqrt{\lambda})^2 e^T e^{-\frac{2T}{\sqrt{\lambda}}} + (1-\sqrt{\lambda})^2 e^T + 8\sqrt{\lambda} e^{-\frac{T}{\sqrt{\lambda}}} \right]^2} \right] = \\
& = \frac{0}{(e^T - e^{-T})^2} = 0
\end{aligned}$$

$$\begin{aligned}
& \lim_{\lambda \rightarrow 0} \left[\alpha^2 \frac{\sqrt{\lambda}}{1+\sqrt{\lambda}} \left(e^{-(1+\frac{1}{\sqrt{\lambda}})T} - 1 \right) G_{13} \right] = \\
& = \lim_{\lambda \rightarrow 0} \left[\frac{\sqrt{\lambda} \left(e^{-(1+\frac{1}{\sqrt{\lambda}})T} - 1 \right) \left(-2\sqrt{\lambda} e^T e^{-\frac{T}{\sqrt{\lambda}}} - (1-\sqrt{\lambda}) e^{-\frac{2T}{\sqrt{\lambda}}} + (1+\sqrt{\lambda}) \right)}{\left[(1-\sqrt{\lambda})^2 e^{-T} e^{-\frac{2T}{\sqrt{\lambda}}} - (1+\sqrt{\lambda})^2 e^{-T} - (1+\sqrt{\lambda})^2 e^T e^{-\frac{2T}{\sqrt{\lambda}}} + (1-\sqrt{\lambda})^2 e^T + 8\sqrt{\lambda} e^{-\frac{T}{\sqrt{\lambda}}} \right]^2} \times \right. \\
& \left. \times \left((1-\sqrt{\lambda}) e^{-T} e^{-\frac{T}{\sqrt{\lambda}}} + (1+\sqrt{\lambda}) e^T e^{-\frac{T}{\sqrt{\lambda}}} - 2 \right) \right] = \frac{0}{(e^T - e^{-T})^2} = 0
\end{aligned}$$

$$\begin{aligned}
 & \lim_{\lambda \rightarrow 0} \left[\alpha^2 \frac{\sqrt{\lambda}}{1 - \sqrt{\lambda}} \left(e^{-(1 - \frac{1}{\sqrt{\lambda}})T} - 1 \right) G_{14} \right] = \\
 & = \lim_{\lambda \rightarrow 0} \left[\frac{\sqrt{\lambda} \left(e^{-T} - e^{-\frac{T}{\sqrt{\lambda}}} \right) \left(-2\sqrt{\lambda} e^T e^{-\frac{T}{\sqrt{\lambda}}} - (1 - \sqrt{\lambda}) e^{-\frac{2T}{\sqrt{\lambda}}} + (1 + \sqrt{\lambda}) \right)}{\left[(1 - \sqrt{\lambda})^2 e^{-T} e^{-\frac{2T}{\sqrt{\lambda}}} - (1 + \sqrt{\lambda})^2 e^{-T} - (1 + \sqrt{\lambda})^2 e^T e^{-\frac{2T}{\sqrt{\lambda}}} + (1 - \sqrt{\lambda})^2 e^T + 8\sqrt{\lambda} e^{-\frac{T}{\sqrt{\lambda}}} \right]^2} \times \right. \\
 & \left. \times \left(-(1 + \sqrt{\lambda}) e^{-T} - (1 - \sqrt{\lambda}) e^T + 2e^{-\frac{T}{\sqrt{\lambda}}} \right) \right] = \frac{0}{(e^T - e^{-T})^2} = 0
 \end{aligned}$$

$$\begin{aligned}
 & \lim_{\lambda \rightarrow 0} \left[\alpha^2 \frac{\sqrt{\lambda}}{1 - \sqrt{\lambda}} \left(e^{(1 - \frac{1}{\sqrt{\lambda}})T} - 1 \right) G_{23} \right] = \\
 & = \lim_{\lambda \rightarrow 0} \left[\frac{\sqrt{\lambda} \left(e^T e^{-\frac{T}{\sqrt{\lambda}}} - 1 \right) \left(1 - 2\sqrt{\lambda} \right) \left(2\sqrt{\lambda} e^{-T} e^{-\frac{T}{\sqrt{\lambda}}} - (1 + \sqrt{\lambda}) e^{-\frac{2T}{\sqrt{\lambda}}} + (1 - \sqrt{\lambda}) \right)}{\left[(1 - \sqrt{\lambda})^2 e^{-T} e^{-\frac{2T}{\sqrt{\lambda}}} - (1 + \sqrt{\lambda})^2 e^{-T} - (1 + \sqrt{\lambda})^2 e^T e^{-\frac{2T}{\sqrt{\lambda}}} + (1 - \sqrt{\lambda})^2 e^T + 8\sqrt{\lambda} e^{-\frac{T}{\sqrt{\lambda}}} \right]^2} \times \right. \\
 & \left. \times \left((1 - \sqrt{\lambda}) e^{-T} e^{-\frac{T}{\sqrt{\lambda}}} + (1 + \sqrt{\lambda}) e^T e^{-\frac{T}{\sqrt{\lambda}}} - 2 \right) \right] = \frac{0}{(e^T - e^{-T})^2} = 0
 \end{aligned}$$

$$\begin{aligned}
 & \lim_{\lambda \rightarrow 0} \left[\alpha^2 \frac{\sqrt{\lambda}}{1 + \sqrt{\lambda}} \left(e^{(1 + \frac{1}{\sqrt{\lambda}})T} - 1 \right) G_{24} \right] = \\
 & = \lim_{\lambda \rightarrow 0} \left[\frac{\sqrt{\lambda} \left(e^T - e^{-\frac{T}{\sqrt{\lambda}}} \right) \left(1 + 2\sqrt{\lambda} \right) \left(2\sqrt{\lambda} e^{-T} e^{-\frac{T}{\sqrt{\lambda}}} - (1 + \sqrt{\lambda}) e^{-\frac{2T}{\sqrt{\lambda}}} + (1 - \sqrt{\lambda}) \right)}{\left[(1 - \sqrt{\lambda})^2 e^{-T} e^{-\frac{2T}{\sqrt{\lambda}}} - (1 + \sqrt{\lambda})^2 e^{-T} - (1 + \sqrt{\lambda})^2 e^T e^{-\frac{2T}{\sqrt{\lambda}}} + (1 - \sqrt{\lambda})^2 e^T + 8\sqrt{\lambda} e^{-\frac{T}{\sqrt{\lambda}}} \right]^2} \times \right. \\
 & \left. \times \left(-(1 + \sqrt{\lambda}) e^{-T} - (1 - \sqrt{\lambda}) e^T + 2e^{-\frac{T}{\sqrt{\lambda}}} \right) \right] = \frac{0}{(e^T - e^{-T})^2} = 0.
 \end{aligned}$$

The limit of the regular cost \mathcal{C}_R (see Eq. (1.35)) as λ approaches 0 is additive:

$$\begin{aligned}
 \lim_{\lambda \rightarrow 0} \mathcal{C}_R &= -\frac{1}{2} \left(e^{-2T} - 1 \right) \frac{1}{2 \sinh^2 T} + \frac{1}{2} \left(e^{2T} - 1 \right) \frac{1}{2 \sinh^2 T} = \frac{1}{4 \sinh^2 T} \left(e^{2T} - e^{-2T} \right) = \\
 &= \frac{\sinh T \cosh T}{\sinh^2 T} = \coth T = \mathcal{C}_s.
 \end{aligned}$$

We conclude that the regular cost, when $\lambda \rightarrow 0$, converges to the singular cost \mathcal{C}_s just as we expected.

1.5.3

Limit of the Derivative of Regularized Cost

As we mentioned before, because of singularities we are not able to plot the dependency of the regularized cost on the regularization parameter λ for $\lambda \ll 1$. Here, we will make that point clearer and find out the direction of the curvature when $\lambda \rightarrow 0$.

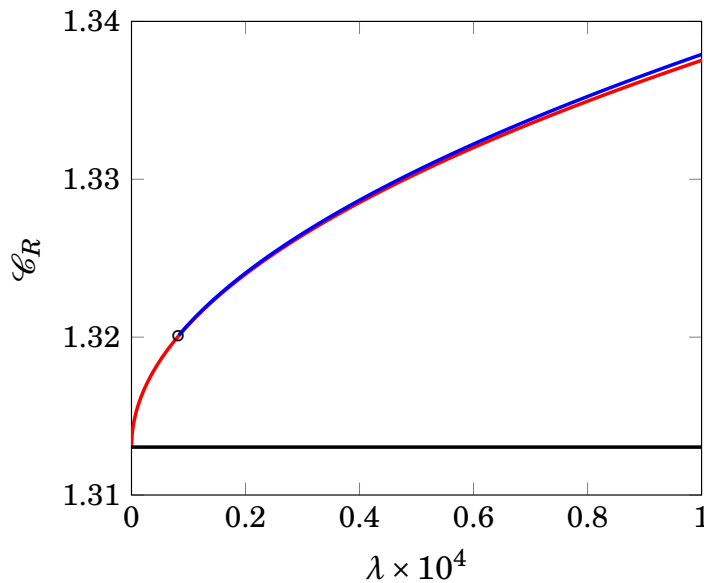


Figure 1.8: Plot of the regularized cost functional \mathcal{C}_R as a function of the parameter λ (solid blue or dark gray line). The solid horizontal black line indicates the value of the minimum cost functional $\coth 1$ which corresponds to the singular solution. The solid red or light gray line is a square-root fit $\coth 1 + \sqrt{6\lambda}$ of \mathcal{C}_R around $\lambda = 0$. The black circle indicates the minimum value $\lambda = 8.2 \times 10^{-6}$ for which \mathcal{C}_R has been numerically computed. Dimensionless units are used.

Although the analytic expression of the derivative of the regular cost is too long to be given here or even to be considered in the scope of this research, it is quite possible to treat the problem numerically. Mathematical intuition led us to a guess, which was later numerically confirmed, that the derivative of the regularized cost when $\lambda \rightarrow 0$ diverges approximately with the speed $1/\sqrt{\lambda}$. In other words, the regularized cost behaves as $\sqrt{\lambda}$ over the values of λ near 0. As a part of our numerical computations, the function "Limit" in the environment of "Mathematica" was also used to confirm our guess. What we claim is illustrated in Fig. 1.8 where the dependencies of the regularized cost \mathcal{C}_R and fitting function $\coth 1 + \sqrt{6\lambda}$ on the parameter λ are plotted.

Summary

- We have rigorously proven that the exponential or regular solution coincides with the singular one in the limit when $\lambda \rightarrow 0$, where λ is the regularization parameter.
- We have also proven that the regularized cost converges toward the singular cost when λ approaches 0.
- The derivative of the regularized cost has been shown to diverge with the rate $\simeq 1/\sqrt{\lambda}$ when $\lambda \rightarrow 0$.
- In Sec. 1.6 we generalize our approach to the case of higher order boundary constraints.

1.6**Generalization to Higher Orders**

All we have done above can be generalized to the case of constraints including higher order derivatives. In this general case, the problem is to steer the system between the initial $\mathbf{x}(0) = \mathbf{0}$ and target states $\mathbf{x}(T) = \mathbf{1}$ under constraints including higher, up to n th order derivatives $\dot{\mathbf{x}}(0) = \ddot{\mathbf{x}}(0) = \dots = \mathbf{x}^{(n)}(0) = \mathbf{0}$ and $\dot{\mathbf{x}}(T) = \ddot{\mathbf{x}}(T) = \dots = \mathbf{x}^{(n)}(T) = \mathbf{0}$. In the following, we first introduce the basics of Linear Quadratic Optimal Control Theory (LQOCT) [75], then we apply this theory to the particular model we have discussed above.

1.6.1**Generalized Problem**

The model is described by a simple linear differential equation, and LQOCT is fully applicable (see Sec. 1.6.3):

$$(1.58) \quad \dot{\mathbf{x}} + \mathbf{x} = \mathbf{u}$$

The problem is to find the optimal field to steer the system from the state $\mathbf{x}(0) = \mathbf{0}$ to the state $\mathbf{x}(1) = \mathbf{1}$, while insuring that all the derivatives up to n th order vanish at the initial and final times: $\dot{\mathbf{x}}(0) = \dots = \mathbf{x}^{(n)}(0) = \mathbf{0}$ and $\dot{\mathbf{x}}(1) = \dots = \mathbf{x}^{(n)}(1) = \mathbf{0}$. For the optimization procedure we enlarge the space of variables by introducing extra coordinates $\mathbf{x}_1 = \dot{\mathbf{x}}$, $\mathbf{x}_2 = \ddot{\mathbf{x}}$, \dots , $\mathbf{x}_n = \mathbf{x}^{(n)}$ and $\mathbf{z}_0 = \mathbf{u}$, $\mathbf{z}_1 = \dot{\mathbf{u}}$, $\mathbf{z}_2 = \ddot{\mathbf{u}}$, \dots , $\mathbf{z}_{n-1} = \mathbf{u}^{(n-1)}$. This way we replace the boundary conditions on the derivatives by conditions on the state of the system. The new control is $\mathbf{v} = \mathbf{u}^{(n)}$. The dimension of the state of the system is $n + 1$, $(\mathbf{x}_n, \mathbf{z}_{n-1}, \dots, \mathbf{z}_1, \mathbf{z}_0)$. The differential system to control can be

expressed as:

$$(1.59) \quad \begin{cases} \dot{x}_n + x_n = v \\ \dot{z}_{n-1} = v \\ \dot{z}_{n-2} = z_{n-1} \\ \dots \\ \dot{z}_k = z_{k+1} \\ \dots \\ \dot{z}_1 = z_2 \\ \dot{z}_0 = z_1, \end{cases}$$

with the boundary conditions $x_n(0) = x_n(1) = 0$, $z_{n-1}(0) = z_{n-1}(1) = 0$, \dots , $z_1(0) = z_1(1) = 0$, $z_0(0) = 0$, $z_0(1) = 1$. The cost functional in the regular case can be written as:

$$(1.60) \quad \mathcal{C}_R = \int_0^T [(z_0 - x_1)^2 + x_1^2 + \lambda v^2] dt$$

with

$$(1.61) \quad x_1 = z_1 - z_2 + z_3 + \dots + (-1)^n z_{n-1} - (-1)^n x_n$$

Before the derivation of the regular control let us show that the singular control is the same for all orders. The singular case is obtained in the limit when $\lambda \rightarrow 0$. Pontryagin's singular Hamiltonian can be expressed as:

$$H_S = p_n(v - x_n) + p_{n-1}v + p_{n-2}z_{n-1} + \dots + p_0z_1 - \frac{1}{2} [(z_0 - x_1)^2 + x_1^2],$$

where the adjoint states p_n, p_{n-1}, \dots, p_1 and p_0 are associated respectively to x_n, z_{n-1}, \dots, z_1 and z_0 . Using H_S , and Hamilton's equation $\dot{p} = -\frac{\partial H_s}{\partial x}$, where x is the state, and p is the corresponding adjoint state, we also deduce the differential equations governing the dynamics of the adjoint states:

$$(1.62) \quad \begin{cases} \dot{p}_n = p_n + (-1)^{n+1}(2x_1 - z_0) \\ \dot{p}_k = -p_{k-1} + (-1)^{k+1}(2x_1 - z_0), \quad k = n-1, \dots, 1 \\ \dot{p}_0 = z_0 - x_1 \end{cases}$$

The singular control satisfies **PMP** $\frac{\partial H_s}{\partial v} = 0$ which leads to $p_n + p_{n-1} = 0$. Since this statement is valid in a non-zero time interval, the time derivatives of $p_n + p_{n-1}$ are equal to 0. We therefore obtain a series of constraints given by:

$$\begin{cases} p_n - (-1)^{n-k} p_k = 0, \quad k = n-1, \dots, 0 \\ p_n + (-1)^{n+1} x_1 = 0 \\ z_1 = z_0 \end{cases}$$

where each relation is obtained by derivating with respect to time the preceding one. From $z_1 = z_0$ and Eqs. (1.59), we deduce that $z_0 = z_1 = z_2 = \dots = z_{n-2} = z_{n-1} = v$ for the singular trajectory. From Eqs. (1.59) we deduce that $\dot{z}_0 = z_0$. Substituting the solution of this equation $z_0(t) = Z e^t$ into the first inhomogeneous first-order differential equation of Eqs. (1.59) $\dot{x}_n + x_n = v$ we obtain the singular trajectories:

$$\begin{cases} z_0(t) = z_1(t) = \dots = z_{n-1}(t) = v(t) = Z e^t \\ x_n(t) = Y e^{-t} + Z \sinh t \end{cases}$$

In the same way, as it has been done in Sec. 1.3.1, we can show that the control field has a discontinuity at initial and final times. In other words, it is a B—S—B pulse, where B means bang and S singular pulses. Otherwise, we can not sew the boundary conditions to the trajectory. For the constants Z and Y we obtain the same expressions as in Sec. 1.3.1. More importantly, the singular control is indeed the same for any order n .

1.6.2 Regular Control

In this section we find the regular control by using LQOCT. Pontryagin's regularized Hamiltonian has the form:

$$(1.63) \quad H_R = p_n(v - x_n) + p_{n-1}v + p_{n-2}z_{n-1} + \dots + p_0z_1 - \frac{1}{2} \left[(z_0 - x_1)^2 + x_1^2 + \lambda v^2 \right].$$

Pay attention to the fact that $H_R = H_s - \frac{1}{2}\lambda v^2$. Since the dynamics of the adjoint state follows the Hamiltonian equation $\dot{p}_i = -\frac{\partial H}{\partial x_i}$, we arrive at Eqs. (1.62). The regular control satisfies PMP $\frac{\partial H_R}{\partial v} = 0$ which leads to $v = \frac{1}{\lambda}(p_n + p_{n-1})$. We rewrite Eqs. (1.59) in a matrix form:

$$(1.64) \quad \frac{d}{dt} \begin{pmatrix} x_n \\ z_{n-1} \\ z_{n-2} \\ \vdots \\ z_1 \\ z_0 \end{pmatrix} = \begin{pmatrix} -1 & 0 & \dots & 0 & 0 \\ 0 & 0 & \dots & 0 & 0 \\ \hline 0 & & & & 0 \\ \vdots & & \mathbf{I}_{n-1} & & \vdots \\ 0 & & & & 0 \end{pmatrix} \times \begin{pmatrix} x_n \\ z_{n-1} \\ z_{n-2} \\ \vdots \\ z_1 \\ z_0 \end{pmatrix} + \begin{pmatrix} 1 \\ 1 \\ 0 \\ \vdots \\ 0 \\ 0 \end{pmatrix} v.$$

Comparing Eq. (1.64) with Eq. (1.71) we observe:

$$(1.65) \quad x = \begin{pmatrix} x_n \\ z_{n-1} \\ z_{n-2} \\ \vdots \\ z_1 \\ z_0 \end{pmatrix}, \quad A = \begin{pmatrix} -1 & 0 & \dots & 0 & 0 \\ 0 & 0 & \dots & 0 & 0 \\ \hline 0 & & & & 0 \\ \vdots & & \mathbf{I}_{n-1} & & \vdots \\ 0 & & & & 0 \end{pmatrix}, \quad B = \begin{pmatrix} 1 \\ 1 \\ 0 \\ \vdots \\ 0 \\ 0 \end{pmatrix},$$

where \mathbf{I}_{n-1} is an identity matrix of size $n-1$. Then substituting Eq. (1.61) into Eqs. (1.62) we obtain:

$$(1.66) \quad \begin{cases} \dot{p}_n = p_n - 2(-1)^{2n+1}x_n + 2(-1)^{2n+1}z_{n-1} + \cdots + 2(-1)^{n+1}z_3 - \\ - 2(-1)^{n+1}z_2 + 2(-1)^{n+1}z_1 - (-1)^{n+1}z_0; \\ \vdots \\ \dot{p}_k = -p_{k-1} - 2(-1)^{n+k+1}x_n + 2(-1)^{n+k+1}z_{n-1} + \cdots + 2(-1)^{k+1}z_3 - \\ - 2(-1)^{k+1}z_2 + 2(-1)^{k+1}z_1 - (-1)^{k+1}z_0; \quad k = n-1, \dots, 1 \\ \vdots \\ \dot{p}_0 = (-1)^n x_n - (-1)^n z_{n-1} + \cdots - z_3 + z_2 - z_1 + z_0, \end{cases}$$

where $\mathbf{p} = (p_n, p_{n-1}, \dots, p_1, p_0)^\top$ is the adjoint state. Comparing Eq. (1.66) with Eq. (1.75), we find out:

$$(1.67) \quad W = \begin{pmatrix} 2(-1)^{2n} & \cdots & 2(-1)^{n+k} & \cdots & (-1)^n \\ \vdots & \ddots & \vdots & \ddots & \vdots \\ 2(-1)^{n+k} & \cdots & 2(-1)^{2k} & \cdots & (-1)^k \\ \vdots & \ddots & \vdots & \ddots & \vdots \\ (-1)^n & \cdots & (-1)^k & \cdots & (-1)^0 \end{pmatrix}$$

Comparing Eq. (1.60) and Eq. (1.72), we deduce that $U = \lambda$. Since we have the expressions for matrices \mathbf{A} , \mathbf{B} , \mathbf{U} and \mathbf{W} , we also have the block matrix \mathbf{M} . We recall that $\dot{x} + x = u$ and hence $x = z_0 - x_1$. On the other hand $x_1 = z_1 - z_2 + z_3 + \cdots + (-1)^n z_{n-1} - (-1)^n x_n$, thus according to Eq. (1.84) the state x can be expressed in the following way:

$$(1.68) \quad x = \sum_{j=1}^{2n} a_j e^{\lambda_j t},$$

where the coefficients a_j are defined from the boundary conditions. Equation (1.85) holds true with \mathbf{C}_i being a vector of coefficients a_j and $\mathbf{V}_i = (0, 1, 0, \dots, 0)^\top$. Numerically inverting the matrix \mathbf{L} one can find the coefficients a_j . In a second step, by taking the derivatives of x we can calculate the regular optimal control in the initial and modified coordinates:

$$(1.69) \quad u = \dot{x} + x = \sum_{j=1}^{2n} a_j (1 + \lambda_j) e^{\lambda_j t}$$

$$(1.70) \quad v = \dot{x}_n + x_n = \sum_{j=1}^{2n} a_j \lambda_j^n (1 + \lambda_j) e^{\lambda_j t}.$$

The simulations have been done according to Eq. (1.69) and Eq. (1.70).

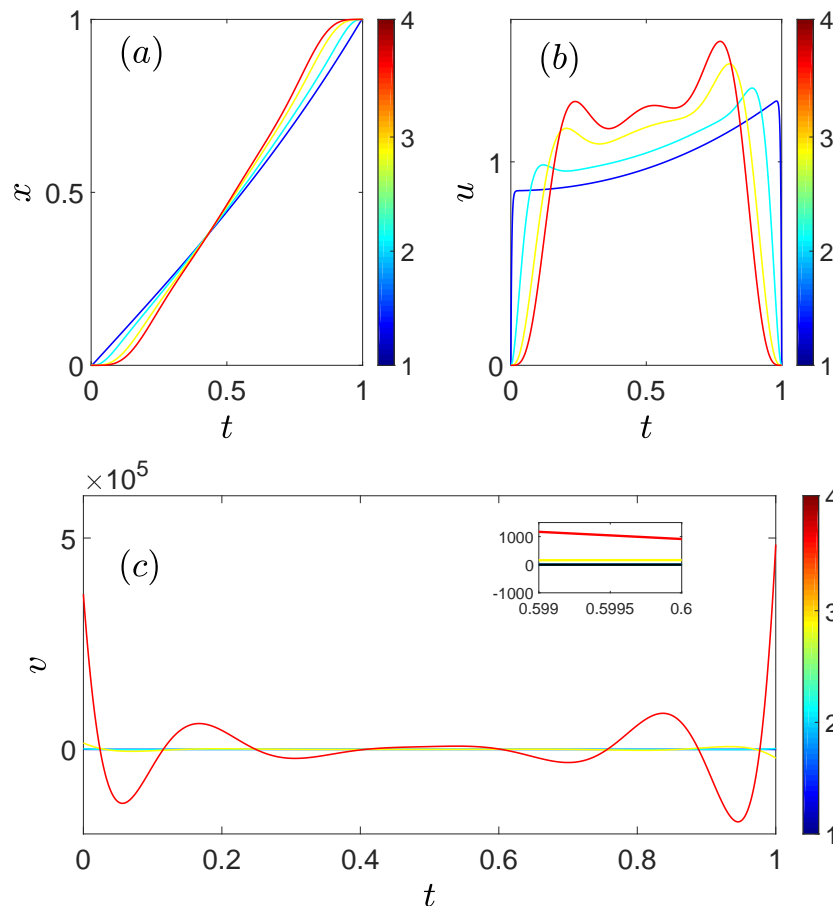


Figure 1.9: Plot of the time evolution of the optimal trajectories (a) and of the regular optimal controls u (b) and v (c). The colorbar indicates the value of the order n . The parameter λ is set to 10^{-5} , 5×10^{-7} , 5×10^{-9} and 10^{-11} respectively for $n = 1, 2, 3$ and 4 . The black line in the small inset represents the singular optimal solution. Dimensionless units are used.

The analysis of the generalized problem is summarized in Fig. 1.9. Notice that in the middle of the time interval, the control field is singular independently of the order n .

1.6.3

Linear Quadratic Optimal Control Theory

This problem could also be solved by applying the LQOCT. The control problem is given by the dynamical equation:

$$(1.71) \quad \dot{x} = Ax + Bu,$$

where $x \in \mathbb{R}^n$ is the state of the system and $u \in \mathbb{R}^m$ is the control field, $A \in M_n(\mathbb{R})$ and $B \in M_{nm}(\mathbb{R})$ are two constant matrices. The linear dynamics modeled as in Eq. (1.71) is ensemble controllable [76, 77]. Starting from the state $x(0) = x_0$, the goal is to reach the state $x(T) = x_f$ at time T under the additional constraints $\dot{x}(0) = \dot{x}_0$, $\ddot{x}(0) = \ddot{x}_0, \dots, x^{(n-1)}(0) = x_0^{(n-1)}$ and $\dot{x}(T) = \dot{x}_f$, $\ddot{x}(T) = \ddot{x}_f, \dots$,

$x^{(n-1)}(T) = x_f^{(n-1)}$ while minimizing the cost functional \mathcal{C} defined by:

$$(1.72) \quad \mathcal{C} = \int_0^T [x^T W x + u^T U u] dt,$$

where $W \in M_n(\mathbb{R})$ and $U \in M_m(\mathbb{R})$ are two constant symmetric matrices which are respectively positive and positive definite. The Pontryagin Hamiltonian H_p of the system can be written as:

$$(1.73) \quad H_p = p^T A x + p^T B u - \frac{1}{2} (x^T W x + u^T U u),$$

where $p \in \mathbb{R}^n$ is the adjoint state. The dynamics of p is governed by the Hamiltonian equation:

$$(1.74) \quad \dot{p} = -\frac{\partial H_p}{\partial x},$$

or in vector components:

$$\begin{aligned} \dot{p}_i &= -\frac{\partial H_p}{\partial x_i} = -\frac{\partial}{\partial x_i} \left[\sum_{j,k=1}^n p_j A_{jk} x_k - \frac{1}{2} \sum_{j,k=1}^n x_j W_{jk} x_k \right] = -\sum_{j,k=1}^n p_j A_{jk} \delta_{ki} + \frac{1}{2} \sum_{j,k=1}^n \delta_{ij} W_{jk} x_k + \\ &+ \frac{1}{2} \sum_{j,k=1}^n x_j W_{jk} \delta_{ki} = -\sum_{j=1}^n p_j A_{ji} + \frac{1}{2} \sum_{k=1}^n W_{ik} x_k + \frac{1}{2} \sum_{j=1}^n x_j W_{ji} = \\ &= -\sum_{j=1}^n A_{ij}^T p_j + \frac{1}{2} \sum_{j=1}^n W_{ij} x_j + \frac{1}{2} \sum_{j=1}^n W_{ij}^T x_j \end{aligned}$$

Since W is a symmetric matrix $W^T = W$, we arrive at:

$$(1.75) \quad \dot{p} = -A^T p + W x$$

The optimal control satisfies the maximization condition of PMP $\frac{\partial H_p}{\partial u} = 0$, which can be written by means of vector components:

$$\begin{aligned} 0 &= \frac{\partial}{\partial u_i} \left[\sum_{j=1}^n \sum_{k=1}^m p_j B_{jk} u_k - \frac{1}{2} \sum_{j=1}^m \sum_{k=1}^m u_j U_{jk} u_k \right] = \sum_{j=1}^n \sum_{k=1}^m p_j B_{jk} \delta_{ki} - \frac{1}{2} \sum_{j=1}^m \sum_{k=1}^m \delta_{ij} U_{jk} u_k - \\ &- \frac{1}{2} \sum_{j=1}^m \sum_{k=1}^m u_j U_{jk} \delta_{ki} = \sum_{j=1}^n p_j B_{ji} - \frac{1}{2} \sum_{k=1}^m U_{ik} u_k - \frac{1}{2} \sum_{j=1}^m u_j U_{ji} = \\ &= \sum_{j=1}^n B_{ij}^T p_j - \frac{1}{2} \sum_{j=1}^m U_{ij} u_j - \frac{1}{2} \sum_{j=1}^m U_{ij}^T u_j \end{aligned}$$

Since U is symmetric $U^T = U$, we obtain:

$$(1.76) \quad B^T p - U u = 0 \quad \text{or} \quad u = U^{-1} B^T p.$$

From Eqs. (1.71), Eq. (1.75) and Eq. (1.76) we finally obtain:

$$(1.77) \quad \begin{pmatrix} \dot{x} \\ \dot{p} \end{pmatrix} = \begin{pmatrix} A & B U^{-1} B^T \\ W & -A^T \end{pmatrix} \begin{pmatrix} x \\ p \end{pmatrix}.$$

We introduce the following notation:

$$(1.78) \quad X = \begin{pmatrix} x \\ p \end{pmatrix}, \quad M = \begin{pmatrix} A & BU^{-1}B^T \\ W & -A^T \end{pmatrix}$$

Now we can rewrite Eq. (1.77) in the following way:

$$(1.79) \quad \dot{X} = MX.$$

The formal solution is well-known:

$$(1.80) \quad X(t) = e^{Mt} X(0),$$

where $X \in \mathbb{R}^{2n}$, and $M \in \mathcal{M}_{2n,2n}(\mathbb{R})$. For deriving an explicit expression of the matrix exponential e^{Mt} we have to find the eigenvalues and eigenvectors of M . Suppose the eigenvalues and eigenvectors of M are given respectively by $\{\lambda_1, \lambda_2, \dots, \lambda_{2n}\}$, and $\{S_1, S_2, \dots, S_{2n}\}$. Note that $\lambda_i \in \mathbb{R}$, and $S_i \in \mathcal{M}_{2n,1}(\mathbb{R})$; $i = 1, 2, \dots, 2n$. Let us define the matrices of eigenvectors and eigenvalues:

$$(1.81) \quad P = (S_1 \ S_2 \ \dots \ S_{2n}), \quad D = \begin{pmatrix} \lambda_1 & 0 & \dots & 0 \\ 0 & \lambda_2 & \dots & 0 \\ \vdots & \vdots & \ddots & \vdots \\ 0 & 0 & \dots & \lambda_{2n} \end{pmatrix}$$

The basic properties of eigenvalues and eigenvectors impose: $MP = PD$, or $M = PDP^{-1}$. Therefore by expanding e^{Mt} into Taylor series, we can ensure that:

$$(1.82) \quad e^{Mt} = P e^{Dt} P^{-1}.$$

The vector $e^{Mt} X(0)$ can be represented in the following way:

$$(1.83) \quad e^{Mt} X(0) = \begin{pmatrix} c_{11} e^{\lambda_1 t} + c_{12} e^{\lambda_2 t} + \dots + c_{1,2n} e^{\lambda_{2n} t} \\ c_{21} e^{\lambda_1 t} + c_{22} e^{\lambda_2 t} + \dots + c_{2,2n} e^{\lambda_{2n} t} \\ \vdots \\ c_{2n,1} e^{\lambda_1 t} + c_{2n,2} e^{\lambda_2 t} + \dots + c_{2n,2n} e^{\lambda_{2n} t} \end{pmatrix}$$

Taking into account Eq. (1.80) we can rewrite the last relation in a compact form:

$$(1.84) \quad X_i = \sum_{j=1}^{2n} c_{ij} e^{\lambda_j t}.$$

The coefficients c_{ij} are defined from the boundary conditions: $X_i(0) = X_{i0}$, $X_i(T) = X_{if}$, $\dot{X}_i(0) = \dot{X}_{i0}$, $\dot{X}_i(T) = \dot{X}_{if}$, \dots , $X_i^{(n-1)}(0) = X_{i0}^{(n-1)}$, $X_i^{(n-1)}(T) = X_{if}^{(n-1)}$; $i = 1, 2, \dots, 2n$. Taking the derivatives of Eq. (1.84) up to the order $n-1$ we obtain:

$$LC_i = V_i,$$

or

$$(1.85) \quad C_i = L^{-1}V_i,$$

where

$$(1.86) \quad C_i = \begin{pmatrix} c_{i1} \\ c_{i2} \\ \vdots \\ c_{i,2n-1} \\ c_{i,2n} \end{pmatrix}, \quad V_i = \begin{pmatrix} X_{i0} \\ X_{if} \\ \vdots \\ X_{i0}^{(n-1)} \\ X_{if}^{(n-1)} \end{pmatrix}$$

and

$$(1.87) \quad L = \begin{pmatrix} 1 & 1 & \cdots & 1 & 1 \\ e^{\lambda_1 T} & e^{\lambda_2 T} & \cdots & e^{\lambda_{2n-1} T} & e^{\lambda_{2n} T} \\ \vdots & \vdots & \vdots & \vdots & \vdots \\ \lambda_1^{n-1} & \lambda_2^{n-1} & \cdots & \lambda_{2n-1}^{n-1} & \lambda_{2n}^{n-1} \\ \lambda_1^{n-1} e^{\lambda_1 T} & \lambda_2^{n-1} e^{\lambda_2 T} & \cdots & \lambda_{2n-1}^{n-1} e^{\lambda_{2n-1} T} & \lambda_{2n}^{n-1} e^{\lambda_{2n} T} \end{pmatrix}.$$

Substituting the coefficients c_{ij} into Eq. (1.84) we obtain the solution of the control problem given by Eq. (1.71).

Summary

- We have applied LQOCT to the general problem with higher order boundary constraints.
- The singular control has been shown to be the same for any maximum order of the boundary constraints.
- We have compared the regular and singular solutions.
- The application of LQOCT is discussed for this problem in Sec. 1.6.3.

1.7

Conclusions

In this chapter, we apply OCT and STA control protocols in the same linear system, where two main requirements are to be fulfilled. First, we aim to find the global optimal solution, which corresponds to the minimum energy cost. Second, we ensure to be robust against time interval variations. To this end, higher order boundary constraints are imposed on the state of the system. Our research findings claim the suitability of OCT protocols for finding the global optimal solution. In contrast, STA protocols are well suited to fulfill higher order boundary

constraints while ensuring the robustness against time interval variations. Remarkably, we have proved that **OCT** protocols can be adapted to satisfy higher order boundary constraints by enlarging the dimension of the phase space. Alternatively, inspired by **OCT** protocols we have shown the high efficiency of exponential **STA** solutions. We have discussed the drawbacks of each protocol and paved a way to make the **OCT** and **STA** protocols benefit from each other. The application of **LQOCT** is discussed for this particular problem.

Ensemble Control of Springs and Spins

Manipulating large ensembles of dynamical systems by a single control is a challenging task due to inherent parameter variations for each individual component of the considered ensemble. The direct problem of calculating the time evolution of an ensemble of dynamical systems corresponding to a given control pulse can be solved through a numerical integration, whereas the inverse problem of designing a control pulse that produces the desired distribution of final states is much more difficult [38, 62]. In this chapter, we consider the control problem of an ensemble of springs and spins [78]. Thanks to the linearity of the dynamics, analytic control pulses can easily be designed to control an ensemble of springs. To this end, different methods can be used such as [STA](#) or [OCT](#). Contrary to that, analytic approaches for the control of an ensemble of spins have not been sufficiently developed due to the non-linearity of the spin dynamics. An alternative to designing high-fidelity broadband pulses to steer spin systems by using a non-trivial dynamic connection between non-linear spring and linear spin systems has been presented in [62]. This alternative claims, under some conditions, that nonlinear pulse design is equivalent to designing controls for steering linear spring systems under optimal forcing. Furthermore, this surprising dynamic connection has been proven to be true even under non-optimal forcing [79]. By mapping spins to springs, one may achieve excitation and inversion of a spin population in a given bandwidth of Larmor frequencies of the spins [62]. We have extended this dynamic connection to [STA](#) protocols with motion planning approach [79]. In Sec. 2.1 we present the control problem of a single spring by two-component control pulse. In Sec. 2.2, we explore the controllability limits of an ensemble of springs and present some simulation results as well as other attempts. In Sec. 2.3, we present results about the behavior of the fidelity as a function of control time, spring frequencies and the distribution of offset frequencies. In Sec. 2.4, we describe and give an original explanation to the idea of mapping spins to springs firstly suggested by Prof. Jr-Shin Li et al. for an ensemble

of spins [62]. In Sec. 2.5 we present the STA protocols to control an ensemble of springs and spins.

2.1

Optimal Control of a Single Spring

Control of a single spring is a trivial matter. Nevertheless, it is worth to first solve this problem as it will help the reader to follow the development of methods in this direction. The time evolution of a driven harmonic oscillator or a spring is expressed through a system of first order differential equations [79]:

$$(2.1) \quad \frac{d}{dt} \begin{bmatrix} x \\ y \end{bmatrix} = \begin{bmatrix} 0 & -\omega \\ \omega & 0 \end{bmatrix} \begin{bmatrix} x \\ y \end{bmatrix} + \begin{bmatrix} u_x \\ u_y \end{bmatrix},$$

where ω is the spring frequency, (u_x, u_y) the two components of the control field and (x, y) the state of the dynamical system. The goal of the control is to steer the system from its initial state $(x(0) = x_0, y(0) = y_0)$ to the target one $(x(T) = x_1, y(T) = y_1)$ by means of the (u_x, u_y) control field while minimizing the pulse energy, namely the following cost functional:

$$(2.2) \quad \mathcal{E} = \frac{1}{2} \int_0^T (u_x^2 + u_y^2) dt.$$

In this manuscript, we consider only this particular cost functional that corresponds to the energy minimum. In general a time-minimum cost functional could also be considered [80]. The control time T is fixed. In order to optimize the trajectory of the harmonic oscillator, we introduce the Pontryagin Hamiltonian H_p according to the mathematical theory of optimal processes of Pontryagin-Boltyanski-Gamkrelidze [68] (see Sec. A.1):

$$(2.3) \quad H_p = p_x \dot{x} + p_y \dot{y} - \frac{1}{2}(u_x^2 + u_y^2),$$

where (p_x, p_y) is the adjoint state. The latter can be rewritten in the form:

$$(2.4) \quad H_p = p_x(-\omega y + u_x) + p_y(\omega x + u_y) - \frac{1}{2}(u_x^2 + u_y^2).$$

By the help of the Hamilton equations, we recover the time-evolution of the state of the system (x, y) and obtain that for the adjoint state (p_x, p_y) :

$$(2.5) \quad \begin{cases} \dot{x} = \frac{\partial H_p}{\partial p_x} = -\omega y + u_x \\ \dot{y} = \frac{\partial H_p}{\partial p_y} = \omega x + u_y \\ \dot{p}_x = -\frac{\partial H_p}{\partial x} = -\omega p_y \\ \dot{p}_y = -\frac{\partial H_p}{\partial y} = \omega p_x \end{cases}$$

Hereafter, for the sake of simplicity, we introduce complex representations of the state (x, y) , adjoint state (p_x, p_y) and control pulse (u_x, u_y) :

$$z = x + iy, \quad p = p_x + ip_y, \quad u = u_x + iu_y.$$

The solutions of the differential equations are found by the method of constant variation (see Sec. B.3):

$$(2.6) \quad p(t) = p(0)e^{i\omega t}$$

$$(2.7) \quad z(t) = z(0)e^{i\omega t} + \int_0^t u(\tau)e^{i\omega(t-\tau)} d\tau.$$

According to the maximization condition of PMP [68], the partial derivatives of the Pontryagin Hamiltonian with respect to u_x and u_y are zero at (u_x^*, u_y^*) ¹:

$$(2.8) \quad \begin{cases} \frac{\partial H_p}{\partial u_x} = 0 \\ \frac{\partial H_p}{\partial u_y} = 0 \end{cases}$$

We deduce that:

$$(2.9) \quad \begin{cases} u_x^*(t) = p_x(t) \\ u_y^*(t) = p_y(t) \end{cases}$$

or according to Eq. (2.6):

$$(2.10) \quad u^*(t) = p_0 e^{i\omega t},$$

where $p_0 = p(0)$ is the initial adjoint state. In other words, the optimal field is a sum of cosine and sine functions and is known up to a constant that is defined by the following boundary conditions:

$$\begin{cases} z(T) = x(T) + iy(T) = x_1 + iy_1 = z_1 \\ z(0) = x(0) + iy(0) = x_0 + iy_0 = z_0. \end{cases}$$

According to Eq. (2.7):

$$(2.11) \quad \int_0^T u^*(\tau)e^{-i\omega\tau} d\tau = e^{-i\omega T} z_1 - z_0,$$

where the optimal control field is defined from Eq. (2.10). The latter integral condition finally yields:

$$(2.12) \quad p_0 = \frac{1}{T} \left(e^{-i\omega T} z_1 - z_0 \right).$$

¹the asterisk next to any function indicates that the function is extremal

From Eq. (2.7) we obtain the optimal trajectory:

$$(2.13) \quad z^*(t) = (z_0 + tp_0)e^{i\omega t}.$$

The real and imaginary parts of the optimal field are given by the following expressions:

$$(2.14) \quad u_x^*(t) = \frac{1}{T}(x_1 \cos \omega T + y_1 \sin \omega T - x_0) \cos \omega t - \frac{1}{T}(y_1 \cos \omega T - x_1 \sin \omega T - y_0) \sin \omega t$$

$$(2.15) \quad u_y^*(t) = \frac{1}{T}(y_1 \cos \omega T - x_1 \sin \omega T - y_0) \cos \omega t + \frac{1}{T}(x_1 \cos \omega T + y_1 \sin \omega T - x_0) \sin \omega t$$

Similarly, parametric equations of the optimal trajectory can be derived:

$$(2.16) \quad x^*(t) = \left[x_0 \left(1 - \frac{t}{T}\right) + (x_1 \cos \omega T + y_1 \sin \omega T) \frac{t}{T} \right] \cos \omega t - \left[y_0 \left(1 - \frac{t}{T}\right) + (y_1 \cos \omega T - x_1 \sin \omega T) \frac{t}{T} \right] \sin \omega t$$

$$(2.17) \quad y^*(t) = \left[y_0 \left(1 - \frac{t}{T}\right) + (y_1 \cos \omega T - x_1 \sin \omega T) \frac{t}{T} \right] \cos \omega t + \left[x_0 \left(1 - \frac{t}{T}\right) + (x_1 \cos \omega T + y_1 \sin \omega T) \frac{t}{T} \right] \sin \omega t$$

The control problem is solved for the frequency ω . In other words, the solution we have derived works exactly for the spring with frequency ω . To evaluate the efficiency of our solution, we calculate the final states of springs with frequencies $\Omega \in [-1; 1]$. The final states of these springs do not coincide with the desired target state. However, the final and target states could be sufficiently close. The closer they are, the better our solution is. The difference between the target and final states and hence the efficiency of the solution is measured by the fidelity \mathcal{F} :

$$(2.18) \quad \mathcal{F}(\Omega) = 1 - |z^*(\Omega, T) - z_1|^2.$$

$z^*(\Omega, T)$ is the final state of the spring with a frequency Ω driven by the optimal control pulse $u^*(t)$ that is computed for a spring $\omega = 0.25$. By direct substitution of the optimal pulse into the trajectory of springs, we arrive at:

$$(2.19) \quad z^*(\Omega, T) = \left[z_0 + \frac{T}{2} \zeta(\Omega) \right] e^{i\Omega T}$$

with the $\zeta(\Omega)$ function given by:

$$(2.20) \quad \zeta(\Omega) = 2e^{-i(\Omega-\omega)T/2} \operatorname{sinc} \left[\frac{(\Omega-\omega)T}{2} \right] p_0.$$

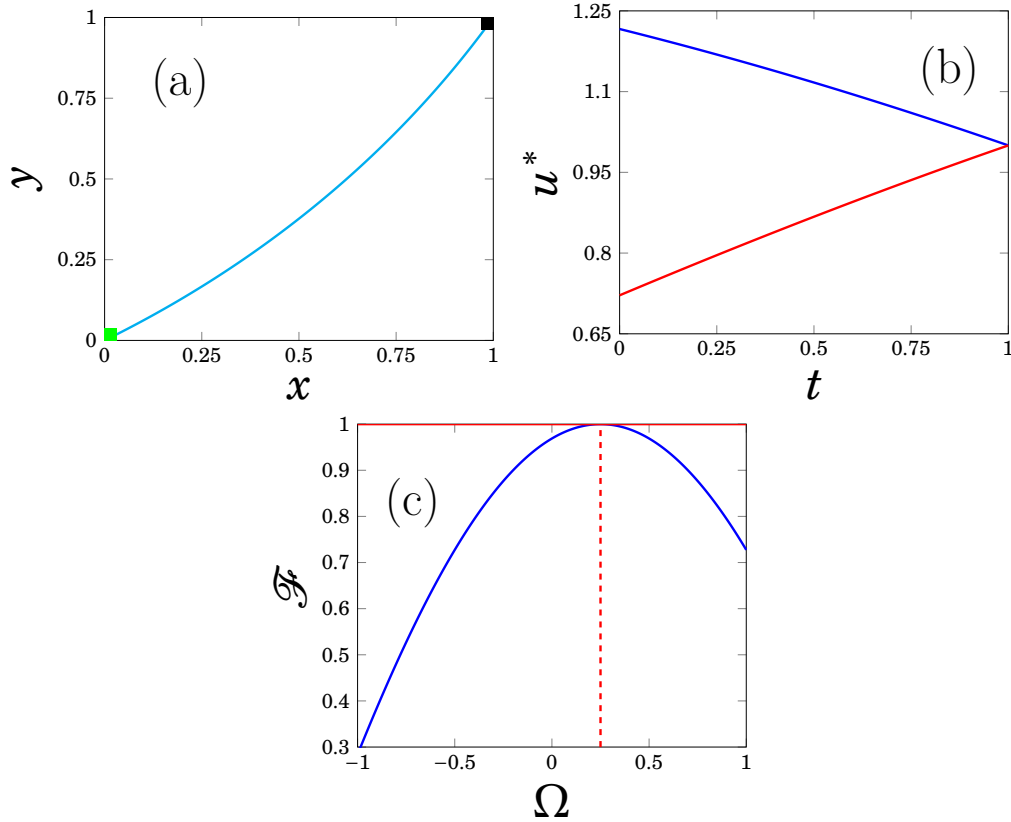


Figure 2.1: (a) Optimal trajectory of the spring with $\omega = 0.25$ in the (x, y) space. The initial state $z_0 = (0, 0)$ is indicated with a green filled square, and the target state $z_1 = (1, 1)$ with a black filled square. (b) The time evolution of the optimal control pulse u^* is depicted via its components u_x^* (blue solid line) and u_y^* (red solid line). The control time T is set to $T = 1$. (c) The dependence of the fidelity \mathcal{F} on the frequencies $\Omega \in [-1; 1]$ is computed by using Eqs. (2.18) and (2.19). The best performance of the algorithm is reached at the points of intersection of the fidelity curve and the line $\mathcal{F} = 1$ (red solid line).

As one could anticipate, the target state is reached only if $\Omega = \omega = 0.25$. The optimal solution is not robust against frequency variations. As it is shown in Subsec. 2.2.1, a robust control field can be designed by considering the simultaneous control of an ensemble of harmonic oscillators with different frequencies.

Summary

- We have obtained the optimal control pulse to steer a spring between the desired initial and target states (see Fig. 2.1).
- The fidelity or the efficiency of the control process turns out to be not sufficient in case of a single offset.
- In Sec. 2.2 we explore the ensemble control of springs.

2.2

Ensemble Controllability

We start our discussion from the second remark that has been proven in [76]. It will help us to dive deeper in the control problem of an ensemble of springs. An ensemble of springs with different offset frequencies ω driven by a single control pulse u obeys the following dynamics:

$$(2.21) \quad \frac{d}{dt} \begin{bmatrix} x_\omega \\ y_\omega \end{bmatrix} = \begin{bmatrix} 0 & -\omega \\ \omega & 0 \end{bmatrix} \begin{bmatrix} x_\omega \\ y_\omega \end{bmatrix} + \begin{bmatrix} u \\ 0 \end{bmatrix},$$

where $u(t) \in \mathbb{R}$, and we assume that the initial state $(x_\omega(0), y_\omega(0)) = (x_0, y_0)$ does not depend on the offset frequencies $\omega \in [\omega_{min}, \omega_{max}]$.

Theorem 2.1. *Ensemble of springs is not controllable if one of the control components is not available (in our case, $u_y \equiv 0$ and $u_x \equiv u$: see Eq. (2.21)).*

The proof to this theorem that is given in [76] is based on a coordinate transformation. This proof shows that the trajectories of springs have to be symmetric about the x axis meaning that the ensemble is not controllable for arbitrary initial and target states. Here, we prove another theorem, which provides us a better understanding of the controllability limits.

Theorem 2.2. *Let $u \in \mathbb{R}$ and $v \in \mathbb{R}$ be the control pulses steering two different ensembles of springs with the respective offset frequencies $\omega \in [\omega_{min}, \omega_{max}]$ and $\omega \in [-\omega_{max}, -\omega_{min}]$ from the initial state z_0 to the target state z_1 in a fixed time t_f , then*

$$z_0 \in \mathbb{R}, z_1 \in \mathbb{R} \Leftrightarrow u \equiv v$$

First, let us prove the necessary condition. We are given $z_0 \in \mathbb{R}$ and $z_1 \in \mathbb{R}$, and the goal is to prove that $u \equiv v$. Equation (2.21), which describes the time evolution of an ensemble of springs, is solved in Sec. B.3:

$$(2.22) \quad z_\omega(t) = z_0 e^{i\omega t} + e^{i\omega t} \int_0^t e^{-i\omega\tau} u(\tau) d\tau.$$

According to Eq. (2.22), the control pulses u and v must satisfy the following equations:

$$(2.23) \quad \int_0^{t_f} e^{-i\omega\tau} u(\tau) d\tau = z_1 e^{-i\omega t_f} - z_0$$

$$(2.24) \quad \int_0^{t_f} e^{i\omega\tau} v(\tau) d\tau = z_1 e^{i\omega t_f} - z_0,$$

where $\omega \in [\omega_{min}, \omega_{max}]$. The complex conjugate of Eq. (2.23) combined with the conditions $z_0 \in \mathbb{R}$ and $z_1 \in \mathbb{R}$ yields:

$$\int_0^{t_f} e^{i\omega\tau} [u(\tau) - v(\tau)] d\tau = 0.$$

The above expression is true for any $\omega \in [\omega_{min}, \omega_{max}]$ and any t_f . We therefore conclude $u(t) \equiv v(t)$. The necessity has been proved. Next, we prove the sufficient condition. We are given $u(t) \equiv v(t)$ and are required to prove that the initial and target states are real. However, we will go even further and prove that the trajectories are symmetric about the $y = 0$ axis. From Eq. (2.23), (2.24) and the condition $u(t) \equiv v(t)$ we obtain:

$$(2.25) \quad e^{i\omega t_f} z_1^* - z_0^* = e^{i\omega t_f} z_1 - z_0.$$

The complex conjugate of this equation is:

$$e^{-i\omega t_f} z_1 - z_0 = e^{-i\omega t_f} z_1^* - z_0^*.$$

Combining the above two equations we arrive at:

$$e^{-i\omega t_f} (z_1 - z_1^*) = e^{i\omega t_f} (z_1 - z_1^*),$$

or in a compact form:

$$(z_1 - z_1^*) \sin \omega t_f = 0.$$

The latter is true for any $\omega \in [\omega_{min}, \omega_{max}]$ and any t_f . We thus conclude $z_1 = z_1^*$ and consequently (see Eq. (2.25)) $z_0 = z_0^*$ meaning that the initial and target states z_0 and z_1 are real. The sufficiency has been proved. To observe the symmetry we go back to Eq. (2.21). Since $u \equiv v$, we can rewrite the same equation also for $-\omega$. We have:

$$\begin{cases} \dot{x}_\omega = -\omega y_\omega + u \\ \dot{y}_\omega = \omega x_\omega \\ \dot{x}_{-\omega} = \omega y_{-\omega} + u \\ \dot{y}_{-\omega} = -\omega x_{-\omega} \end{cases}$$

We define new variables $X_\omega := x_\omega - x_{-\omega}$ and $Y_\omega := y_\omega + y_{-\omega}$. From the above set of equations we obtain:

$$\begin{cases} \dot{X}_\omega = -\omega Y_\omega \\ \dot{Y}_\omega = \omega X_\omega. \end{cases}$$

The corresponding dynamical equation for the complex variable $Z_\omega = X_\omega + iY_\omega$ has the following form:

$$\dot{Z}_\omega = i\omega Z_\omega.$$

The solution of this differential equation is given by:

$$Z_\omega = Z_\omega(0)e^{i\omega t}.$$

Returning to the real coordinates we obtain:

$$\begin{cases} X_\omega(t) = X_\omega(0)\cos\omega t - Y_\omega(0)\sin\omega t \\ Y_\omega(t) = Y_\omega(0)\cos\omega t + X_\omega(0)\sin\omega t. \end{cases}$$

Since the initial state (x_0, y_0) is the same for all the springs and we have already proved that $y_0 = 0$, we arrive at:

$$\begin{cases} X_\omega(0) = x_\omega(0) - x_{-\omega}(0) = x_0 - x_0 = 0 \\ Y_\omega(0) = y_\omega(0) + y_{-\omega}(0) = y_0 + y_0 = 0, \end{cases}$$

whence we deduce:

$$X_\omega(t) \equiv 0, \quad Y_\omega(t) \equiv 0$$

or in the old coordinates:

$$x_\omega(t) = x_{-\omega}(t), \quad y_\omega(t) = -y_{-\omega}(t).$$

The above equation is the mathematical formulation of the symmetry about the $y = 0$ axis. As a logical conclusion, by disclaiming the necessary and the sufficient conditions of this theorem, one may rewrite the theorem in another form:

Theorem 2.3. *Let $u \in \mathbb{R}$ and $v \in \mathbb{R}$ be the control pulses steering two different ensembles of springs with the respective offset frequencies $\omega \in [\omega_{min}, \omega_{max}]$ and $\omega \in [-\omega_{max}, -\omega_{min}]$ from the initial state z_0 to the target state z_1 in a fixed time t_f , then*

$$\Im(z_0)^2 + \Im(z_1)^2 \neq 0 \Leftrightarrow u(t) \neq v(t)$$

One oscillator with non-zero offset frequency is always controllable even if one of the control inputs is not available. Note, however, that one oscillator with zero offset frequency can be driven solely along the $y = y_0$ axis due to the absence of circular motion. Although the mathematical formalism is introduced in Subsec. 2.2.1, we plot a specific case of a control as a logical conclusion. In Fig. 2.2 we illustrate the ensemble controllability of springs with negative offset frequencies that are steered along an axis other than x . The target state z_1 is not real and therefore $u(t) \neq v(t)$ but $u(t)$ exists with the only difference that it does not drive the springs with positive offset frequencies between the same states. We define the fidelity as $\mathcal{F}(\Omega) = 1 - |z(\Omega, T) - z_1|^2$ with $z(\Omega, T)$ being the final state of the spring Ω . The frequency range is regularly discretized for computational reasons. In other words, it allows us to transform the initial infinite dimensional dynamical system to a finite one which can be used from a numerical point of view. This is a standard procedure that we follow throughout the whole manuscript.

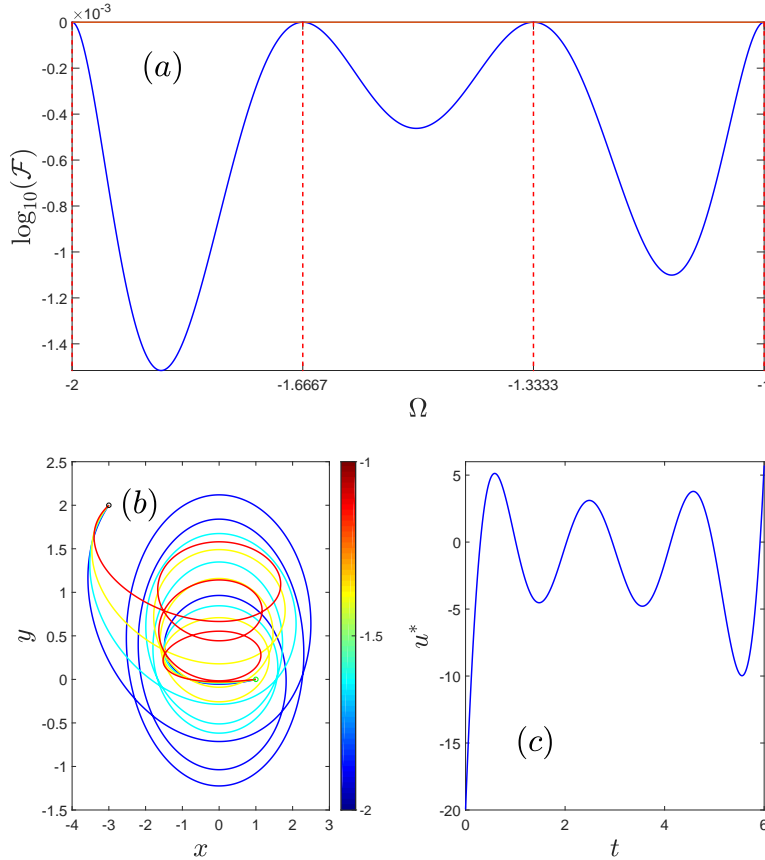


Figure 2.2: Panel (a) displays the dependence of the fidelity \mathcal{F} on the frequency Ω in a logarithmic scale. The dashed vertical red lines represent the $N = 4$ offset frequencies ω_i with $i = 1, 2, 3, 4$ in the frequency range $\Omega \in [-2, -1]$. The trajectories of springs in the phase space (x, y) are plotted in panel (b). The colorbar shows the values of the offset frequencies. The initial state $z_0 = (1, 0)$ and the target state $z_1 = (-3, 2)$ are depicted respectively with green and black circles. Panel (c) displays the time evolution of the unconstrained optimal ensemble control u^* . The control time T is set to $T = 6$.

2.2.1 Control of an Ensemble of Springs

Our goal is to design an optimal control pulse, which steers the dynamical system (see Eq. (2.21)) with N discrete frequencies ω_i from its initial state to the target state:

$$(x_i(0), y_i(0)) = (x_0, y_0) \rightarrow (x_1, y_1) = (x_i(T), y_i(T)),$$

while minimizing the cost functional:

$$\mathcal{E} = \frac{1}{2} \int_0^T u^2 dt.$$

With the discretization of the frequencies, we obtain a finite-dimensional dynamical system and we can apply the standard procedure of PMP. This procedure of controlling an ensemble of

systems with dispersion in the values of one or several parameters (in our case the only parameter is the frequency), which has been widely explored in quantum control e.g. by OCT [81], is a standard tool for improving robustness. The cost functional \mathcal{C} physically corresponds to energy expenditure. The Pontryagin Hamiltonian H_p is given by:

$$H_p = \sum_{i=1}^N \left(p_{xi}(-\omega_i y_i + u) + p_{yi} \omega_i x_i \right) - \frac{1}{2} u^2.$$

The Hamilton equations:

$$(2.26) \quad \begin{cases} \dot{x}_i = -\omega_i y_i + u \\ \dot{y}_i = \omega_i x_i \\ \dot{p}_{xi} = -p_{yi} \omega_i \\ \dot{p}_{yi} = p_{xi} \omega_i. \end{cases}$$

can easily be solved as shown in Sec. B.3:

$$(2.27) \quad \begin{cases} z_i(t) = z_0 e^{i\omega_i t} + \int_0^t u(\tau) e^{i\omega_i(t-\tau)} d\tau \\ p_i = p_i(0) e^{i\omega_i t}. \end{cases}$$

The new variables z_i and p_i are defined in the following way: $z_i := x_i + i y_i$ and $p_i := p_{xi} + i p_{yi}$. The optimal control pulse must satisfy the maximization condition of PMP:

$$\frac{\partial H_p}{\partial u} = 0,$$

hence we obtain the optimal pulse u^* :

$$(2.28) \quad u^* = \sum_{i=1}^N p_{xi} = \sum_{i=1}^N \left(p_{xi}(0) \cos \omega_i t - p_{yi}(0) \sin \omega_i t \right).$$

By direct substitution of the optimal control into Eqs. (2.27), we obtain the optimal trajectory of the offset ω_i :

$$(2.29) \quad z_i^*(t) = \left[z_0 + \frac{t}{2} \xi_i(t) \right] e^{i\omega_i t},$$

where

$$(2.30) \quad \xi_i(t) = \sum_{j=1}^N A_{ij}^-(t) p_j(0) + \sum_{j=1}^N A_{ij}^+(t) \overline{p_j(0)},$$

and

$$A_{ij}^-(t) = e^{-i(\omega_i - \omega_j)t/2} \operatorname{sinc} \left[\frac{(\omega_i - \omega_j)t}{2} \right]$$

$$A_{ij}^+(t) = e^{-i(\omega_i + \omega_j)t/2} \operatorname{sinc} \left[\frac{(\omega_i + \omega_j)t}{2} \right].$$

Equation (2.30) combined with its conjugate yields:

$$(2.31) \quad \begin{pmatrix} A^-(t) & A^+(t) \\ \overline{A^+(t)} & \overline{A^-(t)} \end{pmatrix} \begin{pmatrix} p(0) \\ \overline{p}(0) \end{pmatrix} = \begin{pmatrix} \xi(t) \\ \overline{\xi}(t) \end{pmatrix},$$

where \overline{A} is the complex conjugate of A . From the boundary conditions $z_i(0) = z_0$ and $z_i(T) = z_1$ we get the initial adjoint state:

$$(2.32) \quad \begin{pmatrix} p(0) \\ \overline{p}(0) \end{pmatrix} = \begin{pmatrix} A^-(T) & A^+(T) \\ \overline{A^+(T)} & \overline{A^-(T)} \end{pmatrix}^{-1} \begin{pmatrix} \xi(T) \\ \overline{\xi}(T) \end{pmatrix},$$

where $\xi(T)$ is defined from Eq. (2.29):

$$(2.33) \quad \xi_i(T) = \frac{2}{T} (z_1 e^{-i\omega_i T} - z_0).$$

We can obtain $\xi(t)$ from Eq. (2.31). In summary, we now have the initial adjoint state p_0 and the constant vector $\xi(T)$, and hence the optimal control pulse $u^*(t)$ and the optimal trajectory $z_i^*(t)$ for the offsets ω_i (see Eqs. (2.29) and (2.28)). The fidelity and the final state are given respectively by Eq. (2.18) and Eq. (2.19). However, the function $\zeta(\Omega)$ is different. The counterpart of Eq. (2.20) is obtained by direct substitution of the optimal control pulse into the trajectory of springs:

$$(2.34) \quad \zeta(\Omega) = \sum_{j=1}^N e^{-i(\Omega-\omega_j)T/2} \operatorname{sinc} \left[\frac{(\Omega-\omega_j)T}{2} \right] p(0) + \sum_{j=1}^N e^{-i(\Omega+\omega_j)T/2} \operatorname{sinc} \left[\frac{(\Omega+\omega_j)T}{2} \right] \overline{p}(0).$$

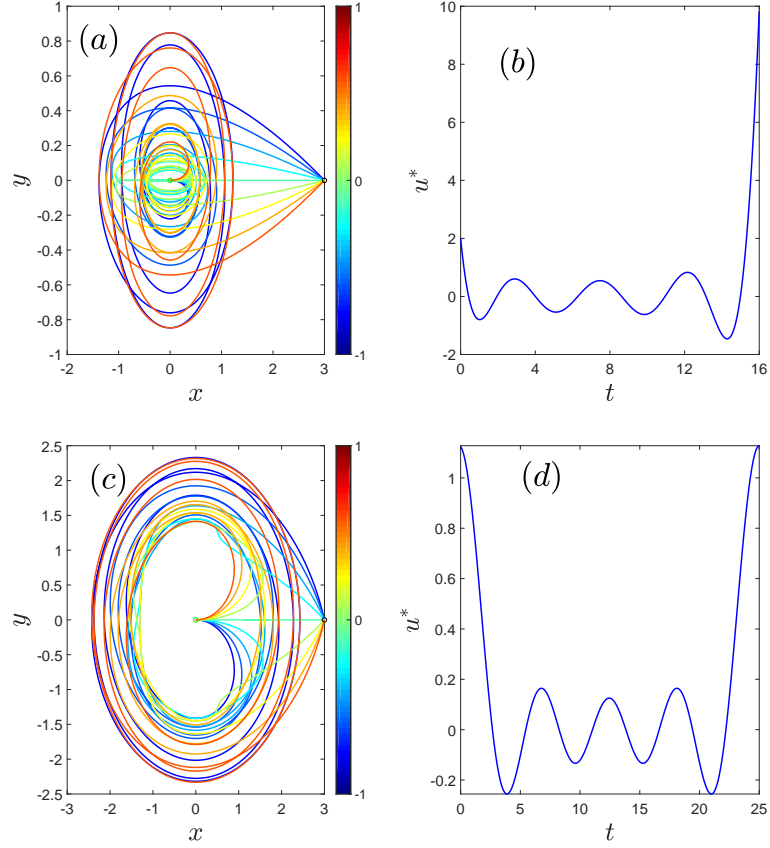


Figure 2.3: We consider $N = 9$ offset frequencies ω_i with $i = 1, 2, \dots, 9$ in the frequency range $\Omega \in [-1, 1]$. The colorbar shows the values of the offset frequencies. The initial state $z_0 = 0$ and the target state $z_1 = 3$ are depicted respectively with green and black circles. Panels (a) and (c) display the trajectories of springs in the space (x, y) . Panels (b) and (d) display the time evolution of the unconstrained optimal ensemble control u^* . In panels (a) and (b) the control time T is set to $T = 16$ and the mean value of the fidelity over Ω is $\langle \mathcal{F} \rangle \approx 0.998$, whereas in panels (c) and (d) $T = 25$ and $\langle \mathcal{F} \rangle \approx -3.866$.

The matrix of Eq. (2.32), which we invert in the simulations, is numerically singular i.e. its determinant is zero to the numerical precision of the computation. However, this matrix has a Moore-Penrose pseudo-inverse, which successfully runs the code. The matrix inversion can also be done by using the discrete prolate spheroidal sequences [80]. In the end, the important point is that the solution steers the ensemble between the desired states. From the practical point of view, we just care about the control pulse, and not about the way we obtain it. The results of our simulations for $\Omega \in [-1, 1]$ are presented in Fig. 2.3. The initial and target states are real, and therefore the trajectories are symmetric about the $y = 0$ axis. The larger the control duration is the more the springs circulate, which results in decreased values of maxima of the control pulse and increased deviation of off-resonance springs from the desired trajectories thereby decreasing the fidelity. This is the reason for the low fidelity corresponding to the

illustrations of panels (c) and (d) in Fig. 2.3. When driving the springs along $y = \text{const}$ axis, the second control pulse component u_y , if available, does not affect the results since $u_y \sim 10^{-13}$. We assume that the N offset frequencies are regularly distributed in the interval $\Omega \in [\omega_1, \omega_2]$, but other choices may be more efficient, and the frequency step is chosen small enough to avoid the discretization effect. The same approach is used in NMR to control a spin ensemble [23, 24, 82]. The control time, which we have chosen for the simulations, is relatively long to ensure the smoothness of the control field but also short enough to ensure sufficient fidelity. Our designed control pulse eventually has to be implemented in experiments. To this end, first and foremost, the amplitude of the control pulse must be limited. One of the naive options that we thought could help us restrain the maximum amplitude of the control pulse, but in fact it did not appear to be helpful in any way, was to cut the pulse at a fixed time t_0 . We choose t_0 such that $|u(t)| \leq u_0$ for $t \leq t_0$ and $|u(t)| > u_0$ for $t > t_0$, where u_0 is the threshold. The cutting is done in two different ways. Either the control pulse u fulfills the condition $u(t > t_0) = 0$ or $u(t > t_0) = u_0$. Even in the latter case, when $u(t > t_0) = u_0$, the fidelity is just 0.65 (with the parameters: $z_0 = 0$, $z_1 = 3$, $w_1 = -1$, $w_2 = 1$, $N = 6$, $T = 3.5$ and $t_0 = 3.4$) which is not a satisfying result. Alternatively, we came up with another idea that we thought could help us restrain the amplitude of the control pulse. We include a constant u_0 directly in the cost functional:

$$\mathcal{C} = \frac{1}{2} \int_0^T (u - u_0)^2 dt.$$

In this case, the optimal control pulse u^* , the optimal trajectory of offset frequencies $z_i^*(t)$ and the components of the vector $\xi(T)$ have slightly different forms:

$$(2.35) \quad \begin{aligned} u^*(t) &= u_0 + \sum_{i=1}^N p_{x_i} = u_0 + \sum_{i=1}^N \left(p_{x_i}(0) \cos \omega_i t - p_{y_i}(0) \sin \omega_i t \right) \\ z_i^*(t) &= \left[z_0 + \frac{t}{2} \xi_i(t) + u_0 t e^{-i\omega_i t/2} \text{sinc} \left(\frac{\omega_i t}{2} \right) \right] e^{i\omega_i t} \\ \xi_i(T) &= \frac{2}{T} \left[z_1 e^{-i\omega_i T} - z_0 - u_0 T e^{-i\omega_i T/2} \text{sinc} \left(\frac{\omega_i T}{2} \right) \right]. \end{aligned}$$

The initial adjoint state $p(0)$, and thus the optimal control field $u^*(t)$ and the optimal trajectory $z^*(t)$, can numerically be computed (see Eq. (2.32)). The term $-u_0 T e^{-i\omega_i T/2} \text{sinc} \left(\frac{\omega_i T}{2} \right)$ in $\xi(T)$ introduces a shift in the initial adjoint state $p(0)$ and therefore in $\xi(t)$. However, this shift is compensated by the additional terms u_0 and $u_0 t e^{-i\omega_i t/2} \text{sinc} \left(\frac{\omega_i t}{2} \right)$ correspondingly in $u^*(t)$ and $z_i^*(t)$ such that the numerical results do not depend on u_0 . This has been confirmed by numerical computations. In brief, this approach does not help to limit the maximum amplitude of the control pulse.

Summary

- We have considered a control problem of an ensemble of springs and found out that not all target states are reachable if the second control component is unavailable. Starting from the origin one can reach all the states along the x axis. The rest is reachable if and only if there are no offsets of opposite signs (see Theorems 2.1, 2.2, 2.3).
- The fidelity or the efficiency of the control process depends on the control time and number of offsets. The smaller the control time and the larger the number of offsets are, the more efficient is the solution (see Fig. 2.3).
- In Sec. 2.3 we discuss the dependency of the fidelity on the control time and distribution of offsets in the considered frequency range.

2.3

Fidelity Plots

In this section, we present some numerical simulations and figures, which contain dense information about the dependence of the fidelity \mathcal{F} on the control time T and on the distribution of offset frequencies ω_i within the frequency range $\Omega \in [\omega_1, \omega_2]$.

2.3.1

Fidelity of the Control Process

Here, we illustrate the behavior of the fidelity for different control times. Note that in this section, the fidelity \mathcal{F} is defined in a different way due to illustrative reasons:

$$\mathcal{F} = 1 - |z(\Omega, T) - z_1|.$$

In the definition of the fidelity, we take the square of the modulus to avoid the singularity at the origin. However, for the contour plots of the current subsection we derive higher resolution figures if we take the modulus. We follow the new definition only in this subsection.

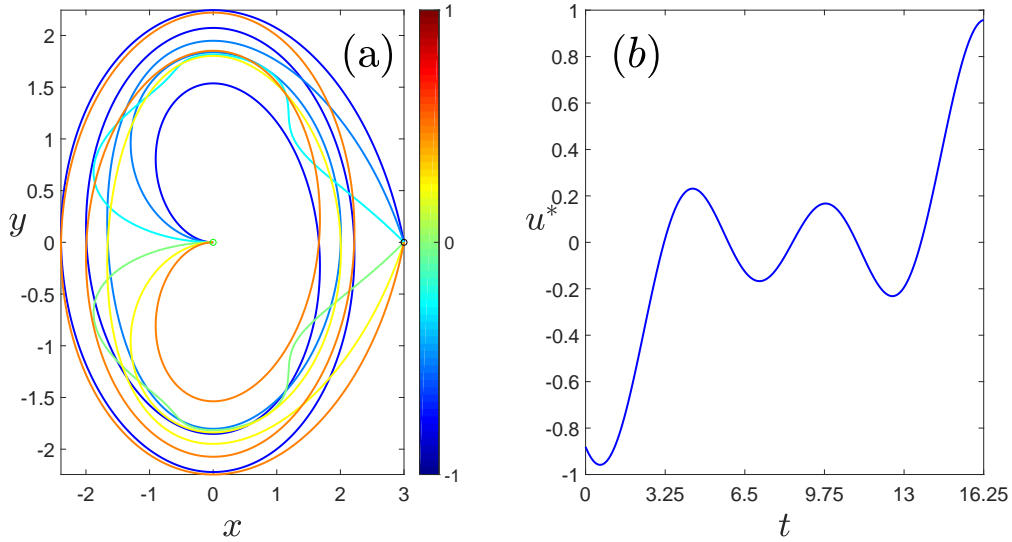


Figure 2.4: Similar to Figs. 2.3, the trajectories of the springs are depicted in panel (a), and the control pulse in panel (b). $N = 6$ offset frequencies ω_i with $i = 1, 2, \dots, 6$ are regularly distributed in the frequency range $\Omega \in [-1; 1]$. The initial and target states respectively are $z_0 = 0$ and $z_1 = 3$. The control time is $T = 16.25$.

We consider the control problem presented in Fig. 2.4. By varying the control time T we observe the change of the fidelity plot. This means one fidelity plot corresponds to each control duration. Graphically we can assure ourselves from Fig. 2.5 that the shorter is the control time the higher is the fidelity as we have already stated in the previous subsection. Until here, we have just considered the regular distribution of offset frequencies. In fact, the fidelity plot is different for different distributions of offset frequencies that we consider in the optimization process (see Fig. 2.6). Moreover, the regular distribution appears to be one of the worst. We consider a pair of offsets (ω_1, ω_2) in the interval $\Omega \in [-1; 1]$ (see Fig. 2.6). An important conclusion of our results on the optimal choice of the distribution of two offsets that is summarized in Fig. 2.6 is that a high fidelity can be reached by setting $(\omega_1; \omega_2) = (-0.1515; 0.1313)$. The mean value of the fidelity, in this case, is $\langle \mathcal{F} \rangle \approx 0.91$. The optimal choice of the two offsets $(\omega_1; \omega_2) = (-0.29, 0.7)$ provides the highest possible mean fidelity in this setting $\langle \mathcal{F} \rangle = 0.96257$. Due to the symmetry of the system, the sign of the offset does not make a difference. The fidelity drops down on the diagonals. For instance, the mean value of the fidelity is just $\langle \mathcal{F} \rangle \approx 0.24$ for $(\omega_1; \omega_2) = (-0.5; 0.5)$. The second diagonal corresponds to the case of a single offset. Because of the symmetry of the dynamics, the control pulse designed for a positive frequency steers the negative one between the desired states and therefore the fidelity drops down even on the first diagonal but rapidly goes up when we introduce an infinitely small frequency shift.

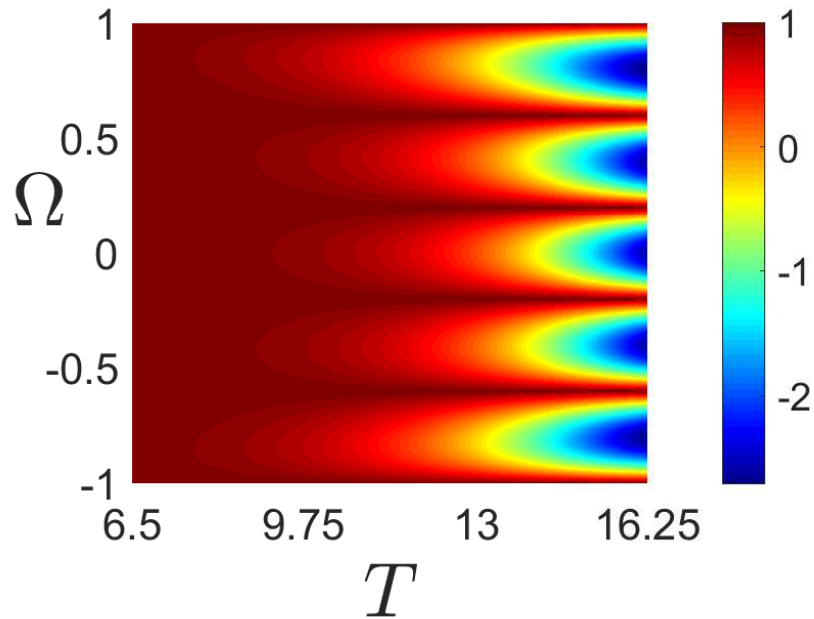


Figure 2.5: Dependence of the fidelity \mathcal{F} on the control time $T \in [6.5; 16.25]$ and on the spring frequency Ω . $N = 6$ offset frequencies ω_i are regularly distributed in the frequency range $\Omega \in [-1, 1]$. The colorbar corresponds to the magnitude of the fidelity.

Summary

- We have plotted the dependence of the fidelity on the control time and frequencies.
- The more we decrease the control time, the more the fidelity increases (see Fig. 2.5).
- The regular distribution of offsets is not the optimal choice. We have found the optimal pair of offsets for a particular setting. Due to symmetry of the system, the fidelity drops down when the distribution of offsets is symmetric (see Fig. 2.6).
- In Sec. 2.4 we discuss the ensemble control of spins or Bloch systems.

2.4

Mapping Spins to Springs

The control of one spin has been studied in the last century and is well-known [31]. Here we discuss the optimal control of an ensemble of two-level quantum systems [83]. Our aim is to generalize the method introduced by Prof. Jr. Shin-Li and Prof. S. J. Glaser [62] in which they

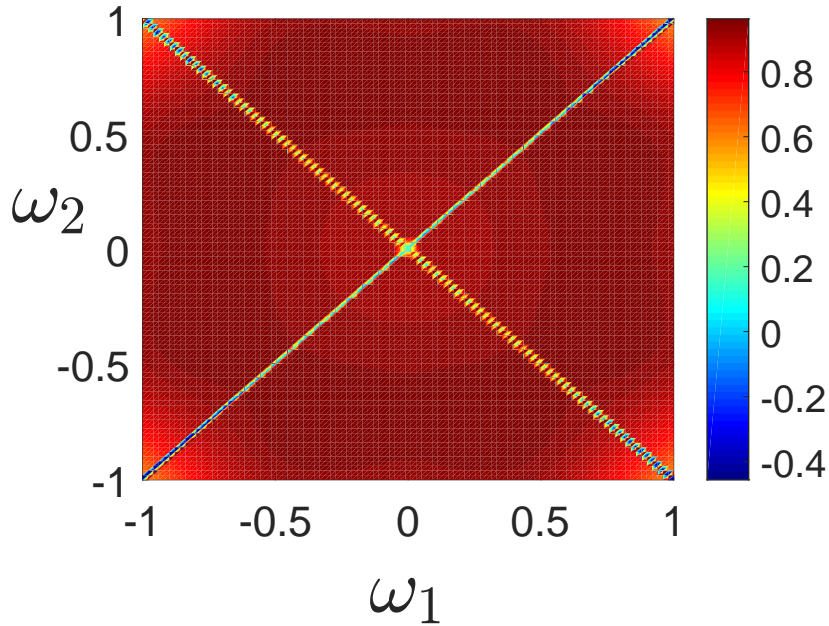


Figure 2.6: $N = 2$ offset frequencies ω_1 and ω_2 are considered in the frequency range $\Omega \in [-1; 1]$. The average fidelity over spring frequencies $\Omega \in [-1; 1]$ is different for different values of offset pairs $(\omega_1; \omega_2)$. The initial and target states respectively are $z_0 = \pi/2$, $z_1 = 0$. The control time T is set to $T = 5$. The colorbar corresponds to the mean value of the fidelity.

introduce a nontrivial dynamic connection between nonlinear spin and linear spring systems. We have made one step forward in understanding this connection. To have a self-consistent and easy-to-understand introduction of this chapter, we first introduce the method of mapping springs to spins developed by Prof. Jr. Shin-Li et al. [62].

The semi-classical Bloch model of the time evolution of a two-level system can mathematically be represented as a first order matrix differential equation [77, 80, 84]:

$$(2.36) \quad \frac{d}{dt} \begin{bmatrix} M_x(t, \omega) \\ M_y(t, \omega) \\ M_z(t, \omega) \end{bmatrix} = \begin{bmatrix} 0 & -\omega & u(t) \\ \omega & 0 & -v(t) \\ -u(t) & v(t) & 0 \end{bmatrix} \begin{bmatrix} M_x(t, \omega) \\ M_y(t, \omega) \\ M_z(t, \omega) \end{bmatrix}$$

Here we neglected the relaxation effects by assuming a very short control duration compared to the relaxation time. Now, consider separately the dynamics of an undamped driven harmonic oscillator:

$$(2.37) \quad \frac{d}{dt} \begin{bmatrix} x(t, \omega) \\ y(t, \omega) \end{bmatrix} = \begin{bmatrix} 0 & -\omega \\ \omega & 0 \end{bmatrix} \begin{bmatrix} x(t, \omega) \\ y(t, \omega) \end{bmatrix} + \begin{bmatrix} u(t) \\ v(t) \end{bmatrix}$$

We steer the Bloch system from $M_0 = (1, 0, 0)$ to $M_F = (0, 0, 1)$, and the spring system from $X_0 = (\pi/2, 0)$ to $X_F = (0, 0)$. It is worth to notice that these two dynamics become even more

similar when the external forces $u(t)$ and $v(t)$ are missing. We might expect a similar evolution under external forcing. Based on this insight, a dynamical projection between the endpoints of the trajectory of a spin to that of a spring has been established. To this end, a complex projection is constructed:

$$(2.38) \quad f(t) = \frac{M_x(t) + iM_y(t)}{a(t) + M_z(t)},$$

where $0 \leq t \leq T$ is the pulse duration and $a(t) = a_1(t) + ia_2(t)$ is a complex-valued function satisfying the Riccati equation with the initial condition $a(0) = 1$ and depending on the time-varying RF pulse:

$$(2.39) \quad \dot{a} = -\frac{u\beta}{2m}a^2 - \frac{uM_z(\beta-1)}{m}a + \frac{u(1+M_z^2-M_z^2\beta)}{2m},$$

where $\beta = e^{2i\omega t}$ and $m = M_x + iM_y$, then f follows:

$$(2.40) \quad \dot{f} = i\omega f + \frac{1}{2}uf^2 + \frac{1}{2}\beta u$$

with $f(0) = 1$ since $m(0) = 1$, $z(0) = 0$, and $a(0) = 1$. If $a(t) = 1$ over the entire duration, then $f(t)$ simply becomes the stereographical projection. Using the fact that the magnitude of the vector $\|\mathbf{M}\| = 1$, we can compose conditions on $f(t)$ and $a(t)$ to ensure that the dynamic projection corresponds to a valid (i.e., noncomplex-valued and unique) Bloch trajectory. The necessary and sufficient condition to have a one-to-one projection between the trajectories of spins and springs is formulated by the following bound on $f(t)$:

$$(2.41) \quad 0 \leq |f|^2 < \frac{1 - |a|^2 + \sqrt{(1 - |a|^2)^2 + 4a_2^2}}{2a_2^2},$$

where $|a|^2 = a_1^2 + a_2^2$. This condition also indicates why the stereographic projection fails to provide a mapping in the general case.

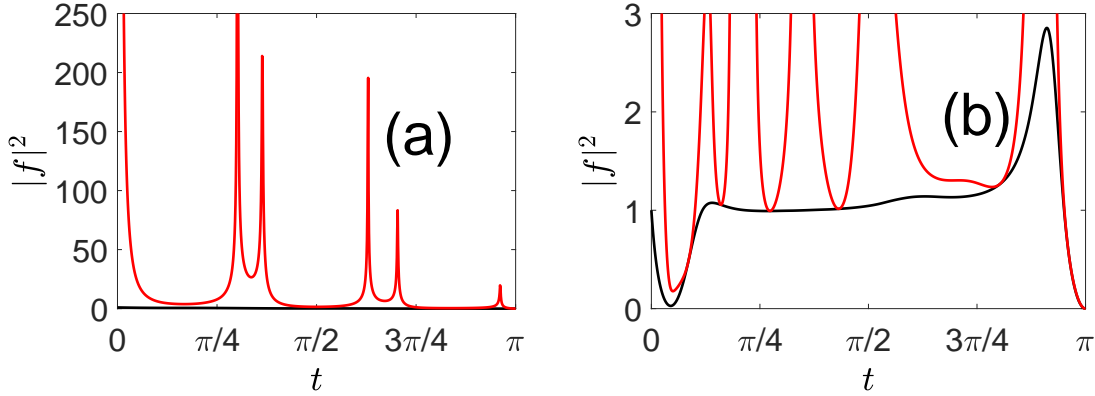


Figure 2.7: The feasibility of pulse design is illustrated. We plot the trajectory of $|f|^2$ (black) and the corresponding bound (red) given by the right side of Eq. (2.41) resulting from the (a) minimum-energy control $u_{\pi/2}^* = -\cos(3t)$ and (b) a quadratic control $u(t) = (18t^2 + 4 - 9\pi^2)/8$ that steer the spring from $X_0 = (\pi/2, 0)$ to $X_F = (0, 0)$. In (a) the trajectory of $|f|^2$ is much smaller than the bound appearing as a horizontal line at the bottom of the figure.

The control problem of an ensemble of springs is linear whereas that of an ensemble of Bloch systems is bi-linear. If the conditions we have imposed on f are satisfied then the optimal pulse to steer an ensemble of springs is applicable to an ensemble of Bloch systems. Note that the corresponding pulse does not correspond to the optimal solution of the non-linear system. In summary, this method is of great scientific importance as it allows to analytically explore a bi-linear control problem. A negative aspect of this approach is the fact that in general Eq. (2.41) is very difficult to verify in practice (see Fig. 2.7).

2.4.1

Spin Systems vs Nonlinear Oscillators

Here, we present an original explanation to the method of mapping spins to springs. Two main dynamical equations are taken into consideration [62]. One describes the semi-classical Bloch model of a two-level system:

$$(2.42) \quad \frac{d}{dt} \begin{bmatrix} M_x(t, \omega) \\ M_y(t, \omega) \\ M_z(t, \omega) \end{bmatrix} = \begin{bmatrix} 0 & -\omega & u(t) \\ \omega & 0 & -v(t) \\ -u(t) & v(t) & 0 \end{bmatrix} \begin{bmatrix} M_x(t, \omega) \\ M_y(t, \omega) \\ M_z(t, \omega) \end{bmatrix}$$

and the other one describes the dynamics of an undamped harmonic oscillator:

$$(2.43) \quad \frac{d}{dt} \begin{bmatrix} x(t, \omega) \\ y(t, \omega) \end{bmatrix} = \begin{bmatrix} 0 & -\omega \\ \omega & 0 \end{bmatrix} \begin{bmatrix} x(t, \omega) \\ y(t, \omega) \end{bmatrix} + \begin{bmatrix} u(t) \\ v(t) \end{bmatrix}.$$

To make the similarity of the two dynamics even more appealing and to give an original explanation to the method of mapping spins to springs, we exchange the variables M_x, M_y, M_z

with x, y, z . We go from Cartesian (x, y, z) to spherical (r, θ, φ) coordinates in the spin systems:

$$\begin{cases} x = r \cos \varphi \sin \theta \\ y = r \sin \varphi \sin \theta \\ z = r \cos \theta \end{cases}$$

and from Cartesian (x, y) to polar coordinates (r, φ) in the spring systems:

$$\begin{cases} x = r \cos \varphi \\ y = r \sin \varphi. \end{cases}$$

Assuming that the radius of the Bloch sphere is constant ($r = \text{const}$) and substituting the derivatives of x, y, z in spherical:

$$\begin{cases} \dot{x} = -r \sin \varphi \sin \theta \dot{\varphi} + r \cos \varphi \cos \theta \dot{\theta} \\ \dot{y} = r \cos \varphi \sin \theta \dot{\varphi} + r \sin \varphi \cos \theta \dot{\theta} \\ \dot{z} = -r \sin \theta \dot{\theta} \end{cases}$$

and polar coordinates:

$$\begin{cases} \dot{x} = \cos \varphi \dot{r} - r \sin \varphi \dot{\varphi} \\ \dot{y} = \sin \varphi \dot{r} + r \cos \varphi \dot{\varphi} \end{cases}$$

into Eqs. (2.42), (2.43) we correspondingly obtain:

$$(2.44) \quad \begin{cases} -\sin \varphi \sin \theta \dot{\varphi} + \cos \varphi \cos \theta \dot{\theta} = -\omega \sin \varphi \sin \theta + u \cos \theta \\ \cos \varphi \sin \theta \dot{\varphi} + \sin \varphi \cos \theta \dot{\theta} = \omega \cos \varphi \sin \theta - v \cos \theta \\ -\sin \theta \dot{\theta} = -u \cos \varphi \sin \theta + v \sin \varphi \sin \theta \end{cases}$$

$$(2.45) \quad \begin{cases} \cos \varphi \dot{r} - r \sin \varphi \dot{\varphi} = -\omega r \sin \varphi + u \\ \sin \varphi \dot{r} + r \cos \varphi \dot{\varphi} = \omega r \cos \varphi + v \end{cases}$$

For the spin system, multiplying the first and the second equations of Eqs.(2.44) respectively by $\sin \varphi$ and $\cos \varphi$ and then subtracting the first equation from the second one we get:

$$(2.46) \quad \begin{cases} \sin \theta \dot{\varphi} = \omega \sin \theta - (u \sin \varphi + v \cos \varphi) \cos \theta \\ -\sin \theta \dot{\theta} = -u \cos \varphi \sin \theta + v \sin \varphi \sin \theta \end{cases}$$

We assume that $\sin \theta \neq 0$ and we divide both sides of Eqs. (2.46) by $\sin \theta$:

$$(2.47) \quad \begin{cases} \dot{\varphi} = \omega - (u \sin \varphi + v \cos \varphi) \cot \theta \\ \dot{\theta} = u \cos \varphi - v \sin \varphi. \end{cases}$$

For the spring system, we multiply the first and the second equations of Eqs. (2.45) respectively by $\sin \varphi$ and $\cos \varphi$, then we subtract the first equation from the second one. In the next step, we multiply the same equations in the same order by $\cos \varphi$ and $\sin \varphi$ respectively, then we sum both equations. Finally we arrive at:

$$(2.48) \quad \begin{cases} \dot{\varphi} = \omega - (u \sin \varphi - v \cos \varphi)/r \\ \dot{r} = u \cos \varphi + v \sin \varphi. \end{cases}$$

Equations (2.47), (2.48) are the main equations to be considered in this section. To further visualize the similarity of these equations, let us expand the function $\cot \theta$ into Taylor series. The well-known formula of the Taylor series of the function $\cot x$ has the following form:

$$\cot x = \frac{1}{x} - \frac{1}{3}x - \frac{1}{45}x^3 - \frac{2}{945}x^5 - \dots - \frac{2^{2n} \mathcal{B}_n}{(2n)!} x^{2n-1} - \dots, \quad 0 < |x| < \pi,$$

where $\mathcal{B}_0 = 1$, $\mathcal{B}_1 = 1/6$, $\mathcal{B}_2 = 1/30$, $\mathcal{B}_3 = 1/42$, ..., \mathcal{B}_n are the Bernoulli numbers. Since $0 < \theta < \pi$, this formula is applicable for $\cot \theta$ as well. In further discussions we only need the first three terms of that expansion. Substituting it into Eqs. (2.47) we arrive at:

$$(2.49) \quad \begin{cases} \dot{\varphi} = \omega - (u \sin \varphi + v \cos \varphi) \left(\frac{1}{\theta} - \frac{1}{3}\theta - \frac{1}{45}\theta^3 - \dots \right) \\ \dot{\theta} = u \cos \varphi - v \sin \varphi. \end{cases}$$

The similarity of Eqs. (2.47) and Eqs. (2.48) becomes obvious. The azimuthal angle is defined the same way for both cases ($\varphi \sim \theta$). However, the counterpart of the polar angle in the spring systems is the radial coordinate ($\theta \sim r$). Assume that we have found the required control field (u, v) for a spring system (see Eqs. (2.48)). Then $(u, -v)$ will be a control field for a spin system (if we take only the first term in the expansion) steering the system between the same initial and target states. In other words, the dynamics of a spring system is nothing more than that of a linear approximation of a spin system. This is how an idea of a nonlinear spring system is being naturally risen. The dynamics of a nonlinear spring system unlike the linear one (see (2.48)) has the following form:

$$(2.50) \quad \begin{cases} \dot{\varphi} = \omega - (u \sin \varphi - v \cos \varphi) \left(\frac{1}{r} - \frac{1}{3}r - \frac{1}{45}r^3 - \dots \right) \\ \dot{r} = u \cos \varphi + v \sin \varphi. \end{cases}$$

Hereafter, the state of a spring system will be described by (r, φ) and that of a spin system by (θ, φ) . The control (u, v) which steers an ensemble of linear springs from $(\pi/2, 0)$ to $(0, 0)$ has been proven to approximately steer an ensemble of spins from $(\pi/2, 0)$ to $(0, 0)$ when considering the same Larmor dispersion in frequencies for both systems [62]. It is important to note that this approximation works best for small polar angles. The generalization we try to make is based on Eqs. (2.49), (2.50). The idea is to solve the linear control problem of a spring system and then apply the obtained solution to the spin systems. The linear spring system can easily be analyzed by analytic methods. We use numeric methods only for inversion of a matrix.

2.4.2

Simulations for One Control Case

In this subsection, we assume that $v = 0$ and we consider one control u along the x direction. Equations (2.49), (2.50) respectively take the forms:

$$(2.51) \quad \begin{cases} \dot{\varphi} = \omega - u \sin \varphi \left(\frac{1}{\theta} - \frac{1}{3}\theta - \frac{1}{45}\theta^3 - \dots \right) \\ \dot{\theta} = u \cos \varphi \end{cases}$$

$$(2.52) \quad \begin{cases} \dot{\varphi} = \omega - u \sin \varphi \left(\frac{1}{r} - \frac{1}{3}r - \frac{1}{45}r^3 - \dots \right) \\ \dot{r} = u \cos \varphi. \end{cases}$$

In the simulations, we take the optimal solution of the linear control problem of a spring system and apply it to steer the spin systems and the nonlinear spring systems. For illustrations, we have chosen a specific frequency of a spring and of a spin. We have taken 500 points for discretization of the range $\Omega \in [-1, 1]$. With these parameters in the case when two control pulse components u_x and u_y are available, the results barely differ from the case with $u_y = 0$. This is because we steer the ensemble of springs along the $y = 0$ axis (see the values of parameters in the caption of Fig. 2.8), which means that one control pulse component u is sufficient.

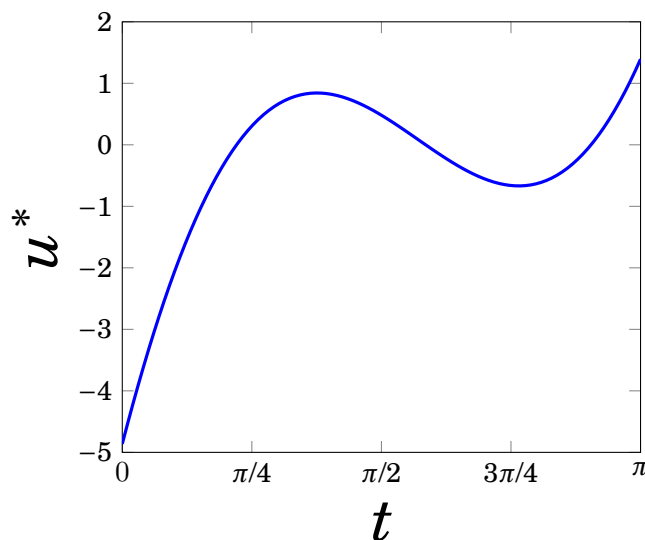


Figure 2.8: The evolution of an optimal control pulse. $N = 4$ offset frequencies are regularly distributed in the frequency range $\Omega \in [-1; 1]$. The control time is set to $T = \pi$. The initial and target states are respectively $z_0 = \pi/3$ and $z_1 = 0$.

We apply the control pulse depicted in Fig. 2.8 to steer an ensemble of spins. The trajectories of springs and spins under this optimal forcing is depicted in Fig. 2.9. The difference of

counterpart states of springs and spins, namely $\theta - r$ and $\phi - \phi$ is depicted in Fig. 2.10. The fidelity of spins is defined as $\cos[\theta(\omega)]$, and is about 0.9998.

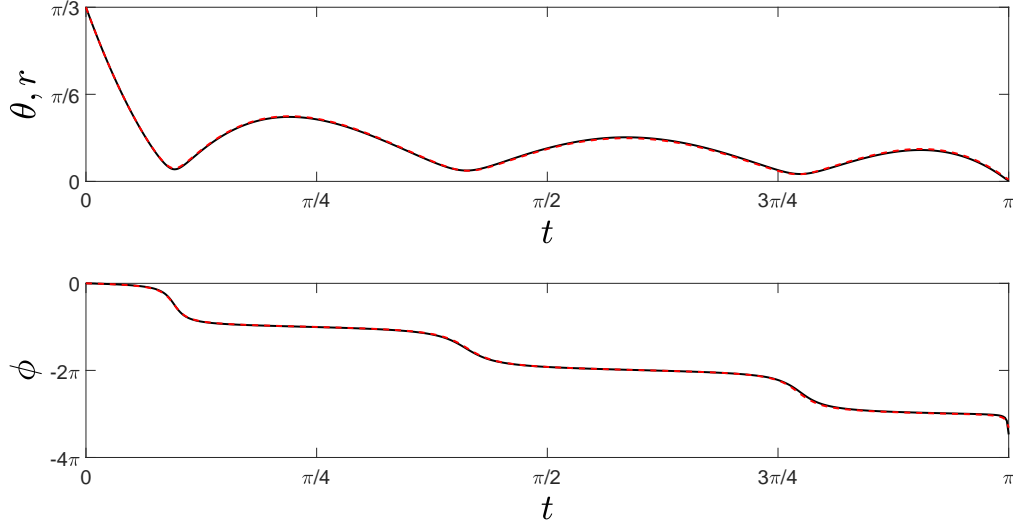


Figure 2.9: Trajectories of a spin and of a spring. The black solid line and the dashed red line correspond respectively to the polar angle and the radius. The spin dynamics is computed using the exact dynamical equations. A linear spring system is considered. All curves correspond to the offset frequency $\Omega \approx -0.57114$.

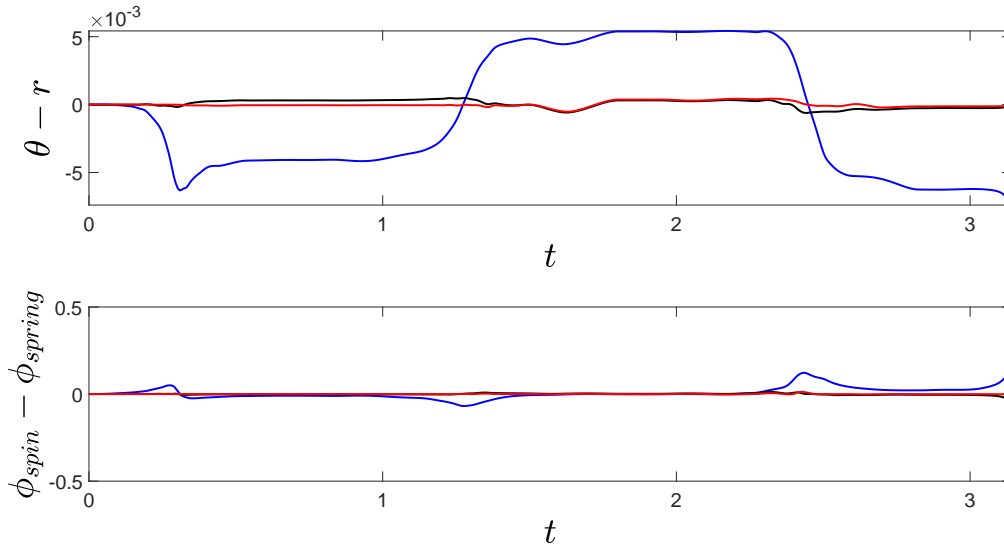


Figure 2.10: Comparison between trajectories of a spin and of a spring. The blue, black and red lines correspond respectively to linear, 1st and 2nd order nonlinear spring systems. The spin dynamics is exactly computed using the exact dynamical equations. All curves correspond to the offset frequency $\Omega \approx -0.57114$.

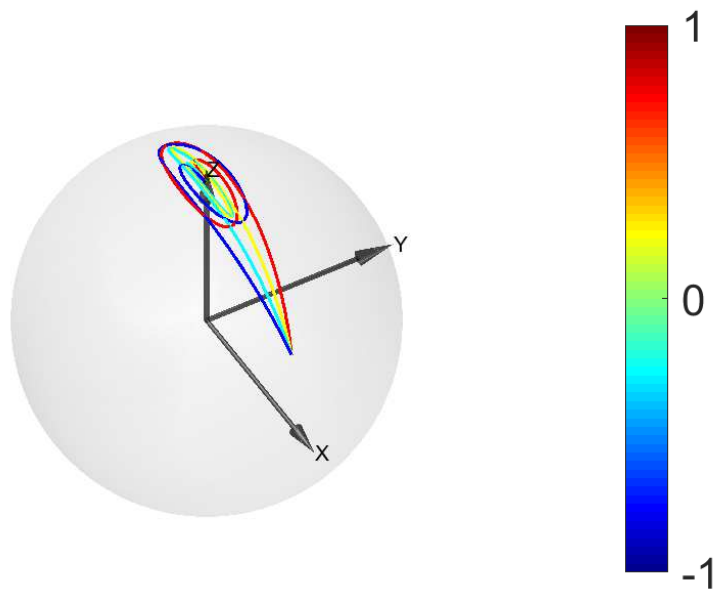


Figure 2.11: $N = 4$ offset frequencies are regularly distributed in the frequency range $\Omega \in [-1; 1]$. The control time is set to $T = \pi$. The initial and the target states of springs are respectively $z_0 = \pi/3$ ($\theta = \pi/3$ for spins) and $z_1 = 0$ ($\theta = 0$ for spins). The colorbar corresponds to the frequency Ω .

As we can see in Figs. 2.9 and 2.10, linear approximation of Bloch equations under OCT pulses for small polar angles is already a good approximation. The trajectories of spins on a Bloch sphere are depicted in Fig. 2.11.

Summary

- We have introduced the method of mapping spins to springs.
- We have presented an original explanation to the method of mapping spins to springs.
- We have applied this method to control an ensemble of spins.
- In Sec. 2.5 we discuss the ensemble control of spins or Bloch systems under STA control pulses.

2.5

STA Solutions

In the computations of the optimal solution by LQOCT, we are required to compute an inverse of a matrix, which may cause numerical problems. In this section, we introduce a STA solution that allows us to avoid these problems. STA methods generally exploit the algebraic structure

of quantum mechanics [47–50]. We propose a general STA protocol for linear dynamical systems based on a motion planning approach, known in control theory as Brunovki form [85, 86].

2.5.1 One Control Input: Springs

We assume from now on that $z_0 = (0, 0)$ and $z_1 = (1, 0)$, thus the goal of the control problem is to find a solution, which fulfills the relation:

$$(2.53) \quad \int_0^{t_f} e^{-i\omega\tau} u(\tau) d\tau = e^{-i\omega t_f}$$

for $\omega \in [\omega_{min}, \omega_{max}]$. We propose to adapt the method introduced in [67]. We first consider the case of two frequencies ω_1 and ω_2 . We introduce an auxiliary function $g(t)$ such that:

$$(2.54) \quad u(\tau) = g^{(4)}(\tau) + (\omega_1^2 + \omega_2^2)g^{(2)}(\tau) + \omega_1^2\omega_2^2g(\tau).$$

After integrating by parts we have:

$$(2.55) \quad \int_0^{t_f} e^{-i\omega\tau} u(\tau) d\tau = e^{-i\omega t_f} + (\omega^2 - \omega_1^2)(\omega^2 - \omega_2^2)G(t_f),$$

where the function g obeys the following boundary conditions:

$$(2.56) \quad g(0) = g(t_f) = g'(0) = g'(t_f) = g^{(2)}(0) = g^{(2)}(t_f) = 0; g^{(3)}(0) = 0; g^{(3)}(t_f) = 1$$

and

$$G(t_f) = \int_0^{t_f} e^{-i\omega\tau} g(\tau) d\tau.$$

The condition Eq. (2.53) is satisfied for the two frequencies ω_1 and ω_2 (see Eq. (2.55)). A possible g function is of the form:

$$(2.57) \quad g(t) = \frac{(-t_f)^3}{3!} \left(\frac{t}{t_f}\right)^4 \left(1 - \frac{t}{t_f}\right)^3.$$

It is then straightforward to generalize this computation to the case of N offsets. The only non zero boundary condition is $g^{(2N-1)}(t_f) = 1$. The control field is given by the expression:

$$(2.58) \quad u(t) = \sum_{k=1}^{N+1} P_{k-1} g^{2(N-k+1)}(t),$$

where the factors P_k are the coefficients of the characteristic polynomial of the matrix $W = -diag(\omega_i^2)_{i=1}^N$ ($\mathbf{P}^N = \det(\lambda\mathbf{I} - W) = P_0\lambda^N + P_1\lambda^{N-1} + \dots + P_{N-1}\lambda + P_N\lambda^0$). As a possible g function we can choose:

$$(2.59) \quad g(t) = \frac{(-t_f)^{2N-1}}{(2N-1)!} \left(\frac{t}{t_f}\right)^{2N} \left(1 - \frac{t}{t_f}\right)^{2N-1}.$$

The energy and the control pulse are very similar to the ones in Fig. 2.12. The trajectories and the fidelity are similar to the case with additional boundary constraints (see Fig. 2.13). At the order N we have $4N$ constraints to fulfill, thus we have to consider at least a polynomial of order $4N - 1$. The behavior of the control field at $t = 0$ and t_f can be adjusted by adding some new constraints: $g^{(2N)}(0) = g^{(2N)}(t_f) = 0$. This way we ensure to have $u(t) = 0$ at the initial and final times. We thus need another function $h(t) = v(t)g(t)$, which will satisfy the additional constraints alongside with others. Here v is an auxiliary finite-value function. According to Leibniz derivation rule of products:

$$(2.60) \quad h^{(n)}(t) = \sum_{k=0}^n C_n^k g^{(k)}(t) v^{(n-k)}(t).$$

Note that $g(0)$, $g(t_f)$ and all derivatives of g are 0 except $g^{(2N-1)}(t_f) = 1$. According to the definition of $h(t)$ and Eq. (2.60) and independently of $v(t)$ this leads to: $h(0) = h(t_f) = h'(0) = h'(t_f) = \dots = h^{(2N-2)}(0) = h^{(2N-2)}(t_f) = h^{(2N-1)}(0) = 0$. The $h(t)$ function is required to fulfill also the constraint $h^{(2N-1)}(t_f) = 1$ and the additional constraints $h^{(2N)}(0) = h^{(2N)}(t_f) = 0$. From the constraint $h^{(2N-1)}(t_f) = 1$ and Eq. (2.60), we derive:

$$(2.61) \quad v(t_f) = h^{(2N-1)}(t_f) = 1.$$

Notice that $g^{(2N)}(0)$ and $g^{(2N)}(t_f)$ have the following values (see Eq. (2.59) and Eq. (2.60)):

$$(2.62) \quad g^{(2N)}(0) = (-1)^{2N-1} \frac{2N}{t_f}, \quad g^{(2N)}(t_f) = \frac{(2N)^2}{t_f}.$$

From the condition $h^{(2N)}(0) = 0$ and Eq. (2.60) we derive:

$$(2.63) \quad v(0)g^{(2N)}(0) = -\frac{2N}{t_f}v(0) = h^{(2N)}(0) = 0 \Rightarrow v(0) = 0$$

From the condition $h^{(2N)}(t_f) = 0$ and Eq. (2.60) we derive:

$$(2.64) \quad 2Nv'(t_f) + v(t_f)g^{(2N)}(t_f) = 2Nv'(t_f) + \frac{(2N)^2}{t_f} = h^{(2N)}(t_f) = 0,$$

whence we deduce:

$$(2.65) \quad v'(t_f) = -\frac{2N}{t_f}.$$

We finally arrive at:

$$(2.66) \quad v(0) = 0, \quad v(t_f) = 1, \quad v'(t_f) = -\frac{2N}{t_f}$$

There are three conditions to be satisfied for v therefore v must be at least a 2nd order polynomial:

$$(2.67) \quad v(t) = a_0 + a_1t + a_2t^2.$$

From the boundary conditions set on v we get for the coefficients a_0 , a_1 and a_2 :

$$(2.68) \quad a_0 = 0, \quad a_1 = \frac{1}{t_f}(2+2N), \quad a_2 = -\frac{1}{t_f^2}(1+2N)$$

thus $v(t)$ takes the form:

$$(2.69) \quad v(t) = \frac{t}{t_f} \left[1 + (2N+1) \left(1 - \frac{t}{t_f} \right) \right].$$

Higher order polynomials can work as well. The general form of $v(t)$ of any order is:

$$(2.70) \quad v(t) = \left(\frac{t}{t_f} \right)^n \left[1 + (2N+n) \left(1 - \frac{t}{t_f} \right) \right]$$

where the order $n \geq 1$. For higher orders, Fig. 2.13 remains almost the same. Starting from

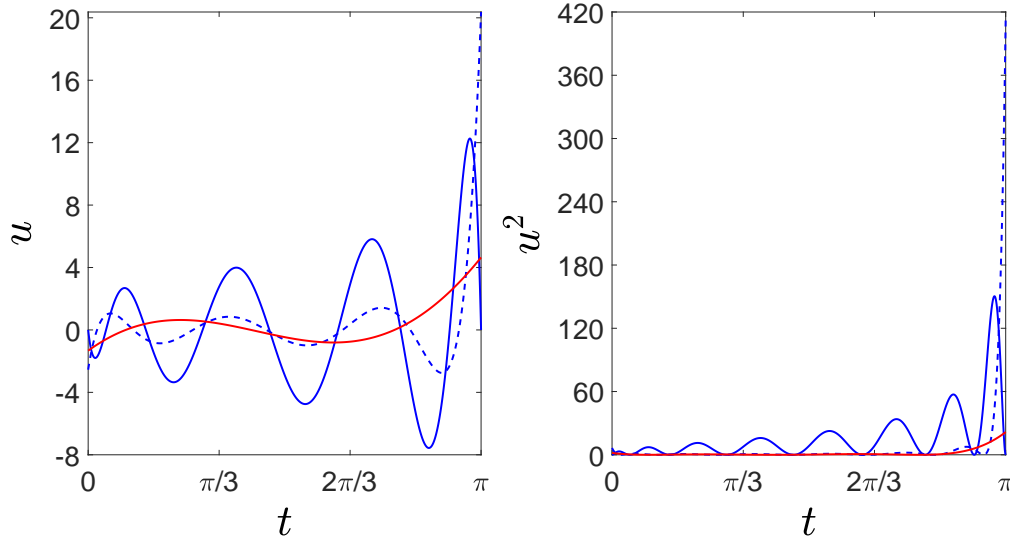


Figure 2.12: The final radii of springs are $r \sim 0.999719$. STA without additional constraints (blue dashed line), STA with additional constraints (blue solid line) and OCT (red solid line) control fields and energies are compared. The parameters are set to $z_0 = (0,0)$, $z_1 = (1,0)$, $t_f = \pi$, $n = 1$, $N = 4$.

$n = 21$ the angular distribution of springs is linear. The $h(t)$ function or the new $g(t)$ function with additional constraints for any order $n \geq 1$ has the following final form:

$$(2.71) \quad g(t) = \frac{(-t_f)^{2N-1}}{(2N-1)!} \left(\frac{t}{t_f} \right)^{2N+n} \left(1 - \frac{t}{t_f} \right)^{2N-1} \left[1 + (2N+n) \left(1 - \frac{t}{t_f} \right) \right]$$

We plot the energies in Fig. 2.12 to graphically show that OCT consumes less energy compared to STA, moreover OCT consumes the least energy among all the possible solutions. It is worth mentioning, however, that we use a specific cost functional and that OCT could minimize the time instead, for instance. The control pulse depicted in Fig. 2.12 can also be applied to steer an ensemble of spins by using the method of mapping spins to springs.

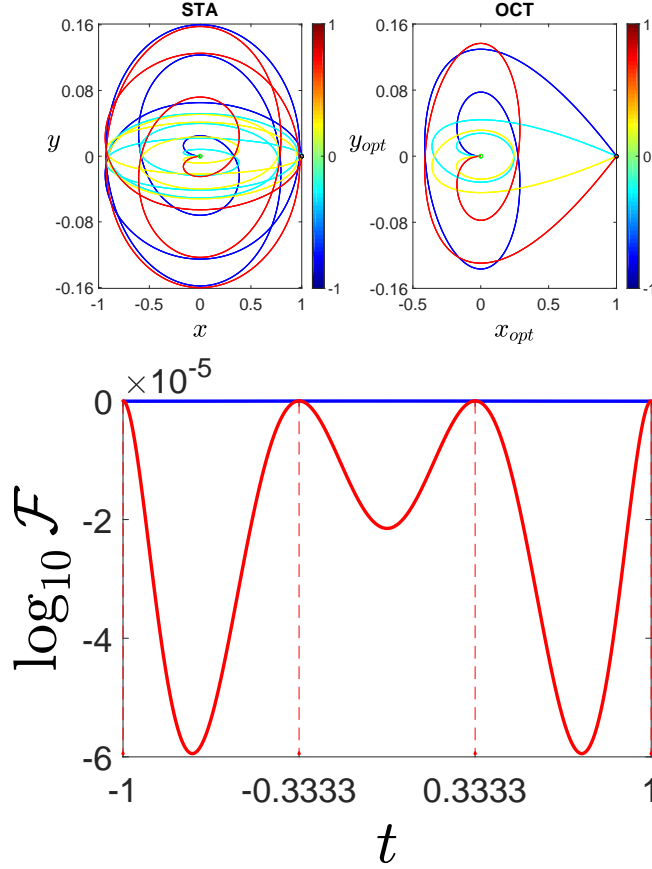


Figure 2.13: **STA** and **OCT** trajectories as well as **STA** (blue) and **OCT** (red) fidelities are compared. The fidelity is defined as $1 - |z_f - z_1|^2$. The order is $n = 1$. $N = 4$ offsets are considered in the frequency range $\Omega \in [-1; 1]$. The control time is $t_f = \pi$, and the initial and target states respectively are $z_0 = (0, 0)$, $z_1 = (1, 0)$. The best performance of the algorithm is reached at the points of intersection of the fidelity curve and the line $\mathcal{F} = 1$.

2.5.2

One Control Input: Spins

Here, we apply the **STA** solution in spin systems. The goal of the control problem, unlike the case of the springs, is to steer the system $\Omega \in [-1; 1]$ in a fixed time $t_f = \pi$ from the initial state $z_0 = (1, 0, 0)$ to the final state $z_1 = (0, 0, 1)$. Although the direction of steering is reversed, the **STA** solution obtained in Subsection 2.5.1 can still be applied by reversing the control field (see Eq. (B.15)). In the simulations, we use the Bloch equations in spherical coordinates. Function g for N offset frequencies without or with additional constraints of any order $n \geq 1$ is given respectively by Eq. (2.59) and Eq. (2.71). The **STA** control field can be expressed in terms of the derivatives of g (see Eq. (2.58)). The fidelity of an ensemble of spins is defined as $\cos(\theta(\omega))$. As we can see in Fig. 2.15, linear approximation of Bloch equations under **STA** pulses for small polar angles is already a good approximation. Note that the control pulses in Fig. 2.14 are the

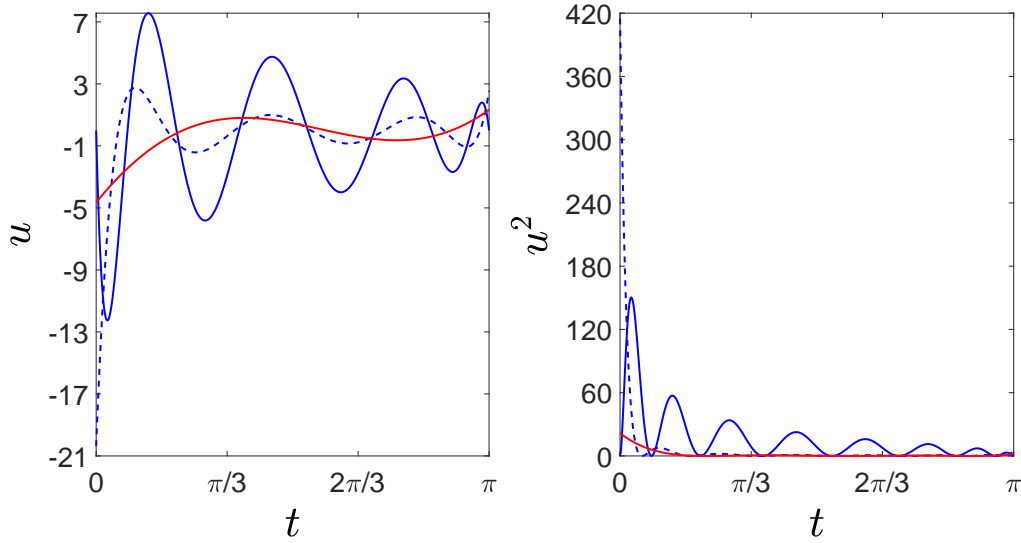


Figure 2.14: The initial and target states respectively are $z_0 = (1, 0)$ and $z_1 = (0, 0)$. $N = 4$ offset frequencies are considered in the frequency range $\Omega \in [-1, 1]$. The control time is $t_f = \pi$. OCT (solid red line) and STA control fields and energies with (solid blue line) and without (dashed blue line) additional constraints are compared. The order is $n = 1$.

negatives of the control pulses in Fig. 2.12 reversed in time. In Sec. 2.5.4 we give a detailed explanation to this.

2.5.3 Two Control Inputs: Springs

We consider in this subsection the control of an ensemble of springs by two control fields $u(t)$ and $v(t)$, $\alpha(t) = u(t) + i v(t)$. The goal of the control procedure is to steer the ensemble of springs from the initial state $z_0 = (0, 0)$ to the final state $z_1 = (1, 0)$. In other words, the goal is to find a solution to the following equation:

$$(2.72) \quad \int_0^{t_f} e^{-i\omega\tau} \alpha(\tau) d\tau = e^{-i\omega t_f}.$$

We first consider the case with two frequencies ω_1 and ω_2 . We assume that the control α can be expressed as:

$$(2.73) \quad \alpha(t) = g^{(2)}(t) - i(\omega_1 + \omega_2)g^{(1)}(t) - \omega_1\omega_2g(t),$$

where $g(t) \in \mathbb{C}$ is an auxiliary function which satisfies the following boundary conditions:

$$g(0) = g(t_f) = 0; g^{(1)}(0) = 0; g^{(1)}(t_f) = 1.$$

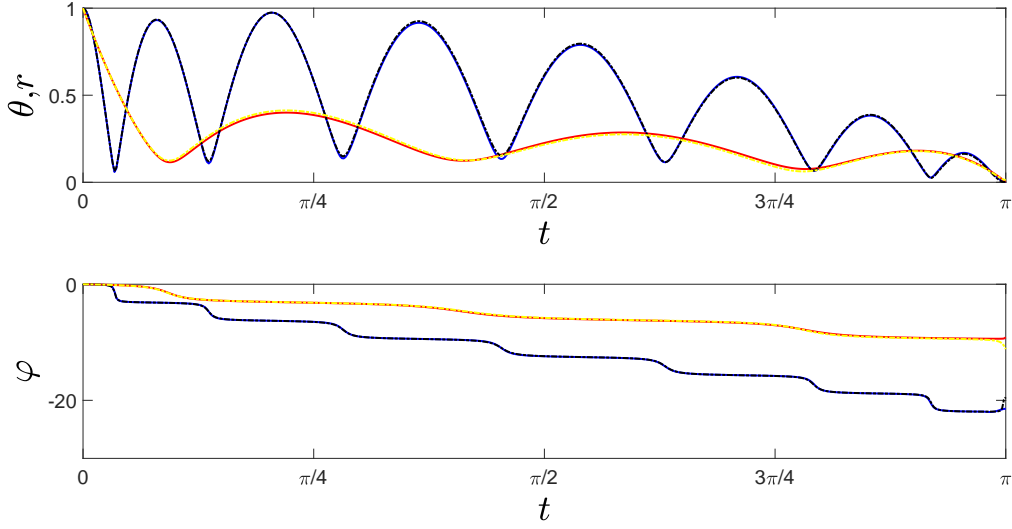


Figure 2.15: The initial and target states respectively are $z_0 = (1, 0)$ and $z_1 = (0, 0)$. $N = 4$ offset frequencies are considered in the frequency range $\Omega \in [-1, 1]$. The control time is $t_f = \pi$. Trajectories of spins (θ, φ) and linear springs (r, φ) are depicted. Red and blue curves correspond respectively to **OCT** and **STA** trajectories of spins, yellow and black dashed curves correspond respectively to **OCT** and **STA** trajectories of linear springs. Additional constraints are taken into account. All curves correspond to the offset frequency $\Omega \approx -0.9519$. The parameter n is set to $n = 1$. The minimum values of **STA** and **OCT** fidelities respectively are $\min(\mathcal{F}^{STA}) \approx 0.9674$ and $\min(\mathcal{F}^{OCT}) \approx 0.9999$.

Substituting $\alpha(t)$ into the left hand side of Eq. (2.72) and integrating by parts we obtain:

$$(2.74) \quad \int_0^{t_f} e^{-i\omega\tau} \alpha(\tau) d\tau = e^{-i\omega t_f} - (\omega - \omega_1)(\omega - \omega_2)G(t_f),$$

where $G(t_f) = \int_0^{t_f} e^{-i\omega\tau} g(\tau) d\tau$. Equation (2.72) is satisfied and thus the control process is performed for both frequencies ω_1 and ω_2 . As a possible $g(t)$ function we can consider:

$$(2.75) \quad g(t) = (-t_f) \left(\frac{t}{t_f} \right)^2 \left(1 - \frac{t}{t_f} \right).$$

The generalization to the case of N offset frequencies leads to the following form of $g(t)$:

$$(2.76) \quad g(t) = \frac{(-t_f)^{N-1}}{(N-1)!} \left(\frac{t}{t_f} \right)^N \left(1 - \frac{t}{t_f} \right)^{N-1}$$

with boundary conditions given by:

$$(2.77) \quad \begin{aligned} g(0) = g(t_f) = g'(0) = g'(t_f) = \dots = g^{(N-2)}(0) = g^{(N-2)}(t_f) = 0 \\ g^{(N-1)}(0) = 0; g^{(N-1)}(t_f) = 1 \end{aligned}$$

The control α will be expressed as:

$$(2.78) \quad \alpha(t) = \sum_{k=1}^{N+1} P_{k-1} g^{(N-k+1)}(t),$$

where P_k are the coefficients of the characteristic polynomial of the matrix $W = -\text{diag}(-i\omega_i)_{i=1}^N$.

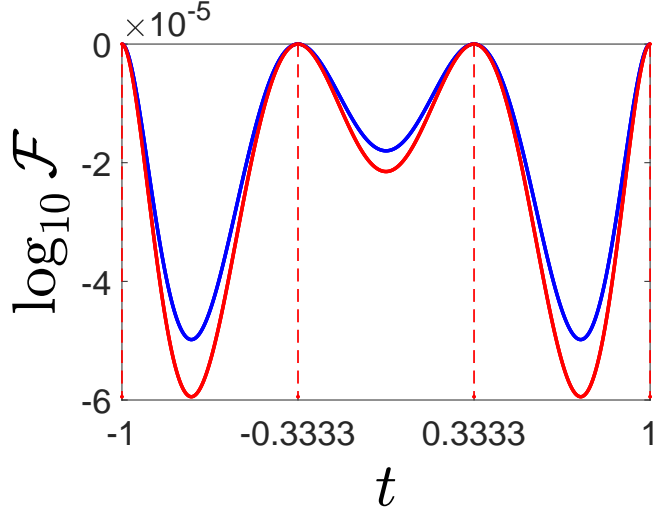


Figure 2.16: $N = 4$ offset frequencies are considered in the frequency range $\Omega \in [-1; 1]$. The control time is $t_f = \pi$. The initial and target states respectively are $z_0 = (0, 0)$, $z_1 = (1, 0)$. STA fidelity (blue line), OCT fidelity (red line) are depicted. The fidelity is defined as $\mathcal{F} = 1 - |z_f - z_1|^2$. STA is the one without additional constraints. Two control inputs are considered.

At order N , we have $2N$ constraints to fulfill, thus we have to consider at least a polynomial of order $2N - 1$. The behavior of the control field at $t = 0$ and t_f can be adjusted by adding some new constraints: $g^{(N)}(0) = g^{(N)}(t_f) = 0$. This way we ensure to have $\alpha(t) = 0$ at the initial and final times. We thus need another function $h(t) = \eta(t)g(t)$ which will satisfy the additional constraints alongside with others. Here η is an auxiliary finite-value function. The steps that lead to the derivation of the function $\eta(t)$ are similar to the ones taken in Subsec. 2.5.1:

$$(2.79) \quad \eta(t) = \frac{t}{t_f} \left[1 + (N+1) \left(1 - \frac{t}{t_f} \right) \right].$$

Higher order polynomials can work as well. The general form of $\eta(t)$ of any order is:

$$(2.80) \quad \eta(t) = \left(\frac{t}{t_f} \right)^n \left[1 + (N+n) \left(1 - \frac{t}{t_f} \right) \right]$$

where the order $n \geq 1$. In the next simulations parameters are the same as for the latter. The $h(t)$ function or the new $g(t)$ function with additional constraints for any order $n \geq 1$ has the

following final form:

$$(2.81) \quad g(t) = \frac{(-t_f)^{N-1}}{(N-1)!} \left(\frac{t}{t_f}\right)^{N+n} \left(1 - \frac{t}{t_f}\right)^{N-1} \left[1 + (N+n) \left(1 - \frac{t}{t_f}\right)\right]$$

Notice that STA fidelity increases as we increase the order n (see Fig. 2.17). It is worth noticing

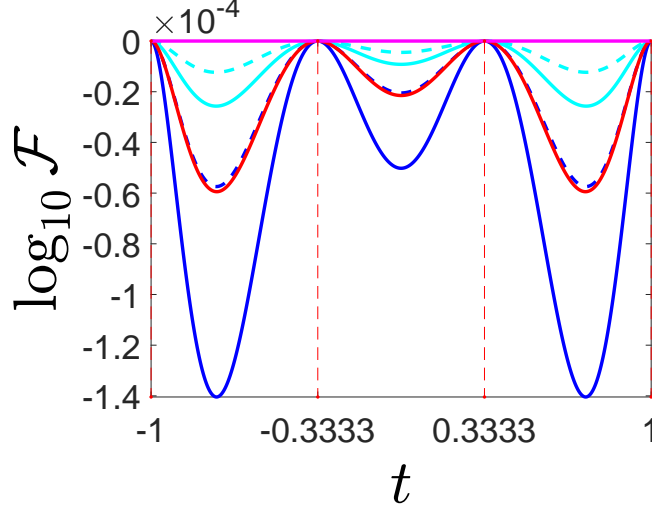


Figure 2.17: $N = 4$ offset frequencies are considered in the frequency range $\Omega \in [-1; 1]$. The control time is $t_f = \pi$. The initial and target states respectively are $z_0 = (0, 0)$, $z_1 = (1, 0)$. The fidelity is defined as $1 - |z_f - z_1|^2$. OCT fidelity (red line), STA fidelities of the orders $n = 1$ (blue line), $n = 2$ (dashed blue line), $n = 3$ (cyan line), and $n = 4$ (dashed cyan line) are depicted.

that the fidelity is higher in the case of one control compared to the case with two controls. When one control is unavailable, the frequency of the pulse is higher, and so is the full width in the reciprocal space [87]. In other words, in the latter case the pulse is in resonance with a wider range of frequencies, and therefore the fidelity is higher.

2.5.4 Two Control Inputs: Spins

Here, we apply the STA solution in spin systems. The goal of the control problem, unlike the case of the springs, is to steer the system $\Omega \in [-1, 1]$ in a fixed time $t_f = \pi$ from the initial state $z_0 = (1, 0, 0)$ to the final state $z_1 = (0, 0, 1)$. Although the direction of steering is reversed, the STA solution obtained in the previous section can still be applied by reversing the control field (see Eq. (B.15)). In the simulations, we use the modified form of Bloch equations (see Eq. (2.49)). Function g for N offset frequencies without or with additional constraints of any order $n \geq 1$ is given respectively by Eq. (2.76) and Eq. (2.81). The STA control field can be expressed in terms of the derivatives of function g (see Eq. (2.78)). Linear approximation of the Bloch equations is already satisfying also in the case of two controls as it is illustrated in Fig. 2.20. The control pulse of Fig. 2.19 is the negative of the one in Fig. 2.18 reversed in time.

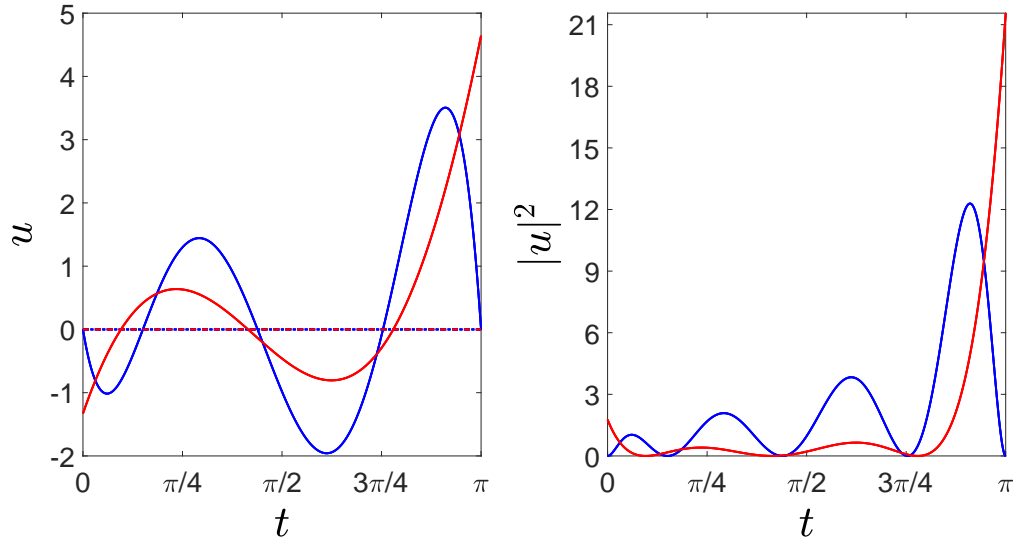


Figure 2.18: $N = 4$ offset frequencies are considered in the frequency range $\Omega \in [-1; 1]$. The control time is $t_f = \pi$. The initial and target states respectively are $z_0 = (0, 0)$, $z_1 = (1, 0)$. **OCT** and **STA** control fields and energies are compared. Solid red, dashed red, solid blue and dashed blue curves correspond respectively to **OCT** (u_x or $|u|^2$), **OCT** (u_y), **STA** (u_x or $|u|^2$) and **STA** (u_y) solutions. The order is $n = 1$. The mean value of radii is $\langle r \rangle \sim 1.002$.

2.5.5 Continuous Case

Here we consider a control problem of an ensemble of springs. The goal is to steer the ensemble from $z_\omega(0) = 0$ to $z_\omega(t_f) = 1$. With these initial and target states the evolution of the system must satisfy the following integral equation:

$$(2.82) \quad e^{i\omega t_f} = \int_0^{t_f} e^{i\omega\tau} u(\tau) d\tau,$$

for $\omega \in [\omega_{min}, \omega_{max}]$. Until here we discretized the range of frequencies. Otherwise the **STA** and **OCT** solutions would coincide. Here, we show the existence and the uniqueness of the control solution for a continuous set of frequencies. A different proof was given in [88]. We assume that $u \in L^2([0, t_f])$, i.e., u is a square integrable function with a compact support included in the interval $[0, t_f]$, u is zero outside of this interval. Its Fourier transform \hat{u} is an analytic function which is known over the interval $[\omega_{min}, \omega_{max}]$. Since the zeros of a nonzero analytic function are isolated, we deduce that there is at most one solution to Eq. (2.82). Indeed, if we consider two solutions u_1 and u_2 to that, then $\hat{u}_1 - \hat{u}_2$ is zero over $[\omega_{min}, \omega_{max}]$, which contradicts the previous result. The map \mathbf{F} defined by

$$L^2([0, t_f]) \rightarrow L^2([\omega_{min}, \omega_{max}]),$$

$$u \rightarrow \hat{u}|_{[\omega_{min}, \omega_{max}]}$$

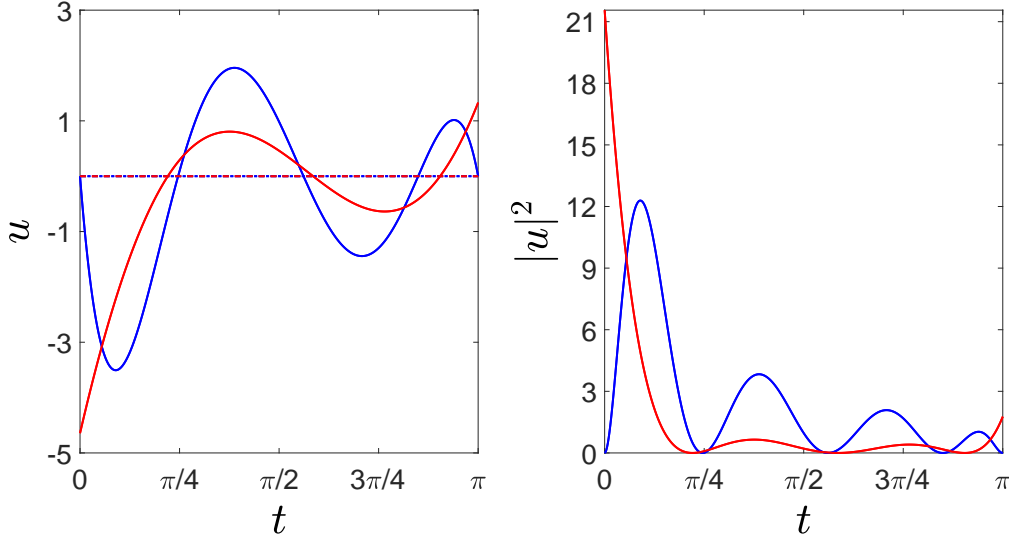


Figure 2.19: The initial and the target states respectively are $z_0 = (1, 0)$, $z_1 = (0, 0)$. $N = 4$ offset frequencies are considered in the frequency range $\Omega \in [-1, 1]$. The control time is $t_f = \pi$. **OCT** and **STA** control fields and energies are compared. The fidelity of an ensemble of spins is defined as $\cos(\theta(\omega))$. Solid red, dashed red, solid blue and dashed blue curves correspond respectively to **OCT** (u_x or $|u|^2$), **OCT** (u_y), **STA** (u_x or $|u|^2$) and **STA** (u_y) solutions. **STA** solution is with additional constraints. The order is $n = 1$. The **STA** fidelity is $\mathcal{F} \sim 0.9998$ and the **OCT** fidelity $\mathcal{F} \sim 0.999943$.

is thus injective. The surjectivity of \mathbf{F} can be described from the Paley-Wiener theorem which states the following property. The function \hat{u} fulfills the condition

$$|\hat{u}(\omega)| \leq C e^{t_f |\omega|},$$

where $C > 0$, if and only if there exists $u \in L^2([0, t_f])$ such that

$$\hat{u}(\omega) = \int_0^{t_f} e^{-i\omega\tau} u(\tau) d\tau$$

and we can choose $C = \int_0^{t_f} |u(\tau)| d\tau$. Satisfying the conditions of this theorem by a judicious choice of target states ensures the existence of a solution to Eq. 2.82. In the example under study, this condition is fulfilled since $|\hat{u}(\omega)| = |e^{i\omega t_f}| = 1$.

To summarize, these results establish the existence and uniqueness of an ideal mathematical control field $u(t)$ for a continuous set of frequencies. However, for practical applications, it is more interesting to consider a finite set and to take into account additional constraints on the control field. This idea has been developed for **OCT** and **STA** procedures in the previous sections where the set of frequencies is discretized. Note that the two fields converge toward the same solution when the discretization step goes to 0.

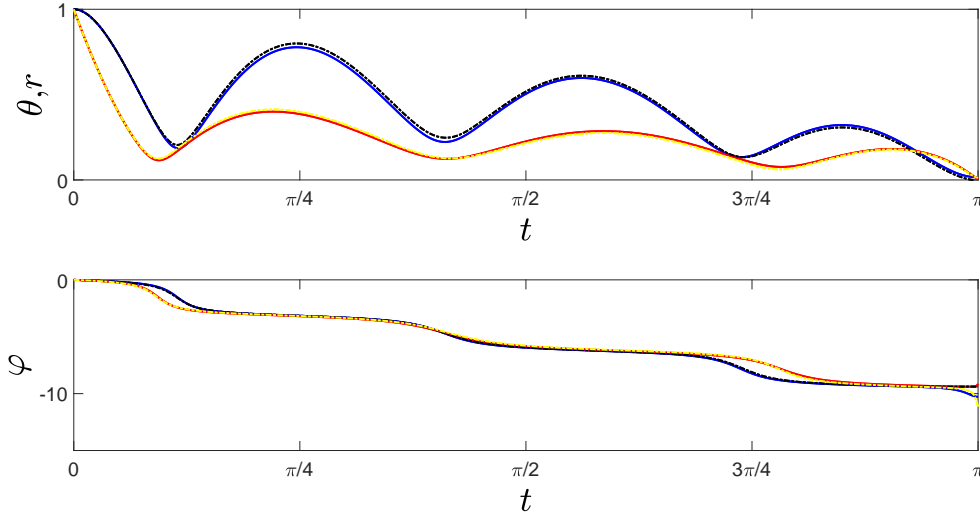


Figure 2.20: The initial and the target states respectively are $z_0 = (1, 0)$, $z_1 = (0, 0)$. $N = 4$ offset frequencies are considered in the frequency range $\Omega \in [-1, 1]$. The control time is $t_f = \pi$. Trajectories of spins (θ , φ) and linear springs (r , φ) are depicted. Red and blue curves correspond respectively to **OCT** and **STA** trajectories of spins, yellow and black dashed curves correspond respectively to **OCT** and **STA** trajectories of linear springs. **STA** solution is with additional constraints. The order n is set to $n = 1$. All curves correspond to the offset frequency $\Omega \approx -0.9519$.

Summary

- We have introduced **STA** control pulses with motion planning approach to control an ensemble of springs and applied them to an ensemble of spins. This is also a good demonstration of the applicability of the method of mapping spins to springs even under not optimal forcing.
- We have discussed the case of one control and two control components. The algorithm is different for these two cases. The **STA** fidelity of one control input is higher than that of two control inputs.
- We have also compared the **STA** and **OCT** solutions. In the case of one control, the **STA** fidelity is higher than the **OCT** fidelity. In the case of two controls, starting from the order $n = 2$ the **STA** fidelity is higher than the **OCT** fidelity for the particular parameters we consider since the **OCT** objective is to minimize the energy but not to maximize the fidelity.
- We have discussed the important case of continuous set of frequencies and proved the existence and uniqueness of the control field.

2.6 Pulses

The ultimate goal of ensemble control theory is to develop a route to steer an ensemble of systems between the given initial and target distributions of states. This problem can be broken into smaller parts. To this end, we design a broadband, narrowband ultrahigh fidelity and selective pulses. Broadband pulses are robust with respect to a wide range of frequencies. The narrowband pulses that we consider are robust and hold an ultrahigh fidelity with respect to a narrow range of frequencies. Selective pulses steer a specific range of frequencies while not affecting the outsiders. In this section, we also derive an adiabatic pulse.

2.6.1 Excitation Pulse

Our goal in Sec. 2.5.1 is to steer an ensemble of springs from $z_0 = (0, 0)$ to $z_1 = (1, 0)$ in a fixed time t_f . To drive an ensemble from $z_0 = (0, 0)$ to $z_1 = (\pi/2, 0)$ instead (see Fig. 2.5.1), we have to introduce some modifications into the dynamics. There is no need to go through the calculations again. It is sufficient to rewrite the modified equations for this case. Equation (2.53) reads:

$$(2.83) \quad \int_0^{t_f} e^{-i\omega\tau} u(\tau) d\tau = \frac{\pi}{2} e^{-i\omega t_f}.$$

Equations (2.54), (2.55) respectively read:

$$(2.84) \quad u(\tau) = \frac{\pi}{2} \left(g^{(4)}(\tau) + (\omega_1^2 + \omega_2^2) g^{(2)}(\tau) + \omega_1^2 \omega_2^2 g(\tau) \right)$$

$$(2.85) \quad \int_0^{t_f} e^{-i\omega\tau} u(\tau) d\tau = \frac{\pi}{2} e^{-i\omega t_f} + \frac{\pi}{2} (\omega^2 - \omega_1^2) (\omega^2 - \omega_2^2) G(t_f).$$

For the general case of N offsets Eq. (2.58) will read:

$$(2.86) \quad u(t) = \frac{\pi}{2} \sum_{k=1}^{N+1} P_{k-1} g^{2(N-k+1)}(t).$$

Similarly Eq. (2.55) will be modified into:

$$(2.87) \quad \int_0^{t_f} e^{-i\omega\tau} u(\tau) d\tau = \frac{\pi}{2} e^{-i\omega t_f} + \frac{\pi}{2} \prod_{k=1}^N (\omega^2 - \omega_k^2) G(t_f).$$

The rest of the discussions and equations in Sec. 2.5.1 remain unchanged.

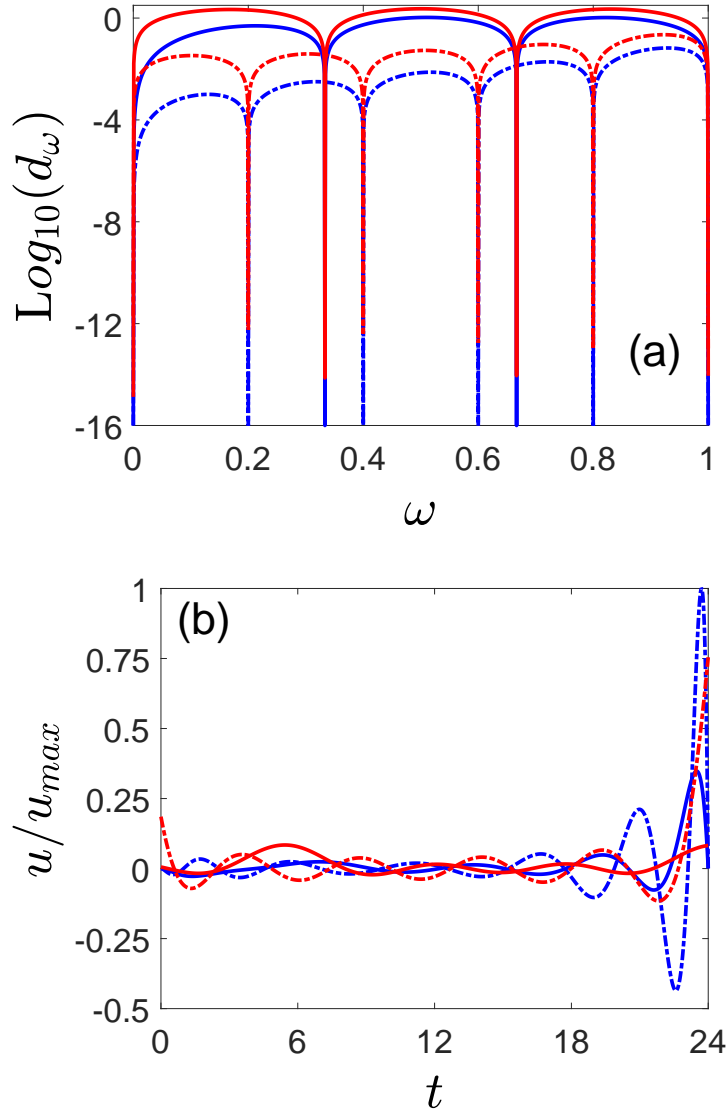


Figure 2.21: The control time is set to $t_f = 24$, $z_0 = (0, 0)$, $z_1 = (\pi/2, 0)$. Dimensionless units are used. STA with additional constraints (blue line) and optimal (red line) excitations of an ensemble of springs are illustrated in the range of frequencies $\Omega \in [0, 1]$. The pulses have been computed for a regular distribution of $N = 4$ (solid line) and $N = 6$ (dashed line) springs. Panels (a) and (b) display, respectively, the distance to the target state $d_\omega = \left| \frac{\pi}{2} (\omega^2 - \omega_1^2) (\omega^2 - \omega_2^2) G(t_f) \right|$ and the corresponding control fields.

We can also go backwards, in other words from $z_0 = (\pi/2, 0)$ to $z_1 = (0, 0)$. In order to do that, we just need to reverse the control field in time and take its negative value as indicated in Sec. B.2).

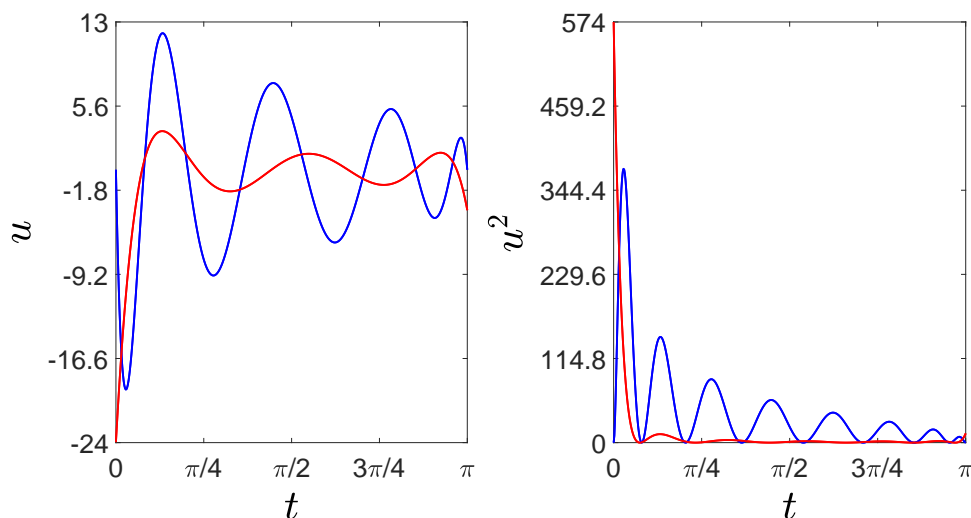


Figure 2.22: STA (blue line) and OCT (red line) pulses and energies are compared. The surface areas under the squares of control pulses indicate the magnitudes of energies. As one could anticipate, $E_{OCT} < E_{STA}$. $N = 4$ regularly distributed springs (harmonic oscillators) are considered in the range of frequencies $\Omega \in [0, 1]$. Control time is set to $t_f = \pi$. The order is $n = 1$. The initial and target states are $z_0 = (\pi/2, 0)$ and $z_1 = (0, 0)$.

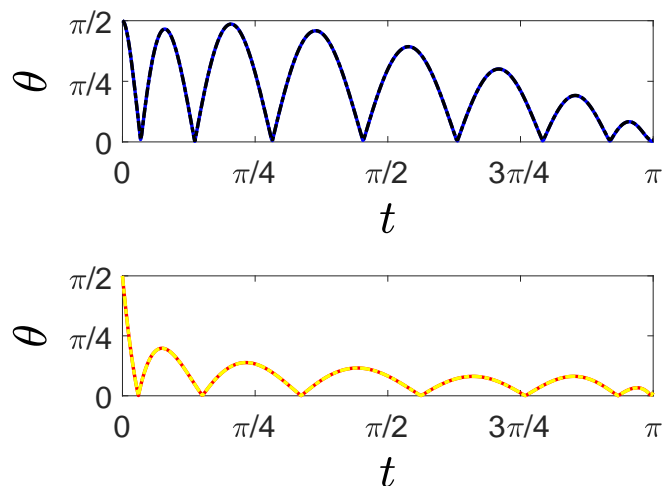


Figure 2.23: STA (blue and black lines) and OCT (red and yellow lines) trajectories of spins are depicted. The exact dynamical equation (blue and red lines) and linear approximation are used (black and yellow lines). $N = 4$ regularly distributed springs (harmonic oscillators) are considered in the range of frequencies $\Omega \in [0, 1]$. Control time is set to $t_f = \pi$. The order n is set to $n = 1$. The initial and the target states are $z_0 = (\pi/2, 0)$ and $z_1 = (0, 0)$. All curves correspond to the offset frequency $\Omega \approx 0.024$.

Although OCT solution corresponds to the minimum energy but at the endpoints the

maximum amplitude could be very large. It is not the case for the [STA](#) pulse due to the boundary constraints we additionally impose on the solution (see [Fig. 2.22](#)). The pulse depicted in [Fig. 2.22](#) steers the spins from the equatorial plane to the north pole (see [Fig. 2.23](#)).

2.6.2 Concatenated Pulse

Here we present a practical tool to design an efficient control pulse for an ensemble of spins. The symmetry of the Bloch equations and the dynamics of springs entail two important properties of control pulses which are discussed in the next lines. To interchange the initial and target states, we have to inverse the pulse in time and take its negative value:

$$(2.88) \quad v(t) = -u(t_f - t).$$

To inverse the direction of steering from the equatorial plane, we have to take the negative value of the control pulse:

$$(2.89) \quad v(t) = -u(t).$$

In summary, we can inverse spins by applying a π pulse or 2 successive $\pi/2$ pulses. When steering the spins from the north pole to the south pole, the two successive $\pi/2$ pulses are $u_{\pi/2}(t)$ and $u_{\pi/2}(t_f - t)$. To apply these pulses, we first give a formal solution of the Bloch equations. Equation (2.42) with $v = 0$ can be rewritten in the following form:

$$(2.90) \quad \frac{d}{dt} \begin{bmatrix} M_x \\ M_y \\ M_z \end{bmatrix} = \omega \begin{bmatrix} 0 & -1 & 0 \\ 1 & 0 & 0 \\ 0 & 0 & 0 \end{bmatrix} \begin{bmatrix} M_x \\ M_y \\ M_z \end{bmatrix} + u \begin{bmatrix} 0 & 0 & 1 \\ 0 & 0 & 0 \\ -1 & 0 & 0 \end{bmatrix} \begin{bmatrix} M_x \\ M_y \\ M_z \end{bmatrix}$$

We can give a more compact form to it by denoting:

$$\begin{bmatrix} M_x \\ M_y \\ M_z \end{bmatrix} := \vec{M}, \quad \begin{bmatrix} 0 & -1 & 0 \\ 1 & 0 & 0 \\ 0 & 0 & 0 \end{bmatrix} := R_z, \quad \begin{bmatrix} 0 & 0 & 1 \\ 0 & 0 & 0 \\ -1 & 0 & 0 \end{bmatrix} := R_y$$

We finally arrive at:

$$(2.91) \quad \dot{\vec{M}} = \omega R_z \vec{M} + u R_y \vec{M}$$

or

$$(2.92) \quad \dot{\vec{M}} = (\omega R_z + u R_y) \vec{M}.$$

In a very short period of time dt , the control pulse u can be treated as a constant. In other words, we assume that the control pulse is a piece-wise constant function, which is a common

assumption in NMR control problems. With this said, we can represent the solution in the following way:

$$(2.93) \quad \vec{M}(t+dt) = e^{(\omega R_z + u(t)R_y)dt} \vec{M}(t).$$

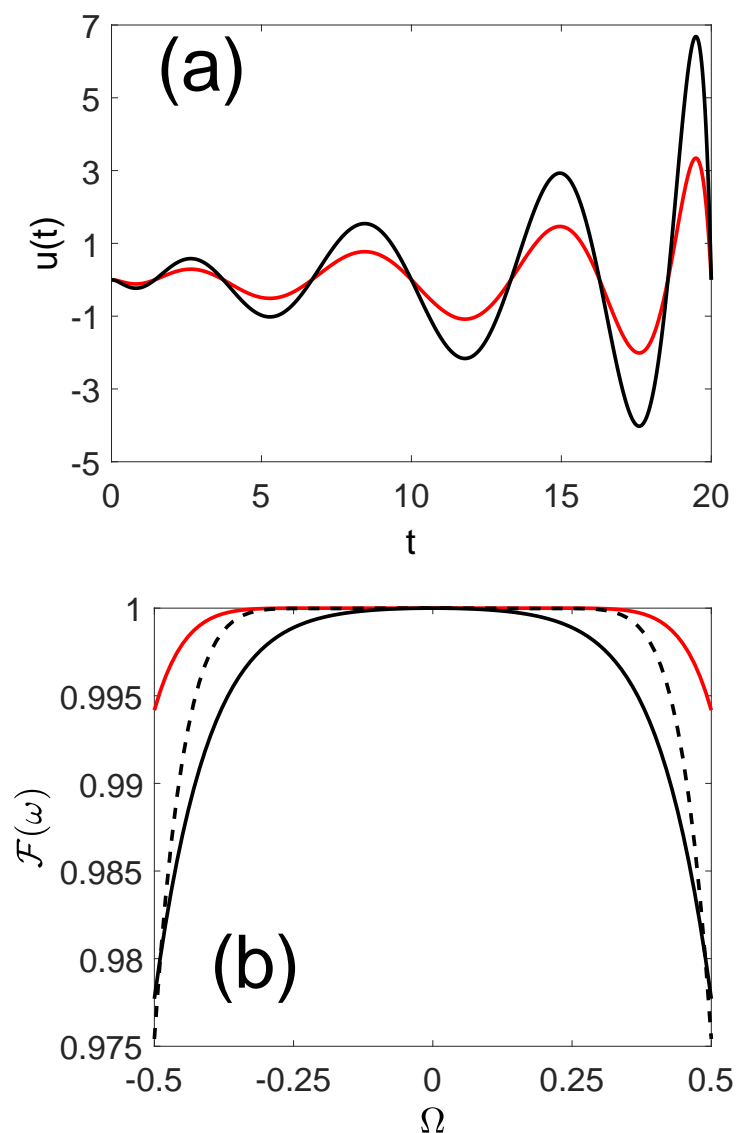


Figure 2.24: $N = 4$ equal offsets are considered $\omega_1 = \omega_2 = \omega_3 = \omega_4 = 0$. The control time is set to $t_f = 20$. $\pi/2$ (red solid line) and π (black solid line) STA pulses are compared in label (a) and the corresponding ultrahigh fidelities in label (b). The efficiency of two successive $\pi/2$ pulses is depicted in label (b) with black dashed line. The order is $n = 2$.

Using Eq. (2.93) with iterative steps, we compute the final state of the spins. The linear approximation of Bloch equations is valid for small polar angles. This is why, the fidelity of the π pulse is the least in Fig. 2.24. The linear approximation works sufficiently well for $\pi/2$ pulses.

Although the control duration is twice as long for the concatenated pulses but it works better as the conditions of the linear approximation are sufficiently well satisfied (see Fig. 2.24). This way by applying successive pulses, which change the polar angle not more than by $\pi/2$, we can achieve any state on the Bloch sphere.

2.6.3 Selective Control Pulses

We recall the dynamics of an ensemble of springs (see Eq. (2.21)) with dispersion in natural frequencies. The controllability conditions are satisfied given that the control pulse is homogeneous and both control inputs are available [76, 77, 80, 88].

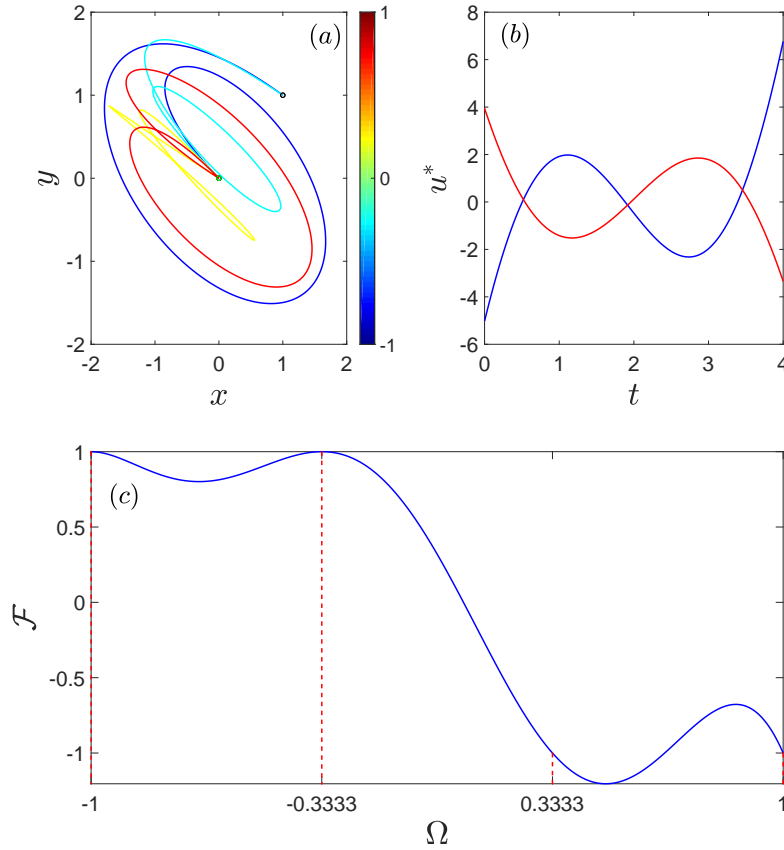


Figure 2.25: $N = 4$ offsets ω_i are regularly distributed in the frequency range $\Omega \in [-1; 1]$. In panel (a) the trajectories of springs are depicted. The positive offsets remain in the initial state $z_0 = 0$ while the negative offsets are driven to the target state $z_1 = 1 + i$. The control inputs are illustrated in panel (b). The fidelity is depicted in panel (c) and is defined as $\mathcal{F} = 1 - |z(\Omega, T) - z_1|^2$ such that the maximum efficiency for the positive frequencies is reached when the fidelity is 1 while for the negative frequencies when the fidelity is -1. The control time is set to $T = 4$.

Here we derive selective compensating pulses which compensate against the dispersion in

natural frequencies and are selective with respect to frequencies. The results we obtained in Sec. 2.2.1 remain unchanged with a single difference that now the initial and target states depend on the offset ω_i . In our simulations, we drive an ensemble of springs from a fixed point z_0 to z_{if} that depends on the offset. The fidelity thus depends on offsets. Figures 2.25 and

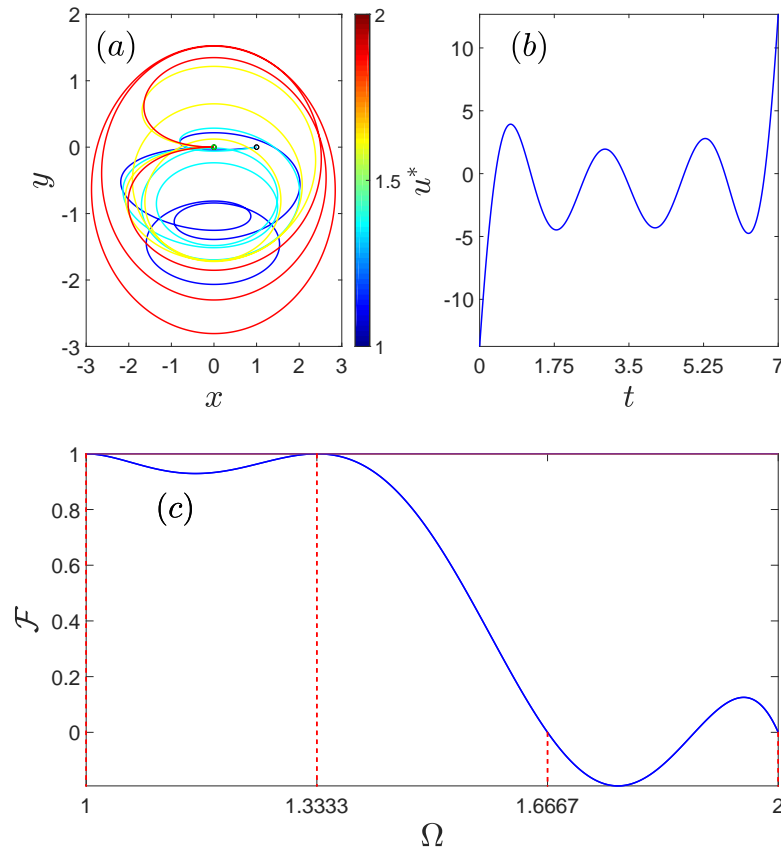


Figure 2.26: $N = 4$ offsets ω_i are regularly distributed in the frequency range $\Omega \in [1;2]$. In panel (a) the trajectories of springs are depicted. The high frequency offsets remain in the initial state $z_0 = \mathbf{0}$ while the low frequency offsets are driven to the target state $z_1 = \mathbf{1}$. The control input is illustrated in panel (b). The fidelity is depicted in panel (c) and is defined as $\mathcal{F} = 1 - |z(\Omega, T) - z_1|^2$ such that the maximum efficiency for the high frequencies is reached when the fidelity is 0 while for the low frequencies when the fidelity is 1. The control time is set to $T = 7$. One control input is sufficient to reach the control objective since here we consider only positive frequencies.

2.26 are given here as illustrative examples. The control pulses are optimal with respect to the energy. Various distributions of target states are achievable. For instance, we can also drive an ensemble of springs without affecting a single spring or vice versa.

2.6.4 Adiabatic Control

Adiabatic control is one of the widely used protocols in control theory [40–43]. It can be expressed as a chirped excitation pulse:

$$(2.94) \quad u(t) = u_0 \cos \left[\omega_0 t + \frac{st^2}{2} \right],$$

where u_0 is the pulse amplitude, ω_0 the initial frequency and s is the sweep rate. We calculate the time evolution of an ensemble of springs both by the stationary phase approximation and by using the Fresnel or imaginary error functions. We assume that $z_0(\omega) \equiv \mathbf{0}$ for all springs. The stationary phase approximation is presented in Sec. C.3. The approximated time evolution of an ensemble of springs is expressed in the following way (see Eqs. (C.22), (C.23)):

$$(2.95) \quad z_\omega(t_f) = e^{i\omega t_f} \int_0^{t_f} e^{-i\omega\tau} u(\tau) d\tau \simeq e^{i\omega t_f} u_0 \sqrt{\frac{\pi}{2s}} e^{i\left(\frac{\pi}{4} - \frac{(\omega - \omega_0)^2}{2s}\right)}.$$

We can, however, express the precise evolution

$$(2.96) \quad z_\omega(t_f) = \frac{u_0}{2} e^{i\omega t_f} \int_0^{t_f} \left(e^{i\left[\frac{st^2}{2} + (\omega_0 - \omega)t\right]} + e^{-i\left[\frac{st^2}{2} + (\omega_0 + \omega)t\right]} \right) dt$$

via the Fresnel or \mathcal{K} function as we have mentioned above (see Sec. C.1):

$$(2.97) \quad z_\omega(t_f) = \frac{u_0}{2} e^{i\omega t_f} \left[\mathcal{K} \left(\frac{s}{2}, \omega_0 - \omega \right) + \mathcal{K} \left(-\frac{s}{2}, -\omega_0 - \omega \right) \right].$$

It is worth to notice that $z_{-\omega}(t_f) = \overline{z_\omega(t_f)}$, and therefore $|z_{-\omega}(t_f)| = |z_\omega(t_f)|$. After the adiabatic excitation, all the springs have almost the same radius $|z_\omega(t_f)|$, but a different phase $\text{Arg}[z_\omega(t_f)]$, which can be expressed as

$$(2.98) \quad \text{Arg} [z_\omega(t_f)] = \omega t_f + \frac{\pi}{4} - \frac{(\omega - \omega_0)^2}{2s}.$$

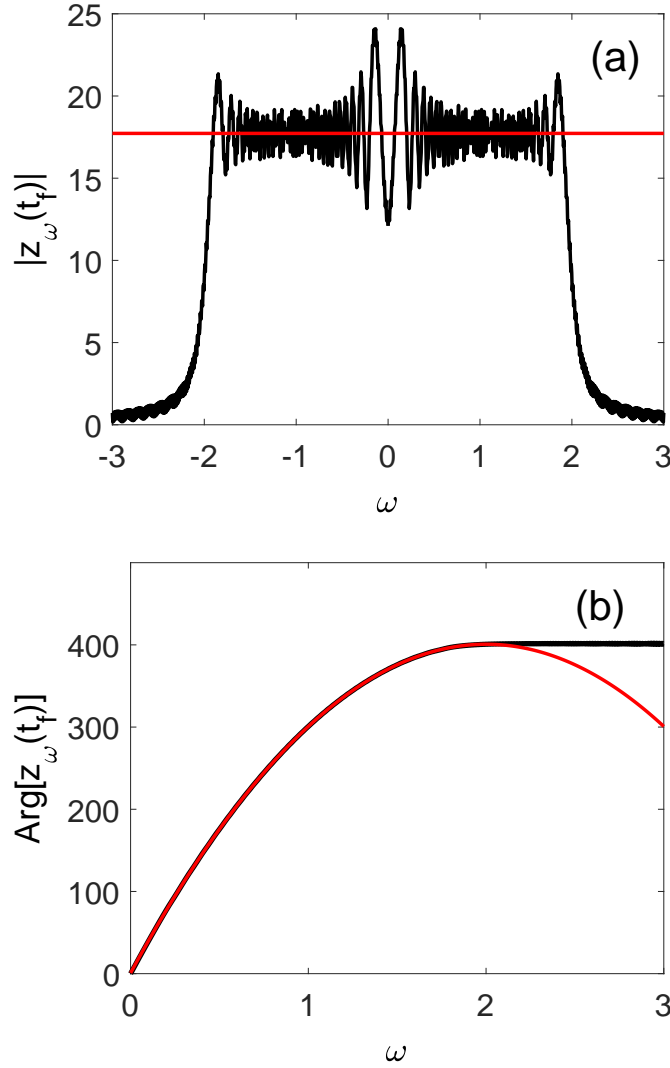


Figure 2.27: Evolution as a function of ω of the radius (a) and phase (b) of an ensemble of springs with $\omega \in [-3, 3]$. The parameters of the adiabatic control field $u(t)$ are set to $u_0 = 1$, $t_f = 400$, $\omega_0 = 0$, $\omega_f = 2$, and $s = \frac{\omega_f - \omega_0}{t_f}$. The solid red (dark gray) lines correspond to the stationary phase approximation, and the solid black lines correspond to the exact solution expressed in terms of the function \mathcal{K} . Only the positive frequencies are plotted for the argument of $z(t_f)$. The different quantities are dimensionless.

As can be seen in Eq. (2.98), this phase is not constant and varies quadratically with the frequency ω . The radius which can be expressed as

$$(2.99) \quad |z_\omega(t_f)| = u_0 \sqrt{\frac{\pi}{2s}}$$

can be fixed by adjusting either the amplitude of the pulse u_0 or the sweeping rate s . A numerical example is given in Fig. 2.27, showing the accuracy of the adiabatic approximation for a long control time t_f in the range of excited springs. The main problem with this approach

is its lack of flexibility since only a specific family of target states can be reached. This adiabatic solution will be used in Chapter 3 for FT-ICR applications.

2.6.5 Optimal Control

In this subsection we add a parameter λ to account the weight of energy as opposed to the distance from the target state in the minimization process [68, 89–91]. We refer the reader to the standard references [68, 90, 92] for technical details. We consider an approach where the distance to the target states (for a finite set of frequencies ω) is defined in the cost functional \mathcal{C} to minimize. The cost functional \mathcal{C} can be expressed as

$$(2.100) \quad \mathcal{C} = \frac{1}{2} \sum_k \left([x_k(t_f) - x_{kf}]^2 + [y_k(t_f) - y_{kf}]^2 \right) + \frac{\lambda}{2} \int_0^{t_f} u^2 dt$$

where λ is a positive penalty factor chosen to weight the importance of the pulse energy. The Pontryagin Hamiltonian is

$$(2.101) \quad H_p = \sum_k \Re [i\omega_k z_k \bar{p}_k + p_k u] - \frac{\lambda u^2}{2}$$

and the optimal control is given by

$$(2.102) \quad u^* = \frac{1}{\lambda} \sum_k \Re [p_k].$$

The time evolution of p_k can be expressed as

$$(2.103) \quad p_k(t) = p_k(0) e^{i\omega_k t} = p_k(t_f) e^{i\omega_k(t-t_f)}$$

with the final condition

$$p_k(t_f) = z_{kf} - z_k(t_f).$$

After straightforward computation, we deduce that

$$\frac{2\lambda}{t_f} z_j(t_f) = \sum_k \left(e^{i(\omega_j - \omega_k)t_f/2} \operatorname{sinc} \left[\frac{(\omega_j - \omega_k)t_f}{2} \right] p_k(t_f) + e^{i(\omega_j + \omega_k)t_f/2} \operatorname{sinc} \left[\frac{(\omega_j + \omega_k)t_f}{2} \right] \bar{p}_k(t_f) \right),$$

which can be expressed as

$$(2.104) \quad \frac{2\lambda}{t_f} z_j(t_f) = \sum_k \left(C_{jk} [z_{kf} - z_k(t_f)] + D_{jk} [\bar{z}_{kf} - \bar{z}_k(t_f)] \right),$$

with

$$(2.105) \quad C_{jk} = e^{i(\omega_j - \omega_k)t_f/2} \operatorname{sinc} \left[\frac{(\omega_j - \omega_k)t_f}{2} \right],$$

$$(2.106) \quad D_{jk} = e^{i(\omega_j + \omega_k)t_f/2} \operatorname{sinc} \left[\frac{(\omega_j + \omega_k)t_f}{2} \right].$$

Equation (2.104) and its complex conjugate give the dynamical state at time t_f , and thus the final adjoint state. We then obtain the control field $u(t)$. Numerical results with this approach are provided in Subsecs. 3.2.2, 3.2.3.

Summary

- The $\pi/2$ pulse has been derived and applied to an ensemble of spin systems.
- The concatenated pulses have appeared to have ultra-high fidelity and be more robust with respect to Larmor dispersion than a simple inversion pulse.
- We have achieved selectivity frequency-wise.
- It is possible to control the final radius of springs by adiabatic excitation simply adjusting the control amplitude and sweep rate.
- We obtain the optimal pulse with a second approach by introducing the distance to the target state and balancing the weight of energy in the optimization process.

2.7

Conclusions

We have reviewed in this study different approaches to control the dynamics of an inhomogeneous ensemble of springs. The different methods presented in this chapter can be used in any linear control system. They also provide interesting alternatives to design pulses controlling two-level quantum systems. We have shown the relative advantages and drawbacks of STA and OCT protocols. OCT minimizes the energy consumption, but in contrary we have less control over the pulse behavior at initial and final times. On the other hand, we can impose additional boundary constraints on STA solutions at the endpoints of time interval. Moreover, in some cases STA control pulses appear to be more robust against dispersion of Larmor frequencies. Any target state and control duration can be formally chosen, which can lead, e.g., to robust or selective control protocols. In order to satisfy experimental limitations on the shape of the control field, additional constraints have to be accounted for. For the two methods, only a finite set of frequencies (with a regular discretization) are considered. This frequency set can be optimized in a practical application to improve the efficiency of the control process. The efficiency of the derived control fields is comparable. Another future research direction is the extension of this approach to other nonlinear dynamical systems. From a mathematical point of view, this method can be applied in a neighborhood of a fixed point of the dynamics. A major limitation of this idea is related to the size of the region around the fixed point that can be considered to reach the target state with a given accuracy. As shown in this study, this size is quite large for a two-level quantum system because robust or selective excitation processes can

be realized from the linearized system. This characteristic is not known a priori and has to be determined in each practical case.

Ion Cyclotron Resonance Mass Spectrometry

This chapter is dedicated to the investigation of the efficiency of optimal control techniques in Two Dimensional (2D) FT-ICR MS. To the best of our knowledge, it is the first time that such methods are applied in this domain. We consider a simple control protocol composed of an excitation and detection processes. This chapter is organized as follows. At first we give a short description of the experimental setup. This experimental technique is designed for measuring the masses of ions by exciting them with homogeneous magnetic and time-varying electric fields. While circulating, electrically charged ions induce charge redistribution and current on the detecting plates which is the output signal. We can then measure the charge to mass ratio by Fourier analysis of the output signal. The interested reader can find more details in [93–97]. Then we investigate the control of an ensemble of ions with cyclotron frequencies $\omega_i \in [\omega_{min}, \omega_{max}]$. We consider an electric field with one or two components. We analytically and numerically show that the complete and simultaneous control of the speed and of the position of ions is not possible. A partial control either of the speed or of the position of ions can be realized. Different numerical results are presented. A comparison with the standard adiabatic and SWIFT solutions is also provided.

3.1

Experimental Setup

FT-ICR MS is designed to measure the masses of ions and their relative abundance. The ions are injected with a very small velocity in the center of the cell. A schematic illustration is given in Fig. 3.1. The ions are subjected to a uniform and static magnetic field which forces the ions to rotate in a plane perpendicular to the field. The Newton's second law with the Lorentz force

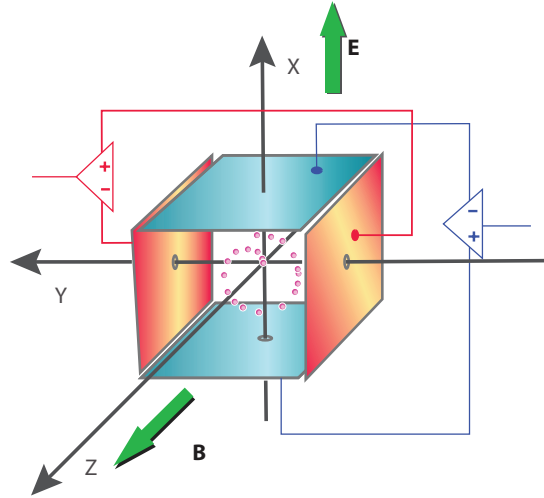


Figure 3.1: Experimental Cell of **FT-ICR MS**: The ions are subjected to the electric field \vec{E} and the magnetic field \vec{B} along the x - and z - directions respectively. The opposite plates orthogonal to the x - axis are the excitation plates, while the ones perpendicular to the y - axis are the detection plates. The distance d between each pair of opposite plates is of the order of 10 cm. The origin O of the laboratory frame coincides with the center of the cell.

acting on the ions is given by:

$$m \frac{d\vec{v}}{dt} = \vec{F} = q\vec{v} \times \vec{B},$$

and leads to the following expression of the angular cyclotron frequency ω_c :

$$\omega_c = \frac{v}{r} = \frac{qB}{m}.$$

We stress that ω_c is inversely proportional to m . The standard mass unit in **FT-ICR** is the Dalton:

$$1 \text{ u} = 1.660539 \times 10^{-27} \text{ kg}.$$

1 u is of the order of the mass of Hydrogen atom. For a standard magnetic field of $7T$, we deduce that $\nu_c = \omega_c/(2\pi)$ ranges from 1 kHz to 1 MHz . The experimental values are summarized in the following table.

Parameter	Value
B	8T
ν	1 KHz < ν < 1 MHz
T_{ex}	5 μs
r	$\simeq 1cm$
E	$\simeq 10Vm^{-1}$

Table 3.1: Experimental Values of **2D FT-ICR MS**.

The initial velocity of the ions can be estimated with the temperature T of the sample. The equipartition theorem gives:

$$\frac{1}{2}mv^2 = k_B T,$$

and from the Newton-Lorentz law

$$m \frac{v^2}{r} = qvB$$

we conclude:

$$(3.1) \quad r = \frac{\sqrt{2mk_B T}}{qB}.$$

At room temperature, an ion of mass $m = 100 u$ subjected to a magnetic field $B = 3T$ with $q = 1e$ has a radius $r \approx 0.08mm$. The ion cyclotron motion is not detectable by the detection plate due to a too small radius and to the fact that the packet of ions is not spatially coherent (the spatial phase is random). Such problems can be overcome by using an excitation process with an electric field $\vec{E}(t)$. The excitation plates with a time-dependent voltage generate a time-varying uniform electric field exciting the ions. The excitation pulse increases the orbital radius of the ions up to a few centimeters. While approaching the conducting plates of the cell, the ions induce charge difference and current in the detecting plates which obey Eqs. (3.27), (3.28). The Fourier Transform of the S signal provides us the sequence of the cyclotron frequencies which leads to the sequence of the charge-to-mass ratio of the ions in the cell. Next, we investigate the control of the motion of the ions in such mutually transverse electromagnetic fields. In the next sections, we discuss the dynamics of ions in the experimental cell. Then we explore the detection process. We will investigate each pulse and technique separately with its own detection process.

3.1.1 Model Dynamics

We consider the simplest modeling of ion trajectories in FT-ICR. The different ions in the experimental cell are confined in the (x, y) -plane and are subjected to a constant magnetic field \vec{B} and a time-dependent electric field \vec{E} , respectively, along the z - and x -axes of the laboratory frame. Note that optimal control techniques can also be used if two control fields along the x - and y -directions are available. The dynamics are governed by the Lorentz's equation:

$$(3.2) \quad m_k \dot{\vec{v}}_k = q_k \vec{E} + q_k (\vec{v}_k \times \vec{B}),$$

where m_k , q_k and \vec{v}_k are the mass, charge and speed of the ion k . $\dot{\vec{v}}_k$ denotes the time derivative of \vec{v}_k . Equation (3.2) can be expressed in Cartesian coordinates:

$$(3.3) \quad \begin{cases} \dot{x}_k = v_{x_k} \\ \dot{y}_k = v_{y_k} \\ \dot{v}_{x_k} = \omega_k (e_x + v_{y_k}) \\ \dot{v}_{y_k} = -\omega_k v_{x_k} \end{cases}$$

with the cyclotron frequency $\omega_k = \frac{q_k B}{m_k}$ and $\vec{e} = \vec{E}/B$. The coordinates (x_k, y_k) and (v_{x_k}, v_{y_k}) describe, respectively, the position and the speed of the ion k in the (x, y) -plane. We assume that the frequency ω_k belongs to the interval $[\omega_{min}, \omega_{max}]$, which is defined by the ion packet under study. As described below, the aim of the control process is to excite the different ions in a robust way with respect to the parameter ω .

The control problem can be defined as follows. Starting from the center of the cell ($x_k = 0$, $y_k = 0$) with a zero speed ($v_{x_k} = 0$, $v_{y_k} = 0$), the goal is to reach at a fixed control time t_f a given radius r_f and phase φ_f . As an illustrative example, we force the phase to vary linearly with ω , contrary to the standard result obtained with chirp pulses, where a quadratic phase dependence is observed (see Sec. 3.2.1 for details). We denote by $r_k(t)$ and $\varphi_k(t)$, respectively, the radius and the phase of ion k at time t . We assume in a first step that there is no constraint on the electric field. A limitation on the maximum pulse intensity is accounted for in Section 3.2.4. To simplify the notations, we omit below the index k . Using Equation (3.3), it is straightforward to show that $\Omega = \omega x + v_y$ is a constant of motion. At $t = 0$, since $x(0) = 0$ and $v_y(0) = 0$, we deduce that $\Omega = 0$ so $v_y(t) = -\omega x(t)$. One of the two coordinates $v_y(t)$ or $x(t)$ can be eliminated. This also means that we cannot control simultaneously the position and the speed of the ion with only one control. We arrive at:

$$\begin{cases} \dot{y} = v_y \\ \dot{v}_y = -\omega^2 V_x \\ \dot{V}_x = v_y + e_x \end{cases}$$

where $V_x = v_x/\omega$. We introduce the vector $X = (y, v_y, V_x)$ whose dynamics are governed by:

$$(3.4) \quad \dot{X} = AX + Ce_x,$$

with

$$A = \begin{pmatrix} 0 & 1 & 0 \\ 0 & 0 & -\omega^2 \\ 0 & 1 & 0 \end{pmatrix}, C = \begin{pmatrix} 0 \\ 0 \\ 1 \end{pmatrix}$$

The dynamics of this linear system can be explicitly integrated as follows. The eigenvalues of A are $(0, i\omega, -i\omega)$ and the corresponding eigenvectors can be written as:

$$X_0 = \begin{pmatrix} 1 \\ 0 \\ 0 \end{pmatrix}, X_+ = \begin{pmatrix} 1 \\ i\omega \\ 1 \end{pmatrix}, X_- = \begin{pmatrix} 1 \\ -i\omega \\ 1 \end{pmatrix}$$

At time t_f , the state of the system is given by:

$$X(t_f) = \int_0^{t_f} e^{A(t_f-s)} C e_x(s) ds.$$

We have:

$$e^{At} = P e^{Dt} P^{-1},$$

where $D = \text{diag}(0, i\omega, -i\omega)$ and

$$P = \begin{pmatrix} 1 & 1 & 1 \\ 0 & i\omega & -i\omega \\ 0 & 1 & 1 \end{pmatrix}, P^{-1} = \begin{pmatrix} 1 & 0 & -1 \\ 0 & -0.5i/\omega & 0.5 \\ 0 & 0.5i/\omega & 0.5 \end{pmatrix}$$

We deduce that:

$$e^{At} = \begin{pmatrix} 1 & \sin(\omega t)/\omega & -1 + \cos(\omega t) \\ 0 & \cos(\omega t) & -\omega \sin(\omega t) \\ 0 & \sin(\omega t)/\omega & \cos(\omega t) \end{pmatrix}$$

and

$$(3.5) \quad X(t_f) = \int_0^{t_f} ds e_x(s) \begin{pmatrix} -1 + \cos[\omega(t_f - s)] \\ -\omega \sin[\omega(t_f - s)] \\ \cos[\omega(t_f - s)] \end{pmatrix}$$

The existence of the integral of motion implies the impossibility of simultaneous control of velocities and positions of ions. We can control either the velocities or the positions.

3.1.2 Rotating Wave Approximation

We describe in this section the [RWA](#) which allows to simplify the control of [FT-ICR](#) processes. Using this approximation, we show that the control of ions reduces to the control of an ensemble of springs of different frequencies.

The oscillating excitation field e_x applied only along the x - axis can be expressed as the sum of two rotating fields, one in the same direction as the ions and the other in the opposite direction. We introduce the [RWA](#) which assumes that the field rotating in opposite direction to the ions has a negligible effect on their trajectories. This approximation is verified if the range of frequencies around the central frequency ω_o is not too large, as discussed in [Appendix C.4](#). Note that [RWA](#) is a standard tool in [NMR](#) [[22](#), [98](#), [99](#)] where it is derived in a similar but different way due to the non-linearity of the system [[100](#)]. In particular for [FT-ICR](#), this approximation does not depend on the amplitude of the excitation. Using [RWA](#), we show below that the control of ions is equivalent to the control of an ensemble of springs of different frequencies [[62](#), [88](#)]. The derivation starts with the control of speeds which fulfill:

$$\begin{cases} \dot{v}_{xk} = \omega_k v_{yk} + \omega_k e_x \\ \dot{v}_{yk} = -\omega_k v_{xk} \end{cases}$$

In complex coordinates, we have:

$$(3.6) \quad \dot{\mathbf{v}}_k = -i\omega_k \mathbf{v}_k + \omega_k e_x(t),$$

where $\mathbf{v}_k = v_{xk} + iv_{yk}$. We consider that $\omega_k \in [\omega_0 - \delta\omega, \omega_0 + \delta\omega]$ where ω_0 is the carrier frequency of the electric field, $e_x(t) = e_0(t)\cos(\omega_0 t + \phi(t))$, and $\delta\omega$ is small compared to ω_0 . We also assume that the amplitude $e_0(t)$ and the phase $\phi(t)$ vary slowly in time with respect to the frequency ω_0 . We express the speed as: $\mathbf{v}_k = \tilde{\mathbf{v}}_k e^{-i\omega_0 t}$, where $\tilde{\mathbf{v}}_k$ is the complex speed in the frame rotating at frequency ω_0 . We deduce that:

$$\dot{\tilde{\mathbf{v}}}_k = -i\Delta\omega_k \tilde{\mathbf{v}}_k + \omega_k \frac{e_0}{2} (e^{-i\phi} + e^{2i\omega_0 t + i\phi}),$$

where $\Delta\omega_k = \omega_k - \omega_0$ is the detuning term. In the [RWA](#), we neglect the rapidly oscillating term $\exp(2i\omega_0 t)$ and we arrive at:

$$(3.7) \quad \dot{\tilde{\mathbf{v}}}_k \simeq -i\Delta\omega_k \tilde{\mathbf{v}}_k + \omega_k \frac{e_0}{2} e^{-i\phi}.$$

It is worth noting here that, in the rotating frame, the dynamics are driven by two control parameters, $e_0 \cos\phi$ and $e_0 \sin\phi$. Note that we recover the control of an ensemble of springs. An additional step can be done for the position of the ion k , $\mathbf{x}_k = x_k + iy_k$. We set $\mathbf{x}_k = \tilde{\mathbf{x}}_k e^{-i\omega_0 t}$. It is then straightforward to show that:

$$\dot{\tilde{\mathbf{x}}}_k - i\omega_0 \tilde{\mathbf{x}}_k = \tilde{\mathbf{v}}_k(t)$$

Since $\tilde{\mathbf{x}}_k$ varies slowly with respect to $e^{i\omega_0 t}$, we can neglect the time derivative $\dot{\tilde{\mathbf{x}}}_k$, which gives:

$$\tilde{\mathbf{x}}_k = \frac{i}{\omega_0} \tilde{\mathbf{v}}_k(t).$$

If the [RWA](#) is valid, we deduce that the speed control leads also to the control of the position of ions. In this study, the validity of [RWA](#) is verified in the different examples by a numerical integration of Eq. (3.5).

Summary

- The experimental setup of [FT-ICR MS](#) is presented. We briefly discussed the excitation and detection processes.
- The dynamics of ions is derived. We also obtain an integral of motion which reduces the dimension of state by one.
- We show that in the regime of [RWA](#), one can apply, to excite ions, the control pulses that we have developed for an ensemble of springs.

3.2

Pulses

In this section, we discuss a number of pulses that are used to excite the ions in FT-ICR. We describe the detection process with some simulation results in Sec. 3.3. Although monochromatic and square pulses can be used but the efficient means of excitation are adiabatic, SWIFT and OCT pulses. Next subsections are devoted to the description of their properties.

3.2.1

Adiabatic Excitation

The goal of this paragraph is to compute the final states of the ions in the case of an adiabatic excitation of the form $e_x = e_0 \cos(\omega_i t + \frac{s}{2} t^2)$ where ω_i is the initial frequency and s the sweep rate. We recall that integrals of the form

$$\mathcal{K}(\alpha, \beta) = \int_0^{t_f} e^{i(\alpha t^2 + \beta t)} dt$$

can be expressed by the Fresnel function (see Sec. C.1). This result allows to exactly compute the dynamics of the system. Starting from Eq. (3.5), the final state of the FT-ICR process can be expressed as follows:

$$X(t_f) = e_0 \int_0^{t_f} dt \begin{pmatrix} -\cos(\omega_i t + st^2/2) + \cos(st^2/2 + (\omega_i - \omega)t + \omega t_f)/2 + \cos(st^2/2 + (\omega_i + \omega)t - \omega t_f)/2 \\ -\omega[\sin(st^2/2 + (\omega_i - \omega)t + \omega t_f)/2 - \sin(st^2/2 + (\omega_i + \omega)t - \omega t_f)/2] \\ \cos(st^2/2 + (\omega_i - \omega)t + \omega t_f)/2 + \cos(st^2/2 + (\omega_i + \omega)t - \omega t_f)/2 \end{pmatrix}$$

and we finally obtain:

$$\begin{cases} x_\omega(t_f)/e_0 = \Im[\frac{e^{i\omega t_f}}{2} \mathcal{K}(\frac{s}{2}, \omega_i - \omega) - \frac{e^{-i\omega t_f}}{2} \mathcal{K}(\frac{s}{2}, \omega_i + \omega)] \\ y_\omega(t_f)/e_0 = \Re[-\mathcal{K}(\frac{s}{2}, \omega_i) + \frac{e^{i\omega t_f}}{2} \mathcal{K}(\frac{s}{2}, \omega_i - \omega) + \frac{e^{-i\omega t_f}}{2} \mathcal{K}(\frac{s}{2}, \omega_i + \omega)] \end{cases}$$

This dynamics can be approximated by using the stationary phase approximation. For that purpose, we start from Equation (3.6) and we assume that $\int_0^{t_f} e_x(t) dt = 0$. For a proper justification of the assumption, we recall that e_0 changes slowly with respect to the frequency ω_i . Therefore the negative and positive parts of e_x cancel each other surface-wise due to its amplitude modulated nature of a high carrier frequency ω_i . With this said, we arrive at:

$$\mathbf{v}_k(t_f) = \omega_k e^{-i\omega_k t_f} \int_0^{t_f} dt e_x(t) e^{i\omega_k t}.$$

The stationary phase approximation is discussed in Sec. C.3. For a chirp excitation, the phase $\phi(t)$ is defined by $\phi(t) = \omega_i t + \frac{st^2}{2}$. The instantaneous frequency $\omega(t)$ can be expressed as:

$$\omega(t) = \dot{\phi}(t) = \omega_i + st,$$

where $s = \dot{\omega}(t)$. In the example under study, the rate s is given by $s = (\omega_f - \omega_i)/t_f$. We assume that $s > 0$ and we deduce that the Fourier transform of the control field is given by:

$$\hat{e}_x(\omega) = \int_0^{t_f} e_x(t) e^{i\omega t} dt = \frac{e_0}{2} \int_0^{t_f} [e^{-i(\omega_i t + \frac{st^2}{2} - \omega t)} + e^{i(\omega_i t + \frac{st^2}{2} + \omega t)}] dt.$$

We denote by ϕ_1 and ϕ_2 the arguments of the two exponential terms. It is straightforward to verify that $\dot{\phi}_1(t) = 0$ for $t = t_1^{(\omega)} = \frac{\omega - \omega_i}{s}$ and that $\dot{\phi}_2(t) = 0$ for $t = t_2^{(\omega)} = \frac{-\omega - \omega_i}{s}$. Neglecting the second contribution since $t_2^{(\omega)} < 0$ and assuming that $t_1^{(\omega)}$ is not too close to 0 and t_f , we can consider that the integral is defined from $-\infty$ to $+\infty$. We finally get:

$$\hat{e}_x(\omega) = e_0 \sqrt{\frac{\pi}{2s}} e^{i(\frac{\pi}{4} + \phi_1(t_1^{(\omega)}))}.$$

The phase spectrum $\phi(\omega) = \frac{\pi}{4} + \phi_1(t_1^{(\omega)})$ can be written as:

$$\phi(\omega) = \frac{\pi}{4} + \frac{(\omega - \omega_i)^2}{2s}.$$

Coming back to the original control problem, we obtain:

$$(3.8) \quad \mathbf{v}_k(t_f) \simeq \omega_k e_0 \sqrt{\frac{\pi}{2s}} \exp\left[i\left(\frac{\pi}{4} - \omega_k t_f + \frac{(\omega_k - \omega_i)^2}{2s}\right)\right].$$

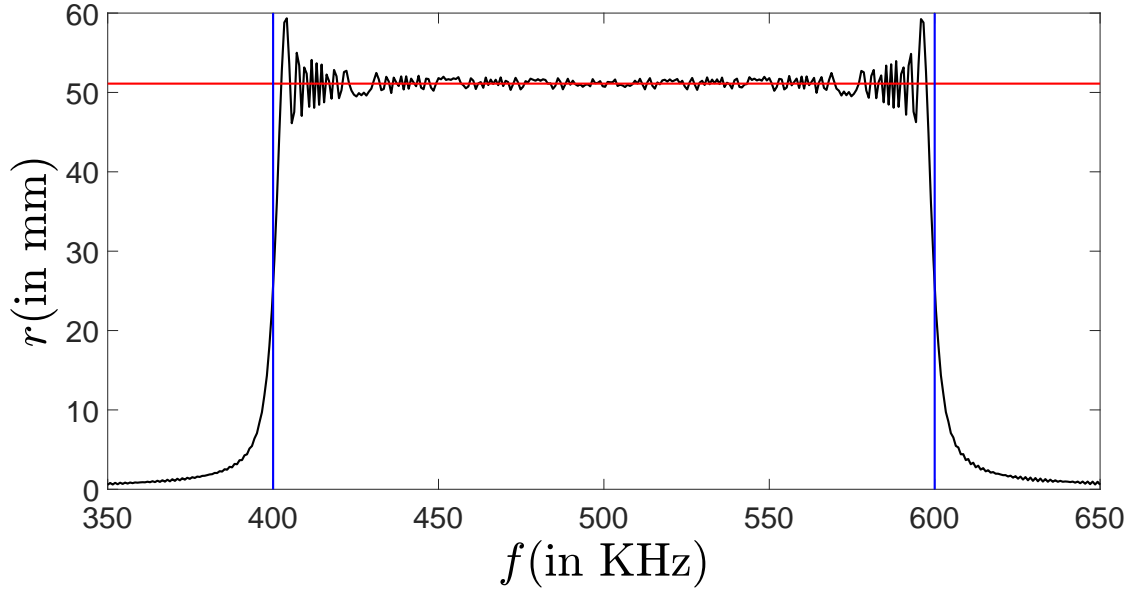


Figure 3.2: Excitation of an ensemble of ions, here, is realized by an adiabatic pulse. The black curve represents the final radii of ions as a function of the frequency while the red solid line represents the stationary phase approximation. The parameters are set to $t_f = 10ms$, $E_0 = 3.2V/m$ and $B_0 = 7T$. The vertical blue solid lines indicate the range of frequency of the pulse.

In the range of validity of this approximation, from Eq. (3.8), we conclude that the final radius of ions $r = |\mathbf{v}_k(t_f)|/\omega_k$ at time $t = t_f$ is a constant and does not depend on the cyclotron frequency of the ion. The phase, however, varies quadratically with the frequency ω_k . A numerical example is given in Fig. 3.2. The frequency of the chirped pulse goes from 400 to 600 kHz.

3.2.2

Optimal Pulse with RWA

We illustrate the optimal control of ions with the following numerical example. We consider the approach presented in Subsec. 2.6.5. We first compute the optimal control $u(t)$ of a spring ensemble with $\omega \in [0, 200]$. The control time t_f is set to 1. At this point, all the quantities are dimensionless. The target states $z_{f\omega}$ depend on the frequency, and the final radius of the trajectory can be expressed as:

$$(3.9) \quad |z_f| = \frac{1}{2} (1 + \tanh[(\omega_s - \omega)\mu]),$$

where $\mu = 0.1$ and $\omega_s = 100$. The target radius is of the order of 1 for $\omega < \omega_s$ and 0 for $\omega > \omega_s$. The smooth transition between the two regions can be adjusted with the parameter μ . The phase of the target state is defined as:

$$z_f(\omega) = |z_{f\omega}| e^{i\omega\eta t_f}$$

with $\eta = 0.5$, the slope of the frequency-dependent phase. We observe numerically that a nonzero slope in a given range ($\eta \in [0, 1]$) helps limit the maximum amplitude of the pulse. The same observation was made for spin control [101, 102]. The parameter λ which weights the importance of the pulse energy in the cost functional, is set to 10^{-3} . A regular discretization of 60 frequencies in the range $[0, 200]$ is taken into account in the optimization. Note that the final result does not change if a sufficient number of frequencies is used. The control field is then expressed in physical units as follows. We define the normalized electric field $e(t)$ as:

$$(3.10) \quad e(t) = \frac{E_0}{B_0} u(t) \cos(\omega_0 t),$$

where $E_0 = 100 \text{V m}^{-1}$, $B_0 = 10 \text{T}$, and $\omega_0/(2\pi) = 500 \text{KHz}$. These values are typical to FT-ICR MS. The intensity of the electric field E_0 is fixed to get a radial excitation of a few centimeters. The control time is assumed to be expressed in ms , leading to a control duration of $1ms$, which is also standard in FT-ICR. We deduce that a range of $\omega/(2\pi) = 100/(2\pi) = 16 \text{kHz}$ is excited around the central frequency $\omega_0/(2\pi)$. Note that the RWA (see Sec. 3.1.2) is justified since $\Delta\omega \ll \omega_0$.

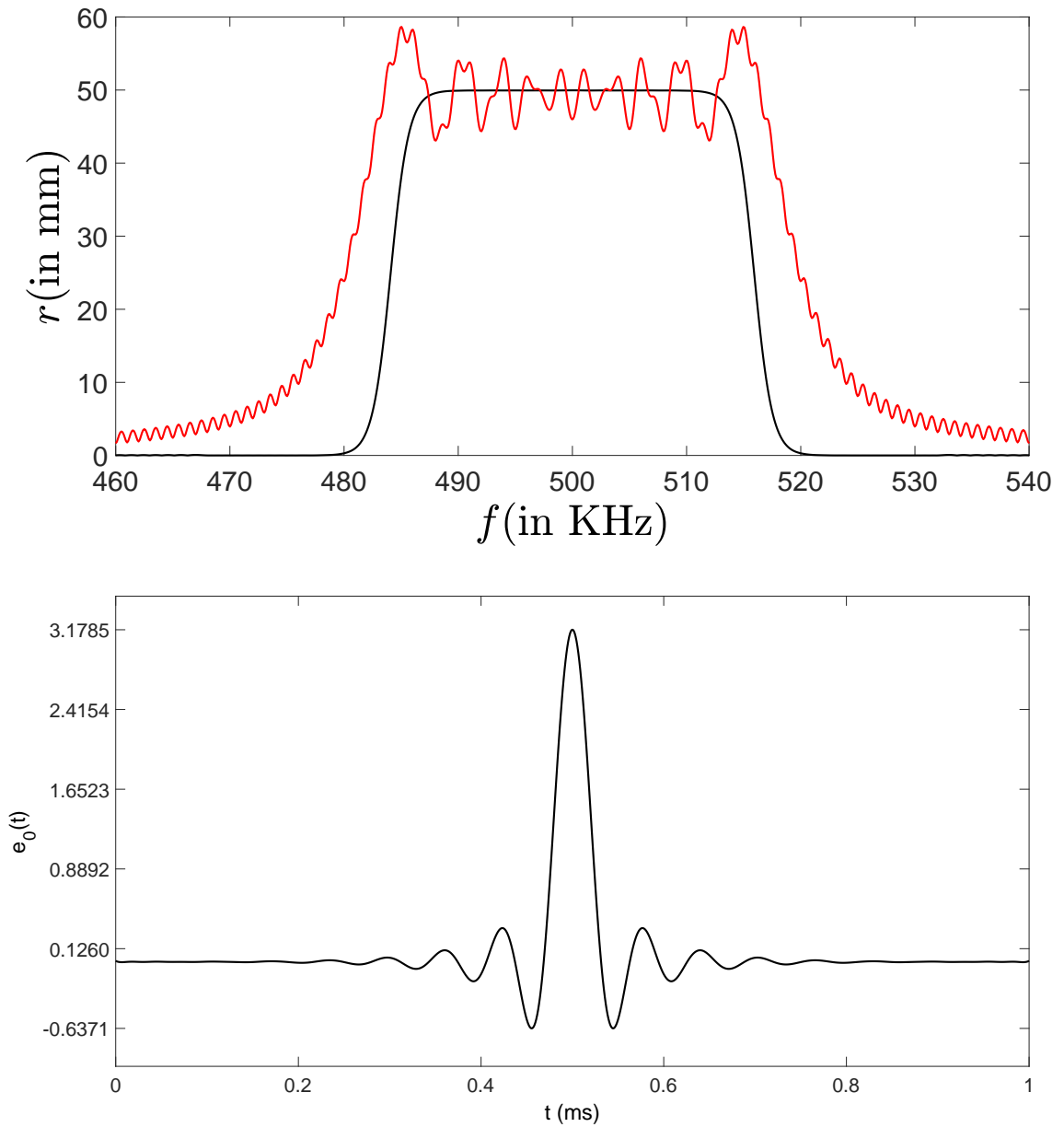


Figure 3.3: Excitation profiles of an ensemble of ions by optimal (black line) and adiabatic (red line) pulses are compared. We depict the final radii r (in mm) of ions as a function of the frequency f in the range of frequencies $[460, 540]kHz$. The optimal control pulse $\mathbf{E}_0(t) = \frac{E_0}{B} \mathbf{u}(t)$ with a duration of $1ms$ is also displayed.

Numerical results are presented in Fig. 3.3. The radius of the ion is denoted r . A comparison can be made with an adiabatic excitation, characterized by the following parameters: $\omega_i/(2\pi) = 480kHz$, $\omega_f/(2\pi) = 520kHz$, $t_f = 1ms$ and an amplitude $E_0 = 0.625kVm^{-1}$. The sweep rate s is defined as $s = \frac{\omega_f - \omega_i}{t_f}$. We observe that the optimal control process generates a very good excitation inside the expected range of frequencies. This control procedure is directly comparable

to the adiabatic process.

3.2.3 SWIFT Pulse

Based on the linearity of ion dynamics, it has been proposed to generate pulses by Fourier synthesis from a given excitation profile, in an approach called **SWIFT** [103–105]. In this paragraph, we describe the application of the **SWIFT** method to the model system. We consider a specific approach in which the control law and the corresponding dynamics can be expressed analytically.

The dynamics are governed by the differential system (3.2). In the **RWA** described in Sec. 3.1.2, the dynamics can be approximated as:

$$\dot{\tilde{\mathbf{v}}}_k = -i\Delta\omega_k \tilde{\mathbf{v}}_k + \frac{\omega_0}{2} e_0 e^{-i\phi},$$

where $\tilde{\mathbf{v}}_k = \tilde{v}_{xk} + i\tilde{v}_{yk}$ and the control field is expressed as $e_x(t) = e_0(t) \cos(\omega_0 t + \phi(t))$. The differential equation can be integrated and leads to:

$$\tilde{\mathbf{v}}_k(t_f) = \int_0^{t_f} e^{-i\Delta\omega_k(t_f-t)} \frac{\omega_0}{2} e_0 e^{-i\phi} dt$$

We deduce that:

$$\tilde{\mathbf{v}}_k^*(t_f) e^{-i\Delta\omega_k t_f} = \int_0^{t_f} e^{-i\Delta\omega_k t} \frac{\omega_0}{2} e_0 e^{i\phi} dt.$$

Introducing $u(t) = e_0 e^{i\phi}$ and assuming that u is different from zero only in the interval $[0, t_f]$, we obtain:

$$\sqrt{2\pi} \frac{\omega_0}{2} \hat{u}(\Delta\omega_k) = \tilde{\mathbf{v}}_k^*(t_f) e^{-i\Delta\omega_k t_f}.$$

where we use the following definition for the Fourier transform:

$$f(t) = \frac{1}{\sqrt{2\pi}} \int_{-\infty}^{+\infty} \hat{f}(\omega) e^{i\omega t} d\omega; \hat{f}(\omega) = \frac{1}{\sqrt{2\pi}} \int_{-\infty}^{+\infty} f(t) e^{-i\omega t} dt.$$

The target states are defined as:

$$\begin{cases} r_{\Delta\omega_k} = r_0 \Pi\left(\frac{\Delta\omega_k}{\delta\omega}\right) \\ \phi_{\Delta\omega_k} = \alpha \Delta\omega_k + \phi_0 \end{cases}$$

where Π is the gate function, with $\Pi(x) = 1$ if $|x| \leq \frac{1}{2}$ and 0 otherwise. The parameter $\delta\omega$ is the width of the distribution and ϕ_0 is an arbitrary constant. We have:

$$\mathbf{x}_k = r_{\Delta\omega_k} e^{i(\alpha\Delta\omega_k + \phi_0)}.$$

In the **RWA** (see Sec. C.4), starting from $\tilde{\mathbf{v}}_k = -i\omega_0 \tilde{\mathbf{x}}_k$, we arrive at:

$$\tilde{\mathbf{v}}_k(t) = -i\omega_0 r_{\Delta\omega_k} e^{i(\alpha\Delta\omega_k + \phi_0)} e^{i\omega_0 t}$$

and

$$\hat{u}(\Delta\omega) = \frac{2i}{\sqrt{2\pi}} r_{\Delta\omega_k} e^{-i\Delta\omega_k(t_f+a)} e^{-i\phi_0 - i\omega_0 t_f},$$

which gives

$$u(t) = \text{FT}^{-1} \left[\frac{2i}{\sqrt{2\pi}} r_{\Delta\omega_k} e^{-i\Delta\omega_k(t_f+a)} e^{-i\phi_0 - i\omega_0 t_f} \right].$$

Since

$$\frac{1}{\sqrt{2\pi}} \int_{-\infty}^{+\infty} \Pi\left(\frac{\omega}{\delta\omega}\right) e^{i\omega t} d\omega = \frac{\delta\omega}{\sqrt{2\pi}} \text{sinc}\left(\frac{\delta\omega t}{2}\right),$$

we obtain:

$$u(t) = \frac{r_0 \delta\omega e^{i\phi_1}}{\pi} \text{sinc}\left[\frac{\delta\omega}{2}(t - t_0)\right],$$

with $t_0 = t_f + a$ and ϕ_1 an arbitrary phase. The original control field $e_x(t) = e_0(t) \cos(\omega_0 t + \phi(t))$ is then given by:

$$e_x(t) = \frac{r_0 \delta\omega}{\pi} \text{sinc}\left(\frac{\delta\omega}{2}(t - t_0)\right) \cos(\omega_0 t + \phi_1).$$

Since the choice of the initial phase ϕ_1 is arbitrary, we finally get:

$$e_x(t) = \frac{r_0 \delta\omega}{\pi} \text{sinc}\left(\frac{\delta\omega}{2}(t - t_0)\right) \cos(\omega_0(t_f - t)).$$

The next step consists in integrating exactly the system dynamics using the original system and Equation (3.5). The final state of the dynamics is given by the following expressions:

$$\begin{cases} x_\omega(t_f) = \int_0^{t_f} dt e_x(t) \sin[\omega(t_f - t)] \\ y_\omega(t_f) = \int_0^{t_f} dt e_x(t) (-1 + \cos[\omega(t_f - t)]). \end{cases}$$

We then deduce:

$$x_\omega(t_f) = \frac{r_0 \delta\omega}{2\pi} [\mathcal{I}_s(t_f, \omega_s, \omega_0 + \omega) - \mathcal{I}_s(0, \omega_s, \omega_0 + \omega) - \mathcal{I}_s(t_f, \omega_s, \omega_0 - \omega) + \mathcal{I}_s(0, \omega_s, \omega_0 - \omega)]$$

and

$$\begin{aligned} y_\omega(t_f) = & \frac{r_0 \delta\omega}{2\pi} [-2\mathcal{I}_c(t_f, \omega_s, \omega_0) + 2\mathcal{I}_c(0, \omega_s, \omega_0) \\ & + \mathcal{I}_c(t_f, \omega_s, \omega_0 + \omega) - \mathcal{I}_c(0, \omega_s, \omega_0 + \omega) + \mathcal{I}_c(t_f, \omega_s, \omega_0 - \omega) - \mathcal{I}_c(0, \omega_s, \omega_0 - \omega)] \end{aligned}$$

with $\omega_s = \frac{\delta\omega}{2}$. The \mathcal{I}_c and \mathcal{I}_s functions are defined in Sec. C.2.

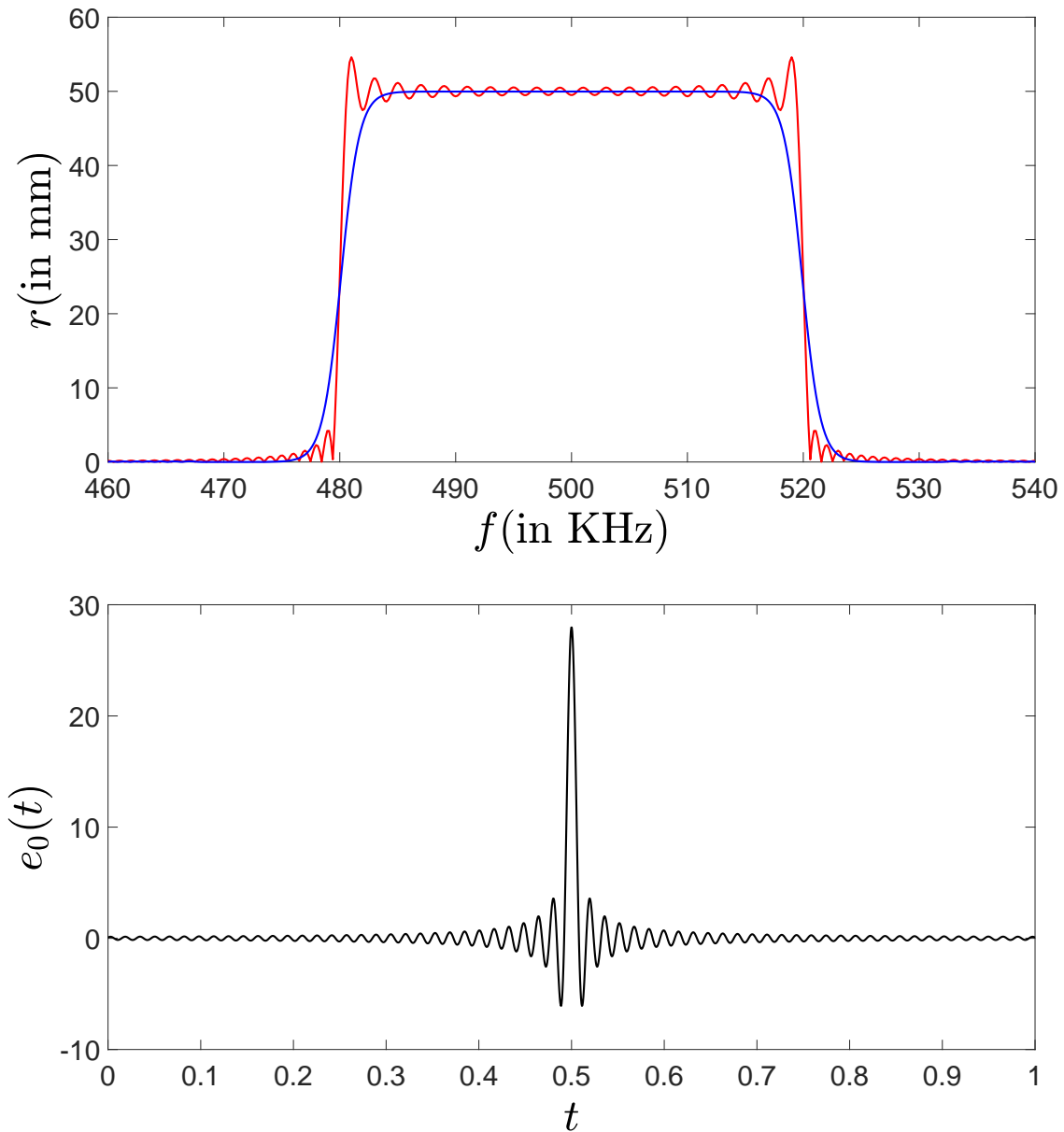


Figure 3.4: Excitation profiles of an ensemble of ions by optimal (blue line) with RWA and SWIFT (red line) pulses are compared. The final radii r (in mm) of ions are depicted as a function of the frequency f in the range of frequencies $[460, 540]kHz$. The optimal control pulse $E_0(t) = E_0 u(t)$ with a duration of $1ms$ is also displayed.

The comparison between the excitation by SWIFT and optimal pulses given in Fig. 3.4 is not really fair. In fact, the gate function is a square for the SWIFT and \tanh function for the optimal pulse. This point partly explains the better efficiency of optimal pulses. The optimal pulse is computed according to Subsec. 2.6.5.

3.2.4

Optimal Gradient-Based Algorithm

The goal of this section is to develop a first-order gradient-based algorithm suited to this control problem [69, 106]. We use a numerical optimization algorithm to take into account field amplitude constraint of the form $|e_x(t)| \leq e_{max}$. Note that this algorithm can be seen as the counterpart of the Gradient Ascent Pulse Engineering (GRAPE) algorithm in NMR [107] and that other limitations such as spectral constraints or bandwidth limitations could be added [108–115]. In the numerical simulations, the control field is described as a piece-wise constant function. Rapid time variations leading to high frequencies may appear in the optimization process. For question of numerical stability and precision, we apply the algorithm in the system with the RWA and then we use the derived control law in the original dynamical system.

We start from the differential system (3.7) written in the rotating frame for the ion k as:

$$\begin{cases} \dot{\tilde{v}}_x^{(k)} = \Delta\omega_k \tilde{v}_y^{(k)} + u_x \\ \dot{\tilde{v}}_y^{(k)} = -\Delta\omega_k \tilde{v}_x^{(k)} + u_y \end{cases}$$

where $u_x = \frac{\omega_0}{2} e_0 \cos\phi$ and $u_y = -\frac{\omega_0}{2} e_0 \sin\phi$. The two controls satisfy the limitation $u_x(t)^2 + u_y(t)^2 \leq u_{max}^2$ with $u_{max} = \frac{\omega_0}{2} e_{max}$. The corresponding target state is $(\tilde{v}_{xf}^{(k)}, \tilde{v}_{yf}^{(k)})$. We consider a cost functional \mathcal{J} with no penalty on the control field defined as:

$$(3.11) \quad \mathcal{J} = \frac{1}{2} \sum_k [(\tilde{v}_{xf}^{(k)} - \tilde{v}_x^{(k)}(t_f))^2 + (\tilde{v}_{yf}^{(k)} - \tilde{v}_y^{(k)}(t_f))^2].$$

The Pontryagin Hamiltonian can be expressed as:

$$H_P = \sum_k [\Delta\omega_k (-p_y^{(k)} \tilde{v}_x^{(k)} + p_x^{(k)} \tilde{v}_y^{(k)}) + u_x p_x^{(k)} + u_y p_y^{(k)}].$$

The adjoint states fulfill the following relations:

$$(3.12) \quad \begin{cases} \dot{p}_x^{(k)} = \Delta\omega_k p_y^{(k)} \\ \dot{p}_y^{(k)} = -\Delta\omega_k p_x^{(k)}. \end{cases}$$

The gradients are given by:

$$\frac{\partial H_P}{\partial u_x} = \sum_k p_x^{(k)}, \quad \frac{\partial H_P}{\partial u_y} = \sum_k p_y^{(k)}$$

The correction to the control fields $\delta u_x(t)$ and $\delta u_y(t)$ at each step of the algorithm is proportional to these gradients [69]. The final adjoint states can be expressed as:

$$\begin{cases} p_x^{(k)}(t_f) = \tilde{v}_{xf}^{(k)} - \tilde{v}_x^{(k)}(t_f) \\ p_y^{(k)}(t_f) = \tilde{v}_{yf}^{(k)} - \tilde{v}_y^{(k)}(t_f). \end{cases}$$

and Eq. (3.12) can be directly integrated backward in time. We thus consider the following gradient-based algorithm.

1. Choose guess fields $u_x(t)$ and $u_y(t)$.
2. Propagate forward the state of every ion k and compute $(v_x^{(k)}(t_f), v_y^{(k)}(t_f))$.
3. Propagate backward the adjoint state of the system from Eq. (3.12).
4. Compute the corrections $\delta u_x(t)$ and $\delta u_y(t)$ to the control fields, $\delta u_x(t) = \epsilon \sum_k p_x^{(k)}$, $\delta u_y(t) = \epsilon \sum_k p_y^{(k)}$ where ϵ is a small positive constant.
5. Define the new control fields $u_x(t) \mapsto u_x(t) + \delta u_x(t)$ $u_y(t) \mapsto u_y(t) + \delta u_y(t)$.
6. Truncate the new control fields $u_x(t)$ and $u_y(t)$ to satisfy the constraint $\sqrt{u_x(t)^2 + u_y(t)^2} \leq u_{max}$:

$$u_x(t) \mapsto \frac{u_x(t)u_{max}}{\sqrt{u_x(t)^2 + u_y(t)^2}}, u_y(t) \mapsto \frac{u_y(t)u_{max}}{\sqrt{u_x(t)^2 + u_y(t)^2}}.$$

7. Go to Step 2 until a given accuracy is reached.

Similar algorithms are used in [NMR](#) for taking into account pulse constraints [23, 24, 82]. Note that the use of a gradient causes this type of algorithm to converge towards a local maximum of the optimization problem. Numerical simulations with different guess fields allow partly overcoming this limitation, even if the global maximum is not reached with certainty.

3.2.5 Application of LQOCT to ICR

We apply in this section the [PMP](#) to [FT-ICR](#) processes in the case without any amplitude constraint. We denote by X_k the state associated with the frequency ω_k as defined in Eq. (3.4) of Section 3.1.1 and by $(X_1^{(k)}, X_2^{(k)}, X_3^{(k)})$ the coordinates. $\{\omega_k\}$ is the set of discrete frequencies used in the numerical optimization. The optimal problem is defined through the cost functional \mathcal{J} to minimize:

$$\mathcal{J} = \frac{1}{2} \sum_k [(X_1^{(k)}(t_f) - X_{1f}^{(k)})^2 + (X_2^{(k)}(t_f) - X_{2f}^{(k)})^2] + \frac{\lambda}{2} \int_0^{t_f} e_x^2 dt.$$

Since there is no final condition on $X_3(t_f)$, this term does not appear in the expression of \mathcal{J} . The Pontryagin Hamiltonian is given by:

$$H_P = \sum_k [p_1^{(k)} X_2^{(k)} - \omega_k^2 p_2^{(k)} X_3^{(k)} + p_3^{(k)} X_2^{(k)} + p_3^{(k)} u] - \frac{\lambda}{2} e_x^2.$$

For the adjoint state, we have:

$$\begin{cases} \dot{p}_1^{(k)} = 0 \\ \dot{p}_2^{(k)} = -p_1^{(k)} - p_3^{(k)} \\ \dot{p}_3^{(k)} = \omega_k^2 p_2^{(k)} \end{cases}$$

with the final conditions:

$$(3.13) \quad \begin{cases} p_1^{(k)}(t_f) = X_{1f}^{(k)} - X_1^{(k)}(t_f) \\ p_2^{(k)}(t_f) = X_{2f}^{(k)} - X_2^{(k)}(t_f) \\ p_3^{(k)}(t_f) = 0 \end{cases}$$

Note that $p_1^{(k)}$ is a constant of the motion. We deduce the dynamics of the adjoint state:

$$(3.14) \quad \begin{cases} p_1^{(k)}(t) = p_1^{(k)}(t_f) \\ p_2^{(k)}(t) = A^{(k)} \cos(\omega_k t) + B^{(k)} \sin(\omega_k t) \\ p_3^{(k)}(t) = -p_1^{(k)}(t_f) + \omega_k [A^{(k)} \sin(\omega_k t) - B^{(k)} \cos(\omega_k t)] \end{cases}$$

with

$$\begin{cases} A^{(k)} = \sin(\omega_k t_f) \frac{p_1^{(k)}(t_f)}{\omega_k} + p_2^{(k)}(t_f) \cos(\omega_k t_f) \\ B^{(k)} = \sin(\omega_k t_f) p_2^{(k)}(t_f) - \frac{p_1^{(k)}(t_f)}{\omega_k} \cos(\omega_k t_f) \end{cases}$$

The optimal control e_x^* can be expressed as:

$$(3.15) \quad e_x^*(t) = \frac{1}{\lambda} \sum_k p_3^{(k)}(t)$$

which can be transformed into:

$$e_x^*(t) = \frac{1}{\lambda} \sum_k [-p_1^{(k)}(t_f) + p_1^{(k)}(t_f) \cos(\omega_k(t_f - t)) - p_2^{(k)}(t_f) \omega_k \sin(\omega_k(t_f - t))].$$

The last step consists in computing the trajectory corresponding to this optimal control field. We obtain for an ion of frequency ω :

$$\begin{aligned} X_1(t_f) &= \frac{1}{\lambda} \sum_k \left[p_1^{(k)}(t_f) \left(t_f - \frac{\sin(\omega t_f)}{\omega} - \frac{\sin(\omega_k t_f)}{\omega_k} \right) + p_2^{(k)}(t_f) (1 - \cos(\omega_k t_f)) \right. \\ &\quad \left. + \frac{p_1^{(k)}(t_f)}{2} \left[\frac{\sin((\omega_k + \omega)t_f)}{\omega_k + \omega} + \frac{\sin((\omega_k - \omega)t_f)}{\omega_k - \omega} \right] + \frac{\omega_k p_2^{(k)}(t_f)}{2} \left[\frac{\cos((\omega_k + \omega)t_f) - 1}{\omega_k + \omega} + \frac{\cos((\omega_k - \omega)t_f) - 1}{\omega_k - \omega} \right] \right] \end{aligned}$$

and

$$\begin{aligned} X_2(t_f) &= \frac{-\omega}{\lambda} \sum_k \left[p_1^{(k)}(t_f) \frac{\cos(\omega t_f) - 1}{\omega} + \frac{p_1^{(k)}(t_f)}{2} \left[\frac{1 - \cos((\omega_k + \omega)t_f)}{\omega_k + \omega} + \frac{\cos((\omega_k - \omega)t_f) - 1}{\omega_k - \omega} \right] \right. \\ &\quad \left. + \frac{\omega_k p_2^{(k)}(t_f)}{2} \left[\frac{\sin((\omega_k + \omega)t_f)}{\omega_k + \omega} - \frac{\sin((\omega_k - \omega)t_f)}{\omega_k - \omega} \right] \right] \end{aligned}$$

Such results can be written in a compact form as follows:

$$\begin{cases} \lambda X_1^{(j)}(t_f) = \sum_k [\mathcal{R}_{jk} p_1^{(k)}(t_f) + \mathcal{S}_{jk} p_2^{(k)}(t_f)] \\ \lambda X_2^{(j)}(t_f) = \sum_k [\mathcal{T}_{jk} p_1^{(k)}(t_f) + \mathcal{U}_{jk} p_2^{(k)}(t_f)] \end{cases}$$

where the matrices \mathcal{R} , \mathcal{S} , \mathcal{T} and \mathcal{U} are known explicitly and the index j labels the ion of the ensemble. We finally arrive at the following system to fulfill:

$$\begin{cases} \sum_k [\mathcal{R}_{jk} X_{1f}^{(k)} + \mathcal{S}_{jk} X_{2f}^{(k)}] = \lambda X_1^{(j)}(t_f) + \sum_k [\mathcal{R}_{jk} X_1^{(k)}(t_f) + \mathcal{S}_{jk} X_2^{(k)}(t_f)] \\ \sum_k [\mathcal{T}_{jk} X_{1f}^{(k)} + \mathcal{U}_{jk} X_{2f}^{(k)}] = \lambda X_2^{(j)}(t_f) + \sum_k [\mathcal{T}_{jk} X_1^{(k)}(t_f) + \mathcal{U}_{jk} X_2^{(k)}(t_f)] \end{cases}$$

In matrix form, for $N = 2$, we have:

$$\begin{pmatrix} \sum_k \mathcal{R}_{1k} X_{1f}^{(k)} + \mathcal{S}_{1k} X_{2f}^{(k)} \\ \sum_k \mathcal{T}_{1k} X_{1f}^{(k)} + \mathcal{U}_{1k} X_{2f}^{(k)} \\ \sum_k \mathcal{R}_{2k} X_{1f}^{(k)} + \mathcal{S}_{2k} X_{2f}^{(k)} \\ \sum_k \mathcal{T}_{2k} X_{1f}^{(k)} + \mathcal{U}_{2k} X_{2f}^{(k)} \end{pmatrix} = \begin{pmatrix} \lambda + \mathcal{R}_{11} & \mathcal{S}_{11} & \mathcal{R}_{12} & \mathcal{S}_{12} \\ \mathcal{T}_{11} & \lambda + \mathcal{U}_{11} & \mathcal{T}_{12} & \mathcal{U}_{12} \\ \mathcal{R}_{21} & \mathcal{S}_{21} & \lambda + \mathcal{R}_{22} & \mathcal{S}_{22} \\ \mathcal{T}_{21} & \mathcal{U}_{21} & \mathcal{T}_{22} & \lambda + \mathcal{U}_{22} \end{pmatrix} \begin{pmatrix} X_1^{(1)}(t_f) \\ X_2^{(1)}(t_f) \\ X_1^{(2)}(t_f) \\ X_2^{(2)}(t_f) \end{pmatrix}$$

This linear system allows computing the final state of the system $X_k(t_f)$, then the adjoint state from Eq. (3.13) and (3.14) and the optimal control field with Eq. (3.15). We observe that the control law is expressed as a linear combination of cosine and sine functions of the frequencies ω_k of the finite discretized set. Note that the same method can be applied in the **RWA** starting from Eq. (3.7) (see [79] for details).

3.2.6

Numerical Computations

We now focus on ion control with amplitude constraint. The numerical simulations were carried out by assuming the **RWA**. The same set of discretized frequencies is chosen. We optimize piecewise constant functions with a time step lower than $1\mu\text{s}$ to avoid discretization effect. The dynamics are integrated numerically through the formulas given in Subsec. 3.1.1. More than 1000 iterations are usually needed to converge to an efficient solution. We can apply the gradient-based algorithm described in Sec. 3.2.4 with only one control field, namely $E_0(t) = e_0(t)\mathbf{B}$, and the phase $\varphi(t)$ of the electric field is set to 0. We consider the same control problem as before and the optimal solutions derived with **LQOCT** are used as guess field for the optimization algorithm.

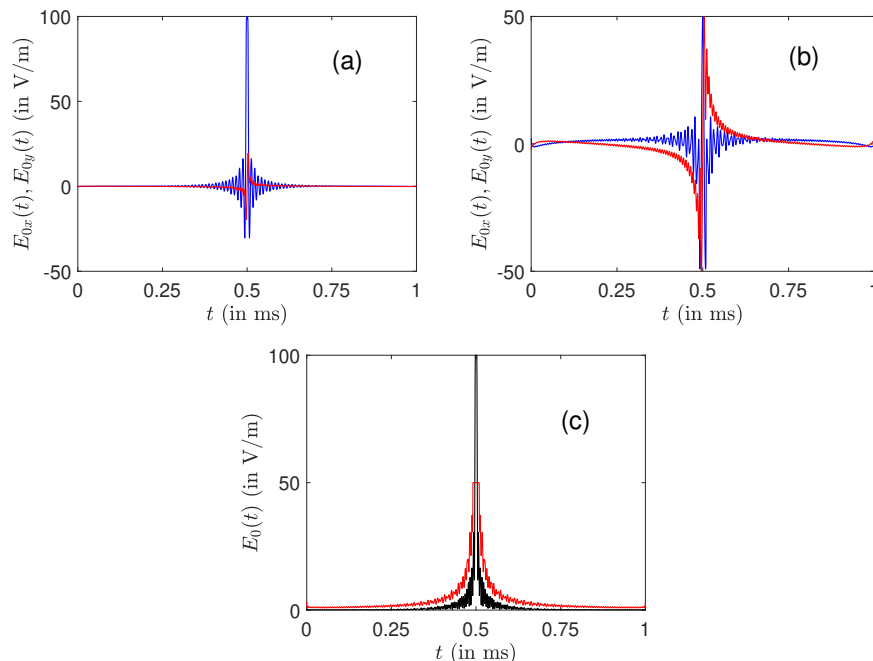


Figure 3.5: The optimal amplitudes E_{0x} (blue line) and E_{0y} (red line) are plotted for a maximum amplitude of 100Vm^{-1} in label (a) and 50Vm^{-1} in label (b). Label (c) corresponds to the total amplitude $E_0 = \sqrt{E_{0x}^2 + E_{0y}^2}$.

The optimization algorithm fails to converge towards a very good excitation profile, when the maximum amplitude is much smaller than 100Vm^{-1} . This obstacle can be partly overcome by considering two control inputs (in the rotating frame) denoted $E_{0x} = e_0B \cos \varphi$ and $E_{0y} = e_0B \sin \varphi$. An example is displayed in Fig. 3.5 for a maximum amplitude of 100 and 50Vm^{-1} . An almost perfect excitation profile is achieved in these two cases. Note the different structures of the inputs along the x and y directions, namely even and odd functions.

Summary

- We have presented the adiabatic pulse, and the stationary phase approximation.
- We have compared the SWIFT and optimal pulses.
- We have compared the adiabatic pulse and OCT pulse with RWA.
- The application of LQOCT is discussed for this particular problem.
- A gradient based algorithm is used to account for experimental limitations on the control pulse amplitude.

3.3 Detection Process

In the previous subsection the excitation phase has been discussed. The next step is to investigate the detection phase. A computer simulation of this process has been carried out. Herein we consider only the adiabatic pulse since the results are quite similar to those of square, SWIFT and optimal pulses. Monochromatic pulses, however, are capable to sense only the ions that are in resonance with the pulse. It is worth to emphasize the importance of excitation pulses in this phase. We deploy our designed pulses to bring all the ions with different frequencies to circulate in a relatively large radius in order to be closer to the detection plates so their frequencies can be recorded in the detected current.

3.3.1 Green's Reciprocity Principle

Before going on with the main task, it is worthwhile to start with the Green's reciprocity principle as all the important calculations are based on it. Suppose we have a charge distribution ρ_1 with its associated potential V_1 , and a completely separate charge distribution ρ_2 with potential V_2 . These two distributions do not co-exist. They are completely different situations. We consider the electric fields \vec{E}_1 and \vec{E}_2 produced by these two distributions and the following integral taken over all space [116]¹:

$$(3.16) \quad \mathcal{I} = \int_V \vec{E}_1 \vec{E}_2 d\vec{r}$$

Recalling two well-known facts from the theory of electricity; $\vec{E} = -\vec{\nabla}\varphi$ and $\vec{\nabla}\vec{E} = \rho/\epsilon_0$, we integrate Eq. (3.16) by parts under the natural assumption that fields vanish when going to infinity:

$$\mathcal{I} = - \int_V \vec{\nabla}\varphi_1 \vec{E}_2 d\vec{r} = \int_V \varphi_1 \vec{\nabla}\vec{E}_2 d\vec{r} = \frac{1}{\epsilon_0} \int_V \varphi_1 \rho_2 d\vec{r}$$

Similarly we get:

$$\mathcal{I} = - \int_V \vec{\nabla}\varphi_2 \vec{E}_1 d\vec{r} = \int_V \varphi_2 \vec{\nabla}\vec{E}_1 d\vec{r} = \frac{1}{\epsilon_0} \int_V \varphi_2 \rho_1 d\vec{r},$$

hence the following statement called Green's reciprocity principle is true:

$$(3.17) \quad \int_V \varphi_1 \rho_2 d\vec{r} = \int_V \varphi_2 \rho_1 d\vec{r}$$

¹Problem 3.43.

3.3.2 Parallel-Plate Capacitor

Assume a uniform electric field \vec{E} with a given potential φ . Then $\vec{\nabla}\varphi = -\vec{E} = \text{const}$, and as the derivative of the potential along an arbitrary direction \vec{n} is given by:

$$\frac{d\varphi}{dn} = (\vec{\nabla}\varphi)\vec{n},$$

it follows that

$$(3.18) \quad \frac{\Delta\varphi}{\Delta n} = \text{const}.$$

Now let us consider a particular case of a uniform electric field bounded inside the parallel-plate capacitor. We assume that the plates are infinite conducting planes. The frame of reference is chosen such that the origin is fixed in an equal distance $d/2$ from all plates, and the ordinate axis is directed perpendicular to the positive plate. From now on we will conventionally name one of the plates positive and the other one negative. The distance between the plates is d . We denote the potentials of the positively and negatively charged plates correspondingly with φ_+ and φ_- . Then according to Eq. (3.18) the following statement holds:

$$(3.19) \quad \frac{\varphi_+ - \varphi_-}{d} = \frac{\varphi_+ - \varphi(y)}{d/2 - y},$$

where $\varphi(y)$ is the potential at a point with an ordinate y inside the capacitor. From here $\varphi(y)$ can be deduced:

$$(3.20) \quad \varphi(y) = \left(\frac{1}{2} + \frac{y}{d}\right)\varphi_+ + \left(\frac{1}{2} - \frac{y}{d}\right)\varphi_-.$$

This relation with the Green's reciprocity principle will be used in the next section.

3.3.3 Charge Induction in the System of Parallel Plates

Suppose the same capacitor with grounded plates, where the Cartesian coordinate system is chosen as before. In this situation the plates are discharged, and their potentials are equal to zero. Now suppose that a charge q is placed between the plates at a distance y from the negative plate. The potentials as well as the total charge in the system will be again equal to zero, but this time a non-zero charge will be induced on the plates to compensate the one between them. Although it is considerably harder to find the charge distribution on the plates, but it is relatively straightforward to find the induced net charge on each plate with the help of Green's reciprocity principle [116]².

To apply the reciprocity theorem we need two distinct charge distributions. For the first, we take the one described. For the second, we just remove the point charge and the condition that the plates are grounded, so each plate can be at a different from zero potential.

²Problem 3.44.

At first consider the distribution as given. Since the two plates are grounded, we have $\varphi_+ = \varphi_- = 0$. Also due to the fact that the induced charge must cancel out the point charge, so there is no net charge in the system. That is $Q_+ + Q_- + q = 0$.

Now consider the distribution without the point charge q . In this case we take the potential of the negative plate to be $\varphi'_- = -\varphi_0$ and of the positive plate to be $\varphi'_+ = \varphi_0$. Note that this time the plates are not grounded. All the corresponding quantities for this case are denoted by prime.

Since the second distribution contains no point charge the potential varies linearly between the two plates as it is reflected in Eq. (3.20):

$$(3.21) \quad \varphi'(y) = \frac{2y}{d} \varphi_0$$

Now we are ready to apply the reciprocity theorem. On one side we have:

$$(3.22) \quad \int_V \varphi_1 \rho_2 d\vec{r} = \varphi_- Q'_- + \varphi_+ Q'_+ = 0,$$

since $\varphi_- = \varphi_+ = 0$

On the other side we have:

$$(3.23) \quad \int_V \varphi_2 \rho_1 d\vec{r} = \varphi_0 Q_+ - \varphi_0 Q_- + \varphi'(y) q = \varphi_0 \left[2Q_+ + \left(\frac{2y}{d} + 1 \right) q \right],$$

since $Q_- = -Q_+ - q$. According to the Green's theorem (3.17) the right hand of Eq. (3.23) must be zero, and therefore:

$$(3.24) \quad Q_+ = -\frac{1}{2} \left(1 + \frac{2y}{d} \right) q$$

$$(3.25) \quad Q_- = \frac{1}{2} \left(-1 + \frac{2y}{d} \right) q$$

$$(3.26) \quad \Delta Q = Q_+ - Q_- = -\frac{2y}{d} q.$$

where ΔQ is the charge difference between the two plates. The same computation can be done for spherical and cylindrical capacitors.

3.3.4

Signal Processing

Finally we can come back to our main problem. In the experimental setup the conducting plates which are allocated for the detection are perpendicular to the ordinate axis. Experimenters can measure both the charge difference and the current induced on these two plates. Each ion gives its own contribution in the signal production. Assume N ions are injected into the experimental setup. We will distinguish them by a subscript i assigned to the characteristic quantities of the

ions:

$$(3.27) \quad S_z(t) = \sum_{i=1}^N \Delta Q_i = - \sum_{i=1}^N \frac{2q_i}{d} y_i(t)$$

$$(3.28) \quad S_v(t) = \sum_{i=1}^N \frac{d}{dt} \Delta Q_i = - \sum_{i=1}^N \frac{2q_i}{d} v_{iy}(t)$$

$S_z(t)$ and $S_v(t)$ are respectively the charge difference and the current induced on the plates. Let us recall some useful formulas which will be used in further discussions. The dynamics of the ions in the mutually transverse electromagnetic field is governed by the general law:

$$(3.29) \quad v_i(t) = v_i(t_0) e^{-i\omega_i(t-t_0)} + \omega_i \int_{t_0}^t e(\tau) e^{-i\omega_i(t-\tau)} d\tau$$

$$(3.30) \quad z_i(t) = z_i(t_0) + \int_{t_0}^t v_i(\tau) d\tau \quad i = 1 \dots N$$

All notations stay the same. In particular be aware that the electric field is directed along the abscissa:

$$e(t) = \frac{E(t)}{B}$$

$$\omega_i = \frac{q_i B}{m_i}$$

For simplicity we assumed that the detection process starts right after the excitation phase. The time intervals for the excitation and detection phases are taken to be respectively in $[0, T_{ex}]$ and $[T_{ex}, T_{ex} + T_{det}]$. In the detection process $e = 0$, therefore:

$$(3.31) \quad v_i(t) = v_i(T_{ex}) e^{-i\omega_i(t-T_{ex})} \quad t \in [T_{ex}, T_{ex} + T_{det}] \quad i = 1 \dots N$$

The imaginary parts of the velocities take the form:

$$(3.32) \quad v_{iy}(t) = v_{iy}(T_{ex}) \cos \left[\omega_i (t - T_{ex}) \right] - v_{ix}(T_{ex}) \sin \left[\omega_i (t - T_{ex}) \right]$$

Substituting it into Eq. (3.28) we get the S_v signal. For the coordinates and their imaginary parts we similarly obtain:

$$(3.33) \quad z_i(t) = z_i(T_{ex}) + v_i(T_{ex}) (t - T_{ex}) e^{-i\omega_i(t-T_{ex})/2} \operatorname{sinc} \left[\frac{\omega_i (t - T_{ex})}{2} \right]$$

$$(3.34) \quad y_i(t) = y_i(T_{ex}) - (t - T_{ex}) \operatorname{sinc} \left[\frac{\omega_i (t - T_{ex})}{2} \right] \left(v_{ix}(T_{ex}) \sin \left[\frac{\omega_i (t - T_{ex})}{2} \right] - v_{iy}(T_{ex}) \cos \left[\frac{\omega_i (t - T_{ex})}{2} \right] \right)$$

Substitution of the last equation into Eq. (3.27) provides us the S_z signal.

3.3.5

Analyzing the Signals

In this section we are going to calculate the Fourier Transformations of these signals which actually provide us the sequence of the frequencies of the injected ions. From now on the hat will assign the state of being Fourier Transformed. Alongside with the following:

$$(3.35) \quad \int_a^b e^{i\alpha x} dx = (b-a)e^{i\alpha(b+a)/2} \operatorname{sinc} \left[\frac{\alpha(b-a)}{2} \right]$$

we recall also the other integral formulae. Some simple calculations lead to a similar set of equations as that of Eqs. (3.27) and (3.28):

$$(3.36) \quad \hat{S}_v(\omega) = - \sum_{i=1}^N \frac{2q_i}{d} \hat{v}_{iy}(\omega)$$

$$(3.37) \quad \hat{S}_z(\omega) = - \sum_{i=1}^N \frac{2q_i}{d} \hat{y}_i(\omega)$$

In order to get the Fourier Transforms of S_v and S_z signals we just need to find those of the velocities and of the coordinates. Note that $v_i(t)$, $z_i(t)$ as well as the S_v and S_z signals are defined in the time range $[T_{ex}, T_{ex} + T_{det}]$. There is no signal detected out of that. In other words we treat $v_i(t)$ and $z_i(t)$ as non-periodic functions of time defined on the real axis, which are zero out of the aforementioned time-range. Hence we arrive:

$$(3.38) \quad \begin{aligned} \hat{v}_{iy}(\omega) &= \int_{-\infty}^{\infty} v_{iy}(t) e^{-i\omega t} dt = \int_{T_{ex}}^{T_{ex}+T_{det}} v_{iy}(t) e^{-i\omega t} dt = \\ &= \frac{iT_{det}}{2} e^{-i\omega T_{ex}} \left\{ \bar{v}_i(T_{ex}) e^{i(\omega_i - \omega)T_{det}/2} \operatorname{sinc} \left[\frac{(\omega_i - \omega)T_{det}}{2} \right] - v_i(T_{ex}) e^{-i(\omega_i + \omega)T_{det}/2} \operatorname{sinc} \left[\frac{(\omega_i + \omega)T_{det}}{2} \right] \right\} \end{aligned}$$

A similar result holds for the coordinates:

$$(3.39) \quad \begin{aligned} \hat{y}_i(\omega) &= \int_{-\infty}^{\infty} y_i(t) e^{-i\omega t} dt = \int_{T_{ex}}^{T_{ex}+T_{det}} y_i(t) e^{-i\omega t} dt = \\ &= T_{det} \left(y_i(T_{ex}) - \frac{v_{ix}(T_{ex})}{\omega_i} \right) e^{-i\omega(2T_{ex}+T_{det})/2} \operatorname{sinc} \left(\frac{\omega T_{det}}{2} \right) + \frac{T_{det}}{2\omega_i} e^{-i\omega T_{ex}} \times \\ &\quad \times \left\{ \bar{v}_i(T_{ex}) e^{i(\omega_i - \omega)T_{det}/2} \operatorname{sinc} \left[\frac{(\omega_i - \omega)T_{det}}{2} \right] + v_i(T_{ex}) e^{-i(\omega_i + \omega)T_{det}/2} \operatorname{sinc} \left[\frac{(\omega_i + \omega)T_{det}}{2} \right] \right\} \end{aligned}$$

The bar stands for the complex conjugate.

These results are common for all type of excitation pulses. The difference that the excitation pulses make are $v_i(T_{ex})$ and $z_i(T_{ex})$, that is the initial values of the velocities and of the coordinates for the detection phase. In the next section, we discuss the numerical results for the detection of ions by means of the adiabatic pulse. The detection results for square and monochromatic pulses are quite similar.

3.3.6
Detection of Ions by Means of the Adiabatic Pulse

The dynamics of ions under the influence of the adiabatic pulse

$$(3.40) \quad e_x(t) = e_0 \cos\left(\omega_0 t + \frac{st^2}{2}\right)$$

has the following form:

$$(3.41) \quad v_i(t_f) = \frac{e_0 \omega_i}{2} e^{-i\omega_i t_f} \left[\mathcal{K}\left(-\frac{s}{2}, -\omega_0 + \omega_i, t_f\right) + \mathcal{K}\left(\frac{s}{2}, \omega_0 + \omega_i, t_f\right) \right].$$

$$(3.42) \quad z_i(t_f) = -i e_0 \Re \left[\mathcal{K}\left(\frac{s}{2}, \omega_0, t_f\right) \right] + \frac{i e_0}{2} e^{-i\omega_i t_f} \left[\overline{\mathcal{K}}\left(\frac{s}{2}, \omega_0 - \omega_i, t_f\right) + \mathcal{K}\left(\frac{s}{2}, \omega_0 + \omega_i, t_f\right) \right].$$

The Fourier transform of the adiabatic pulse is given by:

$$(3.43) \quad \hat{e}_x(\omega) = \frac{e_0}{2} \left[\mathcal{K}\left(\frac{s}{2}, \omega_0 - \omega, T_{ex}\right) + \mathcal{K}\left(-\frac{s}{2}, -\omega_0 - \omega, T_{ex}\right) \right].$$

The Fourier transforms of velocities and positions can be computed by the final velocities and positions (see Eqs. (3.38) and (3.39)).

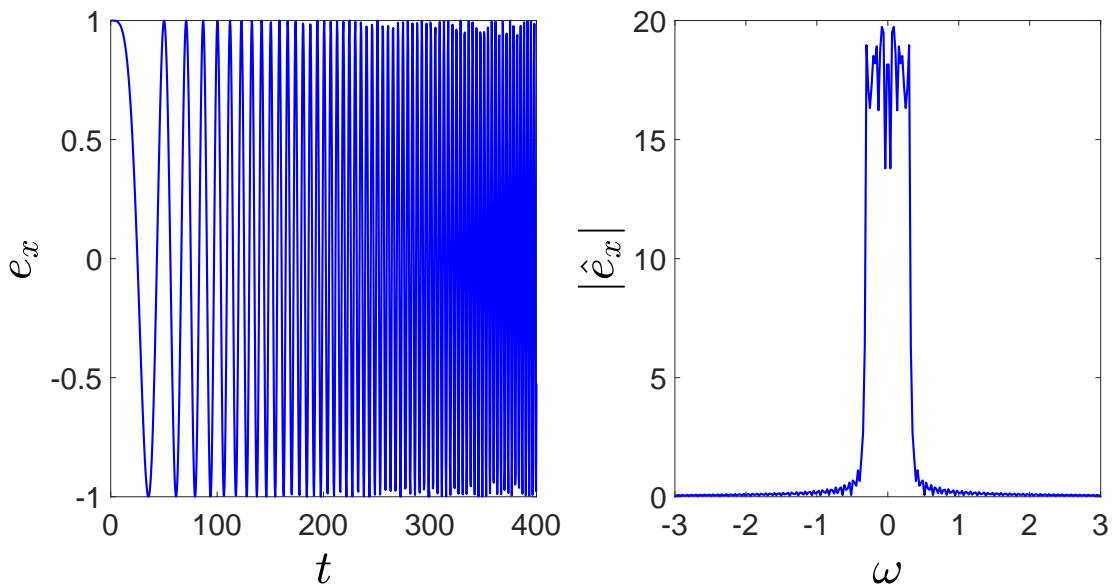


Figure 3.6: The adiabatic pulse and its Fourier transformation are computed via analytic formula. The parameters are set to $e_0 = 1$, $T_{ex} = 400 \mu s$, $s = 5 \times 10^{-3}$, $N = 600$.

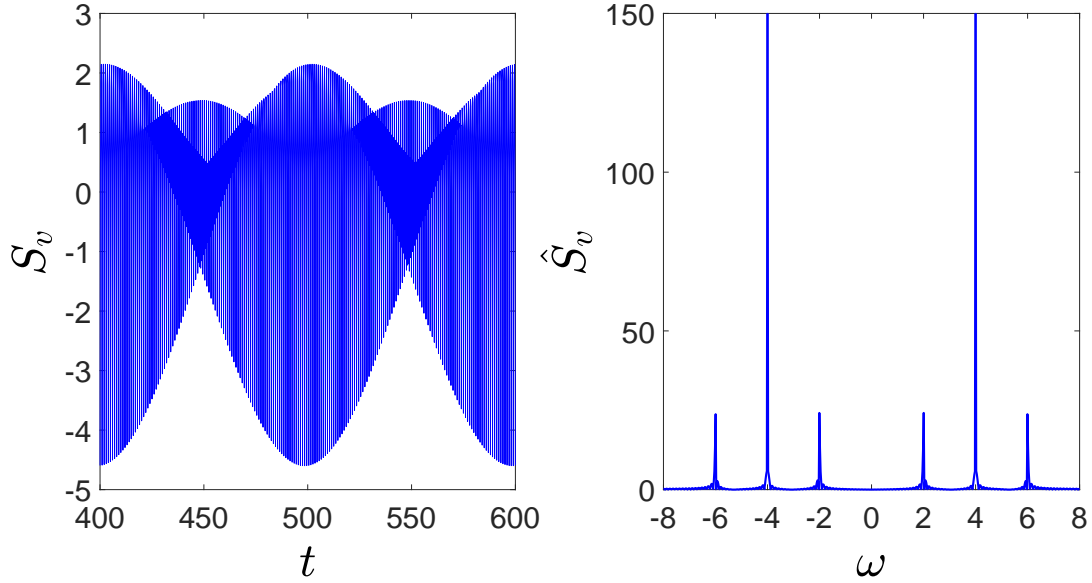


Figure 3.7: The detection pulse and its Fourier transformation are displayed. The parameters are set to $e_0 = 1$, $T_{ex} = 400\mu s$, $s = 5 \times 10^{-3}$, $N = 600$, $T_d = 200\mu s$, $d = 2cm$, $\nu_1 = 2MHz$, $\nu_2 = 4MHz$, $\nu_3 = 6MHz$.

The detection process can also be realized by applying square, [SWIFT](#) and [OCT](#) pulses. The monochromatic pulse is able to see only the on-resonance ion.

Summary

- The detection process is presented along with the Green's reciprocity principle.
- We describe qualitatively and quantitatively the induced charge on the detecting plates.
- We show how to analyze the two types of signals.
- We implement the described techniques to detect the injected ions which circulate under the influence of adiabatic pulse.

3.4

Conclusions

We applied optimal control techniques to the robust excitation of ions in [FT-ICR](#). We considered the simplified but realistic conditions of a [2D](#) trajectory and of a homogeneous magnetic field. In this model system, we propose different ways to solve the optimal control problems. Such methods are directly inspired from [NMR](#) in which [OCT](#) is a standard and efficient tool. In the case without pulse limitation, the linearity of the dynamical equations allows using [LQOCT](#),

which has the advantage to lead to an analytical formula of the control law. Very good results were obtained both for the final radii and phases of the ions. A specific range of frequencies was considered in this study, but the same approach can be extended to broadband excitation from 100 to 900 kHz. However, this solution is both in shape and in amplitude very similar to the [SWIFT](#) pulse. The two solutions are expected to be equal for a continuous range of frequencies. More original control laws are derived when the pulse intensity is limited. Due to this constraint, optimal iterative algorithms have to be used, and we adapt to [FT-ICR](#) the standard GRAPE algorithm, well-known in [NMR](#). Even if this algorithm has some limitations, it allows reducing the pulse intensity, by a factor larger than three in the examples under study. On the basis of [NMR](#) results, this algorithm is expected to be very efficient in the case of other excitation profiles. The very encouraging and promising results obtained in this investigation must now be confirmed by experimental implementation. Numerical simulations of this study are not fully realistic. Effects such as the magnetron motion, field geometry, field inhomogeneities or ion collisions are neglected. However, the model system we consider describes quite faithfully the main cyclotronic behavior and permits to grasp rapidly the main features of ion trajectories. Numerical codes were developed to account for such experimental details. The relative simplicity of the application of numerical optimal algorithms makes it possible to adapt it straightforwardly to a new class of control problems. They could thus be combined with such codes. We are therefore quite confident about the extension of optimization procedures to these additional experimental constraints and limitations.



Basics of Optimal Control Theory

The aim of this chapter is to give a general introduction of PMP as well as to introduce the gradient based algorithm. The interested reader can also find more details in a wide range of scientific literature [6, 8, 9, 68–70, 75, 86, 89, 90, 92].

A.1

Optimal Control Theory: PMP

Here we solve an optimization problem for a continuous system which later can be approximated by a discrete system for a solution on digital computers. Consider the following dynamical system:

$$(A.1) \quad \dot{x}(t) = f[x(t), u(t), t],$$

with $x(t_0)$ given at time t_0 ($t_0 < t < t_f$), where $x \in \mathbb{R}^n$, the state vector, is determined by $u(t) \in \mathbb{R}^m$, the control. The goal is to steer the system from its initial state into the target state at a fixed time t_f . We do not aim to exactly reach the target but rather to be as close as possible to it. In other words, first, we assume there is no terminal constraint on the state vector. We consider a scalar cost of the form:

$$(A.2) \quad \mathcal{J} = \phi[x(t_f), t_f] + \int_{t_0}^{t_f} L[x(t), u(t), t] dt.$$

The problem is to find the control $u(t)$ that minimizes \mathcal{J} . To adjoin the system dynamics (see Eq. (A.1)) to \mathcal{J} we introduce a multiplier vector $p(t) \in \mathbb{R}^n$:

$$(A.3) \quad \bar{\mathcal{J}} = \phi[x(t_f), t_f] + \int_{t_0}^{t_f} L[x(t), u(t), t] dt + \int_{t_0}^{t_f} p^T(t) (\dot{x}(t) - f[x(t), u(t), t]) dt,$$

where ϕ , the terminal cost, is to minimize the distance between the final and the target states. The integrand L is the running cost and p is the Lagrange multiplier, the so called adjoint state in control theory. For convenience, we define a scalar function H_p as follows:

$$(A.4) \quad H_p[x(t), p(t), u(t), t] = p^\top(t)f[x(t), u(t), t] - L[x(t), u(t), t],$$

and we call it Pontryagin Hamiltonian. One of the Hamilton equations is automatically satisfied:

$$(A.5) \quad \dot{x} = \frac{\partial H_p}{\partial p^\top}.$$

Integrating the last term on the right side of Eq. (A.3) by parts, we yield:

$$(A.6) \quad \bar{J} = \phi[x(t_f), t_f] + p^\top(t_f)x(t_f) - p^\top(t_0)x(t_0) - \int_{t_0}^{t_f} (H_p[x(t), p(t), u(t), t] + \dot{p}^\top(t)x(t)) dt.$$

Hereafter we neglect second order or higher variations. The variation in J due to variations in the control vector $u(t)$ for fixed times t_0 and t_f is of the form:

$$(A.7) \quad \delta\bar{J} = \left[\left(\frac{\partial\phi}{\partial x} + p^\top \right) \delta x \right]_{t=t_f} - [p^\top(t)\delta x]_{t=t_0} - \int_{t_0}^{t_f} \left[\left(\frac{\partial H_p}{\partial x} + \dot{p}^\top \right) \delta x + \frac{\partial H_p}{\partial u} \delta u \right] dt.$$

For an extremum, $\delta\bar{J} = 0$ holds true for arbitrary $\delta u(t)$ and $\delta x(t)$. This can happen if and only if:

$$(A.8) \quad \begin{cases} \dot{p} = - \left(\frac{\partial H_p}{\partial x} \right)^\top \\ \frac{\partial H_p}{\partial u} = 0; \quad t_0 \leq t \leq t_f \end{cases}$$

For boundary conditions, there are four options.

1. $x(t_0)$ is fixed and $x(t_f)$ is free, i.e. $\delta x|_{t=t_0} = 0$ and $\delta x|_{t=t_f} \neq 0$. Thus, from $\delta\bar{J} = 0$ it follows:

$$(A.9) \quad p(t_f) = - \left(\frac{\partial\phi}{\partial x} \right)_{t=t_f}^\top.$$

2. $x(t_f)$ is fixed and $x(t_0)$ is free, i.e. $\delta x|_{t=t_f} = 0$ and $\delta x|_{t=t_0} \neq 0$. Thus, from $\delta\bar{J} = 0$ it follows:

$$(A.10) \quad p(t_0) = 0.$$

3. $x(t_0)$ and $x(t_f)$ are both fixed, i.e. $\delta x|_{t=t_0} = \delta x|_{t=t_f} = 0$. Therefore, we have no boundary constraints on the adjoint state.

4. $x(t_0)$ and $x(t_f)$ are both free, i.e. $\delta x|_{t=t_0} \neq 0$, $\delta x|_{t=t_f} \neq 0$. Thus, from $\delta\bar{J} = 0$ it follows:

$$p(t_0) = 0; \quad p(t_f) = - \left(\frac{\partial\phi}{\partial x} \right)_{t=t_f}^\top.$$

In summary, to find a control vector $\mathbf{u}(t)$ that produces a stationary value of the cost \mathcal{J} , we must solve the following coupled differential equations:

$$(A.11) \quad \dot{\mathbf{x}}(t) = f[\mathbf{x}(t), \mathbf{u}(t), t]$$

$$(A.12) \quad \dot{\mathbf{p}}(t) = - \left(\frac{\partial H_p}{\partial \mathbf{x}} \right)^\top$$

$$(A.13) \quad \frac{\partial H_p}{\partial \mathbf{u}} = 0.$$

It is worth to mention that the control input $\mathbf{u}(t)$ depends on the adjoint state $\mathbf{p}(t)$ as it follows from Eq. (A.13) since the Pontryagin Hamiltonian H_p depends on the adjoint state $\mathbf{p}(t)$ in its turn. Therefore, in general, Eqs. (A.11) and (A.12) are coupled. However, we also have to take into account the boundary conditions. Simply put, $\mathbf{x}(t)$ is either fixed at the endpoints of the time interval or is free at least at one of the endpoints. In this case, the missing constraint becomes interchanged with another boundary condition on $\mathbf{p}(t)$ at the same endpoint of the time interval (see Eqs. (A.9), (A.10)). The boundary conditions are said to be split when some are given at t_0 , and some are given at t_f . It may happen that some of the components of the state vector $\mathbf{x}(t)$ are fixed either at the initial or final times or at both endpoints and some are required to satisfy another combination of constraints at the fixed times t_0 and t_f . The same rules apply here. We impose similar boundary constraints on the components of the adjoint state vector $\mathbf{p}(t)$ at the fixed times t_0 and/or t_f in case the corresponding components of the state vector are free. The extremum conditions that we have obtained here are proven to correspond to the minimum of the cost functional [89]. Here, we have found the weak version of PMP where the maximization of the Pontryagin Hamiltonian is replaced by an extremum condition given by the partial derivative with respect to \mathbf{u} . For numerical computations, we interchange the continuous dynamical system with a multistage system by discretizing the time interval [69].

A.2 Gradient Based Algorithm

It is not always possible to solve the coupled differential Eqs. (A.11), (A.12) and (A.13) analytically. Fortunately, there have been developed numerical tools over the years. The one that we use in this manuscript is a gradient based algorithm, a counterpart algorithm of GRAPE used in NMR [107]. We start with Eq. (A.13), the necessary condition for PMP which can also be stated as follows:

$$(A.14) \quad H_p[\mathbf{x}(t), \mathbf{p}(t), \mathbf{u}^*(t)] = \max_{\mathbf{u}} H_p[\mathbf{x}(t), \mathbf{p}(t), \mathbf{u}(t)],$$

where \mathbf{u}^* is the optimal control pulse. This provides us with a numerical tool that we can apply to find a local maximum or a candidate for optimality among control inputs. We expand H_p

into Taylor series in terms of the control pulse:

$$(A.15) \quad H_p \left[x(t), p(t), u(t) + \epsilon \frac{\partial H_p}{\partial u} \right] \approx H_p[x(t), p(t), u(t)] + \frac{\partial H_p}{\partial u} \epsilon \frac{\partial H_p}{\partial u} = H_p[x(t), p(t), u(t)] + \epsilon \left[\frac{\partial H_p}{\partial u} \right]^2,$$

where ϵ is a positive parameter. As one may see, the new control pulse $u_1(t) = u(t) + \epsilon \frac{\partial H_p}{\partial u}$ increases the value of H_p , $H_p[x(t), p(t), u_1(t)] > H_p[x(t), p(t), u(t)]$. The parameter ϵ must be sufficiently small such that we remain in the first-order approximation, but large enough to reduce the number of iterations and the computational time [89]. For a good convergence, we also need to find a guess field $u(t)$ sufficiently close to the optimal solution. We arrive at the same conclusion when considering Eq. (A.7). If $x(t_0)$ is fixed, $p(t)$ satisfies Eqs. (A.9) and (A.12) then we deduce from Eq. (A.7) that:

$$(A.16) \quad \delta \bar{J} = - \int_{t_0}^{t_f} \frac{\partial H_p}{\partial u} \delta u dt.$$

This suggests that a better control can be achieved with a choice $\delta u = \epsilon \frac{\partial H_p}{\partial u}$. Thus the new control is $u_1(t) = u + \delta u = u + \epsilon \frac{\partial H_p}{\partial u}$. The consecutive steps of iterative algorithm can be summarized as follows:

1. Choose a guess control u .
2. Propagate forward the state of the system x from $\dot{x} = f[x(t), u(t), t]$ with the initial condition $x(t_0)$.
3. Propagate backward the adjoint state of the system p from $\dot{p} = - \left(\frac{\partial H_p}{\partial x} \right)^T$ with the terminal constraint $p(t_f) = - \left(\frac{\partial \phi}{\partial x} \right)^T_{t=t_f}$.
4. Compute the correction δu to the control law, $\delta u(t) = \epsilon \frac{\partial H_p}{\partial u}$, where $\epsilon > 0$ is a small parameter.
5. Define the new control $u \rightarrow u + \delta u$.
6. Go to the 2nd step until a given accuracy is reached.

A.3

Application of the Gradient Based Algorithm

We introduce in this paragraph the basic principles of a gradient iterative algorithm in the linear case. The dynamics is governed by:

$$(A.17) \quad \dot{\vec{x}}(t) = A\vec{x}(t) + B\vec{u}(t),$$

where $\vec{x} \in \mathbb{R}^n$ is the state of the system, $\vec{u} \in \mathbb{R}^m$ is the control and $A \in \mathbb{M}_{n,n}$, $B \in \mathbb{M}_{n,m}$ are constant matrices. The goal is to maximize in a fixed time t_f the figure of merit (terminal cost) $\phi = \vec{x}(t_f)\vec{x}_f$ (we are on the Bloch sphere) where \vec{x}_f is the target state (a column vector). The Pontryagin Hamiltonian is given by:

$$(A.18) \quad H_p = \vec{p}A\vec{x} + \vec{p}B\vec{u}.$$

The adjoint state $\vec{p} \in \mathbb{R}^n$ (a row vector) is governed by the following dynamics:

$$(A.19) \quad \dot{\vec{p}} = -\vec{p}A.$$

The general solution of this equation is:

$$(A.20) \quad \vec{p}(t) = \vec{p}(t_f)e^{A(t_f-t)},$$

with the final state:

$$(A.21) \quad \vec{p}(t_f) = \frac{\partial \phi}{\partial \vec{x}}(t_f) = \vec{x}_f^\top.$$

To find a local optimum we calculate the gradient g :

$$(A.22) \quad g = \frac{\partial H_p}{\partial u(t)} = \vec{p}B = \vec{x}_f^\top e^{A(t_f-t)}B.$$

Note that the gradient does not depend on the state of the system. The iterative algorithm can be summarized as follows:

1. guess the initial control \vec{u}_0
2. at step k compute the new field $\vec{u}_{k+1} = \vec{u}_k + \epsilon g^\top$
3. go back to step 2

At each step we can propagate forward the state \vec{x}_k and compute $\phi_k = \vec{x}_k(t_f)\vec{x}_f$:

$$(A.23) \quad \vec{x}_k(t_f) = e^{At_f} \vec{x}_0 + e^{At_f} \int_0^{t_f} e^{-A\tau} B\vec{u}(\tau) d\tau.$$

For a small positive value of ϵ , ϕ_k is an increasing sequence which converges towards a local maximum.

Ensemble of Springs

In this chapter, we go deeper into some of the mathematical details related to the control of an ensemble of springs. Here, we introduce the method of inversion of a matrix with its eigenvalues, control of an ensemble of springs reversed in time, and the solution of the main dynamical equation of an ensemble of springs.

B.1 Inversion of a Matrix Using its Eigenvalues

In this chapter we introduce some helpful mathematical tools which were used in the codes. Suppose we are required to inverse a $N \times N$ square matrix A . Assume that we have found its eigenvalues and eigenvectors:

$$(B.1) \quad A |v_i\rangle = \lambda_i |v_i\rangle; \quad i = 1, 2, \dots, N$$

and the eigenvectors $|v_i\rangle$ are orthonormal:

$$(B.2) \quad \langle v_i | v_k \rangle = \delta_{ik}, \quad i, k = 1, 2, \dots, N$$

Orthonormal eigenvectors form a basis in the given vector space:

$$|w\rangle = \sum_{i=1}^N c_i |v_i\rangle,$$

where $|w\rangle$ is an arbitrary vector, and c_i are its expansion coefficients. From the orthonormality condition (see Eq. B.2) we deduce:

$$A |v_i\rangle = \lambda_i |v_i\rangle = \sum_{k=1}^N \lambda_k |v_k\rangle \langle v_k | v_i \rangle = \left(\sum_{k=1}^N \lambda_k |v_k\rangle \langle v_k | \right) |v_i\rangle,$$

hence

$$(B.3) \quad \hat{\Theta}|v_i\rangle = 0,$$

where

$$(B.4) \quad \hat{\Theta} = A - \sum_{k=1}^N \lambda_k |v_k\rangle \langle v_k|$$

According to Eq. (B.3):

$$\hat{\Theta}|w\rangle = \sum_{i=1}^N c_i \Theta|v_i\rangle = 0$$

Since $|w\rangle$ is arbitrary it follows that:

$$(B.5) \quad \hat{\Theta} = 0,$$

whence according to Eq. (B.4):

$$(B.6) \quad A = \sum_{k=1}^N \lambda_k |v_k\rangle \langle v_k|$$

Given that A^{-1} exists that is $\det(A) \neq 0$ and $\lambda_1 \lambda_2 \cdots \lambda_N \neq 0$ we obtain from Eq. (B.1):

$$A^{-1}|v_i\rangle = \frac{1}{\lambda_i}|v_i\rangle$$

In other words this means that $1/\lambda_i$ and $|v_i\rangle$ are respectively the eigenvalues and eigenvectors of A^{-1} , therefore as it has just been proved (see Eq. (B.6)):

$$(B.7) \quad A^{-1} = \sum_{k=1}^N \frac{1}{\lambda_k} |v_k\rangle \langle v_k|$$

Using the built-in function *eig* of matlab we compute inverse matrices.

B.2

Reversing the Direction of Steering

Suppose we have solved a control problem and found the control $u(\tau)$ which steers in a fixed time T an ensemble of springs with $\omega \in [-\omega_0; \omega_0]$ from z_0 to z_1 :

$$(B.8) \quad z_1 = z_0 e^{i\omega T} + e^{i\omega T} \int_0^T e^{-i\omega\tau} u(\tau) d\tau$$

Since the frequency range is symmetric then:

$$(B.9) \quad z_1 = z_0 e^{-i\omega T} + e^{-i\omega T} \int_0^T e^{i\omega\tau} u(\tau) d\tau$$

We now ask the following question: find the control field $v(\tau)$ which steers the same system in a fixed time T backwards from z_1 to z_0 :

$$(B.10) \quad z_0 = z_1 e^{i\omega T} + e^{i\omega T} \int_0^T e^{-i\omega\tau} v(\tau) d\tau$$

From this equation and Eq. (B.9) it follows that:

$$(B.11) \quad \int_0^T e^{-i\omega\tau} v(\tau) d\tau = z_0 e^{-i\omega T} - z_1 = -e^{-i\omega T} \int_0^T e^{i\omega\tau} u(\tau) d\tau$$

Therefore we get:

$$(B.12) \quad \int_0^T e^{-i\omega\tau} v(\tau) d\tau + \int_0^T e^{-i\omega(T-\tau)} u(\tau) d\tau = 0$$

We make a change of variable in the 2nd integral $T - \tau = t$ and we arrive at:

$$(B.13) \quad \int_0^T e^{-i\omega\tau} v(\tau) d\tau + \int_0^T e^{-i\omega\tau} u(T - \tau) d\tau = 0$$

or equivalently:

$$(B.14) \quad \int_0^T e^{-i\omega\tau} [v(\tau) + u(T - \tau)] d\tau = 0$$

Since this equation is valid for any T and $\omega \in [-\omega_0; \omega_0]$ it follows:

$$(B.15) \quad v(\tau) = -u(T - \tau)$$

Given that the initial and target states are real, we can also go from Eq. (B.8) to Eq. (B.9) and arrive at the same conclusion Eq. (B.15) in the case of one control input even if the frequency distribution is not symmetric.

B.3

Different Ways of Solving the Main Dynamical Equation

Control problems of an ensemble of springs require to solve a linear system of first order inhomogeneous differential equations

$$(B.16) \quad \frac{d}{dt} \begin{bmatrix} x_\omega(t) \\ y_\omega(t) \end{bmatrix} = \begin{bmatrix} 0 & -\omega \\ \omega & 0 \end{bmatrix} \begin{bmatrix} x_\omega(t) \\ y_\omega(t) \end{bmatrix} + \begin{bmatrix} u(t) \\ v(t) \end{bmatrix}$$

— namely the evolution equation of harmonic oscillators. Here, as a supplementary material to what I have already written in the main part of the report, I want to present different ways of solving this system of differential equations.

1st solution: We rewrite Eq. (B.16) in a different form:

$$(B.17) \quad \begin{cases} \dot{x}_\omega(t) = -\omega y_\omega(t) + u(t) \\ \dot{y}_\omega(t) = \omega x_\omega(t) + v(t). \end{cases}$$

For simplicity, in the next steps we omit the time variable

$$z_\omega := x_\omega + iy_\omega, \quad \alpha := u + iv.$$

Summing the equations of Eq.(B.17) and using the newly defined variables we end up with a single 1st order complex inhomogeneous differential equation:

$$(B.18) \quad \dot{z}_\omega = i\omega z_\omega + \alpha.$$

The general solution of the corresponding homogeneous equation

$$(B.19) \quad \dot{z}_\omega = i\omega z_\omega$$

is an exponential function:

$$(B.20) \quad z_\omega = c_\omega e^{i\omega t}.$$

Considering c_ω as a time dependent variable and substituting it in the inhomogeneous differential Eq. (B.18) we obtain:

$$(B.21) \quad c_\omega(t) = c_\omega(0) + \int_0^t \alpha(\tau) e^{-i\omega\tau} d\tau,$$

whence

$$z_\omega(t) = c_\omega(0) e^{i\omega t} + e^{i\omega t} \int_0^t \alpha(\tau) e^{-i\omega\tau} d\tau.$$

$c_\omega(0) = z_\omega(0)$ and therefore:

$$(B.22) \quad z_\omega(t) = z_\omega(0) e^{i\omega t} + e^{i\omega t} \int_0^t \alpha(\tau) e^{-i\omega\tau} d\tau.$$

2nd solution: Introducing new notations:

$$(B.23) \quad \vec{X}_\omega := \begin{bmatrix} x_\omega \\ y_\omega \end{bmatrix}, \quad A = \begin{bmatrix} 0 & -\omega \\ \omega & 0 \end{bmatrix}, \quad \vec{B} = \begin{bmatrix} u \\ v \end{bmatrix},$$

we can rewrite Eq. (B.16) in a form of a linear inhomogeneous differential matrix equation:

$$(B.24) \quad \frac{d\vec{X}_\omega}{dt} = A\vec{X}_\omega + \vec{B}.$$

The general solution of the corresponding homogeneous equation:

$$(B.25) \quad \frac{d\vec{X}_\omega}{dt} = A\vec{X}_\omega$$

gives a matrix exponential:

$$(B.26) \quad \vec{X}_\omega = e^{At} \vec{C}_\omega,$$

where \vec{C}_ω is a constant vector. Coming back to the initial Eq. (B.24) we assume that \vec{C}_ω depends on time and we insert it into Eq. (B.24):

$$(B.27) \quad \vec{C}_\omega(t) = \vec{C}_\omega(0) + \int_0^t e^{-A\tau} \vec{B}(\tau) d\tau.$$

Equation (B.26) combined with Eq. (B.27) gives the solution of our problem. e^{At} is a matrix. To write the solution in an explicit way, first we have to solve the eigenvectors and eigenvalues problem for the matrix A . Let \vec{m} and Ω be respectively an eigenvector and eigenvalue of A :

$$A\vec{m} = \Omega\vec{m}, \quad (A - \Omega\mathbf{I}_n)\vec{m} = 0.$$

We are interested in nontrivial eigenvectors, thus we have:

$$\det(A - \Omega\mathbf{I}_n) = 0.$$

This quadratic equation has two solutions $\Omega_1 = i\omega$ and $\Omega_2 = -i\omega$. The corresponding eigenvectors satisfy the following equations:

$$A\vec{m}_1 = i\omega\vec{m}_1, \quad A\vec{m}_2 = -i\omega\vec{m}_2$$

or

$$(A - i\omega\mathbf{I}_n)\vec{m}_1 = 0, \quad (A + i\omega\mathbf{I}_n)\vec{m}_2 = 0.$$

The corresponding solutions read:

$$\vec{m}_1 = m_{1y} \begin{pmatrix} i \\ 1 \end{pmatrix}, \quad \vec{m}_2 = m_{2y} \begin{pmatrix} -i \\ 1 \end{pmatrix}.$$

These eigenvectors are defined up to a constant, thus they can be normalized:

$$\langle m_i | m_i \rangle = 1; \quad i = 1, 2.$$

The normalization coefficients m_{1y}, m_{2y} will therefore be defined up to a constant phase:

$$m_{1y} = m_{2y} = \frac{1}{\sqrt{2}}.$$

The eigenvectors have the final form:

$$(B.28) \quad \vec{m}_1 = \frac{1}{\sqrt{2}} \begin{pmatrix} i \\ 1 \end{pmatrix}, \quad \vec{m}_2 = \frac{1}{\sqrt{2}} \begin{pmatrix} -i \\ 1 \end{pmatrix}$$

It is important to notice the validity of this statement:

$$AP = PD,$$

where P is a matrix whose columns are the right eigenvectors \vec{m}_1 and \vec{m}_2 , and D is a diagonal matrix of the eigenvalues Ω_1 and Ω_2 :

$$P = (\vec{m}_1, \vec{m}_2) = \frac{1}{\sqrt{2}} \begin{pmatrix} i & -i \\ 1 & 1 \end{pmatrix}, \quad D = \begin{pmatrix} \Omega_1 & 0 \\ 0 & \Omega_2 \end{pmatrix} = \begin{pmatrix} i\omega & 0 \\ 0 & -i\omega \end{pmatrix}.$$

In case P is reversible or in other words the inverse matrix P^{-1} is defined, the last statement can be rewritten in the form:

$$A = PDP^{-1}.$$

A matrix exponential e^M of a matrix M is defined by Taylor expansion:

$$(B.29) \quad e^M = \sum_{k=0}^{\infty} \frac{M^k}{k!}.$$

Notice that if M is a number then $\lim_{k \rightarrow \infty} \frac{M^k}{k!} = 0$. According to Eq. (B.29):

$$(B.30) \quad e^{-At} = e^{P(-Dt)P^{-1}} = P e^{-Dt} P^{-1}.$$

We recall that D is a diagonal matrix, hence:

$$(B.31) \quad e^{-Dt} = \begin{pmatrix} e^{-\Omega_1 t} & 0 \\ 0 & e^{-\Omega_2 t} \end{pmatrix} = \begin{pmatrix} e^{-i\omega t} & 0 \\ 0 & e^{i\omega t} \end{pmatrix},$$

and P is a unitary matrix $P^+P = PP^+ = \mathbb{1}$ or in other words $P^{-1} = P^+$. Inserting the corresponding expressions of P , P^{-1} and e^{-Dt} into Eq. (B.30), and doing some simplifications we obtain:

$$(B.32) \quad e^{-At} = \begin{pmatrix} \cos \omega t & \sin \omega t \\ -\sin \omega t & \cos \omega t \end{pmatrix}.$$

It is useful to mention that e^{-At} is an orthogonal matrix that is $(e^{-At})^T e^{-At} = \mathbb{1}$ or in other words $(e^{-At})^{-1} = (e^{-At})^T = e^{At}$. According to Eq. (B.27) (we recall that $B = (u \ v)^T$):

$$(B.33) \quad \vec{C}_\omega(t) = \vec{C}_\omega(0) + \int_0^t \begin{pmatrix} u \cos \omega \tau + v \sin \omega \tau \\ -u \sin \omega \tau + v \cos \omega \tau \end{pmatrix} d\tau.$$

Eq. (B.26) now reads:

$$(B.34) \quad \begin{bmatrix} x_\omega \\ y_\omega \end{bmatrix} = \begin{bmatrix} \cos \omega t & -\sin \omega t \\ \sin \omega t & \cos \omega t \end{bmatrix} \left\{ \begin{bmatrix} C_\omega^x(0) \\ C_\omega^y(0) \end{bmatrix} + \int_0^t \begin{bmatrix} u \cos \omega \tau + v \sin \omega \tau \\ -u \sin \omega \tau + v \cos \omega \tau \end{bmatrix} d\tau \right\},$$

where $C_\omega^x(t)$ and $C_\omega^y(t)$ are the vector components of $\vec{C}_\omega(t)$. We introduce new variables z_ω , α_ω , α , and for simplicity we omit mentioning the time dependency:

$$(B.35) \quad z_\omega := x_\omega + iy_\omega, \quad \alpha_\omega = C_\omega^x + iC_\omega^y, \quad \alpha := u + iv.$$

After doing the matrix multiplication, summing x and y components of vectors of Eq.(B.34), and after some straightforward calculations we finally arrive at the expected solution (notice that $\alpha_\omega(0) = z_\omega(0)$):

$$(B.36) \quad z_\omega(t) = z_\omega(0)e^{i\omega t} + e^{i\omega t} \int_0^t \alpha(\tau)e^{-i\omega\tau} d\tau.$$



Special Integrals and Approximations

This chapter is aimed to introduce a toolbox of integrals which are used in the manuscript. The two well-known integral functions among others that are presented in the next section are the Fresnel and the imaginary error functions.

C.1

Fresnel and Imaginary Error Functions

Here, we present the Fresnel and imaginary error functions and the relation between them. The simulations we make in the manuscript work with both integral functions. Since most of the simulations of the manuscript are made by "Matlab", we keep the same definitions as there [118]. The imaginary error function is given by the following form:

$$(C.1) \quad \operatorname{erfi}(x) = \frac{2}{\sqrt{\pi}} \int_0^x e^{t^2} dt.$$

The Fresnel sine and cosine integrals of x are respectively given in the following ways [118]:

$$\begin{aligned} \operatorname{fresnels}(x) &= \int_0^x \sin\left(\frac{\pi t^2}{2}\right) dt \\ \operatorname{fresnelc}(x) &= \int_0^x \cos\left(\frac{\pi t^2}{2}\right) dt \end{aligned}$$

For simplicity of the equations, we define a new function which we loosely call Fresnel integral:

$$(C.2) \quad \operatorname{fresnelz}(x) = \int_0^x e^{i\left(\frac{\pi t^2}{2}\right)} dt.$$

By change of a variable $\sqrt{\frac{\pi}{2}}t = \tau$, the Fresnel integral can be represented in a different form:

$$(C.3) \quad \text{fresnelz}(x) = \sqrt{\frac{2}{\pi}} \int_0^{\sqrt{\frac{\pi}{2}}x} e^{i\tau^2} d\tau.$$

We can now express the integral on the right side of the equation with the Fresnel integral:

$$(C.4) \quad \int_0^z e^{i\tau^2} d\tau = \sqrt{\frac{\pi}{2}} \text{fresnelz}\left(\sqrt{\frac{2}{\pi}}z\right).$$

Imaginary error function is expressed by means of the Fresnel function in the following way:

$$(C.5) \quad \text{erfi}(x) = (1+i)\text{fresnelz}\left(\sqrt{\frac{2}{\pi}}e^{-i\frac{\pi}{4}}x\right).$$

In the regime of adiabatic control we encounter an integral of specific form:

$$(C.6) \quad \mathcal{K}(\alpha, \beta) = \int_0^{t_f} e^{i(\alpha t^2 + \beta t)} dt.$$

By completing the square in the argument of the integrand exponential we arrive at:

$$(C.7) \quad \mathcal{K}(\alpha, \beta) = e^{-i\frac{\beta^2}{4\alpha}} \int_0^{t_f} \exp\left(\left[e^{i\frac{\pi}{4}}\sqrt{\alpha}\left(t + \frac{\beta}{2\alpha}\right)\right]^2\right) dt.$$

Integration by substitution can be expressed in terms of imaginary error function:

$$(C.8) \quad \mathcal{K}(\alpha, \beta) = \frac{1}{2}\sqrt{\frac{\pi}{\alpha}} e^{-i\left(\frac{\pi}{4} + \frac{\beta^2}{4\alpha}\right)} [\text{erfi}(b) - \text{erfi}(a)]$$

or in terms of the Fresnel function (see Eq. (C.5)):

$$(C.9) \quad \mathcal{K}(\alpha, \beta) = \sqrt{\frac{\pi}{2\alpha}} e^{-i\frac{\beta^2}{4\alpha}} [\text{fresnelz}(b') - \text{fresnelz}(a')],$$

where the parameters a , b , a' and b' are given in the following way:

$$(C.10) \quad a = e^{i\frac{\pi}{4}}\sqrt{\alpha}\frac{\beta}{2\alpha}, \quad b = e^{i\frac{\pi}{4}}\sqrt{\alpha}\left(t_f + \frac{\beta}{2\alpha}\right), \quad a' = \sqrt{\frac{2\alpha}{\pi}}\frac{\beta}{2\alpha}, \quad b' = \sqrt{\frac{2\alpha}{\pi}}\left(t_f + \frac{\beta}{2\alpha}\right).$$

Fresnel function is a special function that can not be represented as a finite sum of elementary functions. However, representation of the Fresnel function with infinite series is still possible. First of all, it is useful to recall one important result of complex analysis:

$$(C.11) \quad \int_0^{+\infty} e^{it^2} dt = \frac{\sqrt{\pi}}{2} e^{i\frac{\pi}{4}}.$$

We now consider the tail of this integral:

$$(C.12) \quad f(x) = \int_x^{+\infty} e^{i\tau^2} d\tau,$$

where $x > 0$. By using the substitution $\tau^2 = t$, we arrive at:

$$(C.13) \quad f(x) = \frac{1}{2} \int_{x^2}^{+\infty} \frac{e^{it}}{\sqrt{t}} dt.$$

Continuously integrating by parts the right side of Eq. (C.13), we derive a representation of $f(x)$ with infinite series:

$$(C.14) \quad f(x) = \frac{i}{2} \frac{e^{ix^2}}{x} \left[1 + \sum_{n=1}^{\infty} \left(-\frac{i}{2} \right)^n \frac{(2n-1)!!}{x^{2n}} \right].$$

According to Eqs. (C.3), (C.11), (C.12):

$$(C.15) \quad \text{fresnelz}(x) = \sqrt{\frac{2}{\pi}} \left[\int_0^{+\infty} e^{it^2} dt - \int_{\sqrt{\frac{\pi}{2}}x}^{+\infty} e^{it^2} dt \right] = \sqrt{\frac{2}{\pi}} \left[\frac{\sqrt{\pi}}{2} e^{i\frac{\pi}{4}} - f\left(\sqrt{\frac{\pi}{2}}x\right) \right],$$

and finally substituting the infinite series representation of $f\left(\sqrt{\frac{\pi}{2}}x\right)$ from Eq. (C.14) we get the representation of the Fresnel function via infinite series:

$$(C.16) \quad \text{fresnelz}(x) = \frac{e^{i\frac{\pi}{4}}}{\sqrt{2}} - \frac{i}{\pi} \frac{e^{i\frac{\pi}{2}} x^2}{x} \left[1 + \sum_{n=1}^{\infty} \left(-\frac{i}{\pi} \right)^n \frac{(2n-1)!!}{x^{2n}} \right].$$

In the main text, however, we use the built-in Fresnel function of "Matlab". Since the \mathcal{K} function is expressed via Fresnel function by Eqs. (C.9), (C.10) then it can also be represented in infinite series and computed by the built-in Fresnel function. Therefore, in the main work, the final results contain the function \mathcal{K} , which is sufficient.

C.2 Special Integrals

When it comes to calculating the dynamics of ions under the influence of the SWIFT pulse, we encounter a special type of integrals:

$$\begin{cases} \mathcal{I}_c(t, \omega_s, \omega) = \int \text{sinc}(\omega_s(t-t_0)) \cos(\omega(t_f-t)) dt \\ \mathcal{I}_s(t, \omega_s, \omega) = \int \text{sinc}(\omega_s(t-t_0)) \sin(\omega(t_f-t)) dt. \end{cases}$$

For that purpose, we use the sine and the cosine integral functions Si and Ci [118], which are defined by:

$$\text{Si}(x) = \int_0^x \text{sinc}(t) dt, \text{Ci}(x) = - \int_x^{\infty} \frac{\cos t}{t} dt = \gamma + \ln x + \int_0^x \frac{\cos t - 1}{t} dt, x > 0,$$

where γ is the EulerMascheroni constant [118]:

$$(C.17) \quad \gamma = \lim_{n \rightarrow \infty} \left(\sum_{k=1}^n \frac{1}{k} - \ln(n) \right).$$

We have the following results:

$$\begin{aligned} \mathcal{J}_c(t, \omega_s, \omega) &= \frac{\sin[(t_0 - t_f)\omega]}{2\omega_s} (\text{Ci}[(t_0 - t)(\omega + \omega_s)] - \text{Ci}[(t_0 - t)(\omega - \omega_s)]) + \\ &\quad \frac{\cos[(t_0 - t_f)\omega]}{2\omega_s} (\text{Si}[(t_0 - t)(\omega - \omega_s)] - \text{Si}[(t_0 - t)(\omega + \omega_s)]) \\ \mathcal{J}_s(t, \omega_s, \omega) &= \frac{\cos[(t_0 - t_f)\omega]}{2\omega_s} (\text{Ci}[(t_0 - t)(\omega + \omega_s)] - \text{Ci}[(t_0 - t)(\omega - \omega_s)]) + \\ &\quad \frac{\sin[(t_0 - t_f)\omega]}{2\omega_s} (\text{Si}[(t_0 - t)(\omega + \omega_s)] - \text{Si}[(t_0 - t)(\omega - \omega_s)]) \end{aligned}$$

C.3

Stationary Phase Approximation

One approximation that we use in the control of an ensemble of springs and ions is the stationary phase approximation. As a starting point, we consider the following integral:

$$(C.18) \quad \hat{h}(\omega) = \int_{-\infty}^{\infty} h(t) e^{i\varphi(t)} dt$$

where φ is a smooth function, which is assumed to be rapidly varying with respect to h . A stationary point t_0 satisfies $\varphi^{(1)}(t_0) = 0$, where $\varphi^{(n)}$ denotes the n th time derivative of φ . By expanding $\varphi(t)$ into Taylor series around $t = t_0$:

$$(C.19) \quad \varphi(t) = \varphi(t_0) + (t - t_0)\varphi^{(1)}(t_0) + \frac{(t - t_0)^2}{2}\varphi^{(2)}(t_0) + \dots$$

we deduce that

$$(C.20) \quad \hat{h}(\omega) \simeq h(t_0) e^{i\varphi(t_0)} \int_{-\infty}^{\infty} e^{i\frac{\xi^2}{2}\varphi^{(2)}(t_0)} d\xi \simeq \sqrt{\frac{2\pi}{\varphi^{(2)}(t_0)}} h(t_0) e^{i\left[\varphi(t_0) + \frac{\pi}{4}\right]}.$$

For a chirp excitation, the phase $\varphi(t)$ is defined by $\varphi(t) = \omega_i t + \frac{st^2}{2}$. The instantaneous frequency $\omega(t)$ can be expressed as

$$(C.21) \quad \omega(t) = \varphi^{(1)}(t) = \omega_i + st,$$

where $s = \omega^{(1)}(t)$. For a linear evolution of $\omega(t)$ between ω_i and ω_f , the rate s is given by $s = (\omega_f - \omega_i)/t_f$. We assume that $s > 0$. We deduce that the Fourier transform of the control field is given by

$$(C.22) \quad \hat{u}(\omega) = \int_0^{t_f} u(t) e^{-i\omega t} dt = \frac{u_0}{2} \int_0^{t_f} \left[e^{i\left(\omega_i t + \frac{st^2}{2} - \omega t\right)} + e^{-i\left(\omega_i t + \frac{st^2}{2} + \omega t\right)} \right] dt.$$

We denote by φ_1 and φ_2 the arguments of the two exponential terms. It is straightforward to verify that $\varphi_1^{(1)}(t) = 0$ for $t = t_1^{(\omega)} = \frac{\omega - \omega_i}{s}$ and that $\varphi_2^{(1)}(t) = 0$ for $t = t_2^{(\omega)} = \frac{-\omega - \omega_i}{s}$. We neglect the second contribution since $t_2^{(\omega)} < 0$. If $t_1^{(\omega)}$ is not too close to 0 and t_f , we can consider that the integral is defined from $-\infty$ to $+\infty$. We finally arrive at

$$(C.23) \quad \hat{u}(\omega) = u_0 \sqrt{\frac{\pi}{2s}} e^{i\left[\frac{\pi}{4} + \varphi_1(t_1^{(\omega)})\right]},$$

The phase spectrum $\varphi(\omega) = \frac{\pi}{4} + \varphi(t_1^{(\omega)})$ can be written as

$$(C.24) \quad \varphi(\omega) = \frac{\pi}{4} - \frac{(\omega - \omega_i)^2}{2s}.$$

In the time evolution of an ensemble of springs and ions we encounter the very integral of Eq. (C.22). The efficiency of this approximation is illustrated in Fig. 2.27.

C.4

Rotating Wave Approximation

We discuss in this section the validity of the **RWA** described in Sec. 3.1.2. We consider the following dynamical system:

$$(C.25) \quad \dot{z} = -i\omega z + u \cos(\omega_0 t)$$

which corresponds to Eq. (3.6) of the main text. Equation (C.25) describes a spring of frequency $\omega/(2\pi)$ excited by an external field of constant amplitude u and of frequency $\omega_0/(2\pi)$. Introducing the frame rotating at ω_0 with the transformation $z = \tilde{z} e^{-i\omega_0 t}$, we arrive at:

$$\dot{\tilde{z}} = -i\Delta\omega \tilde{z} + \frac{u}{2}(1 + e^{2i\omega_0 t}),$$

where $\Delta\omega = \omega - \omega_0$ is the detuning. In the **RWA**, we neglect the fast oscillating term and we get:

$$\dot{\tilde{z}}_r = -i\Delta\omega \tilde{z}_r + \frac{u}{2}.$$

where \tilde{z}_r denotes the approximate \tilde{z} -variable. We set $\delta\tilde{z} = \tilde{z} - \tilde{z}_r$ and obtain:

$$\delta\dot{\tilde{z}} = -i\Delta\omega \delta\tilde{z} + \frac{u}{2} e^{2i\omega_0 t}.$$

This differential system can be exactly integrated:

$$\delta\tilde{z}(t) = \int_0^t e^{-i\Delta\omega(t-\tau)} \frac{u}{2} e^{2i\omega_0 \tau} d\tau.$$

This leads to:

$$\delta\tilde{z}(t) = e^{i(\omega_0 - \frac{\Delta\omega}{2})t} \frac{u}{2\omega_0 + \Delta\omega} \sin\left(\left(\omega_0 + \frac{\Delta\omega}{2}\right)t\right).$$

We deduce that the relative error due to the RWA can be expressed as:

$$\left| \frac{\delta\tilde{z}}{\tilde{z}_r} \right| = \frac{|\Delta\omega|}{2\omega_0 + \Delta\omega} \left| \frac{\sin\left(\left(\omega_0 + \frac{\Delta\omega}{2}\right)t\right)}{\sin(\Delta\omega t/2)} \right|.$$

A rough approximation gives:

$$\left| \frac{\delta \tilde{z}}{\tilde{z}_r} \right| \simeq \frac{|\Delta \omega|}{2\omega_0 + \Delta \omega}$$

RWA is therefore justified if $|\Delta \omega| \ll 2\omega_0$. Numerical simulations show that this formula overestimates the error and that **RWA** can be used in a quite wide interval around the carrier frequency of the excitation pulse.

Conclusions

In this manuscript, we have applied OCT and STA in three different physical systems. The simplest model that we have considered is RC circuit. This control problem has the decisive advantage of being linear which simplifies considerably the design of control pulses. Here, we apply a simple STA approach based on inverse engineering technique. This allows us to account for local constraints, in particular at time interval boundaries. Contrary to this, OCT protocols are built on a global constraint, the minimization of a cost functional. A few bases of functions for the trajectory to be expanded over are considered. Each of them depends on a finite number of parameters which are determined from the imposed boundary conditions. The remaining free parameters are used to minimize the cost functional. Our findings reflect that real exponential functions inspired by regularized optimal solutions give very efficient results as opposed to polynomial and trigonometric functions. STA protocols can be made robust against uncertainties at the endpoints of the time interval by canceling the successive time derivatives at the same endpoints. OCT solutions are however perfectly suited for a well-defined time interval but fail in case of time interval uncertainties. Inspired by STA local constraints, we have improved the robustness of OCT solutions by enlarging the parameter space of the optimal control problem so as to account for local constraints at time interval boundaries. The findings in this direction can be applied in other linear control problems and also non-linear control problems in the regime of linear approximation.

The second problem that we discuss in the manuscript refers to control of an ensemble of springs with dispersion in their natural frequencies. The different methods we have developed in this area can be used in any linear control system. They also provide interesting alternatives to design control pulses for two-level quantum systems. We have shown the advantages of STA and optimal protocols over adiabatic control. Any target state and control duration can be formally chosen. We have obtained robust broadband, narrowband, selective and ultrahigh fidelity control pulses. In order to satisfy experimental limitations on the shape of the control field, additional constraints have to be accounted for. For the two methods, only a finite set of frequencies (with a regular discretization) are considered. We have also explained how this set of frequencies can be optimized in a practical application to improve the efficiency of the control process. It turns out that the regular distribution of offset frequencies is actually far from being the optimal choice. We have also discussed the relative advantages of the two methods. The efficiency of the derived control fields is comparable. STA allows to derive simple and

smooth control solutions, which can be expanded in a given basis of functions. However, it is difficult to account for additional constraints on the amplitude or the energy of the pulse, requirements that can be fulfilled with [OCT](#). Another future research direction is the extension of this approach to other nonlinear dynamical systems. From a mathematical point of view, this method can be applied in a neighborhood of a fixed point of the dynamics. A major limitation of this idea is related to the size of the region around the fixed point that can be considered to reach the target state with a given accuracy. As shown in this study, this size is quite large for a two-level quantum system because robust or selective excitation processes can be realized from the linearized system. This characteristic is not known a priori and has to be determined in each practical case.

The last example we have considered is the robust excitation of ions in [FT-ICR](#). We considered the simplified conditions of a [2D](#) trajectory and of a homogeneous magnetic field. The study is not fully realistic. Effects such as the magnetron motion, field geometry, field inhomogeneities or ion collisions are neglected. However, the presented model system describes quite well the main cyclotronic behavior and gives the main features of ion trajectories. In the case without pulse limitation, the linearity of the dynamical equations allows us to use [LQOCT](#), which has the advantage to lead to an analytic formula of the control law. Very good results were obtained both for the final radii and phases of the ions. This solution is both in shape and in amplitude very similar to the [SWIFT](#) pulse. The two solutions are expected to be equal for a continuous range of frequencies. More original control laws are derived when the pulse intensity is limited. A well-known optimal iterative algorithm, GRAPE, which is used in [NMR](#), has been adapted to [FT-ICR](#). This algorithm allows reducing the pulse intensity by a factor larger than three in the examples under study. On the basis of [NMR](#) results, this algorithm is expected to be very efficient in the case of other excitation profiles. The very encouraging and promising results obtained in this investigation must now be confirmed by experimental implementation. The relative simplicity of the application of numerical optimal algorithms makes it possible to adapt it straightforwardly to a new class of control problems. There is therefore confidence about the extension of optimization procedures to these additional experimental constraints and limitations.

To summarize, we have completed the toolbox of quantum control by developing and applying [STA](#) and [OCT](#) techniques to linear systems. Such control pulses can also be used under some conditions in non-linear dynamical systems and for quantum dynamics. In this latter case, we only consider in this manuscript state to state transfer for two level quantum systems. A next goal would be to generalize this procedure to quantum gates or state to state transfer in three or four level quantum systems. We have developed [STA](#) protocols with motion planning approach by introducing generating functions for linear systems. It would be interesting to generalize this approach to other non-linear systems. The problem of [FT-ICR](#) has been solved by considering a simple model. The next step is to take into account the magnetron motion and the magnetic field inhomogeneity.

Bibliography

- [1] R. Murray, “Skillful writing of an awful research paper”, [Analytical Chemistry](#) **83**, edited by R. Murray, 633–633 (2011) (cit. on p. v).
- [2] J. C. Adams, *An explanation of the observed irregularities in the motion of Uranus, on the hypothesis of disturbances caused by a more distant planet; with a determination of the mass, orbit, and position of the disturbing body. (From the Appendix to the Nautical Almanac for the Year 1851.)* (W. Clowes & Sons, 1846), 31 pp. (cit. on p. 3).
- [3] U. J. Le Verrier, “Recherches sur les mouvements d’Uranus”, *Astronomische Nachrichten* **25**, 53–80 (1846) (cit. on p. 3).
- [4] H. Weyl, “Über die asymptotische verteilung der eigenwerte”, *Nachrichten von der Gesellschaft der Wissenschaften zu Göttingen, Mathematisch-Physikalische Klasse* **1911**, 110–117 (1911) (cit. on p. 3).
- [5] V. Ambarzumian, “Über die Beziehung zwischen der Lösung und der Resolvente der Integralgleichung des Strahlungs-gleichgewichts”, [Zeitschrift für Physik](#) **52**, 263–267 (1929) (cit. on p. 3).
- [6] M. Athans and P. L. Falb, *Optimal control: an introduction to the theory and its applications* (DOVER PUBN INC, Dec. 1, 2006), 879 pp. (cit. on pp. 4, 121).
- [7] L. Elsgolts, *Differential equations and the calculus of variations* (University Press of the Pacific, Honolulu, Hawaii, 2004) (cit. on p. 4).
- [8] H. Schättler and U. Ledzewicz, *Geometric optimal control* (Springer-Verlag GmbH, June 26, 2012), 640 pp. (cit. on pp. 4, 121).
- [9] M. R. Hestenes, “On variational theory and optimal control theory”, [Journal of the Society for Industrial and Applied Mathematics Series A Control](#) **3**, 23–48 (1965) (cit. on pp. 4, 121).
- [10] A. Bryson, “Optimal control-1950 to 1985”, [IEEE Control Systems](#) **16**, 26–33 (1996) (cit. on p. 4).
- [11] M. Lapert, Y. Zhang, M. Braun, S. J. Glaser, and D. Sugny, “Singular extremals for the time-optimal control of dissipative spin 1/2 particles”, [Physical Review Letters](#) **104**, 083001 (2010) (cit. on pp. 4, 11).

- [12] H. Shen and P. Tsiotras, “Time-optimal control of axisymmetric rigid spacecraft using two controls”, *Journal of Guidance, Control, and Dynamics* **22**, 682–694 (1999) (cit. on p. 4).
- [13] N. Khaneja, R. Brockett, and S. J. Glaser, “Time optimal control in spin systems”, *Physical Review A* **63**, 032308 (2001) (cit. on p. 4).
- [14] U. Boscain and P. Mason, “Time minimal trajectories for a spin 1/2 particle in a magnetic field”, *Journal of Mathematical Physics* **47**, 062101 (2006) (cit. on p. 4).
- [15] A. E. Bryson, M. N. Desai, and W. C. Hoffman, “Energy-state approximation in performance optimization of supersonic aircraft”, *Journal of Aircraft* **6**, 481–488 (1969) (cit. on p. 4).
- [16] S.-W. Liu and T. Singh, “Fuel/time optimal control of spacecraft maneuvers”, *Journal of Guidance, Control, and Dynamics* **20**, 394–397 (1997) (cit. on p. 4).
- [17] E. Torrontegui, I. Lizuain, S. González-Resines, A. Tobalina, A. Ruschhaupt, R. Kosloff, and J. G. Muga, “Energy consumption for shortcuts to adiabaticity”, *Physical Review A* **96**, 022133 (2017) (cit. on p. 4).
- [18] D. Stefanatos, “Fast control of a gun-turret using shortcuts to adiabaticity”, *Journal of Applied Mathematics and Bioinformatics*, vol. 8, no. 2, 17-28 (2018) (cit. on p. 4).
- [19] C. Brif, R. Chakrabarti, and H. Rabitz, “Control of quantum phenomena: past, present and future”, *New Journal of Physics* **12**, 075008 (2010) (cit. on p. 4).
- [20] C. P. Koch, M. Lemesko, and D. Sugny, “Quantum control of molecular rotation”, *Reviews of Modern Physics* **91**, 035005 (2019) (cit. on p. 4).
- [21] M. H. Levitt, *Spin Dynamics: Basics of Nuclear Magnetic Resonance* (Wiley John & Sons, Mar. 7, 2008), 744 pp. (cit. on p. 4).
- [22] R. R. Ernst, A. Wokaun, and G. Bodenhausen, *Principles of nuclear magnetic resonance in one and two dimensions* (OUP Oxford, May 31, 1990), 636 pp. (cit. on pp. 4, 99).
- [23] K. Kobzar, S. Ehni, T. E. Skinner, S. J. Glaser, and B. Luy, “Exploring the limits of broadband 90° and 180° universal rotation pulses”, *Journal of Magnetic Resonance* **225**, 142–160 (2012) (cit. on pp. 4, 59, 109).
- [24] K. Kobzar, T. E. Skinner, N. Khaneja, S. J. Glaser, and B. Luy, “Exploring the limits of broadband excitation and inversion pulses”, *Journal of Magnetic Resonance* **170**, 236–243 (2004) (cit. on pp. 4, 59, 109).
- [25] J. Mao, T. Mareci, K. Scott, and E. Andrew, “Selective inversion radiofrequency pulses by optimal control”, *Journal of Magnetic Resonance* (1969) **70**, 310–318 (1986) (cit. on p. 4).

-
- [26] S. Conolly, D. Nishimura, and A. Macovski, “Optimal control solutions to the magnetic resonance selective excitation problem”, *IEEE Transactions on Medical Imaging* **5**, 106–115 (1986) (cit. on p. 4).
- [27] D. Rosenfeld and Y. Zur, “Design of adiabatic selective pulses using optimal control theory”, *Magnetic Resonance in Medicine* **36**, 401–409 (1996) (cit. on p. 4).
- [28] N. C. Nielsen, C. Kehlet, S. J. Glaser, and N. Khaneja, “Optimal control methods in NMR spectroscopy”, *eMagRes* (2007) (cit. on p. 4).
- [29] M. A. Nielsen and I. L. Chuang, *Quantum Computation and Quantum Information* (Cambridge University Pr., Dec. 1, 2010) (cit. on p. 4).
- [30] D. Stefanatos, N. Khaneja, and S. J. Glaser, “Optimal control of coupled spins in the presence of longitudinal and transverse relaxation”, *Physical Review A* **69**, 022319 (2004) (cit. on p. 4).
- [31] M. A. Bernstein, K. F. King, and X. J. Zhou, *Handbook of MRI pulse sequences* (ACADEMIC PR INC, Aug. 1, 2004), 1017 pp. (cit. on pp. 4, 62).
- [32] M. Lapert, Y. Zhang, M. A. Janich, S. J. Glaser, and D. Sugny, “Exploring the physical limits of saturation contrast in magnetic resonance imaging”, *Scientific Reports* **2** (2012) (cit. on p. 4).
- [33] M. S. Vinding, I. I. Maximov, Z. Tosner, and N. C. Nielsen, “Fast numerical design of spatial-selective RF pulses in MRI using Krotov and quasi-Newton based optimal control methods”, *The Journal of Chemical Physics* **137**, 054203 (2012) (cit. on p. 4).
- [34] I. I. Maximov, M. S. Vinding, D. H. Tse, N. C. Nielsen, and N. J. Shah, “Real-time 2D spatially selective MRI experiments: comparative analysis of optimal control design methods”, *Journal of Magnetic Resonance* **254**, 110–120 (2015) (cit. on p. 4).
- [35] D. Stefanatos, “Optimal efficiency of a noisy quantum heat engine”, *Physical Review E* **90**, 012119 (2014) (cit. on p. 4).
- [36] X. Chen, E. Torrontegui, D. Stefanatos, J.-S. Li, and J. G. Muga, “Optimal trajectories for efficient atomic transport without final excitation”, *Physical Review A* **84**, 043415 (2011) (cit. on pp. 4, 7).
- [37] D. Stefanatos, J. Ruths, and J.-S. Li, “Frictionless atom cooling in harmonic traps: a time-optimal approach”, *Physical Review A* **82**, 063422 (2010) (cit. on pp. 4, 7).
- [38] S. J. Glaser, U. Boscain, T. Calarco, C. P. Koch, W. Köckenberger, R. Kosloff, I. Kuprov, B. Luy, S. Schirmer, T. Schulte-Herbrüggen, D. Sugny, and F. K. Wilhelm, “Training Schrödinger’s cat: quantum optimal control”, *The European Physical Journal D* **69** (2015) (cit. on pp. 4, 47).
- [39] S. Campbell and S. Deffner, “Trade-off between speed and cost in shortcuts to adiabaticity”, *Physical Review Letters* **118**, 100601 (2017) (cit. on p. 4).

- [40] J. P. Carvalho and A. J. Pell, “Frequency-swept adiabatic pulses for broadband solid-state MAS NMR”, [Journal of Magnetic Resonance](#) **324**, 106911 (2021) (cit. on pp. 4, 89).
- [41] N. V. Vitanov, A. A. Rangelov, B. W. Shore, and K. Bergmann, “Stimulated Raman adiabatic passage in physics, chemistry, and beyond”, [Reviews of Modern Physics](#) **89**, 015006 (2017) (cit. on pp. 4, 89).
- [42] N. V. Vitanov, T. Halfmann, B. W. Shore, and K. Bergmann, “Laser-induced population transfer by adiabatic passage techniques”, [Annual Review of Physical Chemistry](#) **52**, 763–809 (2001) (cit. on pp. 4, 89).
- [43] U. V. Boscain, F. Chittaro, P. Mason, and M. Sigalotti, “Adiabatic Control of the Schrödinger Equation via Conical Intersections of the Eigenvalues”, [IEEE Transactions on Automatic Control](#) **57**, 1970–1983 (2012) (cit. on pp. 4, 89).
- [44] X. Chen, I. Lizuain, A. Ruschhaupt, D. Guéry-Odelin, and J. G. Muga, “Shortcut to adiabatic passage in two- and three-level atoms”, [Physical Review Letters](#) **105**, 123003 (2010) (cit. on p. 4).
- [45] D. Daems, A. Ruschhaupt, D. Sugny, and S. Guérin, “Robust quantum control by a single-shot shaped pulse”, [Physical Review Letters](#) **111**, 050404 (2013) (cit. on p. 4).
- [46] A. Ruschhaupt, X. Chen, D. Alonso, and J. G. Muga, “Optimally robust shortcuts to population inversion in two-level quantum systems”, [New Journal of Physics](#) **14**, 093040 (2012) (cit. on p. 4).
- [47] E. Torrontegui, S. Ibáñez, S. Martínez-Garaot, M. Modugno, A. del Campo, D. Guéry-Odelin, A. Ruschhaupt, X. Chen, and J. G. Muga, “Shortcuts to adiabaticity”, in [Advances in atomic, molecular, and optical physics](#) (Elsevier, 2013), pp. 117–169 (cit. on pp. 4, 71).
- [48] S. Deffner, C. Jarzynski, and A. del Campo, “Classical and quantum shortcuts to adiabaticity for scale-invariant driving”, [Physical Review X](#) **4**, 021013 (2014) (cit. on pp. 4, 71).
- [49] M. Kolodrubetz, D. Sels, P. Mehta, and A. Polkovnikov, “Geometry and non-adiabatic response in quantum and classical systems”, [Physics Reports](#) **697**, 1–87 (2017) (cit. on pp. 4, 71).
- [50] D. Guéry-Odelin, A. Ruschhaupt, A. Kiely, E. Torrontegui, S. Martínez-Garaot, and J. Muga, “Shortcuts to adiabaticity: concepts, methods, and applications”, [Reviews of Modern Physics](#) **91**, 045001 (2019) (cit. on pp. 4, 71).
- [51] L. Van-Damme, D. Schraft, G. T. Genov, D. Sugny, T. Halfmann, and S. Guérin, “Robust not gate by single-shot-shaped pulses: demonstration of the efficiency of the pulses in rephasing atomic coherences”, [Physical Review A](#) **96**, 022309 (2017) (cit. on p. 4).

-
- [52] D. Stefanatos and E. Paspalakis, “A shortcut tour of quantum control methods for modern quantum technologies”, *EPL (Europhysics Letters)* **132**, 60001 (2020) (cit. on p. 4).
- [53] D. Stefanatos and E. Paspalakis, “Resonant shortcuts for adiabatic rapid passage with only z-field control”, *Physical Review A* **100**, 012111 (2019) (cit. on p. 4).
- [54] A. del Campo and K. Kim, “Focus on shortcuts to adiabaticity”, *New Journal of Physics* **21**, 050201 (2019) (cit. on p. 4).
- [55] J.-F. Schaff, P. Capuzzi, G. Labeyrie, and P. Vignolo, “Shortcuts to adiabaticity for trapped ultracold gases”, *New Journal of Physics* **13**, 113017 (2011) (cit. on p. 4).
- [56] I. A. Martínez, A. Petrosyan, D. Guéry-Odelin, E. Trizac, and S. Ciliberto, “Engineered swift equilibration of a Brownian particle”, *Nature Physics* **12**, 843–846 (2016) (cit. on p. 4).
- [57] E. Torrontegui, S. Martínez-Garaot, A. Ruschhaupt, and J. G. Muga, “Shortcuts to adiabaticity: fast-forward approach”, *Physical Review A* **86**, 013601 (2012) (cit. on p. 4).
- [58] C. Whitty, A. Kiely, and A. Ruschhaupt, “Quantum control via enhanced shortcuts to adiabaticity”, *Physical Review Research* **2**, 023360 (2020) (cit. on p. 4).
- [59] A. del Campo, “Shortcuts to adiabaticity by counterdiabatic driving”, *Physical Review Letters* **111**, 100502 (2013) (cit. on p. 4).
- [60] S. An, D. Lv, A. del Campo, and K. Kim, “Shortcuts to adiabaticity by counterdiabatic driving for trapped-ion displacement in phase space”, *Nature Communications* **7** (2016) (cit. on p. 4).
- [61] A. del Campo and M. G. Boshier, “Shortcuts to adiabaticity in a time-dependent box”, *Scientific Reports* **2** (2012) (cit. on p. 4).
- [62] J.-S. Li, J. Ruths, and S. J. Glaser, “Exact broadband excitation of two-level systems by mapping spins to springs”, *Nature Communications* **8** (2017) (cit. on pp. 5, 47, 48, 62, 63, 65, 67, 99).
- [63] S. Faure, S. Ciliberto, E. Trizac, and D. Guéry-Odelin, “Shortcut to stationary regimes: a simple experimental demonstration”, *American Journal of Physics* **87**, 125–129 (2019) (cit. on pp. 7, 8).
- [64] V. Martikyan, D. Guéry-Odelin, and D. Sugny, “Comparison between optimal control and shortcut to adiabaticity protocols in a linear control system”, *Physical Review A* **101**, 013423 (2020) (cit. on pp. 7, 22).
- [65] Q. Zhang, X. Chen, and D. Guéry-Odelin, “Reverse engineering protocols for controlling spin dynamics”, *Scientific Reports* **7** (2017) (cit. on p. 7).

- [66] Q. Zhang, X. Chen, and D. Guéry-Odelin, “Connection between inverse engineering and optimal control in shortcuts to adiabaticity”, [Entropy](#) **23**, 84 (2021) (cit. on p. 7).
- [67] D. Guéry-Odelin and J. G. Muga, “Transport in a harmonic trap: shortcuts to adiabaticity and robust protocols”, [Physical Review A](#) **90**, 063425 (2014) (cit. on pp. 7, 71).
- [68] L. S. Pontryagin et al., *The mathematical theory of optimal processes* (Wiley-Interscience, London New York, 1962) (cit. on pp. 9, 48, 49, 91, 121).
- [69] A. E. Bryson and Y.-C. Ho, *Applied optimal control* (Routledge, May 2018) (cit. on pp. 9, 108, 121, 123).
- [70] B. Bonnard and D. Sugny, *Optimal control with applications in space and quantum dynamics* (American Institute of Mathematical Sciences, Springfield, MO, 2012) (cit. on pp. 9, 121).
- [71] M. Lapert, E. Assémat, S. J. Glaser, and D. Sugny, “Understanding the global structure of two-level quantum systems with relaxation: vector fields organized through the magic plane and the steady-state ellipsoid”, [Physical Review A](#) **88**, 033407 (2013) (cit. on p. 11).
- [72] R.-B. Wu, R. Long, J. Dominy, T.-S. Ho, and H. Rabitz, “Singularities of quantum control landscapes”, [Physical Review A](#) **86**, 013405 (2012) (cit. on p. 11).
- [73] G. Riviello, C. Brif, R. Long, R.-B. Wu, K. M. Tibbetts, T.-S. Ho, and H. Rabitz, “Searching for quantum optimal control fields in the presence of singular critical points”, [Physical Review A](#) **90**, 013404 (2014) (cit. on p. 11).
- [74] D. Stefanatos, A. Smonias, H. R. Hamedi, and E. Paspalakis, “Ultimate conversion efficiency bound for the forward double- λ atom–light coupling scheme”, [Optics Letters](#) **45**, 6090–6093 (2020) (cit. on p. 11).
- [75] E. Trélat, *Contrôle optimal : théorie et applications* (Vuibert, Paris, 2005) (cit. on pp. 38, 121).
- [76] J.-S. Li and N. Khaneja, “Ensemble control of linear systems”, in [2007 46th IEEE conference on decision and control](#) (2007), pp. 3768–3773 (cit. on pp. 42, 52, 87).
- [77] J.-S. Li and N. Khaneja, “Ensemble control of Bloch equations”, [IEEE Transactions on Automatic Control](#) **54**, 528–536 (2009) (cit. on pp. 42, 63, 87).
- [78] F. C. Chittaro and J.-P. Gauthier, “Asymptotic ensemble stabilizability of the Bloch equation”, [Systems & Control Letters](#) **113**, 36–44 (2018) (cit. on p. 47).
- [79] V. Martikyan, A. Devra, D. Guéry-Odelin, S. J. Glaser, and D. Sugny, “Robust control of an ensemble of springs: application to ion cyclotron resonance and two-level quantum systems”, [Physical Review A](#) **102**, 053104 (2020) (cit. on pp. 47, 48, 111).

-
- [80] J.-S. Li, “Control of inhomogeneous ensembles”, PhD thesis (Harvard University USA, 2006) (cit. on pp. 48, 58, 63, 87).
- [81] L. Van-Damme, Q. Ansel, S. J. Glaser, and D. Sugny, “Robust optimal control of two-level quantum systems”, *Physical Review A* **95**, 063403 (2017) (cit. on p. 56).
- [82] K. Kobzar, T. E. Skinner, N. Khaneja, S. J. Glaser, and B. Luy, “Exploring the limits of broadband excitation and inversion: II. RF-power optimized pulses”, *Journal of Magnetic Resonance* **194**, 58–66 (2008) (cit. on pp. 59, 109).
- [83] D. D’Alessandro and M. Dahleh, “Optimal control of two-level quantum systems”, *IEEE Transactions on Automatic Control* **45**, 866–876 (2001) (cit. on p. 62).
- [84] J.-S. Li and N. Khaneja, “Control of inhomogeneous quantum ensembles”, *Physical Review A* **73**, 030302 (2006) (cit. on p. 63).
- [85] R. Brockett, *Finite dimensional linear systems* (Wiley, New York, 1970) (cit. on p. 71).
- [86] F. Bonnans and P. Rouchon, *Commande et optimisation de systèmes dynamiques* (Éditions de l’École Polytechnique, Palaiseau, 2005) (cit. on pp. 71, 121).
- [87] F. Crawford, *Waves, Berkeley physics course* (McGraw-Hill, New York London, 1968) (cit. on p. 78).
- [88] J.-S. Li, “Ensemble control of finite-dimensional time-varying linear systems”, *IEEE Transactions on Automatic Control* **56**, 345–357 (2011) (cit. on pp. 79, 87, 99).
- [89] U. Boscain, M. Sigalotti, and D. Sugny, “Introduction to the Pontryagin Maximum Principle for Quantum Optimal Control”, *PRX Quantum* **2**, 030203 (2021) (cit. on pp. 91, 121, 123, 124).
- [90] D. Liberzon, *Calculus of variations and optimal control theory* (Princeton University Press, Jan. 8, 2012), 256 pp. (cit. on pp. 91, 121).
- [91] J.-S. Li, J. Ruths, and D. Stefanatos, “A pseudospectral method for optimal control of open quantum systems”, *The Journal of Chemical Physics* **131**, 164110 (2009) (cit. on p. 91).
- [92] A. Bressan and B. Piccoli, *Introduction to the mathematical theory of control* (American Institute of Mathematical Sciences, Springfield, MO, 2007) (cit. on pp. 91, 121).
- [93] A. G. Marshall and T. Chen, “40 years of Fourier transform ion cyclotron resonance mass spectrometry”, *International Journal of Mass Spectrometry* **377**, 410–420 (2015) (cit. on p. 95).
- [94] A. G. Marshall, C. L. Hendrickson, and G. S. Jackson, “Fourier transform ion cyclotron resonance mass spectrometry: a primer”, *Mass Spectrometry Reviews* **17**, 1–35 (1998) (cit. on p. 95).

- [95] M. A. van Agthoven, M.-A. Delsuc, G. Bodenhausen, and C. Rolando, “Towards analytically useful two-dimensional Fourier transform ion cyclotron resonance mass spectrometry”, *Analytical and Bioanalytical Chemistry* **405**, 51–61 (2012) (cit. on p. 95).
- [96] A. A. Sehgal, P. Pelupessy, C. Rolando, and G. Bodenhausen, “Theory for spiralling ions for 2D FT-ICR and comparison with precessing magnetization vectors in 2D NMR”, *Physical Chemistry Chemical Physics* **18**, 9167–9175 (2016) (cit. on p. 95).
- [97] E. N. Nikolaev, R. M. A. Heeren, A. M. Popov, A. V. Pozdnev, and K. S. Chingin, “Realistic modeling of ion cloud motion in a Fourier transform ion cyclotron resonance cell by use of a particle-in-cell approach”, *Rapid Communications in Mass Spectrometry* **21**, 3527–3546 (2007) (cit. on p. 95).
- [98] M. McCoy and L. Mueller, “Nonresonant effects of frequency-selective pulses”, *Journal of Magnetic Resonance* (1969) **99**, 18–36 (1992) (cit. on p. 99).
- [99] L. Emsley and G. Bodenhausen, “Phase shifts induced by transient Bloch-Siegert effects in NMR”, *Chemical Physics Letters* **168**, 297–303 (1990) (cit. on p. 99).
- [100] M. S. Shahriar, P. Pradhan, and J. Morzinski, “Driver-phase-correlated fluctuations in the rotation of a strongly driven quantum bit”, *Physical Review A* **69**, 032308 (2004) (cit. on p. 99).
- [101] N. I. Gershenzon, K. Kobzar, B. Luy, S. J. Glaser, and T. E. Skinner, “Optimal control design of excitation pulses that accommodate relaxation”, *Journal of Magnetic Resonance* **188**, 330–336 (2007) (cit. on p. 103).
- [102] N. I. Gershenzon, T. E. Skinner, B. Brutscher, N. Khaneja, M. Nimbalkar, B. Luy, and S. J. Glaser, “Linear phase slope in pulse design: application to coherence transfer”, *Journal of Magnetic Resonance* **192**, 235–243 (2008) (cit. on p. 103).
- [103] A. G. Marshall, T. C. L. Wang, and T. L. Ricca, “Tailored excitation for Fourier transform ion cyclotron mass spectrometry”, *Journal of the American Chemical Society* **107**, 7893–7897 (1985) (cit. on p. 105).
- [104] S. Guan, “Linear response theory of ion excitation for Fourier transform mass spectrometry”, *Journal of the American Society for Mass Spectrometry* **2**, 483–486 (1991) (cit. on p. 105).
- [105] S. Guan and A. G. Marshall, “Stored waveform inverse Fourier transform (SWIFT) ion excitation in trapped-ion mass spectrometry: theory and applications”, *International Journal of Mass Spectrometry and Ion Processes* **157-158**, 5–37 (1996) (cit. on p. 105).
- [106] V. Martikyan, C. Beluffi, S. J. Glaser, M.-A. Delsuc, and D. Sugny, “Application of optimal control theory to Fourier transform ion cyclotron resonance”, *Molecules* **26**, 2860 (2021) (cit. on p. 108).

-
- [107] N. Khaneja, T. Reiss, C. Kehlet, T. Schulte-Herbrüggen, and S. J. Glaser, “Optimal control of coupled spin dynamics: design of NMR pulse sequences by gradient ascent algorithms”, *Journal of Magnetic Resonance* **172**, 296–305 (2005) (cit. on pp. 108, 123).
- [108] M. Lapert, R. Tehini, G. Turinici, and D. Sugny, “Monotonically convergent optimal control theory of quantum systems with spectral constraints on the control field”, *Physical Review A* **79**, 063411 (2009) (cit. on p. 108).
- [109] T. W. Borneman and D. G. Cory, “Bandwidth-limited control and ringdown suppression in high-Q resonators”, *Journal of Magnetic Resonance* **225**, 120–129 (2012) (cit. on p. 108).
- [110] I. Hincks, C. Granade, T. Borneman, and D. Cory, “Controlling quantum devices with nonlinear hardware”, *Physical Review Applied* **4**, 024012 (2015) (cit. on p. 108).
- [111] W. Rose, H. Haas, A. Q. Chen, N. Jeon, L. J. Lauhon, D. G. Cory, and R. Budakian, “High-resolution nanoscale solid-state nuclear magnetic resonance spectroscopy”, *Physical Review X* **8**, 011030 (2018) (cit. on p. 108).
- [112] F. Motzoi, J. M. Gambetta, S. T. Merkel, and F. K. Wilhelm, “Optimal control methods for rapidly time-varying Hamiltonians”, *Physical Review A* **84**, 022307 (2011) (cit. on p. 108).
- [113] P. E. Spindler, Y. Zhang, B. Endeward, N. Gershernzon, T. E. Skinner, S. J. Glaser, and T. F. Prisner, “Shaped optimal control pulses for increased excitation bandwidth in EPR”, *Journal of Magnetic Resonance* **218**, 49–58 (2012) (cit. on p. 108).
- [114] P. E. Spindler, P. Schöps, W. Kallies, S. J. Glaser, and T. F. Prisner, “Perspectives of shaped pulses for EPR spectroscopy”, *Journal of Magnetic Resonance* **280**, 30–45 (2017) (cit. on p. 108).
- [115] A. Walther, B. Julsgaard, L. Rippe, Y. Ying, S. Kröll, R. Fisher, and S. Glaser, “Extracting high fidelity quantum computer hardware from random systems”, *Physica Scripta* **T137**, 014009 (2009) (cit. on p. 108).
- [116] D. Griffiths, *Introduction to electrodynamics* (Prentice Hall, Upper Saddle River, N.J, 1999) (cit. on pp. 113, 114).
- [118] M. Abramowitz and I. A. Stegun, *Handbook of mathematical functions: with formulas, graphs, and mathematical tables* (DOVER PUBN INC, June 1, 1965), 1046 pp. (cit. on pp. 135, 137, 138).

